FINAL REPORT
Grant Number: NCC3-835

A Preliminary Investigation of the E-Beam Induced Polymerization of Maleimide and Norbornene End-capped Polyimides

Period of Performance: 11/20/2000 - 3/31/2005

Submitted by

Principal Investigator: Giuseppe R. Palmese
Department of Chemical and Biological Engineering, Drexel University
Philadelphia, PA 19104

Submitted to NASA John H. Glenn Research Center

Technical Officer: Michael A. Meador

Grant Administrator: Saundra R. Gage

Bismaleimide and Cyanate Ester Based Sequential Interpenetrating Polymer Networks for High Temperature Application

A Thesis

Submitted to the Faculty

of

Drexel University

by

Xing Geng

in partial fulfillment of the

requirements for the degree

of

Doctor of Philosophy

January 2005

© Copyright 2005
Xing Geng. All Rights Reserved.

DEDICATIONS

This dissertation is dedicated to my parents, Mrs. Cao Xixian and Mr. Geng Yaozong, my wife Tie Liu, as well as my daughter, Helen, for their understanding and encouragement.

What I cannot create, I do not understand.
— Richard P. Feynman

ACKNOWLEDGMENTS

If my work achieves recognition, it will be because of the indispensable help that I have received. In particular, I would like to acknowledge valuable suggestions, advice and assistance from my advisor, Dr. Giuseppe R. Palmese, who made my pursuit of a Ph.D. enjoyable and profitable.

I am also very grateful to my dissertation committee members, Dr. Charles Weinberger, Dr. Anthony Lowman, Dr. Steve Wrenn as well as Dr. Frank Ko for their efforts in guiding my research. Dr. Klosterman of the University of Dayton has provided a great deal of help in EB facility utilization.

Thanks are also due to my group members, John La Scala, Jason Robinette, Vijay Raman, Jihean Lee, Mary Sullivan, Mohamed Aflal, Amutha Jeyarajasingam, for their kind help and encouragement. In particular Jason and Jihean provided great assistance with the EB kinetics study and measurement of mechanical properties.

I would also like to express my appreciation to my fellow graduate students, in particular Dr. Veena Pata, Dr. Manasa V. Gudheti, Jonathan Ayutsede and Lei Lou for their kind support. Special thanks are given to my dear friend Dian S. Zhou and his wife Wei Zheng who made my life here friendly and enjoyable.

I would like to acknowledge the administrative assistance provided by Dorothy Porter and the technical assistance provided by Dan Luu. Particularly, many thanks are also due to Orit Darwish and professor George for their kind help with draft revisions. I gratefully acknowledge the financial support that I received from Drexel University,

NASA NCC3-784 [Dr. Michael Meador, Program Monitor] and AFOSR F49620-02-1-0360 [Dr. Charles Lee, Program Monitor].

Someplace in China far away from here, I owe a considerable debt to my parents, Mrs. Cao Xixian and Mr. Geng Yaozong, as well as my daughter, Helen Geng. My wife Tie has been wonderfully patient in the face of many late nights and early mornings.

TABLE OF CONTENTS

LIST OF TABLES xi

LIST OF FIGURES xiii

ABSTRACT xxiv

CHAPTER 1: INTRODUCTION 1

1.1 Motivation and Objective 1

1.2 Outline of This Dissertation 4

List of References 6

CHAPTER 2: MOTIVATION AND LITERATURE REVIEW 7

2.1 Overview of High Temperature Composite Materials 7

2.1.1 Evolution of high temperature thermosetting polymers 7

2.1.2 Processing techniques for high temperature polymer composite fabrication 12

2.2 Structure-property-processing Relationship of Bismaleimides 13

2.3 Current Research Activities Involving Bismaleimide Modification 14

2.3.1 Modification of bismaleimide to improve toughness 14

2.3.1.1 Modification with diamines 16

2.3.1.2 Modification with epoxy resin 17

2.3.1.3 Modification with olefinic compounds 17

2.3.1.4 Modification with thermoplastics 18

2.3.1.5 Toughening with cyanate ester resins 18

2.3.2 Modification of bismaleimides to improve processibility 21

2.3.2.1 Modification with olefinic compounds 22

2.3.2.2 Modification with cyanate ester resins 26

2.4 Interpenetrating polymer networks (IPNs) 28

2.4.1 Morphology of IPNs 29

2.4.2 Physical and mechanical behavior of IPNs 31

2.4.3 Synthetic routes 32

2.4.3.1 Simultaneous IPNs 32

2.4.3.2 Sequential IPNs 33

2.5 Disadvantages of Current Technology and Significance of Our Study 34

List of references 36

CHAPTER 3: SYNTHESIS AND STRUCTURAL CHARACTERIZATION OF BMI-CE IN-SITU SEQUENTIAL IPNs 45

3.1 Introduction 45

3.2 Experimental 45

3.2.1 Materials 45

3.2.2 Preparation of sequential IPNs and LIPNs 46

3.2.3 Preparation of simultaneous IPNs and LIPNs 47

3.2.4 EB irradiation 48

3.2.5 Chemical and physical characterization 48

3.3 Results and Discussion 49

3.3.1 Selection of cyanate ester resin and appropriate catalyst 49

3.3.2 Selection of reactive diluent 53

3.3.3 Synthetic route of sequential IPNs and LIPNs 54

3.3.4 Verification and significance of sequential IPNs 58

3.3.5 Importance of synthetic route — sequential versus simultaneous IPNs 62

3.3.6 Behavior of IPNs....63

3.4 Summary....65

List of references....68

CHAPTER 4: CATALYSIS AND HYDROLYSIS OF LECY....69

4.1 Experimental....70

4.1.1 Materials....70

4.1.2 Instruments....71

4.1.3 Preparation of LECY sample and hydrolysis study....71

4.1.4 Water uptake study....72

4.2. Results and Discussion....73

4.2.1 Catalysis by metal and the influence of AMP on the conversion of LECY....73

4.2.2 Influence of catalyst on BMI and AMP stability....75

4.2.3 Influence of catalyst on the thermal degradation and hydrolysis of LECY....80

4.2.4 Comparison of water uptake behavior of LECY and BACY....90

4.2.5 Determination of processing conditions — LECY cure kinetics....95

4.3 Summary and Conclusions....100

List of References....102

CHAPTER 5: N-ACRYLOYLMORPHOLINE—A UNIQUE REACTIVE DILUENT FOR BMI COPOLYMERIZATION....105

5.1 Introduction....105

5.2 Experimental....105

5.2.1 Materials 105

5.2.2 Instruments and methods 107

5.2.3 Electron beam curing parameters 108

5.3 Results and Discussion 108

5.3.1 Influence of aggregation state on the conversion of phenylmaleimide under EB irradiation 108

5.3.2 Influence of reactive diluents on phenylmaleimide conversion via EB irradiation 111

5.3.3 Influence of the side groups on the reactivity of reactive diluents ... 119

5.3.4 A new reactive diluent: N-acryloylmorpholine 121

5.4 Summary and Conclusions 130

List of References 133

CHAPTER 6: KINETICS OF EB INDUCED BMI-AMP FREE RADICAL COPOLYMERIZATION 134

6.1 Introduction and Background 134

6.1.1 Kinetics of EB induced free radical polymerization 134

6.1.2 Kinetics and mechanism of copolymerization 137

6.2 Experimental 141

6.2.1 Raw materials and sample preparation 141

6.2.2 Fiber optic Near-IR spectroscopy 142

6.2.3 Electron beam curing parameters 145

6.2.4 FT-NIR monitoring of thermal copolymerization 145

6.3 Results and Discussion 146

6.3.1 Near-IR monitoring of the EB and initiator induced copolymerization 146

6.3.2 Influence of AMP concentration on the final conversion of double bond....150

6.3.3 Influence of dose rate on the conversion of AMP and PMI....154

6.3.4 Determination of the copolymerization parameters under different dose rate....157

6.3.5 Determination of initiator induced thermal copolymerization parameters....162

6.3.6 Influence of temperature on the EB induced copolymerization behavior....166

6.4 Summary....171

List of References....173

CHAPTER 7: PROPERTIES OF THE SEQUENTIAL IPN AND CORRELATIONS WITH STRUCTURE....175

7.1 Effect of AMP Content on the Tg of the Formed Sequential IPNs....175

7.2 Role of the Network Coupler in the Enhancement of Tg of Sequential IPNs....179

7.3 Effect of CPM Amount on the Tg of Inter Linked Sequential IPNs....186

7.4 Fracture Toughness of the Neat Resins....191

7.5 Thermal Stability of the Formed Sequential IPNs....194

7.5.1 Long term performance....194

7.5.2 Thermal degradation temperature (T_d)....198

7.6 Summary....199

List of References....201

CHAPTER 8: PROCESSING AND PROPERTIES OF COMPOSITES....202

8.1 Composite Processing....202

8.1.1 Processibility of IPNs neat resin....202

8.1.2 Composite plaques prepared by liquid molding 203

8.1.3 Electron beam (EB) irradiation 205

8.2 Assessment of Composite Properties 208

8.2.1 High temperature behavior - Tg 208

8.2.2 Interlaminar short beam shear (ILSS) 209

8.3 Summary 210

CHAPTER 9: CONCLUSIONS 211

9.1 Summary 211

9.2 Reactive Diluent Selection 216

9.3 Processing and Materials Parameters 217

9.4 Structure-Property Correlation 217

9.5 Future Work 218

9.6 Concluding Remarks 220

List of References 221

APPENDIX I: SYNTHESISLIST OF 4-CYANATOPHENYL MALEIMIDE (CPM) 222

APPENDIX II: DSC PLOTS IN LECY CURE KINETICS STUDY 230

APPENDIX III: DMA DSC RESULTS IN CPM Tg DETERMINATION 235

APPENDIX IV: MECHANICAL PROPERTIES ASSESSMENT OF IPNS NEAT RESIN AND COMPOSITE 239

APPENDIX V: FIBER CHARACTERISTICS AND MOLD DESIGN 244

VITA 250

LIST OF TABLES

Table 3.1 Solubility and reactivity of some reactive diluents evaluated in this study 54

Table 3.2 Final conversions of functional groups following the thermal cure and EB cure stages for the formation of the LECY-AMP/BMI *in-situ* sequential IPN 61

Table 4.1 Cure conditions for LECY sample for thermal cycling and water uptake 72

Table 4.2 Glass transition temperature values after thermal cycling and water uptake with respect to catalyst amount, species 87

Table 4.3 D_{ini} of LECY and BADCY in water uptake for different Cu^{2+} concentrations 94

Table 6.1 Polymerization rate R_p of different double bonds under different dose rates 156

Table 6.2 Conversions of PMI and AMP at different time span in EB induced copolymerization with different dose rate 159

Table 6.3 Polymerization rate R_p of different double bonds with dose rate as 3.5 kGy/min under different temperatures 167

Table 7.1 Compositions of samples in this study (all blends contained 1% copper naphthenate (6% Cu^{2+})) 176

Table 7.2 Tgs of the various monomers employed in the current study 178

Table 7.3 Compositions of samples in this study (all blends contained 1% copper naphthenate (6% Cu^{2+})) 179

Table 7.4 Compositions of blends in this study (all blends contained 1% copper naphthenate (6% Cu^{2+})) 187

Table 7.5 Fracture toughness of various resins 193

Table 8.1 Processing parameters of the EB irradiation and postcure for composite plaques 207

Table A.I.1 Formulation in the synthesis of HPM 224

Table A.I.2 Formulation in the synthesis of CPM.....226

Table A.IV.1 Neat resin comprising of 50% BMI and AMP (molar ratio 1:2) 50% LECY.....240

Table A.IV.2 Neat resin comprising of 40% BMI and AMP (molar ratio 1:2) 30% LECY 50% CPM.....241

Table A.IV.3 Result summary 243

Table A.V.1 Properties and characteristics of THORNEL Carbon Fiber T-650/35 3K.....244

Table A.V.2 Typical Strand Properties of THORNEL Carbon Fiber T-650/35 3K.....245

Table A.V.3 Specification of parts.....245

LIST OF FIGURES

Figure 2.1 General structures of typical thermosetting polyimides 11

Figure 2.2 Chemical structure of 4,4'-bismalimidodiphenyl methane.....15

Figure 2.3 Reaction scheme for the reaction of BMI with diamine 16

Figure 2.4 Variation of fracture toughness with composition. (redrawn according to reference [61]).....20

Figure 2.5 Reaction scheme for allyl compound with bismaleimides 23

Figure 2.6 Proposed structure of cured bismaleimide resins with diallylbisphenol A showing Diels-Alder and ene-reaction.(redrawn according to reference [90]).....24

Figure 2.7 Structure of cured bismaleimide with diallylbisphenol A obtained using ^{13}C NMR. Redrawn according to reference [44]) 25

Figure 2.8 Scheme for the formation of triazine ring from cyanate ester monomer...26

Figure 2.9 A representation of IPN's structure. One network is represented by solid lines, while the other is shown by dotted lines. The circles represent points at which the chains are crosslinked 29

Figure 3.1 General structures of raw materials used in current study.....46

Figure 3.2 The relationship between the constant viscosity (150mPa.s) temperature of common monomers and their Tgs of the cured thermoset resins. Data courtesy of Ciba-Geigy, wherein BPECN stands for LECY.....51

Figure 3.3 Chemical structure of BACY. The more regular backbone gives it higher melting point compared to LECY 51

Figure 3.4 Scheme illustrating the cure path of LECY 52

Figure 3.5 Scheme illustrating the formation of *in-situ* sequential IPNs based on cyanate ester and BMI 56

Figure 3.6 Scheme illustrating the formation of linked *in-situ* sequential IPNs of cyanate ester with BMI.....57

Figure 3.7 The Mid-IR spectra of blends (50 wt.% BMI and AMP (molar ratio as 1:4) 50 wt.% LECY) concerning first network formation: a) initial; after 105°C (5hrs) and c) after 105°C (5hrs) and 130°C (2hrs). OCN peak at 2266 cm^{-1}, triazine peak at 1570 cm^{-1} 59

Figure 3.8 The Near-FTIR spectra of blends (50 wt.% BMI and AMP (molar ratio 1:4) 50 wt.% LECY) concerning second network formation: (a) initial; (b) after EB radiation and (c) after EB radiation and postcure 60

Figure 3.9 The Mid-FTIR spectra of blends [50 wt.% BMI and AMP (molar ratio 1:4) 50 wt.% LECY] concerning second network formation: (—) initial; (---) after EB radiation 61

Figure 3.10 Dynamic mechanical spectrum of the system of 50 wt.% LECY 50 wt.% BMI and AMP (molar ratio 1:2). (—) synthesized sequentially via EB irradiation, (---) synthesized simultaneously by thermal cure. 63

Figure 3.11 Dynamic mechanical spectra of the IPNs comprised of 50 wt.% BMI and AMP (with molar ratio as 1:2) and 30 wt.% LECY together with 20 wt.% CPM synthesized in different ways . (—) sequentially, (---) simultaneously 65

Figure 4.1 Chemical structures of LECY and selected catalyst for LECY cure 70

Figure 4.2 Influence of AMP on the conversion of LECY with 600ppm Cu^{2+}: (—) 50 wt.% LECY 50 wt.% BMI and AMP (molar ratio 1:2), (---) pure LECY. Reaction temperature is 110°C 75

Figure 4.3 Isothermal DSC thermograms for a mixture of BMI and AMP (1:4 molar ratio) with 600 ppm Cu^{2+} catalyst at 110°C. (—) copper acetylacetonate, (---) copper naphthenate 76

Figure 4.4 Mixing catalyst, BMI, and LECY (75 wt.% LECY, 25 wt.% BMI, and 0.1% DBTDL) at the same time at 130°C. (—) C=C of BMI, (---) –OCN of LECY 78

Figure 4.5 Mixing LECY and catalyst first and adding BMI consequently (composition same to that of Figure 4.4) at 130°C. (—) C=C of BMI, (---) –OCN of LECY 79

Figure 4.6 Heating the mixture of BMI and LECY (weight ratio 1:3) at 130°C for two hours. (—) C=C of BMI, (---) –OCN of LECY 80

Figure 4.7 Scheme for the proposed degradation of the network by hydrolysis of the ester bond followed by hydrolysis of cyanuric acid to ammonia and carbon dioxide. 81

Figure 4.8 Dynamic mechanical spectra of the 300ppm Cu^{2+} catalyzed LECY with three sets of peaks corresponding to (A) 1st run after pre-cure, (B) consecutive thermal cycling in DMA, and (C) after water exposure at 70°C for 5.5 hours. Scan to 330°C at a ramping rate of 10°C/min....83

Figure 4.9 Dynamic mechanical spectra of the 300ppm Sn^{4+} catalyzed LECY with three sets of peaks corresponding to (A) 1st run after pre-cure, (B) consecutive thermal cycling, and (C) after water exposure at 70°C for 5.5 hours. Scan to 330°C at a ramping rate of 10°C/min....84

Figure 4.10 Glass transition temperature changes of Sn^{4+} catalyzed LECY during thermal cycling and water exposure. (■) 0 ppm, (♦) 150 ppm, (▲) 300 ppm. (●) 600 ppm....85

Figure 4.11 Glass transition temperature changes of Cu^{2+} catalyzed LECY during thermal cycling and water exposure. (■) 0 ppm, (♦) 150 ppm, (▲) 300 ppm, (●) 600 ppm....86

Figure 4.12 Different stage of 300 ppm tin catalyzing LECY cure monitored by FT-NIR. (a) cure @ 105°C (5hrs) + 130°C (2hrs), (b) 6 DMA runs up to 330°C, (c) water uptake @ 70°C (5.5hrs), (d) water uptake @ 70°C (5.5hrs) and drying @ 105°C (1hr), (e) DMA run after drying @ 105°C (1hr) 89

Figure 4.13 Water uptake profile of LECY with different amount of Cu^{2+}. 91

Figure 4.14 Water uptake profiles of BACY with different amount of Cu^{2+} 91

Figure 4.15 Water uptake profiles of LECY and BACY with different amount of Cu^{2+}....92

Figure 4.16 Water uptake profiles of LECY and BACY plotted as M_t/M_∞ versus [(square root of time/thickness)] at different concentrations of Cu^{2+}. 93

Figure 4.17 Tg change after water uptake for LECY and BADCY without catalyst. (a, a') BADCY with 0 ppm Cu^{2+}, (b, b') LECY with 0 ppm Cu^{2+}....95

Figure 4.18 Plot of activation energy versus concentration of catalyst....97

Figure 4.19 Mixture of 70% BMI and AMP (molar ratio 1:2) and 30% LECY with 150 ppm Cu^{2+}. (—) –OCN change, (---) C=C of BMI, (·····) C=C of AMP 98

Figure 4.20 Mixture of 70% BMI and AMP (molar ratio 1:2) and 30% LECY with 300 ppm Cu^{2+}. (—) –OCN change, (---) C=C of BMI, (·····) C=C of AMP. 99

Figure 5.1 Chemical structures of materials used in current study. 106

Figure 5.2 DSC thermogram of N-phenylmaleimide with a ramping rate of 10°C/min 109

Figure 5.3 HPLC trace of PMI under EB irradiation at room temperature, (—) PMI before EB irradiation, (----) PMI after EB irradiation, (·····) PMI after EB and post heating to 105°C. 110

Figure 5.4 FTIR spectrum of PMI under different stages, (----) PMI before EB irradiation, (—) PMI with EB irradiating at 100°C. 111

Figure 5.5 HPLC trace of PMI and APE with different molar ratio under EB irradiation, (—) 3:1 molar ratio of PMI to APE, (----) 1:1 molar ratio of PMI to APE, (·····) 1:3 molar ratio of PMI to APE 112

Figure 5.6 FTIR spectra of PMI and APE (molar ratio 1:1) at different stages. (----) before EB, (—) after EB, (·····) after EB and post cure. 113

Figure 5.7 FTIR spectra of PMI and APE (molar ratio 3:1) at different stages. (----) before EB, (—) after EB, (·····) after EB and post cure. 114

Figure 5.8 Conversion of PMI C=C under EB irradiation and postcure as a function of APE molar fraction. (■) EB and (▲) EB + postcure. 115

Figure 5.9 HPLC spectrum of APE under different stages. (—) APE before EB irradiation, (----) APE after EB irradiation, (·····) APE after EB and post heating 116

Figure 5.10 Conversion of PMI under EB with different kinds of vinyl ethers, (□) EHVE, (▲) APE, (●) CHVE. A characteristic maximum is not observed for CHVE. 118

Figure 5.11 DSC thermogram of PMI with CHVE (----) and EHVE (—). Weight ratio of PMI to vinyl ether is of 1:2. 119

Figure 5.12 DSC therogram of PMI with St (—), DVB (---), and NSt (·····). Weight ratios of PMI to various diluents are of 1:2.....121

Figure 5.13 Viscosity change of three systems with the increase of temperature. (-▲-) molar ratio of BMI to AMP 1:2, (-●-) molar ratio of BMI to AMP 1:3, (-■-) molar ratio of BMI to AMP 1:4.....123

Figure 5.14 Overlay DSC plots of BMI, AMP, and mixture of BMI and AMP (molar ratio 1:4), (—) BMI+AMP (molar ratio 1:4), (----) BMI, (·····) AMP. 124

Figure 5.15 FTIR spectra of BMI and AMP mixture (molar ratio 1:4), (—) before EB irradiation, (----) after EB irradiation at room temperature. 125

Figure 5.16 Conversion of PMI C=C under EB irradiation at room temperature as a function of AMP concentration. 128

Figure 5.17 *In-situ* NIR monitoring of AMP C=C variation under EB irradiation with dose rate at 3.5 KGy/min and temperature of 22°C, (—) before EB irradiation, (----) after 5 sec of EB irradiation, (·····) after 10 sec of EB irradiation.....129

Figure 5.18 Conversion of AMP C=C with time under EB irradiation with dose rate as 3.5 KGy/min and temperature as 22°C. 130

Figure 6.1 Chemical structure of monomers used in current study.....141

Figure 6.2 Schematic of sample cell configuration.....143

Figure 6.3 Schematic diagram of the entire set-up for remotely monitoring EB cure.....144

Figure 6.4 *In-situ* NIR spectra of the PMI/AMP system (dose rate = 3.5 kGy/min, T = 22°C, molar ratio PMI to AMP = 1:3).....146

Figure 6.5 Plots of C=C conversion versus time under EB irradiation (dose rate = 3.5 kGy/min, T = 22°C, molar ratio PMI to AMP = 1:3): (-■-) PMI C=C, (-□-) AMP C=C. 147

Figure 6.6 Plots of C=C conversion versus time for thermal induced copolymerization of PMI and AMP (molar ratio 3:1, T=110°C, 0.1 mol% Luperox 101): -■-) PMI C=C conversion, -□-) AMP C=C conversion.....148

Figure 6.7 PMI C=C conversion with the increase of AMP amount (EB irradiation at 22°C): (▲) 3.5 kGy/min, (●) 4.4 kGy/min, (■) 7 kGy/min, (×) Thermal copolymerization (T = 110°C).....151

Figure 6.8 AMP C=C conversion with the change of AMP amount (EB irradiation at 22°C): (▲) 3.5 kGy/min, (●) 4.4 kGy/min, (■) 7 kGy/min, (×) Thermal copolymerization (T = 110°C).....152

Figure 6.9 PMI C=C residual after EB and thermal (EB irradiation at 22°C): (▲) 3.5 kGy/min, (●) 4.4 kGy/min, (■) 7 kGy/min, (×) Thermal copolymerization (T = 110°C).....153

Figure 6.10 AMP C=C residual after EB and thermal (EB irradiation at 22°C): (▲) 3.5 kGy/min, (●) 4.4 kGy/min, (■) 7 kGy/min, (×) Thermal copolymerization (T = 110°C).....154

Figure 6.11 Plots of conversion vs. time for molar ratio of PMI to AMP as 1:3 with different dose rate at ambient temperature: (-■-) PMI (7 kGy/min), (-▲-) PMI (3.5 kGy/min), (-□-) AMP (7 kGy/min), (-Δ-) AMP (3.5 kGy/min).....155

Figure 6.12 Initial stage plots of conversion vs. time for molar ratio of PMI to AMP as 1:3 with different dose rate at ambient temperature: (-■-) PMI (7 kGy/min), (-▲-) PMI (3.5 kGy/min), (-□-) AMP (7 kGy/min), (-Δ-) AMP (3.5 kGy/min).....156

Figure 6.13 Copolymerization results with dose rate as 3.5 kGy/min (T = 22°C): (-■-) 3a1p (t = 10s), (-●-) 2a1p (t = 10s), (-▲-) 1a1p (t = 10s), (-□-) 3a1p (t = 20s), (-○-) 2a1p (t = 20s), (-Δ-) 1a1p (t = 20s), (-+-) 3a1p (t = 30s), (-◊-) 2a1p (t = 30s), (-×-) 1a1p (t = 30s).....160

Figure 6.14 Copolymerization results with dose rate as 4.4 kGy/min (T = 22°C): (-■-) 3a1p (t = 10s), (-●-) 2a1p (t = 10s), (-▲-) 1a1p (t = 15s), (-□-) 3a1p (t = 20s), (-○-) 2a1p (t = 20s), (-Δ-) 1a1p (t = 20s), (-♦-) 3a1p (t = 30s), (-◊-) 2a1p (t = 30s), (-×-) 1a1p (t = 30s), (-+-) 1a1p (t = 35s).....161

Figure 6.15 Copolymerization results with dose rate as 7 kGy/min (T = 22°C): (-■-) 3a1p (t = 10s), (-●-) 2a1p (t = 10s), (-▲-) 1a1p (t = 10s), (-□-) 3a1p (t = 20s), (-○-) 2a1p (t = 20s), (-Δ-) 1a1p (t = 20s), (-♦-) 3a1p (t = 30s), (-◊-) 2a1p (t = 30s), (-×-) 1a1p (t = 30s).....162

Figure 6.16 Copolymerization results for thermally polymerization at 110°C (Luperox 101 as initiator with concentration as 0.1 mol.%): (-■-)1a1p (t = 22min), (-●-) 1a1p (t = 25min), (-▲-) 1a1p (t = 30min), (-♦-) 1a1p (t = 35min), (-×-) 1a1p (t = 50min), (-□-) 1a2p (t = 16min), (-○-) 1a2p (t = 25min), (-Δ-) 1a2p (t = 30min), (-◊-) 1a2p (t = 35min). Three groups of lines correspond to three reaction stages I, II, and III in copolymerization of AMP and PMI at a molar ratio 3:1. 163

Figure 6.17 Plots of conversion vs. time for molar ratio of PMI to AMP as 1:3 with dose rate as 3.5 kGy/min under different temperatures: (-■-) PMI (22°C), (-●-) PMI (50°C), (-▲-) PMI (80°C), (-□-) AMP (22°C), (-○-) AMP (50°C), (-Δ-) AMP (80°C). 167

Figure 6.18 Temperature variation during the EB radiation at 50°C for 1:3 molar ratio of PMI to AMP (dose rate = 3.5 kGy/min). 168

Figure 6.19 Temperature variation during the EB radiation at 80°C for 1:3 molar ratio of PMI to AMP (dose rate = 3.5 kGy/min). 169

Figure 6.20 Copolymerization results with temperature as 50°C (dose rate = 3.5 kGy/min): (-■-) 3a1p (t = 5s), (-●-) 2a1p (t = 5s), (-▲-) 1a1p (t = 5s), (-□-) 3a1p (t = 7s), (-○-) 2a1p (t = 7s), (-Δ-) 1a1p (t = 7s), (-♦-) 3a1p (t = 10s), (-◊-) 2a1p (t = 10s), (-×-) 1a1p (t = 10s).....170

Figure 6.21 Copolymerization results with temperature as 80°C (dose rate = 3.5 kGy/min): (-■-) 3a1p (t = 5s), (-●-) 2a1p (t = 5s), (-▲-) 1a1p (t = 5s), (-□-) 3a1p (t = 8s), (-○-) 2a1p (t = 7s), (-Δ-) 1a1p (t = 8s), (-*-) 3a1p (t = 10s), (-◊-) 2a1p (t = 13s), (-×-) 1a1p (t = 10s), (-+-) 3a1p (t = 4s).....171

Figure 7.1 Tg results for the samples of 50 wt.% BMI and AMP 50 wt.% LECY with different amount of AMP: (—) lower bound (obtained by Fox's rule), (---) upper bound (obtained by weighted average rule), (-▲-) without adding of CPM, (-□-) after adding 10 wt.% to 20 wt.% of CPM, (-+-) predicted values of IPNs with different amount of CPM.....177

Figure 7.2 Tgs of copolymer of CPM and AMP with varied weight fraction of CPM (by DMA): (---) upper bound calculated by weighted average rule (obtained with presumed Tg of CPM as 580 °C).....181

Figure 7.3 Tgs of copolymer of CPM and AMP with varied weight fraction of CPM (by DSC): (---) upper bound calculated by weighted average rule (obtained with presumed Tg of CPM as 560 °C).....182

Figure 7.4 Tgs of copolymer of BMI and AMP with varied weight fraction of BMI (by DMA): (---) upper bound calculated by weighted average rule, (—) lower bound calculated by Fox's rule (both bounds were obtained with Tg of BMI as 450 °C).....183

Figure 7.5 Tgs of copolymer of BMI and AMP with varied weight fraction of BMI (by DSC): (---) upper bound calculated by weighted average rule, (—) lower bound calculated by Fox's rule (both bounds were obtained with Tg of BMI as 430°C).....184

Figure 7.6 Dynamic mechanical spectra (storage modulus) of the interlinked IPNs: (a) BA2-30-40, (b)BA2-30-30, (c) BA2-30-20.....188

Figure 7.7 Dynamic mechanical spectra (Loss modulus) of the interlinked IPNs: (a) BA2-30-40, (b) BA2-30-30, (c) BA2-30-20.....189

Figure 7.8 The change of Tg with the variation of CPM amount for IPN via different path: (-□-) Thermal cure, (-×-) EB irradiation, (---) upper bound obtained by weighted average rule, (—) lower bound obtained by Fox's rule.....190

Figure 7.9 Dynamic mechanical analysis plots (Storage modulus) of the linked IPN: (—) EB BA2-30-40, (---) Thermal BA2-30-40.....191

Figure 7.10 Tg change after 7 months for the sequential IPN comprised of 30 wt.% LECY and a 2:1 molar mixture of AMP and BMI together with 20 wt.% CPM with 1% Copper naphthenate as catalyst: (—) postcure immediately after EB irradiation (up to 330°C), (----) Postcure 7 months later after EB irradiation (up to 330°C), (·····) Postcured sample 7 months later (drying at 105°C @3hrs).....195

Figure 7.11 Long time storage of pure LECY cured with 600ppm Copper naphthenate: (—) after fully cure at 105°C for 12 hours, (----) 2 years later first scan, (·····) second scan.....196

Figure 7.12 Influence of the network coupler amount on the water resistance of the formed sequential IPN: (a, a') 30 wt. % LECY and a 2:1 molar mixture of AMP and BMI together with 20 wt.% CPM with 1% Copper naphthenate as catalyst, (b, b') 40 wt.% LECY and a 2:1 molar mixture of AMP and BMI together with 10 wt.% CPM with 1% Copper naphthenate as catalyst.....197

Figure7.13 TGA curves of different resins under nitrogen, (a) BMI, (b) LECY, (c) IPN, d) AMP.....198

Figure 8.1 Change of IPNs neat resin viscosity with the increase of temperature.....203

Figure 8.2 Schematic of the installation of the air pressure assisted RTM.....204

Figure 8.3 Representative picture of C-stage plaques.....204

Figure 8.4 Schematic of the E-beam irradiation equipment.....206

Figure 8.5 Photo of the cart and composite plaque installation.....207

Figure 8.6 DMA spectrum for the composite based on LIPN resin comprising of 40% BMI and AMP (molar ratio 1:2) 30% LECY 30% CPM.....208

Figure 8.7 Representative ILSS test profile of the composite.....209

Figure A.I.1 DSC spectrum of the recrystallized HPM.....225

Figure A.I.2 Photo of the obtained CPM.....228

Figure A.I.3 DSC spectrum of the recrystallized CPM.....228

Figure A.II.1 DSC thermograms of pure LECY at different ramping rates. (—) 5°C/min, (– –) 10°C/min, (— —) 15°C/min, (·····) 20°C/min.....230

Figure A.II.2 DSC thermograms of LECY with 200ppm Cu^{2+} at different ramping rates. (—) 5°C/min, (– –) 10°C/min, (— —) 15°C/min, (·····) 20°C/min.....231

Figure A.II.3 DSC thermograms of LECY with 300ppm Cu^{2+} at different ramping rates. (—) 5°C/min, (– –) 10°C/min, (— —) 15°C/min, (·····) 20°C/min.....231

Figure A.II.4 DSC thermograms of LECY with 600ppm Cu^{2+} at different ramping rates. (—) 5°C/min, (– –) 10°C/min, (— —) 15°C/min, (·····) 20°C/min 232

Figure A.II.5 DSC thermograms of LECY with 800ppm Cu^{2+} at different ramping rates. (—) 5°C/min, (– –) 10°C/min, (— —) 15°C/min, (·····) 20°C/min 232

Figure A.II.6 DSC thermograms of LECY with 1000ppm Cu^{2+} at different ramping rates. (—) 5°C/min, (– –) 10°C/min, (— —) 15°C/min, (·····) 20°C/min 233

Figure A.II.7 DSC thermograms of LECY with 1200ppm Cu^{2+} at different ramping rates. (—) 5°C/min, (– –) 10°C/min, (— —) 15°C/min, (·····) 20°C/min 233

Figure A.II.8 DSC thermograms of LECY with 1400ppm Cu^{2+} at different ramping rates. (—) 5°C/min, (– –) 10°C/min, (— —) 15°C/min, (·····) 20°C/min 234

Figure A.III.1 DSC plots of CPM and AMP with different compositions. (—) 1 wt.% of CPM, (—) 5 wt.% of CPM, (---) 10 wt.% of CPM, (–·–) 15 wt.% of CPM, (····) 20 wt.% of CPM. Glass transition region will be clearer in small scale for high percentage of CPM. Tgs for these combinations with the increase of CPM amount are as follows: 141.3°C, 146.7°C, 168.4°C, 187.3°C, and 200.1°C 235

Figure A.III.2 DSC plots of BMI and AMP with different compositions. (— –) 0 wt.% BMI (i.e. pure AMP), (—) 1wt.% of BMI, (—) 5 wt.% of BMI, (---) 10 wt.% of BMI, (–·–) 15 wt.% of BMI, (····) 20 wt.% of BMI. Glass transition region will be clearer in small scale for high percentage of BMI. Tgs for these combinations with the increase of BMI amount are as follows: 119.8°C, 132.1°C, 137°C, 157.3°C, 168.3°C, and 192.6°C 236

Figure A.III.3 DMA plots concerning storage modulus of CPM and AMP with different compositions. (—) 1 wt.% of CPM, (—) 5 wt.% of CPM, (---) 10 wt.% of CPM, (–·–) 15 wt.% of CPM, (····) 20 wt.% of CPM. Tgs for these combinations with the increase of CPM amount are as follows: 163°C, 169.9°C, 192.6°C, 203°C, and 213.1°C 237

Figure A.III.4 DMA plots concerning storage modulus of BMI and AMP with different compositions. (—) 1 wt. % of BMI, (– –) 5 wt.% of BMI, (- - -) 10 wt.% of BMI, (–·–) 15 wt.% of BMI, (····) 20 wt.% of BMI, (— –) 50 wt.% of BMI, (——) 75 wt.% of BMI. Tgs for these combinations with the increase of BMI amount are as follows: 157.3°C, 157.2°C, 169.4°C, 185.7°C, 200.2°C, 337.2°C, and 384.9°C 238

Figure A.IV.1 Representative plot of load against extension in fracture toughness measurement. 240

Figure A.V.1 Design scheme for the upper layer 246

Figure A.V.2 Design scheme for the middle layer 247

Figure A.V.3 Design scheme for the bottom layer 248

Figure A.V.4 Photo of the designed mold 249

ABSTRACT

Bismaleimide and Cyanate Ester Based Sequential Interpenetrating Polymer Networks for High Temperature Application

Xing Geng

Giuseppe R. Palmese, Ph.D.

A research area of high activity in connection with aerospace engineering has been the development of polymer thermosetting resins that can resist temperature as high as 300°C while maintaining adequate toughness, and providing ease of processing to enable low temperature and low cost composite fabrication methods. In order to meet such requirements, sequential interpenetrating polymer networks (IPNs) based on bismaleimide (BMI) and cyanate ester (CE) monomers were investigated. In these systems, a polycyanurate network is first formed in the presence of BMI and appropriate reactive diluent monomers and in a second step, a network based on the BMI is created in the presence of a fully formed polycyanurate network. The materials developed can be processed at relatively low temperature (<150°C) and with the aid of electron beam (EB) curing.

Of major importance to the success of this work was the identification of a reactive diluent that improves ease of processing and has tailored reactivity to allow for the controlled synthesis of CE-BMI sequential IPNs. Based on solubility and reactivity of a number of reactive diluents, N-acryloylmorpholine (AMP) was selected as a co-monomer for BMI copolymerization. A donor-acceptor reaction mechanism was suggested to explain the relative reactivity of a variety of reactive diluents towards maleimide functionality. The optimum processing parameters for the formation of the first network were determined through the study of metal catalyzed cure and hydrolysis

of cyanate esters, whereas the reaction behavior for second network formation in terms of the influence of EB dose rate and temperature was elucidated through an *in-situ* kinetics study of maleimide and AMP copolymerization.

Structure-property relationships were developed which allowed for the design of improved resin systems. In particular, appropriate network coupler possessing cyanate ester and maleimide functionality was synthesized to link the polycyanurate first network to the BMI/AMP second network and thus form linked sequential IPNs (LIPNs). Consequently, Tg as high as 370°C was achieved and a fracture toughness of 120 J/m^2 was obtained for resin systems that possess adequately low viscosity for processing using liquid molding techniques at low temperature.

CHAPTER 1: INTRODUCTION

1.1 Motivation and Objective

High-temperature-high-performance polymers, along with the fiber reinforced composites based on them, exhibit superior thermal and mechanical properties compared to common materials. These properties include stability at temperatures in excess of 300°C, low density, high specific strength and stiffness, high toughness, low heat distortion and warpage, and good processibility [1]. High temperature composite materials typically consist of a high modulus fibrous reinforcing material imbedded in a thermosetting polymeric matrix. Reinforcing materials include graphite, glass, and aramid fibers. Bismaleimides, cyanate ester resins and polyimides are common high-temperature thermosetting systems. The behavior characteristics of the composite depend on the properties of the matrix and the reinforcing phases, as well as of the interphase between them. The organic matrix material generally limits the thermal resistance characteristics of the composites. Consequently, studies that aim to develop more advanced high temperature composites involve primarily an improvement in the performance of the thermosetting polymeric matrix in terms of high temperature resistance, toughness and processibility.

The high temperature resistance of a thermosetting polymer can be improved by three means in connection with its molecular structure. These include: (1) improving the rigidity of the polymer chain, (2) synthesizing polymers with the ability to crystallize, and (3) designing materials that undergo crosslinking. On a molecular level, each of these methods aims to restrict the movement of the polymer chain thus increasing the Tg,

and melting temperature, which is a necessary condition of the thermal resistance of the thermosetting polymer. However, very high Tg will result in low toughness of the polymer, which makes some thermosetting polymers inadequate for use as composite matrix materials. The improvement in high temperature resistance is generally achieved at the sacrifice of toughness, and *vice versa*.

Another pivotal issue regarding the use of high temperature thermosetting polymers for composite applications is their processibility. Generally these systems require high temperatures for processing and therefore cannot be effectively used in conjunction with low-cost processing techniques like resin transfer molding (RTM) unless solvents are used to reduce viscosity, as is the case for processes such as SARTM (solvent-assisted resin transfer molding). In SARTM, the removal of solvent complicates processing and the residual solvent can be detrimental to the ultimate properties of the resin. Therefore, as pointed out by researchers at NASA, developing novel high performance thermosetting polymers is a matter of finding the best combination of processing and performance characteristics for the end-use. Of course, the cost of the final component is also a major consideration [2].

Interpenetrating polymer networks (IPNs) refer to an intimate combination of two polymers in network form, where at least one of the polymers is polymerized and/or cross-linked in the immediate presence of the other. In IPNs, the properties possessed by each network can be imparted to the IPNs concurrently, suggesting that the resulting materials might possess performance superior to that of each constituent. In view of this, IPNs become the focus of our investigation to find novel thermosetting polymers used in

high temperature composites that convey high temperature resistance, high toughness, and improved processibility. This method has found limited commercial success [3].

Electron beam (EB) curing of fibre-reinforced polymer composites is a promising new curing technology for fabricating aerospace components. The process reduces the time required to crosslink the polymer matrix compared to conventional heat curing [4]. EB provides high energy efficiency, high throughput and more importantly, low cost associated with combining multiple processing steps needed for the fabrication of large complex composite structure [5]. Particularly, EB processing shows significant promise for high temperature production in that it may provide low temperature processing ease [6].

In light of the challenges associated with the manufacturing high temperature polymer composites discussed above, the general objective of this investigation is to develop a new class of thermosetting polymer systems that are easy to process at low temperatures (<150°C) yet possess good mechanical properties even in high temperature environments (>300°C). We therefore propose to develop sequential IPNs composed of bismaleimides and cyanate ester processed by EB irradiation. Such systems will possess the following features: (1) before cure, the mixture of raw materials possesses low viscosity (<1000 cP) below 100°C; (2) the first network forms at T<150°C in the presence of monomers of the second network; (3) the second network can be generated under EB irradiation; and (4) after minimum postcure, the ultimate Tg of the sequential IPNs will exceed 350°C.

To fulfill the outlined objectives three goals must be met: (1) developing a fundamental understanding of processing parameters on sequential IPNs formation, (2)

developing an understanding of structure-property relationships for the formed sequential IPNs, and (3) developing a design methodology for *in-situ* polymerization of sequential IPNs assisted by EB irradiation. As a result, several questions will be answered by this study: (1) Why and how can EB irradiation assisted *in-situ* synthesis of sequential IPNs be an effective means to obtain high temperature polymer composites? (2) What are the advantages possessed by EB processing, compared with thermal methods, for controlling the morphology of sequential IPNs? 3) What empirical rule can be used to predict the properties of the formed sequential IPNs based on the properties of their constituents?

1.2 Outline of This Dissertation

This dissertation is composed of nine chapters. Chapter 1 provides a general introduction to the study. Chapter 2 is a critical review of the literature available on the topic. By comparing our proposed study with current technology, the significance of sequential IPNs in producing high temperature composite materials is elucidated, and the research plan is presented.

Chapter 3 discusses efforts to demonstrate the methodology used for the *in-situ* synthesis of 4,4'-bismalimidodiphenyl methane (BMI) and bisphenol E cyanate ester (LECY) based sequential IPNs. The feasibility of obtaining such BMI-LECY sequential IPNs and their significance are addressed.

Each of the next three chapters addresses an aspect of how processing parameters affect the ultimate IPN structure and hence their resulting properties. Chapter 4 examines the catalysis and hydrolysis of LECY; the optimum amount of catalyst is determined in conjunction with the appropriate temperature and time needed for the formation of the

first network. Chapter 5 highlights the crucial role of N-acryloylmorphiline (AMP) as a novel reactive diluent to improve the processibility of BMI while enhancing the conversion of BMI under EB irradiation. The fundamental mechanism for the copolymerization of BMI with AMP is elucidated in this chapter. Chapter 6 sheds light on the kinetics and mechanism of EB induced free radical copolymerization involving AMP and BMI by using phenylmaleimide (PMI) as a model compound for BMI. On the basis of the measured copolymerization parameters under different dose rates and temperature conditions, the influence of processing parameters on the conversion of functional groups is addressed. This study then forms the basis for selection of processing parameters for the formation of the second network.

In Chapter 7 the correlation of processing-structure and properties of the IPNs is investigated. Particularly, the influence of initial IPNs composition on structure and Tg is discussed.

Based on the work presented in Chapters 3-7, the corresponding composites can then be fabricated. Chapter 8 describes the procedure employed to produce the composites, including RTM and EB irradiation, together with the measurements to assess their properties.

Finally, Chapter 9 summarizes the accomplishments of this study, and proposes future work based on the findings.

List of References

1. Tant, M.R., J.W. Connell, and H.L.N. McManus. *High-Temperature Properties and Applications of Polymeric Materials.* American Chemical Society, Washington, DC, 1995.

2. Black S., *Are high-temp thermosets ready to go commercial?* High-performance composites, November, 2004.

3. 'BT Resins'. Commercial Data Brochure, 2nd Ed. Mitshbishi Gas Chemical Co. June 1980.

4. Goodman, D.L. and G.R. Palmese, "Curing and bonding of composites using electron beam processing" In *Handbook of polymer blends*, ed. Kulshreshtha A.K. and C. Vasile, p. 459. Shropshire: Rapra Technology Limited, 2002.

5. Saunders, C.B., V.J. Lopata, W. Kremers, M. Tateishi, and A. Singh, *Recent developments in the electron-beam curing of fiber-reinforced composites.* International SAMPE Symposium and Exhibition 37 (Mater. Work. You 21st Century) 1992; 944-54.

6. Abrams, F., T.B. Tolle, *An analysis of electron-beam potential in aerospace composite manufacturing.* International SAMPE Symposium and Exhibition 42 (Evolving Technologies for the Competitive Edge, Book 1), 1997; 548-57.

CHAPTER 2: MOTIVATION AND LITERATURE REVIEW

In Section 2.1, the overview of high temperature composite materials will be presented in terms of the development of high temperature thermosetting polymer matrices and low-cost processing techniques used for composite fabrication. Accordingly, bismaleimide resin is presented as the starting material to develop an advanced high temperature thermosetting polymer system by exploiting its high temperature resistance and its ability to cure via free radical polymerization. The structure-property-processing relationship will be described in Section 2.2 to highlight the shortcomings associated with bismaleimide composite fabrication. Next, modifications to bismaleimide resins designed to control processing and toughness will be introduced in Section 2.3 thus highlighting the significance of this work. Moreover, since the primary technique employed in this study to modify the bismaleimide involves the design of IPNs, this will be described in Section 2.4 in terms of its morphology, synthetic route, physical and mechanical behavior. In Section 2.5, the objectives of this study are summarized.

2.1 Overview of High Temperature Composite Materials

2.1.1 Evolution of high temperature thermosetting polymers

As early as 1960, advances in space and other technologies have produced a continuing and growing need for materials that withstand prolonged exposure to temperatures in excess of 300°C and/or relatively short exposures at much higher temperatures [1-3]. A great amount of research has been done in this area to fulfill the need for the high temperature polymer materials used in many fields including

automobiles, electronics, and industrial applications that rely on items made from fibers, plastics and rubber. With additional impetus from aerospace needs, considerable progress has been made. Frazer [4] summarized the progress obtained during the 1960s and pointed out three aspects wherein efforts had been made to synthesize polymer systems capable of withstanding prolonged exposure to elevated temperatures: (1) improving existing polymers by introducing structural modifications; (2) devising new organic systems tailored to resist the efforts of heat; (3) synthesizing an entirely new class of inorganic and organic-inorganic (semiorganic) polymers that are thermally stable.

The three approaches developed in earlier days to gain high temperature resistant polymers are still applied to current studies, particularly the first two approaches, used in developing thermosetting polymers, which are used for composite materials manufacturing.

When thermosetting polymers are subjected to a high temperature environment, they usually undergo two kinds of changes: (1) physical changes, such as softening, and (2) chemical changes, such as ring-formation, oxidation, hydrolysis, degradation, and decomposition. Consequently, there are two indicators that are employed to characterize the high temperature resistance of thermosetting polymers. Namely, glass transition temperature (Tg) and thermal decomposition temperature (T_d), which are associated with above mentioned changes. The enhancement of high temperature resistance indicated by the increase of Tg can be achieved by the followed means: (1) improving the rigidity of the polymer chain, and (2) subjecting polymer chains to crosslinking.

As the most successful polymer with inherently rigid chains, polyimides, which incorporated the imide group 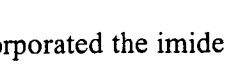 in their repeating units, gained a prominent

position due to their excellent thermal stability, their good mechanical and electrical properties, and their excellent balance of properties, price, and processibility [5]. From production figures it can be inferred that polyimides stand virtually alone with respect to providing useful, available, high temperature technological materials [5].

Traditional linear polyimides have a high melt viscosity that limits processibility and, consequently, end-use. However, by lowering the molecular weight and using reactive end-capping agents to produce thermosetting polyimides, their processibility has been improved. Thermosetting polyimides, originally developed in the 1970s at NASA Lewis for military aircraft engines and airframes, are produced by dissolving an aromatic diamine, a dialkyl ester of tetracarboxylic acid and a monofunctional nadic ester endcapping agent in a solvent, such as alcohol. The resulting solution is typically used to produce prepreg. PMR-15 is the best known of these thermosetting formulations—PMR is shorthand for *in-situ* polymerization of monomer reactants—and it is very successful in producing good thermal and mechanical properties [6].

The introduction of a crosslinking site as an end cap for oligomers is now a general approach to improve the processing and the final properties of aromatic polymers and polyheterocycles [7, 8]. In particular, more recently, cyclic imides with carbon-carbon double bonds were found to be susceptible to polymerization by a radical mechanism or by several other mechanisms, such as photocondensation, Diels-Alder addition, or nucleophilic substitution. Traditionally, they are considered addition polyimides together with other sorts of eng-capped polyimides [5]. The discovery of this sort of thermosetting polyimide widened the range of properties and application possibilities to a great extent [9, 10]. The high temperature composite materials based on

thermosetting polyimides have made a great progress with enhancements of thermal oxidization stability, processibility and mechanical properties [11].

The thermosetting polyimides can be classified into three main types (Figure 2.1) based on the end-capping groups. These types include PMR polyimides (mainly referring to nadimide-end-capped polyimides), acetylene end-capped polyimides, and bismaleimides [12]. From a practical point of view, the monomers commonly used in the fabrication of thermosetting polyimides are bismaleimides [5]. Until 1974, poly(bismaleimides) had actually achieved special importance as technical polymeric materials [13].

Today, bismaleimides resins are a leading class of thermosetting polyimides that exhibit a balance of thermal and mechanical properties, which make them popular for use in advanced composites, structural adhesives, and electronic applications [14, 15]. They are the most important resins currently used in the aerospace industry due to their high performance-to-cost ratio [16-21]. In Section 2.2, the structure-property-processing relationship in regard to bismaleimides will be discussed to highlight the advantages and disadvantages associated with the composite fabrication of bismaleimides.

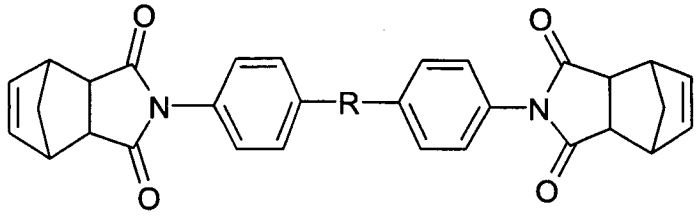

PMR POLYIMIDE

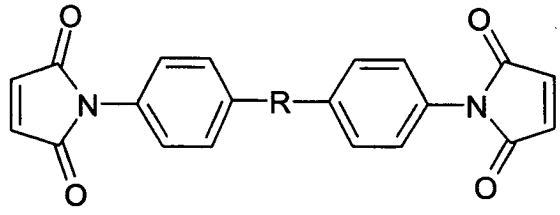

BISMALEIMIDE

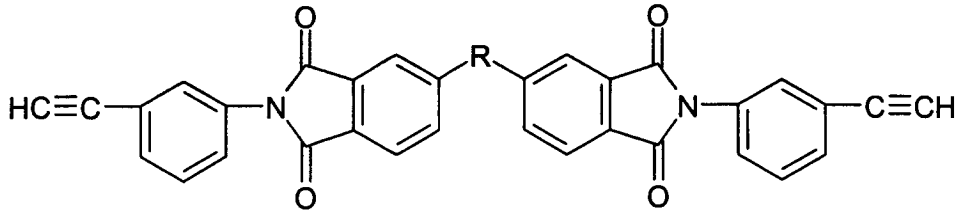

ACETYLENE END-CAPPED POLYIMIDE

Figure 2.1 General structures of typical thermosetting polyimides.

2.1.2 Processing techniques for high temperature polymer composite fabrication

Polymer matrix composite materials are increasingly used for moderately high temperature (200-350°C) applications [22]. High performance composite materials are taken to be those where glass, carbon or aramid fibers are used to reinforce a thermosetting or possibly thermoplastics matrix [23]. Generally, fiberglass laminated polymer composites will exhibit superior high temperature resistance compared to pure resins. The carbon fiber, which is most widely used, can be obtained by the pyrolysis of polyacrylonitrile [24-26] and polymethacrylonitrile [27].

To fabricate fiber reinforced composite articles it is necessary to impregnate fibers with a resin or to put preimpregnated fibers or molding compounds in a mold followed by exposure to heat and pressure [23]. The commonly used processing methods include open molding, closed molding, pultrusion, filament winding, autoclave processing, and liquid molding. Among liquid molding processes, resin transfer molding (RTM) and vacuum assisted resin transfer molding (VARTM) are widely used methods for low temperature and low cost.

Electron beam (EB) processing uses high-energy electrons rather than thermal energy to initiate polymerization and crosslinking reactions in suitable monomers, thus curing the polymer and enhancing specific physical and chemical properties [28]. Curing of composites using EB has the potential to offer several significant advantages over traditional thermally induced cure. The major potential advantages include (1) shorter curing time, (2) low energy consumption, (3) reduced manufacturing costs, and (4) excellent process control. Moreover, EB curing allows fabrication of large structures without the use of autoclaves, allowing the use of low-cost tooling and reducing residual

thermal stresses. The main stumbling block to more widespread composite usage in aerospace structures is their cost [29]. The specific field of EB curing of thermoset composites, particularly thin structures, has been studied since the late 1970s, and for the past several years, it has been actively explored as a method to reduce the processing and fabrication cost of aerospace composites [5, 9, 29].

There are two common EB curing chemistries: (1) vinyl based systems, which cure via the free-radical addition mechanism, and (2) epoxy based systems, which cure via a cationic mechanism [30]. Epoxy based systems have attracted more attention lately because free radical resin systems like acrylates and methacrylates possess high cure shrinkage and relatively lower Tg [31-33]. A new class of EB resins can be processed at room temperature using techniques like VARTM has been developed by Palmese, *et al.* [34]. The system is based on epoxy/amine and acrylate monomer components and is capable of C-staging at room temperature to form handleable solids, which when irradiated, achieve a high degree of conversion, with Tg approaching 200°C. It was found that cure initiated by EB irradiation at ambient temperature results in significantly higher Tg than thermal processing of the same system using peroxide, which makes the low temperature processing high temperature composite materials possible. This class of materials was based on the formation of a sequential interpenetrating polymer network.

2.2 Structure-property-processing Relationship of Bismaleimides

Bismaleimides are a series of resins that are derivatives of polyimide resins. As shown in Figure 2.1, they are bi-functional compounds with maleimide as their active end group. Due to the aliphatic-type linkages employed to make polyaddition possible,

polymers of this type are not as thermally stable as aromatic polyimides. Their better processibility and the relatively low cost of their raw materials have helped them to become a real alternative for long-term use up to 200°C. Therefore, bismaleimides have attracted broad attention in high temperature polymer composite material manufacturing.

Bismaleimide resins are of interest because they process in a manner similar to epoxies, have low cure temperatures, and cure without the evolution of by-products [15]. The imide linking groups impart higher polymer backbone stiffness than epoxies, and the greater crosslinking density of bismaleimides results in materials with improved thermal and hydrolytic resistance relative to epoxies [22]. Thus, the major advantage of bismaleimides is that they possess high temperature resistance yet can be processed more easily than polyimides. With the characteristics of both rigid rings and network forming ability, the final Tg of such systems can reach 400°C. However, unmodified bismaleimide resins suffer from brittleness due to their high crosslinking densities after curing, poor processibility due to their poor solubility in ordinary solvents, high crystalline melting temperatures of the monomers, and narrow processing windows (the temperature difference between the melting point of bismaleimide monomer and its onset point of curing reaction) [35-38]. Therefore, the major challenges regarding the use of bismaleimides for composite applications are improving processibility and fracture toughness [39].

The simplest bismaleimide resin is 4,4'-bismalimidodiphenyl methane as shown in Figure 2.2. Due to its particular structure, it can be used as a functional monomer or crosslinker, and has found applications in fields ranging from biomaterials to insulation materials [40-42]. In particular, due to its rigid ring, regular backbone structure and

network forming ability, it has been widely used for producing high temperature polymer composites [43-47]. More importantly, due to the methyl linkage, it possesses the highest crosslink density among all bismaleimides, and consequently, the Tg can reach 450°C. However, due to the regular backbone structure and hence, high crystallinity, its melting point is close to 150°C, which causes great inconveniences to the processing, particularly in low temperature molding operations, such as RTM and VARTM.

Currently, research on bismaleimides mainly focuses on 4,4'-bismalimidodiphenyl methane as a starting compound and concentrates on its modification with an aim to decrease the viscosity of the resulting melt, thereby improving the processibility and the fracture toughness while retaining thermal stability. These two goals also motivate this study.

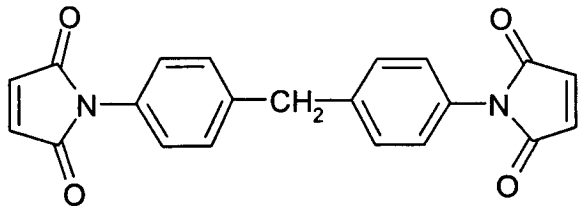

Figure 2.2 Chemical structure of 4,4'-bismalimidodiphenyl methane.

2.3 Current Research Activities Involving Bismaleimide Modification

2.3.1 Modification of bismaleimides to improve toughness

Due to high crosslink density and a rigid polymer structure, bismaleimides exhibit high Tg (> 400°C) and low fracture toughness (with G_{ic} << 50 J/m^2). Therefore,

enhancing toughness of bismaleimides is a key factor for the advancement of these materials. In the following section, several methods for improving the toughness of bismaleimides are summarized including modifications with diamines, epoxy resins, olefinic compounds, thermoplastics, and with cyanate ester resins.

2.3.1.1 Modification with diamines

Modifying bismaleimides by diamines was first studied in 1973 by Crivello who proved it to be a simple way to improve the brittleness of bismaleimides [48]. The reaction is depicted in Figure 2.3.

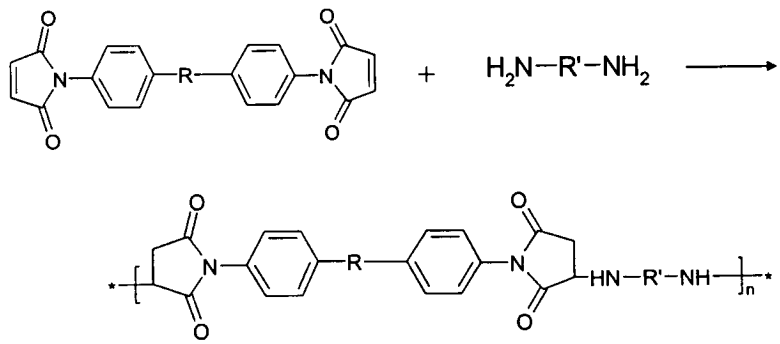

Figure 2.3 Reaction scheme for the reaction of BMI with diamine.

The reaction shown in Figure 2.3 proceeds via Michael Addition mechanism, and the final polymer products are linear (and therefore soluble) or crosslinked, depending upon the starting materials and the precise conditions of preparation. The chain extension and crosslinking of bismaleimides by this method was reported by Leslie R. Dix *et al.* [49]. An attractive feature of this reaction is that it can proceed rapidly at moderate

temperatures without the elimination of volatiles. This technique can be also applied in surface coating and reactive molding.

2.3.1.2 Modification with epoxy resin

Modifying bismaleimides by epoxy is a well-developed technique used to improve their processibility and interfacial adhesion, which also improves toughness. Generally, this modification is realized when used along with other components since epoxy itself does not react readily with bismaleimides, though it has been claimed that epoxy can assist homopolymerization of bismaleimides by the formation of a zwitter ion adduct [50]. One disadvantage associated with this modification method is that the addition of epoxy resin will be detrimental to the heat resistance of bismaleimides. Thus, combining bismaleimides with high Tg polymers such as cyanate esters to improve the toughness of bismaleimides was also reported [51]. (See section 2.3.1.5)

2.3.1.3 Modification with olefinic compounds

There are many kinds of olefinic compounds that can be used as modifiers to enhance the toughness of bismaleimides, however, allyl-type compounds have been the most successful.

Liang, *et al.* [52] points out that one of the most desirable methods for bismaleimide resin modification is the copolymerization of bismaleimides with allyl functional resins. For example, o,o'-diallylbisphenol A (DBA) is one of the most effective modifiers of bismaleimides for improving the processibility and toughness [53].

Allyl compounds are very stable at room temperature. At high temperatures or with peroxide initiators the homopolymerization of allyl functionality is difficult to obtain. This is because the free radicals produced are very stable due to conjugation and thus more unlikely to propagate.

2.3.1.4 Modification with thermoplastics

The toughness of bismaleimides can be improved greatly by using good heat resistant thermoplastics. Currently, the most widely used thermoplastics are: polybenzimidazole (PBT), polyethersulfone (PES), and polyetherimide (PEI). The toughening effect depends on the thermoplastics chain structure, molecular weight, particle size, and end groups. Toughening by thermoplastics is a successful method of bismaleimide modification [54, 55]. However, accompanying the enhancement of toughness, the viscosity of bismaleimides is also increased, thus resulting in poor processibility of the resin system. Additionally, the lower Tg associated with thermoplastic modifiers is detrimental to the high temperature resistance of the resin system.

2.3.1.5 Toughening with cyanate ester resins

Cyanate ester resins represent another important class of thermosetting high performance materials that are being evaluated for structural and electronic applications, and more importantly, for advanced composites [56, 57]. Cyanate ester resins are cured through the condensation of the cyanate ester group and form thermally stable cyanurate rings.

In light of their advantages, like excellent adhesion characteristics, good toughness, and ease of processing [58], cyanate esters have been used extensively to modify bismaleimide resins. It was pointed out by Hamerton in 1996 that cyanate esters and bismaleimides do not co-react [59], but instead form an interpenetrating polymer network [60]. The cyanate ester-bismaleimide based IPNs are expected to yield improvements in performance resulting from potential synergism arising from constituent specific structure. The cyanate ester imparts processibility and toughness, while the bismaleimide confers thermal stability to the blend system. Thus the product may have good toughness while maintaining a high Tg.

The influence of the cyanate ester constituent on the toughness of cyanate ester-bismaleimide blends, was investigated by Chaplin, *et al.* by using bisphenol A cyanate ester and low melting eutectic of several bismaleimide monomers as two model compounds [61]. The results are given in Figure 2.4.

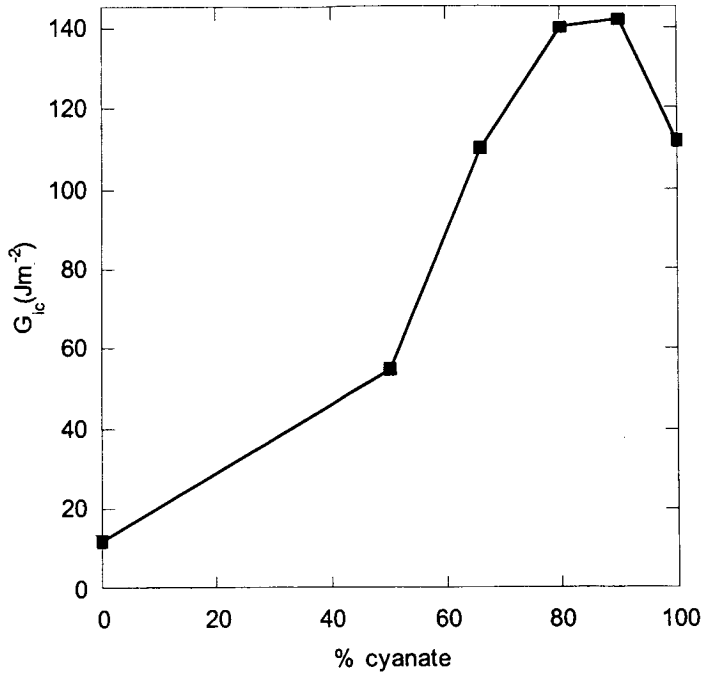

Figure 2.4 Variation of fracture toughness with composition. (redrawn according to reference [61])

As seen on the chart, the cyanate ester exhibits a significantly high fracture energy (G_{ic}) of 112 J/m^2 whereas the bismaleimide demonstrates extreme brittleness with only 11 J/m^2. The results are of considerable interest in that they demonstrate a positive deviation from linearity, for a particular composition range (approximately 10-20% bismaleimide), which has toughness characteristics superior to both neat polymer systems. The reason for this striking result was believed to be due to morphological factors [61].

Cyanate ester toughened bismaleimides based on IPN structure overcome disadvantages such as loss of thermal resistance, poor processibility, and lower stiffness that are associated with the toughening methods described in previous sub-sections. Cyanate esters possess low water absorption characteristics that may also improve the

water resistance of bismaleimides. Accordingly, the use of cyanate ester-bismaleimide can lead to further improvements in performance, and reduction in cost. This has been the subject of research beginning in the 1990's and many investigations have been carried out [53, 62-66] resulting in some commercial success.

2.3.2 Modification of bismaleimides to improve processibility

Another critical issue in the application of bismaleimides is their processibility. Bismaleimides have been modified by the following five methods [67] to improve their processibility. (1) synthesis of bismaleimides with flexible or long segments in the backbone [68, 69]; (2) use of aromatic diamines as a chain extender to react with bismaleimides through the Michael addition reaction [70, 71]; (3) blending of bismaleimides with epoxies [72-74]; (4) copolymerization of bismaleimides with olefinic compounds via the Diels-Alder reaction [75, 76]; and (5) use of aromatic dicyanate esters to blend with bismaleimides [77, 78]. The first three methods have the disadvantage of lowering the glass transition temperature of the cured resins. The fourth and the fifth methods have less severe adverse effects on the high temperature properties and processibility. Bismaleimides have a tendency to recrystallize from the mixture with aging [79] and the prepared resin system often shows inconsistent properties from batch to batch. Nevertheless, the latter two methods for obtaining a good high temperature performance are promising and will be discussed in more detail in the following section.

2.3.2.1 Modification with olefinic compounds

Introducing liquid coreactants, known as reactive diluents, in order to provide a processible and useful resin for composite fabrication, is of marked significance. The range of suitable liquid reactive diluents containing unsaturated carbon-carbon double bonds, however, is currently very limited [80]. As mentioned earlier, the most successful reactive diluents for processing of bismaleimides are allyl functional compounds. Of them, o,o'-diallylbisphenol A (DBA) is one of the most effective modifiers for bismaleimides used to improve their processibility. Much work based on these compounds has been done to improve the processibility of bismaleimides [81-83]. In addition, in the pursuit of high temperature resistance, other kinds of allyl-type modifiers have been investigated. It was claimed that with allylamine as a modifier, the recrystallization of bismaleimides in processing can be prevented, and the Tg can reach up to 349°C [67]. Marks and co-workers also copolymerized bismaleimides with allyl-type compounds, and after curing, ultra-high Tg (up to 350°C) polymer systems were obtained [84]. However, the fracture toughness of these two-component bismaleimide systems is not yet sufficient for use as composite matrices [85].

At room temperature, o,o'-diallylbisphenol A is an amber liquid with viscosity of 12~20 Pa.s, and at temperatures above 100°C, it can dissolve bismaleimides by stirring [53]. Then, at temperatures above 150°C, it is thought to react with bismaleimides through the Diels-Alder mechanism rather than the free radical copolymerization mechanism, which is shown in Figure 2.5.

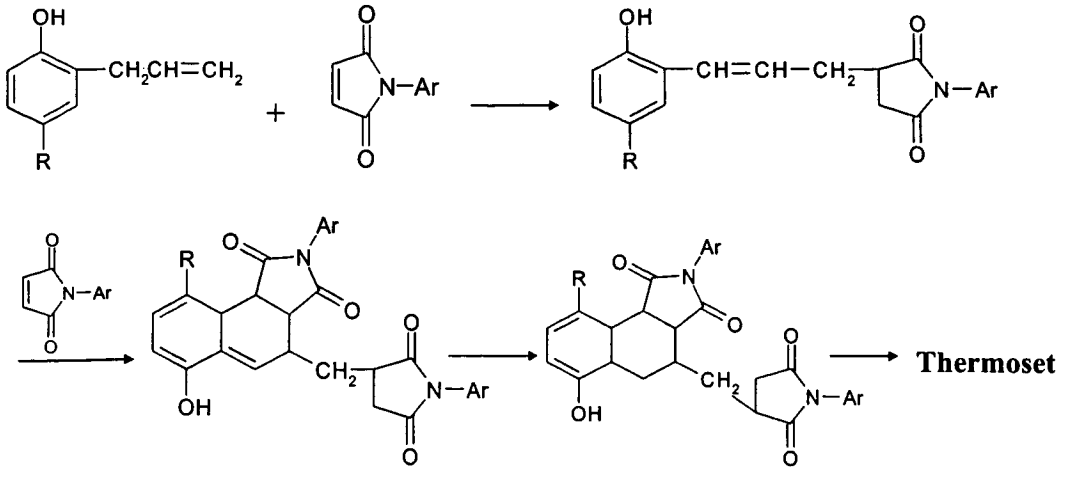

Figure 2.5 Reaction scheme for allyl compound with bismaleimides.

However, the fundamental mechanism by which the reaction of the allyl group with bismaleimides takes place is still controversial [86-92]. It is suggested [87-89] that the reaction mechanism of bismaleimide resin with diallylbisphenol A proceeds via 'ene-reaction' for chain extension, and by 'Diels-Alder' reaction for crosslinking as shown in Figure 2.6. In Reyx's work [90], the occurrence of an ene-reaction and further Diels-Alder and retro Diels-Alder reactions, with rise in temperature, was suggested based on results of a study using N-phenylmaleimide and 2-allylphenol as a model system.

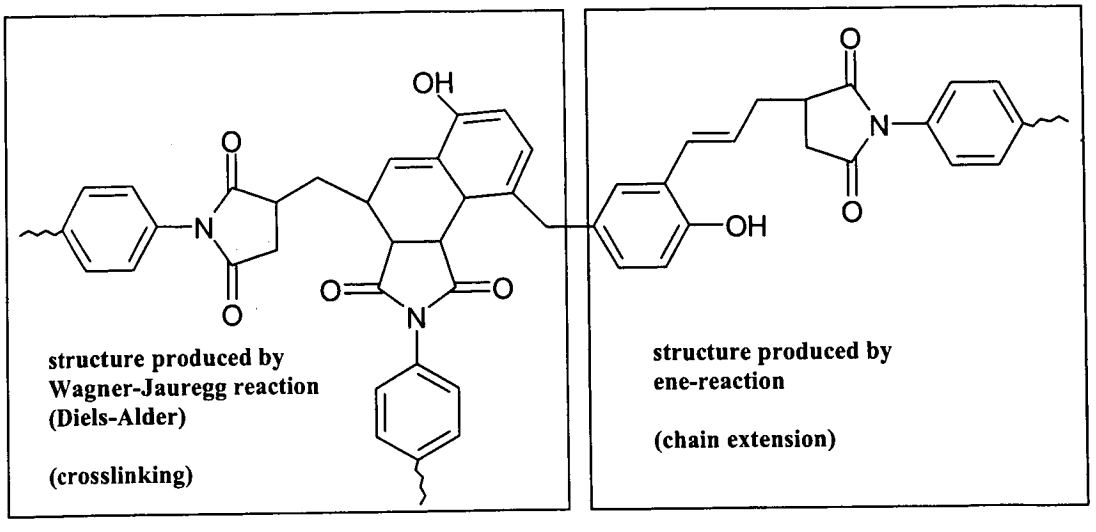

Figure 2.6 Proposed structure of cured bismaleimide resins with diallylbisphenol A showing Diels-Alder and ene-reaction. (redrawn according to reference [90])

Another viewpoint regarding the mechanism of the allyl group with the maleimide group is from Lin [67]. His work showed, using mass spectrometry, that allylamine can accelerate the polymerization of bismaleimides; the accelerated effects of adducted allylamine on the polymerization of bismaleimides were believed to be attributable to the 'charge transfer complex' effect in view of the fact that the allyl groups from the adducted allylamine is an electron-rich olefin, and the double bonds of the maleimide groups are an electron poor olefin. The charge transfer mechanism is shown by the following equation:

$$\textbf{Donor} + \textbf{Acceptor} \leftrightarrow [\textbf{Donor-Acceptor}] \longrightarrow \textbf{Free Radicals}$$

However, these two apparently contradictory observations were corroborated by Shibahara's work [91, 92]. In his work, a high resolution solid-state ^{13}C NMR technique revealed that in the presence of allylphenol, Diels-Alder adducts were formed with both BMI and PMI, but Diels-Alder reactions hardly proceeded when diallylbisphenol A was used. Instead, as shown in Figure 2.7, only ene-reaction and polymerization was observed. Thus, mixtures of products obtained by ene reaction and by copolymerization respectively were formed. This shows that the crosslinking of such widely used curing system of diallylbisphenol-A proceeds via a different manner as suggested previously [86]. Whether the Diels-Alder reaction is a significant route for crosslinking is dependent on the structure of the allylphenols.

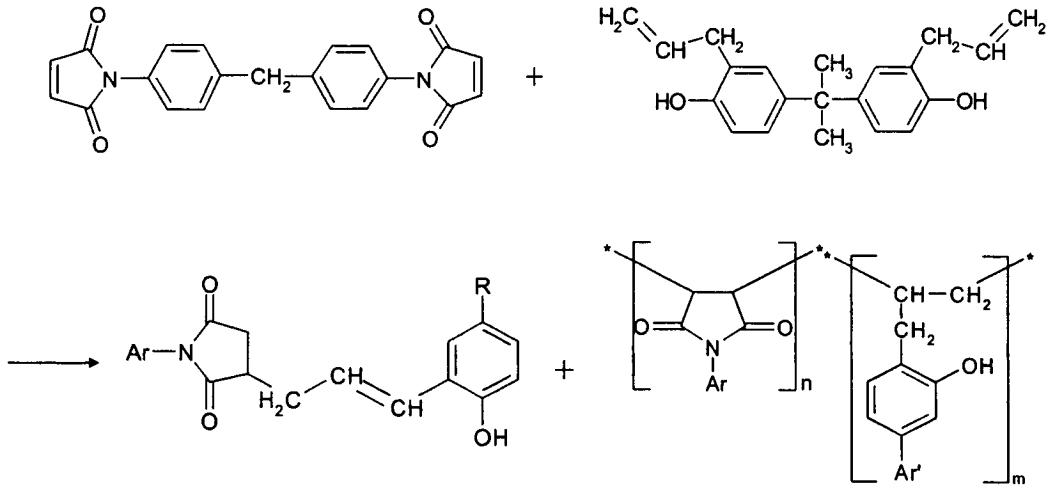

Figure 2.7 Structure of cured bismaleimide with diallylbisphenol A obtained using ^{13}C NMR. (redrawn according to reference [44])

Aside from o,o'-diallylbisphenol A, some other allyl compounds such as allyl phenyl ether, diallylbisphenol S have been employed to modify bismaleimides in order to improve processibility. They have achieved some success [81, 93].

2.3.2.2 Modification with cyanate ester resins

Cyanate ester resins are usually defined as phenol derivatives bearing two or more cyanate ester functional groups. They were found to undergo nearly quantitative conversion to crosslinked cyanate homopolymers by cyclotrimerization to *s*-triazines with the aid of heat and a catalyst as shown in Figure 2.8 [94, 95].

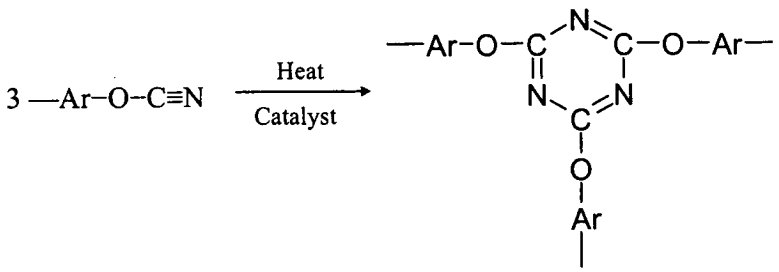

Figure 2.8 Scheme for the formation of triazine ring from cyanate ester monomer.

The cured cyanate ester resin exhibits characteristics such as low dielectric coefficient (2.8~3.2), high glass transition temperature (240~290°C), low shrinkage, low water absorption rate (<1.5%), as well as excellent mechanical properties. In addition, cyanate ester possesses a similar processibility to epoxy resin and can be cured at 177°C

with no volatile molecules produced during the cure process. Currently, cyanate ester resins are established as thermosetting resins for insulating high-speed, high density electronic circuitry; they also can potentially serve as adhesives, active electro-optic components for processing light signals in fiber-optics, matrix resins for aircraft composites, geostationary broadcast satellites, radomes, and antennas [96].

Modifying bismaleimides with cyanate ester resin through the formation of IPNs is currently an exciting area of investigation, focused on improving the toughness and processibility of bismaleimides. However, the service temperature of the formed IPNs is limited by the Tg of the polycyanurate network, which is between 230 and 290° C. One approach used to solve this problem was the development of an alkenyl-functionalized cyanate ester to form linked interpenetrating polymer networks (LIPNs) [60, 85]. Interlinking the two component networks causes an increase in the crosslinking density of the product. As a result, the Tg has been found to attain values as high as 343 ° C, while retaining much of the original morphology of the blend and thus retaining a high fracture toughness. Another study using 4-cyantophenylmaileimide as interlinker was carried out by Nair and coworkers [65, 97]. These investigations used 2,2-bis(4-(4-maleimido phenoxy)phenyl) propane as a starting monomer to solve the solvation problem. However, the introduction of an ether bond in the backbone of bismaleimide reduced Tg greatly. This aspect was proven in that the addition of bismaleimide did not result in any enhancements in the Tg of the blend. The presence of 4-cyanatephenylmaleinide as an interlinker can lead to the increase of Tg by 50° C, but the attainable Tg was still found to be below 300° C.

Recently, work that combined 2,2'-diallylbisphenol and cyanate ester to modify the BMI was done by Hu, *et al.* [53]. They retained the phenol group that is believed to act as a catalyst to the cyclotrimerization of cyanate esters to obtain high conversion [98, 99]. Their model of IPNs structure was based on the facts that CEs form the first network at lower temperatures due to the accelerated effect of the phenol group, and allyl group react with BMI to form the second network by 'ene' and 'Diels–Alder' mechanisms. However, this model is not widely accepted. The only evidence given to show the formation of IPNs is by Differential Scanning Calorimetry (DSC) which is not sufficient. The reaction mechanism that they relied on is also questionable. If the forming process of two networks interfere chemically or physically with each other, the final structure and properties will be altered. This interpretation is substantiated by their result that the Tg of the final IPNs is 282°C, which is lower than each of the two components. The sequential IPNs is therefore not truly formed, and the final Tg is not as high as anticipated.

2.4 Interpenetrating Polymer Networks (IPNs)

Interpenetrating polymer networks, IPNs, are defined as intimate combinations of two polymers in network form, in which at least one of the polymers is polymerized and/or cross-linked in the immediate presence of the other [100]. Thus, they can also be called polymer blends or polymer alloys. A simplified representation of IPNs is shown in Figure 2.9. The main goal of IPNs is to trap two polymer phases in each other thus causing a possible synergistic behavior, or an addition of properties, as opposed to a compromise of properties, as might be expected.

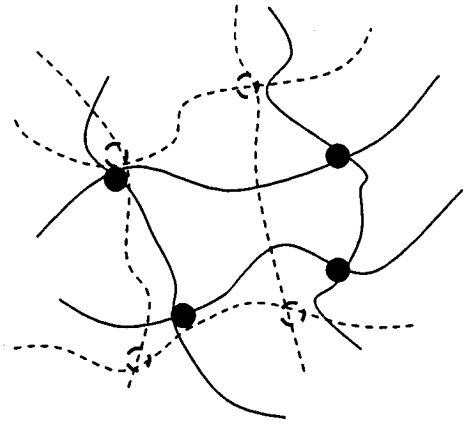

Figure 2.9 A representation of IPN's structure. One network is represented by solid lines, while the other is shown by dotted lines. The circles represent points at which the chains are crosslinked.

IPNs have attracted much attention since first proposed by Sperling [101] and are used in applications including coatings, adhesives, and damping materials. Based mainly on his work, the knowledge of IPNs involving their morphology, and synthesis plus their properties will be reviewed in the following section in relation to this study.

2.4.1 Morphology of IPNs

While ideally polymers should interpenetrate on the molecular level, actual interpenetration may be limited owing to phase separation. Due to the low entropy and the positive heat associated with mixing, most IPNs will undergo phase separation. Therefore, the degree of interpenetration can be on the molecular aggregation state level or on larger domain levels. However, the initial mixing of the two components is good and the continuity of the two phases is often maintained based on kinetic factors.

Generally, IPNs are found to exhibit a characteristic cellular structure with characteristic size ranging from 500~1000 Å, where the first component makes up the cell and the second component, the contents of the cells. The phase constituted by the first component will possess a greater degree of continuity and may exert more influence on the final properties, even though it may be the minor component by weight. Moreover, it was revealed that an additional structure at an exceedingly fine level with an order of 100~200Å existed in the wall and inner part of cell [102].

The various morphologies of IPNs, and hence their subsequent physical and mechanical properties, are controlled by cross-linking and/or mixing. Usually, if the miscibility and crosslinking density of two constituents are greater, then the phase domain of the IPNs is smaller. In addition, kinetics is another factor that determines the final morphologies of IPNs; If the polymers gel before phase separation occurs, the crosslinking of polymer chains will restrict phase separation. On the contrary, if phase separation precedes gelation, the domains will be large and the crosslinks will stabilize the phase separated morphology. Suthar, *et al.* gave a good review with respect to the kinetics studies on the formation of interpenetrating polymer networks [103]. They concluded that the faster the rates of the respective chain extension and crosslinking reactions are and the closer they are to simultaneity, the more homogeneous are the IPNs. In addition, the individual components sometimes can polymerize more rapidly in the IPNs than alone, due to a "solvent effect" of the IPNs.

2.4.2 Physical and mechanical behavior of IPNs

An IPNs is a combination of two crosslinked polymers that (ideally) are not bonded to each other [104], even though sometimes physical crosslinking may exist between two networks, such as hydrogen bonding. Therefore one prominent characteristic feature of IPNs is the existence of glass transitions for each phase, which generally leads to a broad glass transition region. The intensity of each transition is clearly related to the overall composition and phase continuity, while shifts and broadening of the transition indicate the extent of molecular mixing. The two characteristic transitions will restrict the use of IPNs as high temperature materials in that the lower Tg will limit the use temperature of IPNs.

Additionally, for most incompatible polymer blends, they often possess high interfacial tension and weak adhesion at the interfaces between two phases which result in very coarse morphology due to macrophase separation, and, inferior mechanical properties [105].

Compatibilization and limited phase separation with small phase domains are therefore pursued in making high temperature polymers based on IPNs. Usually, the compatibilization associated with IPNs can be ameliorated by introducing a network linker which forces two potentially immiscible networks together and also results in the narrowing of the glass transition region.

Another most active avenue to access this goal, is to employ *in-situ* polymerization. *In-situ* polymerization, according to Walsh, is the polymerization of one monomer in the presence of another polymer [106], which can be performed by reaction in the melt, in solution, or in the solid phase [107]. *In-situ* polymerization in the solid

state is advantageous because of its low cost and large variety of possible modifications, compared to polymerization in solution or in the melt [107].

It is clear that the properties of IPNs can only be tailored by controlling the synthetic routes, processing parameters as well as understanding the influence of these parameters on cure kinetics and structure formation.

2.4.3 Synthetic routes

Because the unique properties of IPNs arise from the intimate mixing of the component polymer systems, the synthetic methodology used to produce these materials is critical. The method employed is determined by the component polymers selected, polymerization mechanisms, miscibility and the anticipated end use of the IPNs [108].

Several synthetic methods are used to prepare IPNs [104]. These methods include sequential IPNs, where the networks are made sequentially; and simultaneous interpenetrating networks, SINs, where both monomers are mixed together and are polymerized by independent and noninterferring routes. These two methods will be described briefly in the following section.

2.4.3.1 Simultaneous IPNs [108]

In simultaneous IPNs, "hard" and "soft" polymer segments are combined in a homogeneous solution containing all the necessary components — such as monomers, crosslinkers, and initiators — to produce the final IPNs. Two non-competing polymerization mechanisms are employed to polymerize the components in the presence of the other to produce the intimate mixing characteristic of IPNs. However, with

polymerization, some phase separation will occur because very few polymer/polymer mixtures are soluble in each other over a wide composition range. Thus, the properties of the final product are determined by the degree of immiscibility.

Moreover, it was pointed out that in SINs, both timing and rate of polymerization to form the two networks are important. It was found in an acrylate-epoxy system, that simultaneous gelation produced materials with inferior properties to those formed by slightly mismatched polymerization rates.

Another example is with respect to polyurethane-poly (n-butyl methacrylate) SINs. In this case, acrylate polymerization was initiated photolytically at various times after the onset of polyurethane formation producing a series of materials, presumably with the same chemical composition, which possessed an average particle size that decreased as the delay time to acrylate polymerization initiation increased [109].

Thus, it can be concluded that in the formation of IPNs, interfering reactions will lead to poor structure and hence to the poor properties, which might therefore be more prominent in SINs.

2.4.3.2 Sequential IPNs [108]

This type of IPN's is generally made in a two step process where mobile monomer, crosslinker, and initiator phase are swollen into and polymerized inside a previously crosslinked three dimensional polymer. Sperling gave a detailed description of the phase continuity and separation that occurred in sequential IPNs [102]. Initially, polymer network I exhibits continuity of structure and its phase. Then monomer II is uniformly applied while swelling polymer I. At this point, polymer network I is

continuous and monomer II is also distributed homogeneously. Upon *in-situ* polymerization of II, some extent of phase separation takes place. Polymer network I is still continuous, but is partially or wholly excluded from some regions of space. Polymer network II exhibits some degree of chain continuity or even phase continuity, however, usually less than polymer network I.

Based on the above, it can be reasonably concluded that phase separation in connection with *in-situ* sequential IPNs formation will occur to a minor extent compared with simultaneous IPNs as a result of restriction of polymer network I. Moreover, the chains of polymer network I are extended by the swelling action of monomer II, and phase domain size is generally reduced.

2.5 Disadvantages of Current Technology and Significance of Our Study

Allyl group compounds as modifiers cannot provide a good matrix for composites. Cyanate ester itself cannot solve the solvation problem of bismaleimides. Combining the cyanate ester and allyl group to achieve high performance resin system seems therefore to be an optimum approach. In fact, this method is popular currently. Although Tg as high as 343°C was obtained by using a multifunctional network coupler, there are still disadvantages: (1) for the methods investigated, the cure temperature has to be as high as 250°C for the bismaleimide monomer to react with allyl functionality. Meanwhile long cure time is also needed to ensure a proper conversion. This results in high production cost; (2) Diallylbisphenol (DBA) as a good reactive diluent can solve the solvation problem of bismaleimides and is widely used. However, 'ene reaction' reduces the final Tg greatly. Meanwhile, the two polymerization mechanisms, either of Diels-

Alder and ene reaction or of copolymerization and ene reaction, could interfere with each other thus result in poor structure as well. Accordingly, from both technological and theoretical aspects, it is significant to find a better method for processing bismaleimide.

A new and more facile processing technique compared to conventional methods for the synthesis of modified bismaleimide resins is envisioned that will result in materials with excellent properties that can be used as matrices for high temperature composites. This work is based on 4,4'-bismalimidodiphenyl methane (simplified as BMI in this study), low temperature processing will be accomplished by finding appropriate reactive diluents that copolymerizes with BMI at low temperature and by using EB radiation in order to mitigate the processing cost of conventional thermal curing. Improving the fracture toughness of this system will be addressed by the use of cyanate ester monomers as a modifier.

Specifically, high toughness and high-temperature thermosetting materials will be produced in this study by synthesizing sequential interpenetrating polymer networks (IPNs) using cyanate esters cured thermally to form the first network in the presence of BMI and a reactive diluent, and in a second step, *in-situ* polymerization of the second BMI-diluent network will be accomplished in the solid state via EB irradiation. Network couplers will be employed to maximize the Tg of these systems. Significant challenges include: (1) finding the appropriate reactive diluent, (2) synthesizing the network couplers, (3) developing a fundamental understanding of the kinetics of polymerization as it relates to IPNs formation (thermal and EB), and (4) developing a basic understanding of structure-property relationship of the thus formed sequential IPNs.

List of References

1. Bartholomew E.R., G.R. Eykamp, and W.E. Gibbs. *High temperature elastomeric compounds and polymers.* Rubber Chem. Technol. 1959;32:1587-1624.

2. Jaffe L.D.. *Effects of Space Environment upon Plastics and Elastomers.* Chem. Eng. Progr. Symp. 1963;59(40):81

3. Ross J.H.. *High-Temperature Fiber Research.* Textile Research Journal 1962;32:768.

4. Frazer A.H.. *High temperature resistant polymers.* Interscience publishers, A division of John Wiley&Sons, 1968.

5. Kricheldorf H.R.. *Handbook of polymer synthesis Part B. Polyimide.* Marcel Dekker Inc., 1991.

6. Black S.. *Are high-temp thermosets ready to go commercial?* High-performance composites, November, 2004.

7. Sillion B. *Recent Advances in Mechanistic and Synthetic Aspects of Polymerization.* (Fontanille, M., and Guyot, A.. eds.), D.Reidel, Paris, p.237, 1987.

8. Takeichi T. and J.K. Stille. *Star and linear imide oligomers containing reactive end-caps: preparation and thermal properties.* Macromolecules 1986;19:2093-2102.

9. Mittal, K.L., ed. *Polyimides. Synthesis, Characterization and Applications.* Dekker, New York, 1984.

10. Margolis, J.M., ed. *Engineering Thermoplastics. Properties and Applications.* Dekker, New York, 1985.

11. Serafini T.T., P. Delvigs, and G.R. Lightsey. *Thermally stable polyimides from solutions of monomeric reactants.* Journal of Applied Polymer Science 1972;16:905-15.

12. Pater R H. Thermosetting polyimides: A review. SAMPE Journal 1994;30(5):29-38.

13. Alvarez, R.T. and F.P. Darmory. *Recent Developments in Processable Polyimides* Soc. Plast. Eng. Tech. Pap. 1974;20:687

14. Stezenberger, H. D. In *Polyimides*; Wilson, D., Stenzenberger, H.D., and Hergenrother, P.M., Eds.; Chapman & Hall: New York, 1990

15. Stezenberger, H. D. In *Structural Adhesives: Developments in Resins and Primers*; Kinloch, A. J. Ed.; Elsevier Applied Science: New York, 1986.

16. Glatz, F. P. and R. Muelhaupt. *Semi-interpenetrating networks of sulfur-containing bismaleimides.* High Performance Polymers 1993;5(4):297-305.

17. Stenzenberger H. D. and P. Koenig. *Bis [3-(2-allylphenoxy)phthalimides]: a new class of comonomers for bismaleimides.* High Performance Polymers 1989;1(2):133-44.

18. Mikroyannidis, J.A. and A.P. Melissaris. *Heat-resistant adhesive resins derived from bismaleimides and bisnadimides containing amide linkages.* Journal of Applied Polymer Science 1989;37(9):2587-601.

19. Chaudhari M., J. King, B. Lee. *A new bismaleimide matrix resin for high-performance advanced composites.* International SAMPE Symposium and Exhibition 32nd (Adv. Mater. Technol. '87) 1987;24-32

20. Jin S.J. and A.F. Yee. *Preparation and characterization of maleimide-terminated poly(arylene ether sulfone) oligomers of various molecular weights.* J of Applied Polymer Science 1991;43(10):1849-58.

21. Lin S.C. and E.M. Pearce. *High-Performance Thermosets, Chemistry, Properties, Applications.* Munich: Hanser, 1993.

22. Tant M.R., J.W. Connell, and H.L.N. McManus. *High-Temperature Properties and Applications of Polymeric Materials.* American Chemical Society, Washington, DC 1995.

23. Kelly A. and S.T. Mileiko. *Handbook of Composites, Vol. 4, Fabrication of Composites,* Elsevier Science Publishers B.V., Netherlands.

24. Houtz R.C.. *"Orlon" acrylic fiber: Chemistry and properties.* Textile Research Journal 1950;20:786-801.

25. Vosburgh W.G.. *The heat treatment of Orlon acrylic fiber to render it fireproof.* Textile Research Journal 1960;30:882-96.

26. Burlant W.J. and J.L. Parsons. *Pyrolysis of polyacrylonitrile.* Journal of Polymer Science 1956;22(101):249-56.

27. Grassie N. and I.C. McNeill. *Thermal degradation of polymethacrylonitrile. Part II. The coloration reaction.* Journal of Polymer Science 1958;27(115):207-18.

28. Saunders C.B., V.J. Lopata, W. Kremers, M. Tateishi, A. Singh. *Recent developments in the electron-beam curing of fiber-reinforced composites.* International SAMPE Symposium and Exhibition 37 (Mater. Work. You 21st Century) 1992;944-54.

29. Crasto A.S., R.Y. Kim, and B.P. Rice. *Electron beam cure of composites for aerospace structure.* 42nd International SAMPE Symposium, May 4-8, 1997

30. Yen A. and E.S. Weiser. *E-Beam curing for In-situ automated tape placement.* 30th International SAMPE Technical Conference, October 20-24, 1998.

31. Farmer J.D., C.J. Janke, and V. J. Lopata. *The electron beam cure of fiberglass/epoxy prepregs.* 29th International SAMPE Technical Conference, October 28-November 1, 1997

32. Roylance M.E., C.J. Janke, and J.M. Tuss. *Affordable composite structures vai electron beam (E Beam) curing.* 43rd International SAMPE Symposium, May 31-June 4, 1998

33. Raghavant J., V.J. Lopata, and R.M. Baillie. *Influence of process parameters on electron beam curing of a polymer composite.* 30th International SAMPE Technical Conference, October 20-24, 1998

34. Goodman D.L., D.L. Birx, and G.R. Palmese. *Composite energy curing with high-energy electron beams.* 41st International SAMPE Symposium and Exhibition, Anaheim, Calif, March 25-28, 1996.

35. Wang C.S., H.J. Hwang. *Synthesis and properties of novel naphthalene-containing bismaleimides.* J. Appl. Polym. Sci. 1996;60(6):857-63.

36. Dao B., D.G. Hawthorne, J.H. Hodgkin, M.B. Jackson, T.C. Morton, *Preparation and characterization of some novel bismaleimide monomers and polymers based on diaminobisimides.* High Performance Polymers 1996;8(2):243-63.

37. Wang C.S. and H.J. Hwang. *Synthesis and properties of novel polyaspartimides from 2,7-bis(4-maleimidophenoxy)naphthalene and aromatic diamines.* Polymer 1996;37(3):499-503.

38. Liu Y.L., Y.J. Chen. *Novel thermosetting resins based on 4-(N-maleimideophenyl)glycidylether: II. Bismaleimides and polybismaleimides.* Polymer 2004;45:1797-1804.

39. Hu X., J. Fan, C.Y. Yue, G.Z. Liang. *Enhancement of the processibility of bismaleimide resins via copolymerization with allyl organo-boron compounds.* Journal of Materials Processing Technology 1999;89-90:544-9

40. DeSilva B.S., G.S. Wilson. *Solid phase synthesis of bifunctional antibodies.* Journal of Innunological Methods 1995;9(19):188.

41. Fabian P.E., T.S. Bauer-McDaniel and R.P. Reed. *Low temperature thermal properties of composite insulation systems.* Cryogenics 1995;35(11):719.

42. Humer K., H.W. Weber, E.K. Tschegg, H. Gerstenberg and B.N. Goshchitskii. *Tensile and fracture behaviour in mode I and mode II of fibre reinforced plastics at 77K following low temperature irradiation.* Cryogenics 1995;35(11):743-5

43. Li C., W.L. Qiu, W.S. Hua , L. Lu, X. Wang, *A study of the thermal stability of metal bismaleimides and the thermal cyclodehydration of their precursors,* Thermochimica Acta 1995;255:355.

44. Jin J.Y., J. Cai, X.L. Tang, Y.F. Ding, S.J. Li, J.C. Wang, Q.S. Zhao, X.Y. Hua, and X.Q. Cai. *On polyetherimide modifies bismaleimide resins, I, Effect of the chemical backbone of polyetherimide.* Macromolecular Chemistry and Physics 1999;200:1956.

45. Torrecillas R., N. Regnier, and B. Mortaigne, *Thermal degradation of bismaleimide and bisnadimide networks-products of thermal degradation and type of crosslinking points.* Polymer Degradation and Stability 1996;51:306.

46. Hao J.J., L.X. Jiang and X.X. Cai, *Investigation on bismaleimide bearing polysiloxane (BPS) toughening of 4,4'-bismaleimido diphenylmethane (BMI) matrix-synthesis, characterization, and toughness.* Polymer 1996;37(16):3721-7.

47. Wang C.S., T.S. Leu, and K.R. Hsu, *Novel bismaleimide with naphthalene side group. 1. From 1-naphthaldehyde and 2,6-dimethayaniline.* Polymer 1998;39(13):2921-7.

48. Crivello J.V., *Polyaspartimides: condension of aromatic diamines and bismaleimide compounds.* Journal of Polymer Science: Polymer Chemistry Edition 1973;11:1185-1200.

49. Dix L.R., J.R. Ebdon, N.J. Flint, P. Hodge, and R. O'dell. *Chain extension and crosslinking of telechelic oligomers — I. Michael additions of bisamines to bismaleimides and bis(acetylene ketone)s.* European Polymer Journal 1995;31(7):647.

50. Kumar A.A., M.A. Lagar, R.M.V.G.K. Rao. *Synthesis and characterization of siliconized epoxy-1,3-bis(maleimide)benzene intercrosslinked matrix materials.* Polymer 2002;43:693-702.

51. Dinakaran K., and M. Alagar. *Studies on thermal and morphological properties of 1,1-bis(3-methyl-4-4cyanatophenyl)cyclohexane-epoxy-bismaleimide matrice.* Polymers for Advanced Technologies 2003;14:544-56.

52. Liang G.Z., A.J. Gu. *New bismaleimide resin with improved tack and drape properties for advanced composites.* Journal of Applied Polymer Science 1997;64:273-9.

53. Hu X., J. Fan, C.Y. Yue. *Rheological study of crosslinking and gelation in bismaleimide/cyanate interpenetrating polymer network.* Journal of Applied Polymer Science 2001;80:2437-45.

54. Jin J.Y., J. Cui, X.L. Tang, Y.F. Ding, S.J. Li, J.C. Wang, Q.S. Zhao, X.Y. Hua, and X.Q. Cai. *On polyetherimide modified bismaleimide resins, 1 Effect of the chemical backbone of polyetherimide.* Macromolecular Chemistry and Physics 1999;200:1956-60.

55. Jin J.Y., J. Cui, X.L. Tang, S.J. Li, J.C. Wang, Q.S. Zhao, X.Y. Hua, and X.Q. Cai. *Polyetherimide-modified bismaleimide resins. II. Effect of polyetherimide content.* Journal of Applied Polymer Science 2001;81:350-8.

56. Takeda S., H. Akiyama and H. Kakiuchi. *Synthesis and properties of bismaleimide resins containing ether bonds.* Journal of Applied Polymer Science 1988;35:1341.

57. Crivello J.V.. *Polyaspartimids: Condensation of aromatic diamines and bismaleimide compounds.* Journal of Polymer Science: Polymer Chemistry Edition 1973;11:1185-1200.

58. Yong D. and G.C. Martin. *Diffusion phenomena during cyanate resin cure.* Polymer 1996;37(16):3593-3601.

59. Morio G.. *Properties and applications of bisphenol A type cyanate resin.* Polymeric Materials Science and Engineering 1994;71:621-2.

60. Hamerton I.. High-performance thermoset—thermoset polymer blends: a review of the chemistry of cyanate ester-bismaleimide blends. High Performance Polymers 1996;8:83-95.

61. Chaplin A., T.J. Davies, D.A. Jones, S.J. Shaw, and G.F. Tudgey. *Novel hydrophobic, tough, and high temperature matrix resins for polymer composite.* Plastics, Rubber, and Composites 1999;28(5):191-200.

62. Fan J., X. Hu, C.Y. Yue. *Static and dynamic properties of modified bismaleimide and cyanate ester interpenetrating polymer networks.* Journal of Applied Polymer Science 2003; 88: 2000-6.

63. Fan J., X. Hu, C.Y. Yue. *Thermal degradation study of interpenetrating polymer network based on modified bismaleimide resin and cyanate ester.* Polymer International 2003;52:15-22.

64. Fan J., X. Hu, C.Y. Yue. *Dielectric properties of self-catalytic interpenetrating polymer networks based on modified bismaleimide and cyanate ester resins.* Journal of Polymer Science: Part B. Polymer Physics 2003;41:1123-34.

65. Nair C.P.R, T. Francis, T.M. Vijayan, K. Krishnan. *Sequential interpenetrating polymer networks from bisphenol A based syanate ester and bismaleimide: properties of the neat resin and composites.* Journal of Applied Polymer Science 1999;74:2737-46.

66. Sisk B.C, K. Chuang and W.P. Pan. *Development of bismaleimide /cyanate ester copolymers.* Materials characterization by dynamic and modulated thermal analytical techniques, ASTM STP 1402, Riga A.T. and L.Judovits, Eds., American Society for Testing and Materials, West Conshohocken, PA, 2001.

67. Lin K.F., J.S. Lin and C.H. Cheng. *High temperature resins based on allylamine/bismaleimides.* Polymer 1996;37(21):4729-37.

68. Rao B.S. Synthesis, characterization, and thermal stability of bismaleimides derived from maleimido benzoic acid. Journal of Polymer Science: Part A. Polymer Chemistry 1989;27(8):2509-18.

69. Takeda S., H. Akiyama, and H. Kakiuchi. *Synthesis and properties of bismaleimide resins containing ether bonds.* Journal of Applied Polymer Science 1988;35:1341-50.

70. Varma I.K., G.M. Fohlen, J.A. Parker. *Synthesis and thermal characteristics of bisimides.* I. Journal of Polymer Science: Polymer Chemistry Edition 1982;20(2):283-97.

71. Di Giulio, C., M. Gautier, B. Jasse. *Fourier transform infrared spectroscopic characterization of aromatic bismaleimide resin cure states.* Journal of Applied Polymer Science 1984;29(5):1771-9.

72. Chaudhari, M., T. Galvin, J. King. *Characterization of bismaleimide system, XU 292.* SAMPE Journal 1985;21(4):17-21.

73. Pater, R.H. *Tough, high performance, addition-type thermoplastic polymers.* U.S Pat 5081198, 1992

74. Lin K.F., J.C. Chen. *Curing, compatibility, and fracture toughness for blends of bismaleimide and a tetrafunctional epoxy resin.* Polymer Engineering and Science 1996;36(2):211-7.

75. Viot J.F., J.C. Seferis. *Process-resolved morphology of bismaleimide matrix composites.* Journal of Applied Polymer Science 1987;34(4):1459-75.

76. Domeier L. A.. *Aromatic bismaleimide and prepreg resin therefrom.* U.S. Pat. 4654407, 1987

77. Grigat E. and R. Putter. *New methods of preparative organic chemistry VI.* Angewandte Chemie International Edition 1967;6:206-18.

78. *'BT Resins'. Commercial Data Brochure.* 2nd Ed. Mitshbishi Gas Chemical Co. June 1980

79. Stenzenberger H. D., W. Roemer, M. Herzog, S. Pierce, M. Canning, K. Fear. *The development of tough bismaleimide resins.* International SAMPE Symposium and Exhibition 31st (Mater. Sci. Future), 1986;920-32.

80. Domeier L.A.. *Bismaleimide formulations containing olefinic ether modifiers.* US patent: 4853449, 1989.

81. Li Z.M., M. Xu, A. Lu, M.D. Zhang, R. Huang. *Dially bisphenol A ether and diallyl phenyl ether modified bismaleimide resin system for resin transfer molding.* Journal of Applied Polymer Science 1999;74(7):1649-53.

82. Iijima T., K. Ohnishi, W. Fukuda, and M. Tomoi. *Modification of bismaleimide resin with N-phenylmaleimide-styrene-p-hydroxystyrene and N-phenylmaleimide-styrene-p-allyloxystyrene terpolymers.* Journal of Applied Polymer Science 1997;65:1451-61.

83. Chattha M.S., R. A. Dickie. *Dynamic mechanical analysis of bismaleimidodiphenyl methane and diallylbisphenol-A crosslinked polymers.* Journal of Applied Polymer Science 1990;40(3-4): 411-6.

84. Marks T.J. and M.A. Ratner. *Design, synthesis, and properties of molecule-based assemblies with large second-order optical nonlinearities.* Angewandte Chemie International Edition in English 1995;34:155-73.

85. Iijima T., K. Ohnishi, W. Fukuda, and M. Tomoi. *Modification of bismaleimide resin with N-phenylmaleimide-styrene-p-hydroxystyrene and N-phenylmaleimide-styrene-p-allyloxystyrene terpolymers.* Journal of Applied Polymer Science 1997;65(8):1451-61.

86. Stenzenberger H.D., P. Koenig, W. Roemer, M. Herzog. *BMI/bis(allylphenoxyphthalimide) copolymers: a new family of resins for advanced composites with improved thermal oxidative stability.* International SAMPE Symposium and Exhibition 1991;36(2):1232-43.

87. Zahir S., M.A. Chaudhari, J. King. *Novel high-temperature resins based on bis(4-maleimidophenyl)methane.* Makromolekulare Chemie, Macromolecular Symposia 25(Eur. Symp. Polym. Mater., 1987, Pt. 4), 1989;141-54.

88. Carduner K.R., M.S. Chattha. *Carbon-13 NMR investigation of the oligomerization of bismaleimidodiphenylmethane with diallylbisphenol A.* Polymeric Materials Science and Engineering 1987;56:660-4.

89. Carduner K.R., M.S. Chattha. *Carbon-13 NMR investigation of the oligomerization of bismaleimidodiphenylmethane with diallyl bisphenol A.* ACS Symposium Series 367 (Cross-Linked Polym.), 1988;379-94.

90. Reyx D., I. Campistron, C. Caillaud. *Thermal reaction between N-phenylmaleimide and 2-allylphenol as a model for the crosslinking reaction to bismaleimide polymerization with diallylbisphenol A.* Macromolecular Chemistry and Physics 1995;196:773-85.

91. Shibahara S.; T. Yamamoto, T. Yamaji, J. Motoyoshiya, S. Hayashi. *Thermal reactions of N-phenyl maleimide and mono- or di-functional allyl phenols.* Polymer Journal (Tokyo) 1998;30(5):404-9.

92. Shibahara S., T. Yamamoto, J. Motoyoshiya, and S. Hayashi. *Curing reactions of bismaleimidodiphenylmethane with mono- or di-functional allylphenols. High resolution solid-state ^{13}C NMR study.* Polymer Journal 1998;30:410.

93. Varma I.K., S. P. Gupta, D. S. Varma. *Blends of bismaleimide resins and bis(allyl phenyl) esters.* Angewandte Makromolekulare Chemie 1991;184(1): 7-18.

94. Grigat E. and R. Putter. Synthesis and reactions of cyanic esters. Angewandte Chemie International Edition in English 1967;6(3):206-18.

95. Grigat E. and R. Putter, Dtsch. Pat. 1183507, assigned to Bayer (1963)

96. Fang T. and D.A. Shimp. *Polycyanate esters: science and applications.* Progress in Polymer Science 1995;20:61-118.

97. Nair C.P.R., T. Francis. *Blends of bisphenol A-based cyanate ester and bismaleimide: cure and thermal characteristics.* Journal of Applied Polymer Science 1999;74:3365-75.

98. Hamerton I.. *Chemistry and Technology of Cyanate Ester Resins.* Blackie Academic and Professional Press; London, 1994; chapter 3

99. Shimp D.A.. *The translation of dicyanate structure and cyclotrimerization efficiency to polycyanurate properties.* Polymeric Materials Science and Engineering 1986;54:107-13.

100. Sperling. L.H.. *Interpenetrating polymer networks and related materials.* Plenum, New York, 1981.

101. Sperling, L.H. and D.W. Friedman. Synthesis and mechanical behavior of interpenetrating polymer networks: Poly(ethyl acrylate) and polystyrene. Journal of Polymer Science Part A-2: Polymer Physics 1969;7(2):425-7.

102. Manson J.A. and L.H. Sperling. *Polymer blends and composites.* Plenum, New York, 1976.

103. Suthar B., H.X. Xiao, D. Klempner, and K.C. Frisch. *A review of kinetic studies on the formation of interpenetrating polymer networks.* Polymers for Advanced Technologies 1996;7(4):221-33.

104. D.R. Paul and L.H. Sperling. *Multicomponent polymer materials* (Advances in chemistry series 211). American Chemical Society, Washington, DC, 1986.

105. Liang B., Y.L. Ji, and J.H. Ma. *In situ polymerization and in situ compatibilization of polymer blends of poly(2,6-dimethyl-1,4-phenylene oxide) and polyamide 6.* Materials Letters 2005;59:1997-2000.

106. Walsh D.J. and C.K. Sham. *In-situ polymerization of n-butyl acrylate in poly(vinyl chloride).* Polymer 1984;25(7):1023-7

107. Shach-caplan M., M. Narkis, and M.S. Silverstein. *Modification of porous suspension-PVC particles by stabilizer-free aqueous dispersion polymerization of absorbed monomers.* Polymer Engineering & Science 2002;42(5):911-24.

108. Fox R.B., J.J. Fay, Usman Sorathia, and L.H. Sperling. *Interpenetrating polymer networks: An overview.* In *Sound and vibration damping with polymer.* ed. Corsaro R.D. and L.H. Sperling. Chapter: 19. American Chemical Society, Washington, DC, 1990.

109. Fox R.B., J.L. Bitner, J.A. Hinkley, and W. Carter. *Dynamic mechanical properties of some polyurethane-acrylic copolymer interpenetrating polymer networks.* Polymer Engineering & Science 1985;25(3):157-63.

CHAPTER 3: SYNTHESIS AND STRUCTURAL CHARACTERIZATION OF BMI-CE IN-SITU SEQUENTIAL IPNs

3.1 Introduction

This chapter details the methodology employed for *in-situ* synthesis of sequential IPNs comprised of a cyanate ester and bismaleimide/reactive diluent monomer combination by means of EB irradiation. These IPNs possess important features including low temperature processing and high temperature performance.

Following the experimental section 3.2, the discussion will be divided into four sections that describe: (1) selection of cyanate ester and catalyst (3.3.1); (2) selection of reactive diluent (3.3.2); (3) synthesis and verification of *in-situ* sequential IPN structure (3.3.3 and 3.3.4); and (4) characterization of the sequential IPNs (3.3.5 and 3.3.6).

This chapter also sets the framework for in depth discussions associated with various aspects of the design and implementation of the novel material systems that will be the subject of chapters that follow.

3.2 Experimental

In this section, basic materials and procedures are summarized.

3.2.1 Materials

1,1'-(methylenedi-4,1-phenylene)-bismaleimide (BMI) and 4-acryloylmorpholine (AMP) were obtained from Aldrich Chemicals and were used without further purification. 4.4'-ethylidene diphenyl cyanate ester (LECY) was obtained from Lonza,

Inc. and was used as received. 4-cyantophenylmaileimide (CPM) was used as a network coupler to connect the two networks. It was synthesized as described in Appendix I. The structures of these monomers are given in Figure 3.1. Copper (II) Naphthenate was obtained from the Shepherd Chemical Company and was used as a catalyst for LECY cure. As a thermal initiator, 2,5-bis(tert-butylperoxy)-2,5-dimethylhexane (Luperox 101) was purchased from Aldrich Chemicals and directly used in the synthesis of simultaneous IPNs and in our copolymerization kinetics study (Chapter 6).

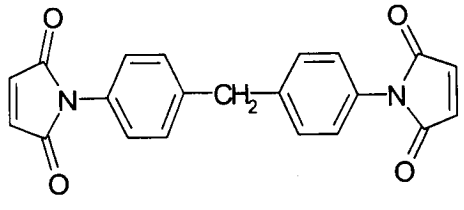

1,1'-(methylenedi-4,1phenylene)-bismaleimide (BMI)

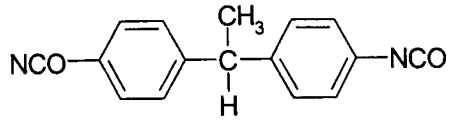

4.4'-ethylidene diphenyl cyanate ester (LECY)

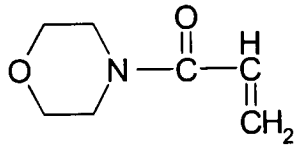

4-acryloylmorpholine (AMP)

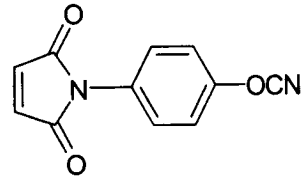

4-cyantophenylmaileimide (CPM)

Figure 3.1 Chemical structure of raw materials used in current study.

3.2.2 Preparation of sequential IPNs and LIPNs

The blends of cyanate ester and reactive diluent were mixed with 300~600ppm copper naphthenate (based on Cu^{++}) at about 120°C until the color of the solution

changed to deep green indicating that a complex between cyanate ester and Cu^{2+} was formed. Consequently, the corresponding amount of BMI and network coupler was added to the solutions to form homogeneous mixtures at 120°C. The mixtures were then cured at 110°C for 5 hours and 130°C for 2 hours to form the cyanurate network. The bismaleimide network formation was realized by a thermal scan to 310~330°C using a DMA instrument or by electron beam irradiation.

3.2.3 Preparation of simultaneous IPNs and LIPNs

The simultaneous IPNs were obtained in a manner similar to the sequential IPNs. First, a solution comprised of BMI, cyanate ester, reactive diluent as well as a catalyst for the cyanate ester cure was prepared as described in section 3.2.1. Second, Luperox 101 was added to the solution and mixed. The mixture was kept 130°C for 3 hours and then at 170°C for 2 hours to allow the two networks to form simultaneously while following two different mechanisms, condensation and free radical copolymerization. Note that the decomposition temperature of Luperox 101 peroxide is 130°C.

Furthermore, the simultaneous LIPNs based on BMI, LECY, and CPM were synthesized by means of thermal cure. In this case, however, Luperox CU90 (cumene hydroperoxide), which has a higher decomposition temperature (10 hour half life at 135°C), was used as a thermal initiator for the copolymerization of BMI and AMP. The system was cured at 145°C for 6 hours.

3.2.4 EB irradiation

Preliminary EB irradiation experiments were conducted to monitor the conversion of relevant functional groups and to verify the formation of IPNs as well. This set of experiments were carried out by irradiating sample plaques at room temperature to a total dose of 200 kGy administrated as follows: 10, 20, 20, 50, 50, 50 kGy. Irradiation was accompanied by a minimal temperature rise of the samples. The irradiated samples were evaluated using differential scanning calorimetry (DSC), dynamic mechanical analysis (DMA) and Fourier transform infrared spectroscopy (FTIR) which are discussed in the following section.

3.2.5 Chemical and physical characterization

Dynamic mechanical analysis (DMA) was performed using a TA Instruments DMA 2980 in an air atmosphere at a frequency of 1Hz and at a heating rate of 5°C/min. Specimens of nominal dimensions 30×10×3 mm^3 were tested in a single cantilever beam loading configuration.

Differential scanning calorimetry (DSC) was performed at a heating rate of 10°C/min using a Perkin Elmer DSC 7 to obtain information regarding the cure behavior of these systems. The typical sample size was 8 mg and the samples were placed in sealed aluminum pans and experiments were conducted using a nitrogen purge gas.

Fourier transform infrared spectroscopy (FTIR) was employed to monitor changes in –OCN and C=C concentration in order to ascertain the formation of sequential IPNs. A Thermo Nicolet Nexus 670 FTIR spectrometer was used. Mid-IR experiments were

conducted in transmission mode at 4 cm^{-1} resolution with 32 scans per spectrum. Near IR spectroscopy with a resolution of 16 cm^{-1} was also used to assess conversion.

The viscosity of the resin system as a function of temperature was measured using a Brookfield digital viscometer to evaluate the processing performance offered by the formulations developed.

3.3 Results and Discussion

3.3.1 Selection of cyanate ester resin and appropriate catalyst

As the constituent employed to improve the processability of BMI, the aggregation state of cyanate ester at room temperature is critical for evaluating its usefulness. In this sense, the viscosity of various cyanate resins at given temperatures along with their final Tgs was compared in order to choose the proper one. Figure 3.2 shows, BPECN, which is 4,4'-ethylidenediphenyl cyanate (simplified as LECY in this study, its structure shown in Figure 3.1) exhibits very low viscosity at room temperature ~100cps@25°C [1]. It is the only non-crystalline compound among all the commercially available dicyanate monomers. Aside from this, LECY's Tg is about 300°C after full cure. It was thus selected in the present study to improve the processability of BMI even though less research on it has been done to date with respect to its modification of BMI compared to another commonly used cyanate ester resin: 2,2'-bis(4-cyanatophenyl) propane(BACY) [2-4], which is represented by BPA cyanate in Figure 3.2. It can be seen that BACY possesses much higher melting point (~100°C) compared to LECY due to its more regular backbone structure, as shown in Figure 3.3. Meanwhile, the higher fracture toughness associated with LECY (1.1 in-lb/in^2) compared to BADCY (0.8 in-lb/in^2)

constitutes another advantage of LECY in modifying the bismaleimides [5]. Accordingly, the small Tg difference between LECY and BACY resins, which is typically within 10~20°C [1, 3, 6-8], will result in a minor effect on the final IPNs according to the weight fraction of cyanate ester resin, and can be completely counteracted by the better toughness and processability provided by LECY [8]. In addition, the hydrolysis associated with these two monomers was investigated and will be reported in Chapter 4. The better performance of LECY in equilibrium water uptake at 100°C leads to the final decision.

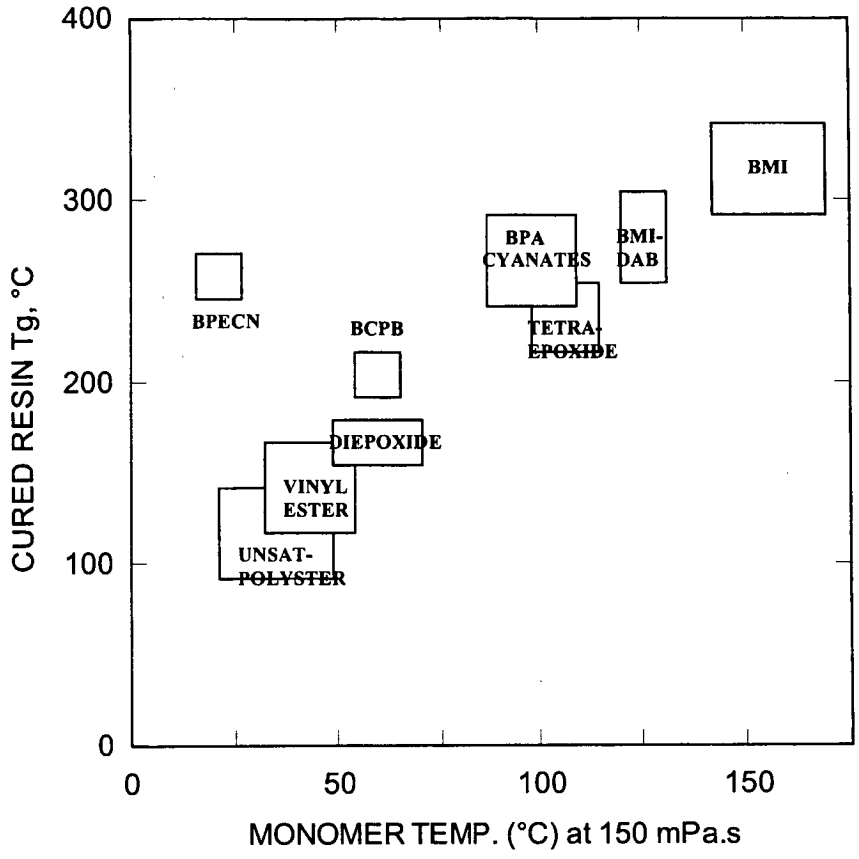

Figure 3.2 The relationship between the constant viscosity (150mPa.s) temperature of common monomers and their Tgs of the cured thermoset resins. Data courtesy of Ciba-Geigy, wherein BPECN stands for LECY. (Redrawn from chart in Ref. 9)

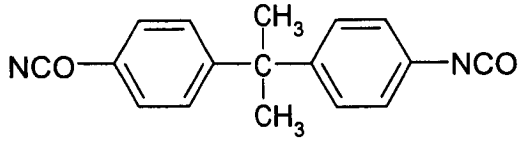

Figure 3.3 Chemical structure of BACY. The more regular backbone gives it higher melting point compared to LECY.

Figure 3.4 shows the cure path of LECY. The cyanate group can form triazine rings at ~110°C with the help of a catalyst, which constitutes the formation of first network of the *in-situ* sequential IPNs. The catalyst for the cure of LECY is a critical component in the resin system in that its presence will ensure that the complete cure of LECY can be attained at low temperatures thus avoiding the polymerization of BMI and the simultaneous occurrence of two interfering reaction mechanisms. Determination of catalyst type and concentration, as well as processing temperature was conducted by studying the catalysis and hydrolysis of LECY. This is discussed in detail in the Chapter 4. As a result of this study, copper naphthenate was selected as a catalyst since its presence can maintain the stability of BMI-reactive diluent combination at the selected processing temperature while the resulting hydrolysis is also kept to a minimum level compared to other metal catalysts.

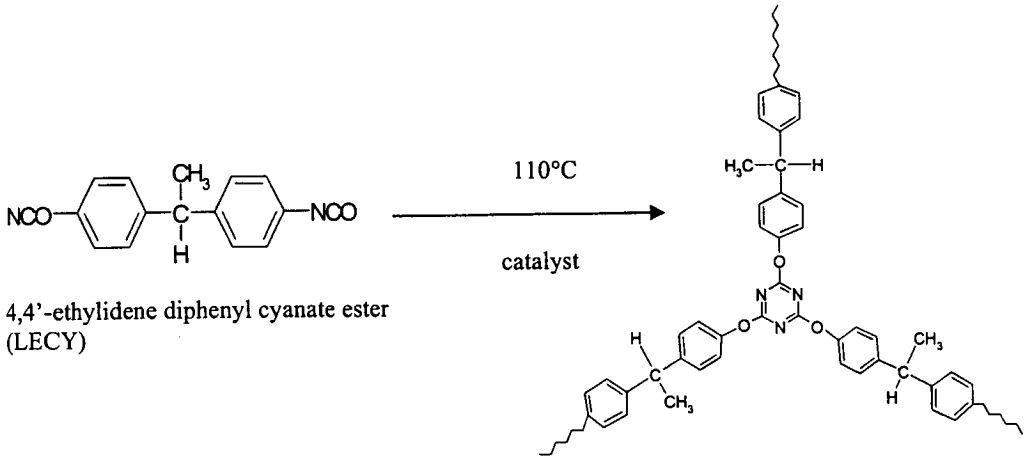

4,4'-ethylidene diphenyl cyanate ester
(LECY)

Polycyanurate

Figure 3.4 Scheme illustrating the cure path of LECY.

3.3.2 Selection of reactive diluent

It is expected, though to a lesser extent than is observed for thermally cured systems, that diffusion limitation will play an important role in determining the final extent of conversion resulting from EB irradiation. Liquid reactive diluents can be used to reduce the influence of diffusion limitations. Additionally, the resulting free radical copolymerization can potentially increase the intrinsic rate of reaction of the system relative to the individual monomers. To ensure the optimum processing and final properties of the formed IPN, there are some critical requirements for the choice of reactive diluents. First, the diluent should possess good solubility to prevent BMI's recrystallization and reduce heating requirements in RTM processing. Secondly, both reactive diluent and BMI should be chemically stable during the formation of the first network without interfering in the formation of the LECY polycyanurate network. Thirdly, the diluent must copolymerize with BMI by a free radical mechanism under EB radiation. Furthermore, use of the diluent should also be beneficial to BMI conversion and network structure in order to obtain a high Tg. Thus reactive diluents were selected based on two attributes: solubility and reactivity. A number of reactive diluents were investigated and the results are presented qualitatively in Table 3.1. Of these, AMP showed good solubility for BMI (i.e. it can dissolve BMI completely at 110°C with 1:2 molar ratio of BMI to AMP). This may be attributed to the similarity in structure between BMI and AMP (see Figure 3.1). Additionally, the BMI and AMP system maintains chemical stability up to 140°C. Thus AMP was selected as the reactive diluent for this study. Note that while it was possible to obtain adequate solubility for a wide variety of diluents, many were not acceptable because they either showed reactivity at too low a

temperature or were not at all reactive via EB free radical polymerization. The fundamental reactivity behavior of a variety of reactive diluents with maleimide under EB irradiation was investigated. These results and more detailed explanations for observed differences in co-monomer reactivity are given in Chapter 5.

Table 3.1 Solubility and reactivity of some reactive diluents evaluated in this study.

Reactive Diluent	Solubility	Reactivity	Comment
2-ethyl-1-hexyl vinyl ether	√	×××	fast
Cyclohexyl vinyl ether	√√	×××	fast
Allyl phenyl ether	√	×	slow EB
2-allylphenol	√√	×	slow EB
Styrene	√	××	fast
4-acetoxy styrene	√√√	××	fast
N-acryloylmorpholine	√√√	√√√	best choice
1-vinyl-2-pyrrolidone	√√√	×××	fast
Poor: ××× very good:√√√			

3.3.3 Synthetic route of sequential IPNs and LIPNs

Based on the preceding discussion, a scheme for the synthesis of sequential IPNs is presented in Figure 3.2 to show that the first network based on LECY can be created in the presence of BMI and AMP by employing a cure temperature below 130°C; then, AMP can copolymerize with BMI to form the second network sequentially by either using high temperature or a peroxide initiator or by EB irradiation.

The term "network coupler" is employed to describe a monomer that possesses dual functionality so that it can be involved in the formation of both IPN networks thus allowing for the formation of linked interpenetrating polymer networks (LIPNs) [10]. Such monomers serve two purposes: First, they can increase the crosslink density of the

IPNs significantly; and secondly, they can link the unreacted sites or defects in one network to the other to improve the overall structure of the IPNs. Accordingly, the direct influence of a network coupler on IPN performance is enhancing the Tg of the system, which is the consequence of the increase of the crosslinking density of the IPNs. In this work, the network coupler 4-(cyanatophenyl)maleimide (CPM) was synthesized according to the procedure described in Appendix I. This coupler has both cyanate and maleimide functionality, which can interlink the two networks as illustrated in Figure 3.5. In view of the chemical structure of CPM, it was expected that this coupler would enhance the compatibility of the whole system providing better polymer mixing at the molecular level.

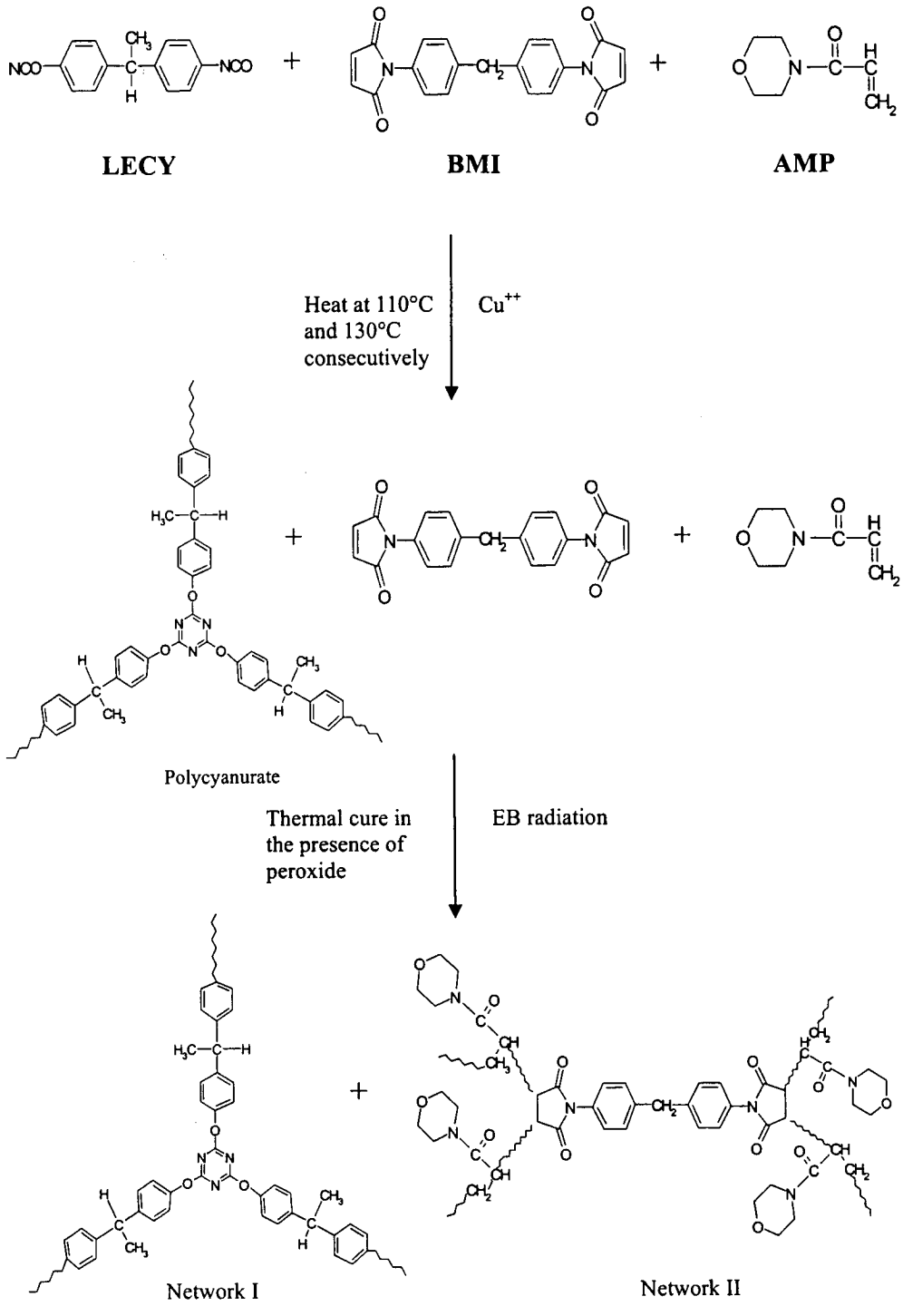

Figure 3.5 Scheme illustrating the formation of *in-situ* sequential IPNs based on cyanate ester and BMI.

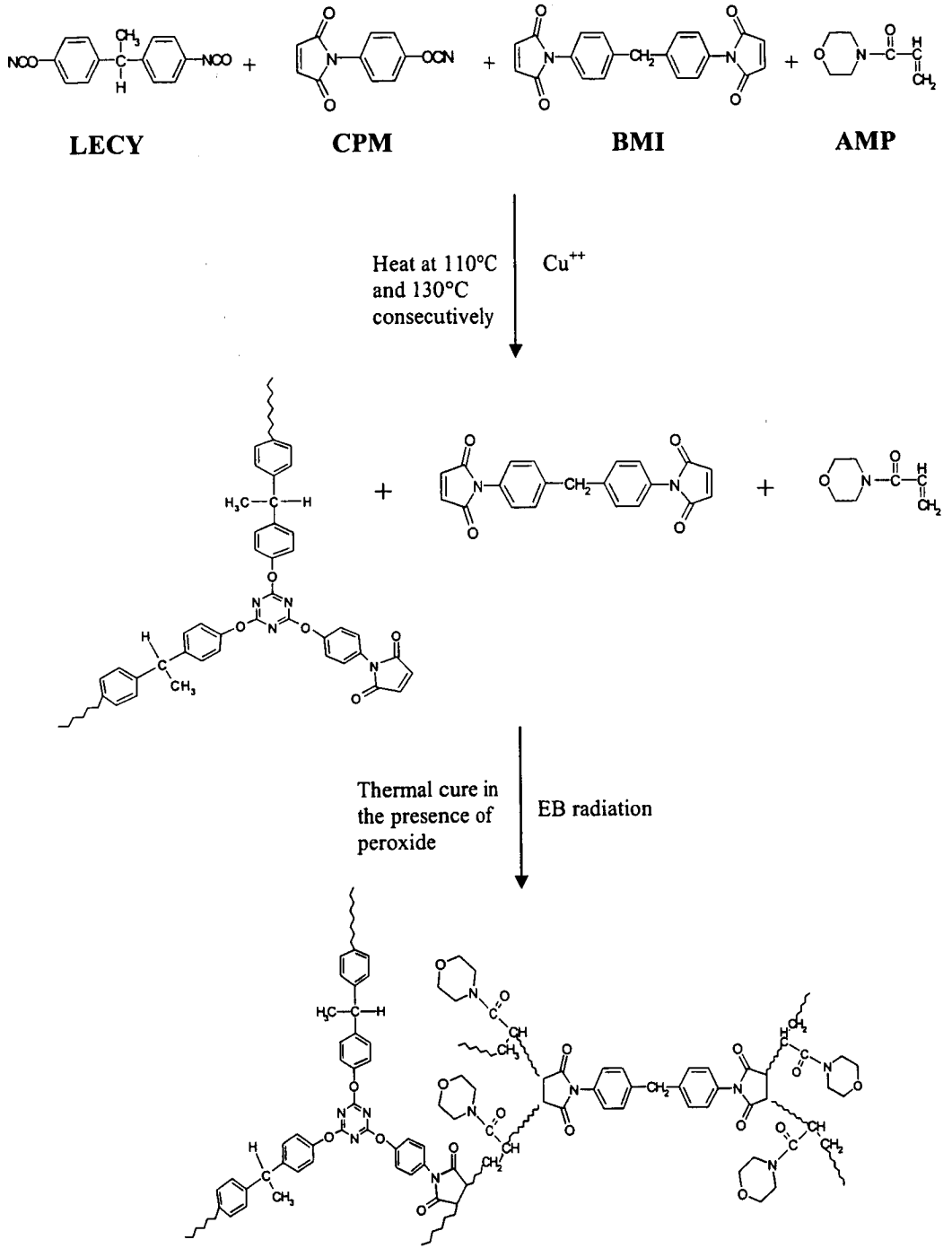

Figure 3.6 Scheme illustrating the formation of linked *in-situ* sequential IPNs of cyanate ester with BMI.

3.3.4 Verification and significance of sequential IPNs

A sample containing 50 wt.% LECY and the remaining 50 wt.% comprised of a 4:1 molar ratio of AMP:BMI was subjected to a cure schedule of 5 hours at 110°C and 2 hours at 130°C in the presence of copper naphthenate (600ppm Cu^{++} based on the total mixture weight) in order to verify the presumed first network formation (shown in Figure 3.5 and 3.6). The Mid-IR technique was employed. A representative spectrum is given in Figure 3.7, in which spectra for a sample at various stages of cure are superimposed. The peak at 2266 cm^{-1} corresponds to the OCN group. The FTIR data revealed that after two consecutive heatings at 110°C and 130°C respectively, a dramatic reduction in the 2266 cm^{-1} peak corresponding to 88% conversion of cyanate ester moieties is achieved whereas only a small portion of the BMI and AMP double bonds react. A peak corresponding to the triazine ring structure at 1570 cm^{-1} appears after cure indicating the polycyanurate network structure has formed.

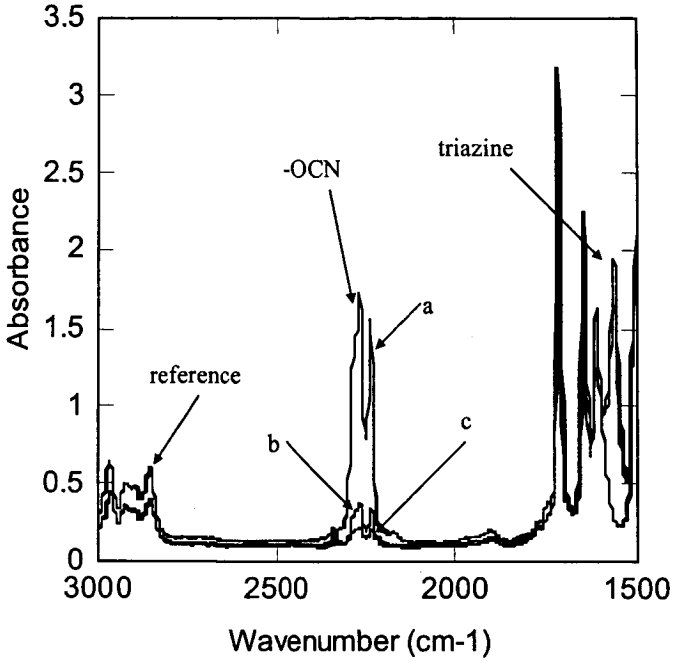

Figure 3.7 The Mid-FTIR spectra of blends (50 wt.% BMI and AMP (molar ratio as 1:4) 50 wt.% LECY) concerning first network formation: a) initial; b) after 105°C (5hrs) and c) after 105°C (5hrs) and 130°C (2hrs). OCN peak at 2266 cm^{-1}, triazine peak at 1570 cm^{-1}.

The second stage involves EB curing by a dose of 200 KGy. During this processing stage, the maximum temperature attained by the sample was not greater than 120°C. Figure 3.8 and Figure 3.9 show the results of Mid-IR and Near-IR spectroscopy on samples before and after irradiation. The NIR absorbance for maleimide double bond is found at 4875 cm^{-1} and the NIR absorbance for the AMP double bond is found at 6153 cm^{-1}. Likewise, the Mid-IR absorbance for the maleimide C=C is at 692 cm^{-1} and for the AMP C=C is at 791 cm^{-1}. It is clear that the peak heights decrease significantly following irradiation. The results are in close agreement and show that BMI conversion is about 50% while AMP conversion is 90%, at the same time, there is almost no change in the

OCN peak. The results substantiate the suggested reaction mechanism of Figure 3.2. The great difference in conversion of the two monomers may be attributed to the initial monomer ratio and to diffusion effects. After postcure, complete conversion of AMP and BMI was achieved.

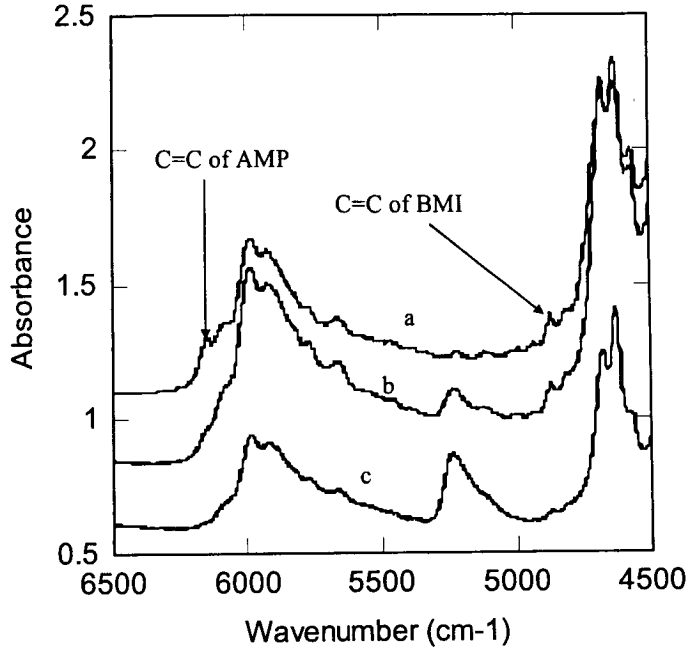

Figure 3.8 The Near-FTIR spectra of blends (50 wt.% BMI and AMP (molar ratio 1:4) 50 wt.% LECY) concerning second network formation: (a) initial; (b) after EB radiation and (c) after EB radiation and postcure.

The relevant peak assignments used for the analysis and the results are summarized in Table 3.2. The data show that it is possible to control processing parameters so as to form *in-situ* sequential IPNs based on polycyanurate networks, cured thermally, followed by EB cured BMI-AMP blends, without the interference of the two reaction mechanisms.

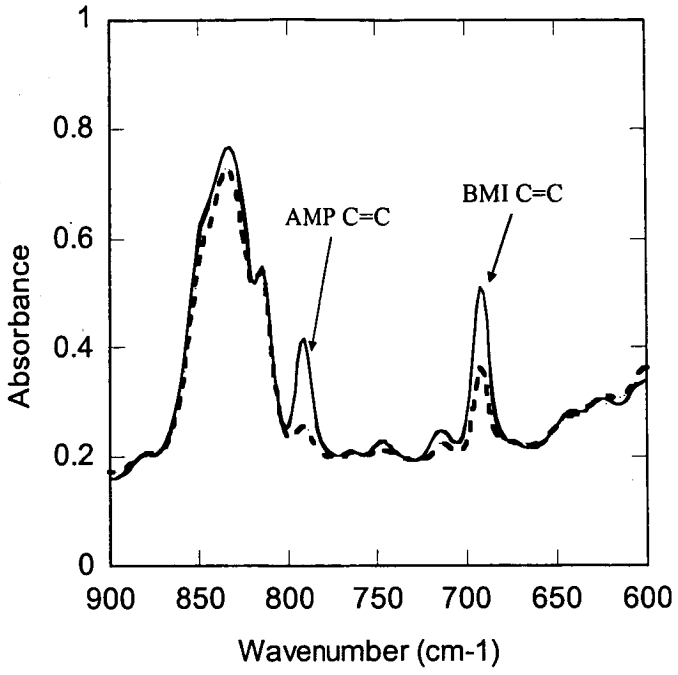

Figure 3.9 The Mid-FTIR spectra of blends [50 wt.% BMI and AMP (molar ratio 1:4) 50 wt.% LECY] concerning second network formation: (—) initial; (---) after EB radiation.

Table 3.2 Final conversions of functional groups following the thermal cure and EB cure stages for the formation of the LECY-AMP/BMI *in-situ* sequential IPN.

FTIR	Peaks		1st Network %conversion		2nd Network %conversion	
	Group	Position (cm^{-1})	105°C (5h)	130°C (2h)	EB	Postcure
MIR	Aromatic C-H	2853	reference	reference	reference	
	-OCN	2266	71	88	0	—
	BMI C=C-H	692	3	9	47	—
	AMP C=C-H	791	3	2	82	—
NIR	Aromatic C-H	4530	—	—	reference	reference
	BMI C=C-H	4875	—	—	50	87
	AMP C=C-H	6153	—	—	89	99

3.3.5 Importance of synthetic route—sequential versus simultaneous IPNs

IPNs with the same initial monomer composition were synthesized sequentially and simultaneously in order to demonstrate the influence of the synthetic method on the final performance just discussed. Figure 3.10 shows the DMA spectra for the IPNs obtained by the two methods described in the experimental section with 50% LECY 50% BMI and AMP (with molar ratio as 1:2). The EB cured IPNs exhibits a higher initial storage modulus and a distinctly sharper Tg peak of 279°C; whereas the Tg of the simultaneous IPNs is just 257°C and is accompanied by a broadened glass transition region. This phenomenon may be attributed to the interference of two concurrent reactions that result in an incomplete reaction or lower crosslinking density. Another possible reason is that with the advancement of polymerization, the macromolecules formed tend to become immiscible with each other resulting in phase separation. The 22°C difference in Tg is a result of the difference in structure arising from the selection of the synthetic route. Therefore, several factors may be conducive to the higher Tg associated with the EB cured sequential IPNs: (1) Phase separation can be prevented maximally via the *in-situ* polymerization of the second network induced by EB radiation which contributes to clean interfaces and small phase domains, (2) the interference between two network forming processes can be avoided in sequential IPN production, (3) miscibility of all components is good, (4) there is a high conversion of all monomers, and (5) high crosslinking density can also force the two networks to maintain small phase domains. The same difference is also observed between thermally cured sequential IPNs and thermally cured simultaneous IPNs.

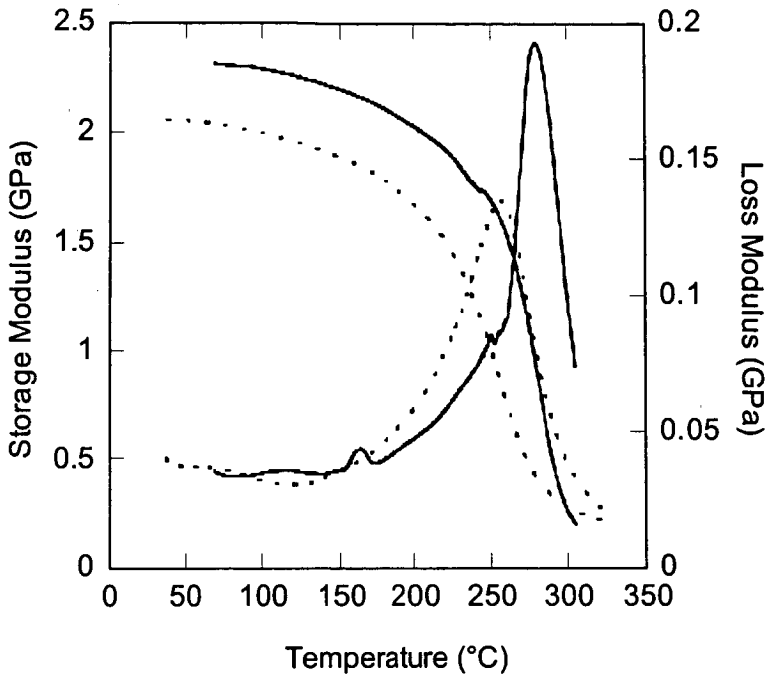

Figure 3.10 Dynamic mechanical spectrum of the system of 50 wt.% LECY 50 wt.% BMI and AMP (molar ratio 1:2). (—) synthesized sequentially via EB irradiation, (---) synthesized simultaneously by thermal cure.

3.3.6 Behavior of LIPNs

We expect that linking the network of the IPNs should result in an increase of Tg. In our work we have used CPM as a network coupler between the cyanate ester and BMI/AMP networks. The dynamic mechanical analysis of linked IPNs synthesized both sequentially and simultaneously is given in Figure 3.11. These are characteristic results for such systems. Compared to the materials in Figure 3.10, part of the LECY was replaced by CPM. Comparison of Figure 3.10 and 3.11 shows that the Tg of networks containing the coupler is ~ 50°C higher than the uncoupled counterparts (329°C versus

279°C and 309°C versus 257°C). Additionally, the storage modulus of the coupled systems is significantly higher: 3.2 GPa and 2.5 GPa versus 2.4 GPa and 2.1 GPa for sequentially and simultaneously IPNs respectively.

The advantage of sequential over simultaneous synthesis in terms of high Tg is also apparent for the LIPNs since the Tg of the sequential LIPN is 20°C higher than the simultaneous one. Figure 3.11 shows that after complete cure some phase separation occurred. This is much more prevalent for materials synthesized simultaneously as shown by the three distinct transition peaks and a correspondingly much lower Tg.

In Chapter 7, the relationship among composition (LECY, BMI, diluent, and coupler) are explored in depth and empirical relations are developed for use as design tools for high temperature IPN systems.

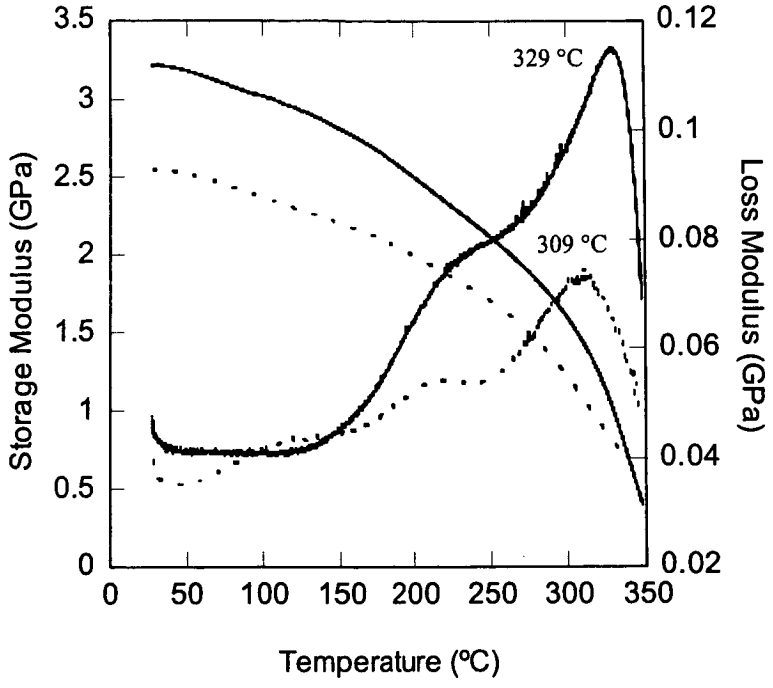

Figure 3.11 Dynamic mechanical spectra of the IPNs comprised of 50 wt.% BMI and AMP (with molar ratio as 1:2) and 30 wt.% LECY together with 20 wt.% CPM synthesized in different ways. (—) sequentially, (---) simultaneously.

3.4 Summary

General process and material parameters have been established for the synthesis of bismaleimide–cyanate ester sequential IPNs that can be processed at low temperature while possessing high temperature performance. The copper naphthenate catalyzed cure of bisphenol E cyanate ester (LECY) results in the formation of the first network and the EB induced copolymerization of 1,1'-(methylenedi-4,1phenylene)-bismaleimide (BMI) with reactive diluent creates the second network. N-acryloylmorphiline (AMP) was found to be a good and uniquely suited reactive diluent due to features such as good solubility for BMI and optimal reactivity—it does not react during the first stage of processing, but

reacts readily with BMI via EB irradiation or at higher temperature with the use of a peroxide initiator. CPM (4-cyanatophenylmaleimide) was employed as a network coupler to enhance the Tg of such systems further by interlinking two networks to produce LIPNs. The resin system produced features low viscosity as well as a high Tg and fracture toughness. Moreover, such systems are amenable to low cost liquid molding processing methods like VARTM and RTM for the fabrication of composite parts at low temperature, which will be demonstrated in Chapter 8.

The *in-situ* synthesis of sequential IPNs at low temperature was accomplished with the aid of EB irradiation and the reactive diluent, which provide a promising way to overcome the high processing/fabrication costs as well as phase separation associated with traditional thermal cure. More importantly, EB irradiation can be used to precisely control the free radical reaction of the second network formation, and consequently results in real sequential IPNs that possess morphology and properties superior to those claimed by current IPNs.

This chapter has summarized some of the key accomplishments of this work. It has provided an overview of the new material systems that have been developed based on *in-situ* sequential interpenetrating polymer networks of cyanate ester with BMI. It also provides the framework for in depth discussions associated with various respects of the design and implementation of these new material systems that are the subject of the chapters that follow. In Chapter 4, the influence of catalyst type, catalyst concentration, and processing condition of the formation of the polycyanurate network is discussed. Chapter 5 describes the selection of reactive diluent, meanwhile the significance of reactive diluent in BMI processing via EB irradiation is highlighted. Chapter 6 illustrates

the kinetics of EB induced copolymerization, based on that, the processing condition of the formation of the second network is discussed. In Chapter 7, the relationship between structure and property of the *in-situ* LECY-BMI sequential IPNs is illuminated. Finally in Chapter 8, the processing technique along with the obtained resin system is described in terms of processing parameters and performance assessments.

List of References

1. Product Information from Lonza Inc.

2. Hu X., J. Fan, C.Y. Yue. *Rheological study of crosslinking and gelation in bismaleimide/cyanate interpenetrating polymer network.* Journal of Applied Polymer Science 2001;80:2437-45.

3. Hamerton I.. High-performance thermoset—thermoset polymer blends: a review of the chemistry of cyanate ester-bismaleimide blends. High Performance Polymers 1996;8:83-95.

4. Nair R.C.P., T. Francis, T.M. Vijayan, K. Krishnan. *Sequential interpenetrating polymer networks from bisphenol A based syanate ester and bismaleimide: properties of the neat resin and composites.* Journal of Applied Polymer Science 1999;74:2737-46.

5. Shimp D.A. and W.M.Craig. *New liquid dicyanate monomer for rapid impregnation of reinforcing fibers.* 34th International SAMPE Symposium, 1336-46, May 8-11, 1989

6. Hamerton I. *Chemistry and Technology of Cyanate Ester Resins.* Blackie Academic and Professional Press; London, 1994; chapter 3

7. Hamerton I., J.M.Barton, A.Chaplin, B.J.Howlin, S.J.Shaw. The development of novel functionalised aryl cyanate esters. Part 2. Mechanical properties of the polymers and composites. Polymer 2001;42:2307-19.

8. Shimp D.A., J.R.Christenson and S.J.Ising. *Cyanate esters-an emerging family of versatile composite resins.* 34th International SAMPE Symposium, May 8-11, 1989

9. Fang T. and D.A. Shimp, *Polycyanate esters: Science and applications*, Progress in Polymer Science 1995;20:61-118.

10. Hamerton I., J. M. Barton, A. Chaplin, B. J. Howlin, S. J. Shaw. *The development of novel functionalized aryl cyanate esters. Part. Mechanical properties of the polymers and composites.* Polymer 2001;42:2307-19.

CHAPTER 4: CATALYSIS AND HYDROLYSIS OF LECY

For the synthesis of the *in-situ* sequential IPNs based on CE and BMI, a primary concern in obtaining optimum structure is to prevent the formation of the second network (BMI-AMP) during the polymerization of the first network (CE). In this work, bisphenol E based cyanate ester (LECY) was selected because it is liquid at room temperature and therefore was thought to provide good processibility for BMI compared to other common CEs that are of higher viscosity and solid at room temperature.

In this chapter, several important factors influencing the reaction of LECY in the presence of BMI and AMP are explored. These include: (1) the influence of catalyst on conversion, (2) the influence of the catalyst and LECY on the stability of the monomers (BMI, AMP) used for second network formation, and (3) the influence of processing conditions on LECY polymerization in the presence of monomers used for second network formation. Thus the appropriate catalyst composition and processing conditions for the preparation of sequential IPNs are established.

Additionally, the influence of catalyst selection on the hydrolysis behavior of CE was investigated. This is important because the performance characteristics of the IPNs will be influenced by the long-term behavior of the first network.

4.1 Experimental

4.1.1 Materials

4.4'-ethylidene diphenyl cyanate ester (LECY) was obtained from Lonza, Inc. and was used as received. Copper (II) naphthenate and Copper (II) acetylacetonate were obtained from the Shepherd Chemical Company. Dibutyl tin dilaurate (DBTDL) was purchased from Aldrich Chemicals. Figure 4.1 gives the chemical structures of these materials. The amount of catalyst was based on the metal concentration in the sample mixtures.

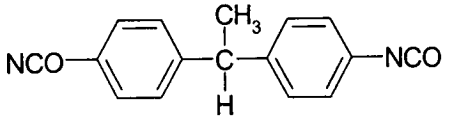

4.4'-ethylidene diphenyl cyanate ester (LECY)

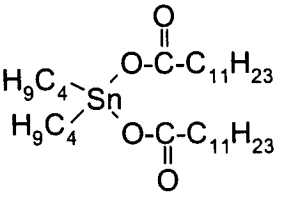

dibutyl tin dilaurate (DBTDL)

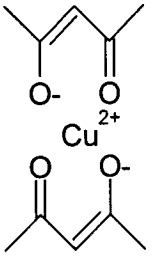

Copper (II) acetylacetonate

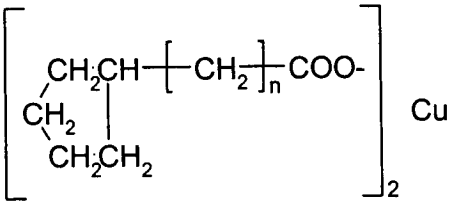

Copper (II) naphthenate

Figure 4.1 Chemical structures of LECY and selected catalysts for LECY cure.

4.1.2 Instruments

Dynamic mechanical analysis (DMA) was performed to measure the Tg and to conduct thermal cycling of cured LECY samples using a TA Instruments DMA 2980 at a frequency of 1 Hz. Heating rate of 5°C/min or 10°C/min was used in different experiments as indicated. Specimens of nominal dimensions 33×11×3.2 mm^3 were tested using a single cantilever beam loading configuration.

Differential scanning calorimetry (DSC) was performed at a heating rate of 10°C/min using Perkin Elmer DSC 7 to obtain information regarding the cure behavior of these systems. The typical sample size was 8 mg, the samples were placed in sealed aluminum pans, and testing was conducted using a nitrogen purge gas.

Fourier transform infrared spectroscopy (FTIR) was used to monitor the concentration change of –OCN and C=C functionality during the cure process of the resin in order to investigate the influence of catalysts on reactivity and to determine the optimum processing conditions for LECY cure. A Thermo Nicolet Nexus 670 FTIR spectrometer was used. Mid IR experiments were conducted in transmission mode at 4 cm^{-1} resolution with 32 scans per data point. Near IR spectroscopy with a resolution of 16 cm^{-1} was used to measure the hydrolysis associated with fully cured LECY exposed to water and thermal cycling.

4.1.3 Preparation of LECY samples and hydrolysis study

Blends of different concentrations of catalyst and LECY were mixed in 100 ml capped polypropylene bottles with a rectangular bottom at 100°C until the catalyst was

fully dissolved. The liquid mixture was processed in an oven according to the conditions shown as Table 4.1.

Table 4.1 Cure conditions for LECY sample for thermal cycling and water uptake.

Catalyst amount	Cure condition
150 ppm Sn^{4+}	105°C (48hrs) + 130°C (2hrs)
*150 ppm Cu^{2+}	145°C (16hrs) + 165°C (8hrs)
300 ppm Sn^{4+}	105°C (5hrs) + 130°C (2hrs)
300 ppm Cu^{2+}	105°C (5hrs) + 130°C (2hrs)
600 ppm Sn^{4+}	105°C (5hrs) + 130°C (2hrs)
600 ppm Cu^{2+}	105°C (5hrs) + 130°C (2hrs)
0 ppm	180°C (25hrs)

* 150 ppm Cu^{2+} cannot make LECY cure at 105°C after a long time that cure temperature has to be elevated.

The size of the samples used for the hydrolysis investigation was the same as that used for DMA evaluation, which was nominally 33×11×3.2 mm^3. The dimensions of these samples did not vary by more than 0.1mm. The samples were placed in a round bottom flask containing deionized water equipped with a reflux funnel, which was placed in an oil bath for conditioning at 70°C for 5.5 hours. Following water uptake, the samples were dried at 105°C for 1 hour and weighed. FTIR measurements were conducted to obtain information regarding composition change and DMA analysis was used to follow changes of Tg resulting from hydrolysis.

4.1.4 Water uptake study

After cure and postcure by DMA, the specimens were dried at 105 °C until a constant weight was obtained prior to immersion in boiling deionized water as discussed in the previous section. Water uptake was recorded by weighing the sample after predetermined exposure times. The percentage gain after a measurement was calculated by the following equation:

$$\text{Water uptake} = (W - W_0)/W_0 \times 100\% \qquad 4.1$$

where W_0 and W denote weights of dry and immersed samples respectively.

4.2 Results and Discussion

4.2.1 Catalysis by metal and the influence of AMP on the conversion of LECY

It is generally accepted that the rate of the cyclotrimerization of cyanate monomers is catalyst-dependent [1]. During commercial processing of cyanate resins, coordination metals are usually used as catalysts and phenols as co-catalysts [2]. The role of the transition metal compound is to gather groups via coordination into ring-forming proximity, while the hydroxyl donates a proton for imidocarbonate formation and step transfer [3]. The ranking of metal ions effectiveness for catalyzing is generally Cu^{2+}~Co^{2+}>Zn^{2+}>Mn^{2+}>Fe^{3+}>Al^{3+} [1]. Two widely used catalyst systems are copper acetylacetonate with nonylphenol and copper naphthenate with nonylphenol. The metal type has a relatively minor effect on the degree of conversion, while the nonylphenol concentration has a significant effect in this regard [4, 5]. This is believed to be because

of the accelerating effect of the phenol group on the formation of the triazine ring along with the plasticizing effect of the nonyl group which retards vitrification. Besides these advantages, the presence of nonylphenol can also be beneficial to the dispersion of copper naphthenate in cyanate ester resin. However, the existence of the nonyl group is detrimental to the final Tg as was reported by Shimp [6]. The detrimental influence of vitrification on conversion of LECY at relatively low temperature can be overcome by the introduction of a reactive diluent. It was found in our study that AMP increases the conversion of LECY greatly under certain conditions. Figure 4.2 demonstrates this effect for a 50 wt.% LECY/50 wt.% BMI and AMP (molar ratio 1:2) mixture. Compared to pure LECY, the increase in conversion is dramatically higher. The reactions were carried out at 110°C. The reason for the greater conversion is the plasticizing effect of the AMP/BMI added to the system. Meanwhile, the dispersion problem of copper naphthenate can also be solved by mixing it with AMP first. Moreover, the second stage polymerization of AMP with BMI which leaves practically no residual AMP diluent eliminates the plasticizing effect associated with nonylphenol. It was also found that AMP aids the dispersion of catalyst by first dissolving the catalyst in AMP.

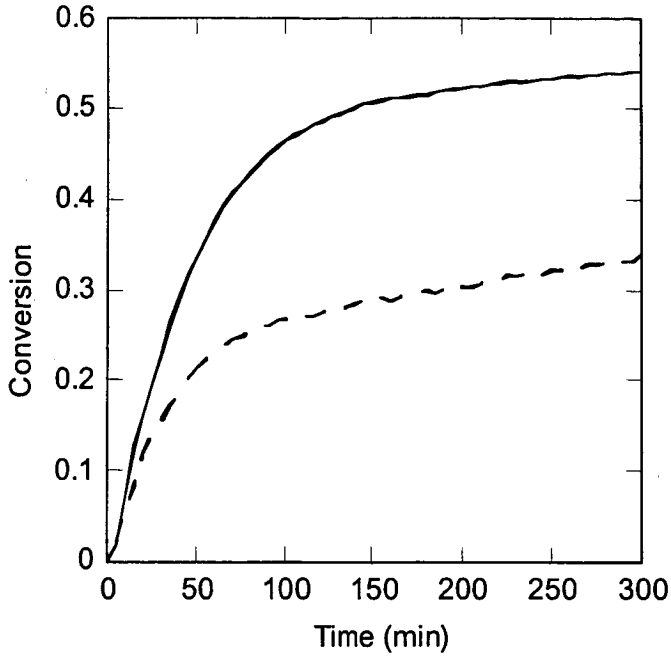

Figure 4.2 Influence of AMP on the conversion of LECY with 600 ppm Cu^{2+}: (—) 50 wt.% LECY 50 wt.% BMI and AMP (molar ratio 1:2), (----) pure LECY. Reaction temperature is 110°C.

4.2.2 Influence of catalyst on BMI and AMP stability

Adding catalyst is expected to catalyze the cure of LECY thus allowing the reaction to occur around 100°C. It is designed so that the stability of BMI should be maintained at this temperature in order to eliminate potential interference of the two reaction mechanisms needed for the formation of the sequential IPNs. Copper acetylacetonate was found not to be a good catalyst. It was apparent that adding copper acetylacetonate leads to a dramatic reaction of BMI and AMP within the first 10 minutes. This is believed to be the result of the double bond of acetylacetonate initiating reaction with BMI and AMP through a donor-acceptor mechanism. This suggestion was tested by mixing AMP and copper acetylacetonate together at 100°C, and again observing a rapid

reaction. For comparison, copper naphthenate, which does not have a double bond, was added to the mixture of BMI and AMP, and as seen in the Figure 4.3 thermogram, no obvious reaction was observed. Copper naphthenate was selected in this study as a catalyst for the LECY cure to ensure the proper synthesis of sequential IPNs based on LECY and BMI/AMP.

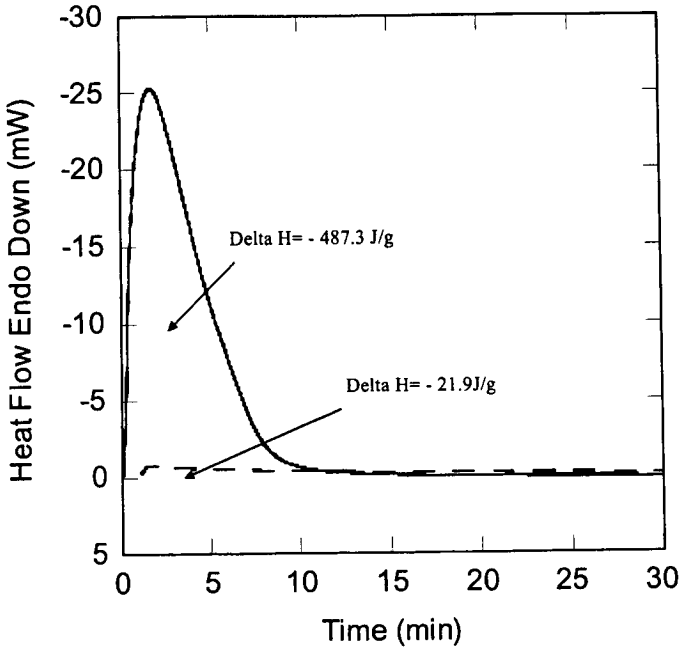

Figure 4.3 Isothermal DSC thermograms for a mixture of BMI and AMP (1:4 molar ratio) with 600 ppm Cu^{2+} catalyst at 110°C. (—) copper acetylacetonate, (---) copper naphthenate.

Another factor that was observed to affect the stability of BMI was the mixing sequence of components that constitute the resin system. It was found that when adding the catalyst to a mixture of LECY, BMI and AMP at 110°C, the mixture would undergo a dramatic reaction resulting in gelation within several minutes making further processing

impossible. For comparison, if the catalyst were first mixed with LECY at 110°C and after the color of solution changes from yellow to deep green, BMI and AMP is added; the resulting solution remains in the liquid state and stable for a long time prior to the occurrence of gelation resulting from the cure of LECY. Therefore, an ample processing window can be provided by this procedure. The difference in outcomes resulted from the difference in mixing sequence. A possible explanation for this is that when the catalyst is mixed with LECY, a complex may be formed that prevents the interaction of the catalyst with BMI and AMP. Experiments with dibutyl tin dilaurate (DBTDL) as a catalyst were carried out using FTIR to observe the influence of mixing order on specific reactions. The reason for selecting DBTDL as a catalyst was its low activation energy in catalyzing the LECY polymerization resulting in a more pronounced catalyzing effect. Figure 4.4 and 4.5 give temporal variations in reaction mixture composition for the case where the catalyst is mixed to the mixture of LECY-BMI and where the catalyst is first added to LECY alone respectively.

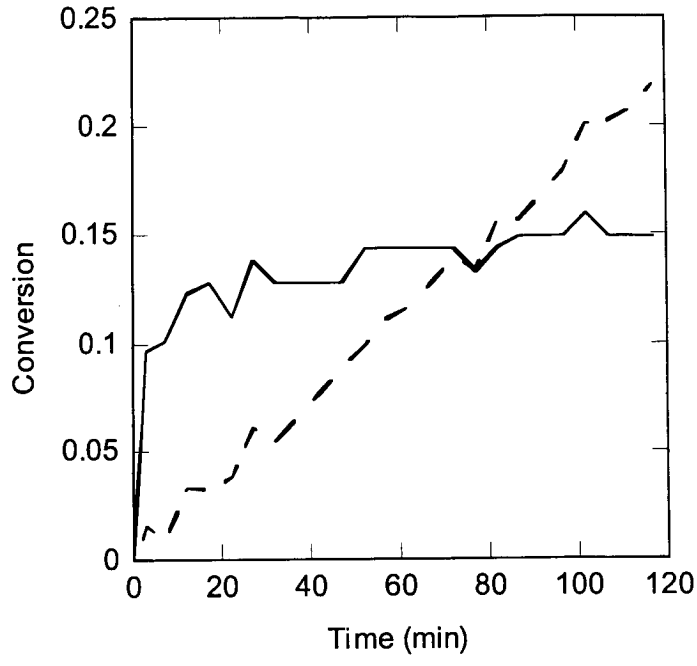

Figure 4.4 Mixing catalyst, BMI, and LECY (75 wt.% LECY, 25 wt.% BMI, and 0.1% DBTDL) at the same time at 130°C. (—) C=C of BMI, (---) –OCN of LECY.

Comparing these figures, it was observed that when mixing the catalyst with LECY first, the conversion of BMI C=C was limited, whereas the conversion of the –OCN group of LECY increased greatly during the same period. More importantly, the dramatic reaction of BMI C=C in the initial stages shown in Figure 4.4, believed to be the reason of the "rapid gelation", was eliminated.

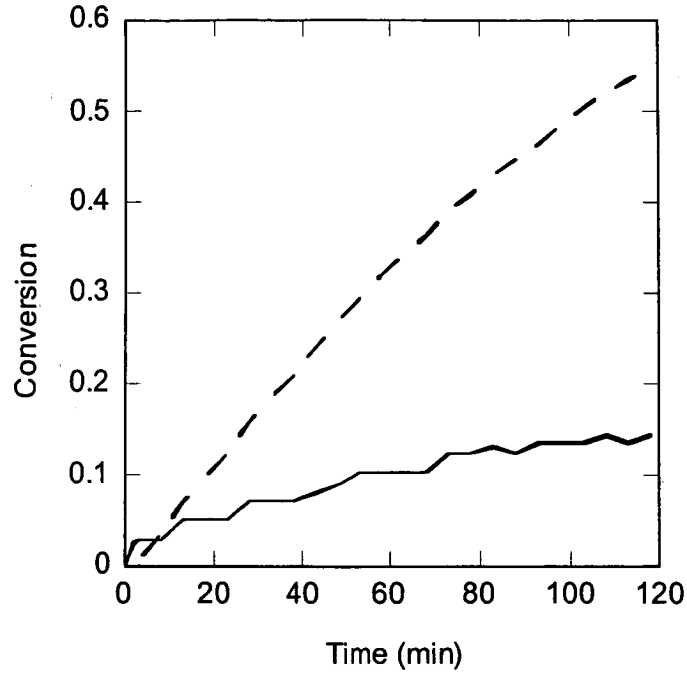

Figure 4.5 Mixing LECY and catalyst first and adding BMI consequently (composition same to that of Figure 4.4) at 130°C. (—) C=C of BMI, (---) –OCN of LECY.

On the other hand, Figure 4.6 shows that without catalyst, when heating the mixture of BMI and LECY (weight ratio 1:3) at 130°C, there is a dramatic reaction of BMI C=C in the initial stages of the process whereas there is almost no change of –OCN concentration from LECY during 2 hours of reaction. It was observed that when heating the mixture of BMI and LECY at 130°C, the resin system gelled after some time. Based on the results shown in Figure 4.6, it can be concluded that this gelation is the result of the reaction of BMI C=C.

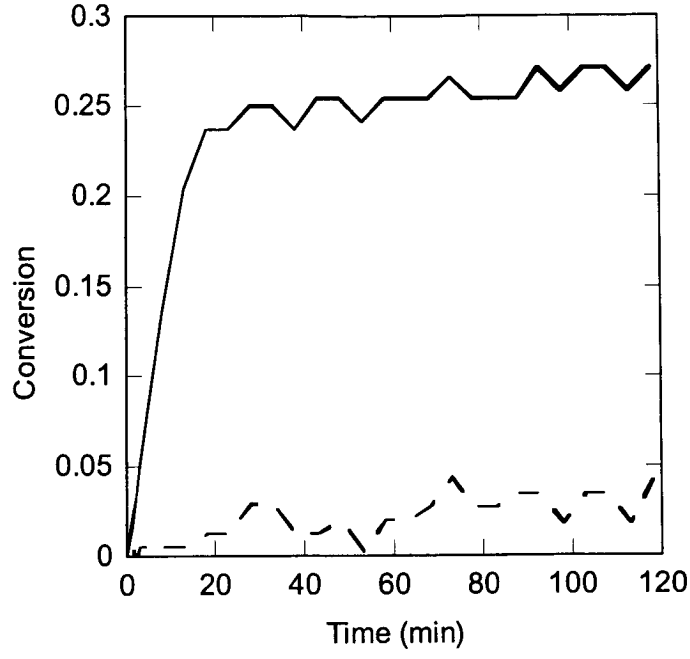

Figure 4.6 Heating the mixture of BMI and LECY (weight ratio 1:3) at 130°C for two hours. (—) C=C of BMI, (---) –OCN of LECY.

In summary, comparison of the results of Figures 4.4, 4.5, and 4.6, suggests that the presence of catalyst, accelerates the reaction of LECY cyanate groups while retarding the reaction of BMI C=C; moreover, the extent of this behavior is highly dependent on the catalyst mixing sequence.

4.2.3 Influence of catalyst on the thermal degradation and hydrolysis of LECY

Hydrolysis can be a serious problem associated with the use of cyanate esters. Figure 4.7 illustrates the mechanism of cyanate ester hydrolysis which was suggested as early as 1974 [7-8] and has been widely cited [9].

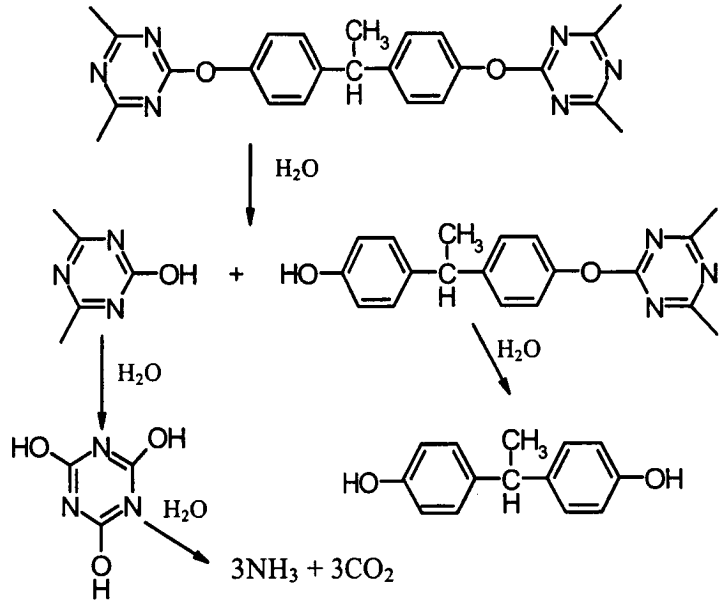

Figure 4.7 Scheme for the proposed degradation of the network by hydrolysis of the ester bond followed by hydrolysis of cyanuric acid to ammonia and carbon dioxide.

It is apparent from the degradation scheme in Figure 4.7 that hydrolysis leads to the fracture of the backbone chain of the polycyanurate. Thus the properties of the cured resin would be unavoidably damaged after hydrolysis, particularly its mechanical properties and Tg. In our study, the effect of hydrolysis on the Tg of cured LECY was investigated in connection with the amount and type of the catalyst. It was reported that Co^{2+}, Cu^{2+} and Mn^{2+} exhibited minimal acceleration of the hydrolysis reactions [3]. DBTDL was thought to be another promising catalyst that possesses minimal acceleration in the hydrolysis of cyanate ester [10]; if that assertion is true, DBTDL would be an ideal candidate for the cyanate ester cure because it combines low activation

energy for polymerization with low propensity for hydrolysis as well as good solubility in LECY. The effect of DBTDL and copper naphthenate catalyst and their concentrations on the hydrolysis of LECY were therefore investigated. The DMA loss modulus spectra of cured LECY catalyzed by copper and tin catalysts in a concentration of 300 ppm are shown in Figure 4.8 and Figure 4.9 respectively. The curves correspond to the thermal cycling and water exposure. The peak position of the loss modulus curves was taken to be the glass transition temperature. The result indicates that tin is a more effective catalyst than copper for polymerization of LECY. This is reflected by the difference in the 1st run peak position after pre-cure under the same conditions. The ultimate Tgs of the fully cured LECY in connection with these two catalysts also exhibited marked differences. The Tgs obtained using copper was much higher than that of tin. Several reasons may account for this phenomenon: (1) the rapid cure of tin catalyzed systems may lead to poor polycyanurate network structure of LECY; (2) the decomposition of LECY at high temperatures may be accelerated more significantly by tin.

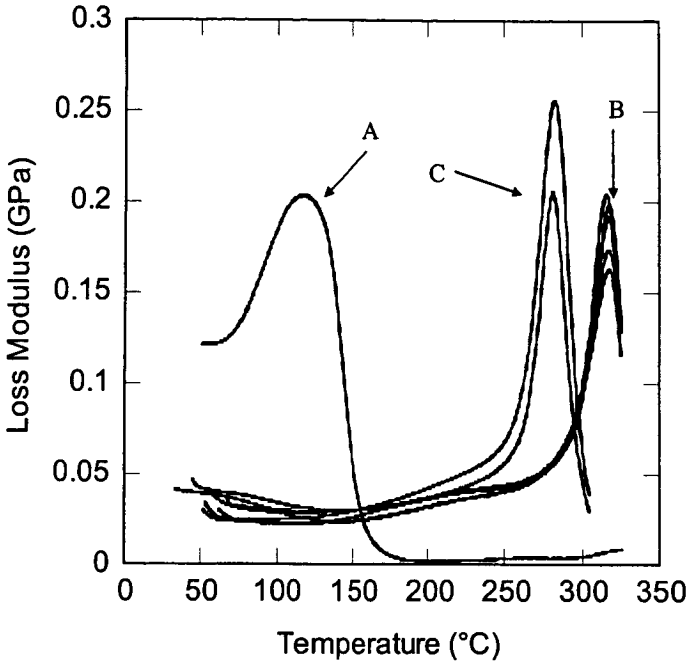

Figure 4.8 Dynamic mechanical spectra of the 300ppm Cu^{2+} catalyzed LECY with three sets of peaks corresponding to (A) 1st run after pre-cure, (B) consecutive thermal cycling in DMA, and (C) after water exposure at 70°C for 5.5 hours. Scan to 330°C at a ramping rate of 10°C/min.

Besides lower Tg, it was found that the curves of tin catalyzed LECY exhibited a broader peak compared to the copper catalyzed LECY. This peak behavior is more pronounced after water uptake, which may suggest the formation of a more heterogeneous network structure in connection with tin as a catalyst. It was also observed that for the 300ppm tin catalyzed sample, after water uptake and subsequent DMA scanning to 330°C, bubbles were formed in the sample that could be easily peeled off, which suggests the production of gas after hydrolysis as suggested by the mechanism in Figure 4.7. The lower Tg of 238°C was the consequence of the hydrolysis induced by the presence of water and high temperature. A similar decrease of Tg was observed for copper catalyzed systems after water uptake and heating.

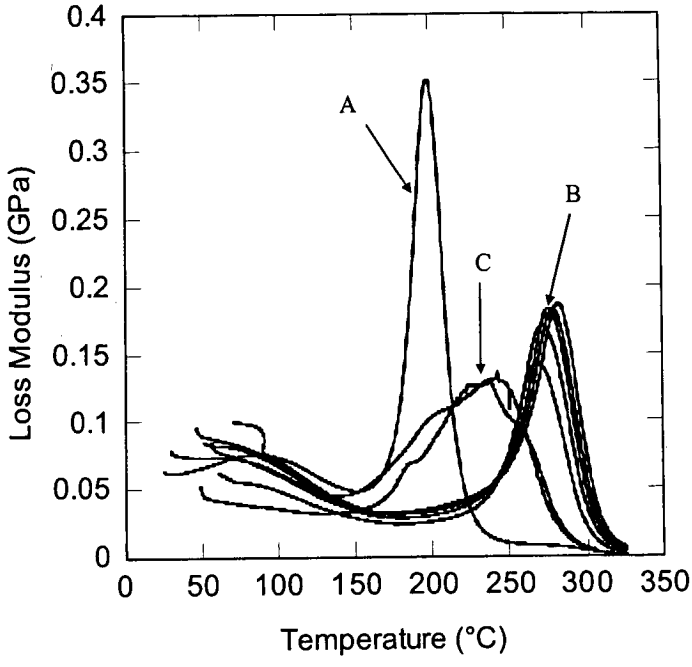

Figure 4.9 Dynamic mechanical spectra of the 300ppm Sn^{4+} catalyzed LECY with three sets of peaks corresponding to (A) 1st run after pre-cure, (B) consecutive thermal cycling, and (C) after water exposure at 70°C for 5.5 hours. Scan to 330°C at a ramping rate of 10°C/min.

To gain a better understanding of the influence of catalyst concentration on the cure reaction as well as on the hydrolysis of LECY, experiments with varying concentrations of catalyst were conducted. The influence of thermal cycling and water exposure on Tg obtained from dynamic mechanical behavior are summarized in Table 4.2. These values correspond to the peak position of the DMA spectra such as those in Figure 4.8 and 4.9 for 300 ppm catalyst loading. The first scan corresponds to the material following pre-cure, scans 2-6 are from repeated scans to 310°C at 10°C/min. Scan 7 and 8 are repeated scans after exposure of the samples to water as described earlier. Note that the initial cure condition (run 1) was different for the uncatalyzed system which required an initial cure temperature of 180°C for reaction.

Figure 4.10 and 4.11 are plots of the data in Table 4.2. From these data it is clear that the degree of cure increases with an increase in the amount of catalyst for either catalyst. LECY cured by 150 ppm tin showed the highest Tg of 320°C compared to the other systems with higher concentrations of catalyst or with copper as catalyst. With increasing scans (i.e. high temperature exposure), for 0 ppm and 150 ppm there is a slight decreasing trend in Tg; for 300 ppm and 600 ppm there is an increasing trend in Tg. The significantly lower Tg obtained with the higher concentration of tin suggests the more serious decomposition reaction associated with high concentrations of tin.

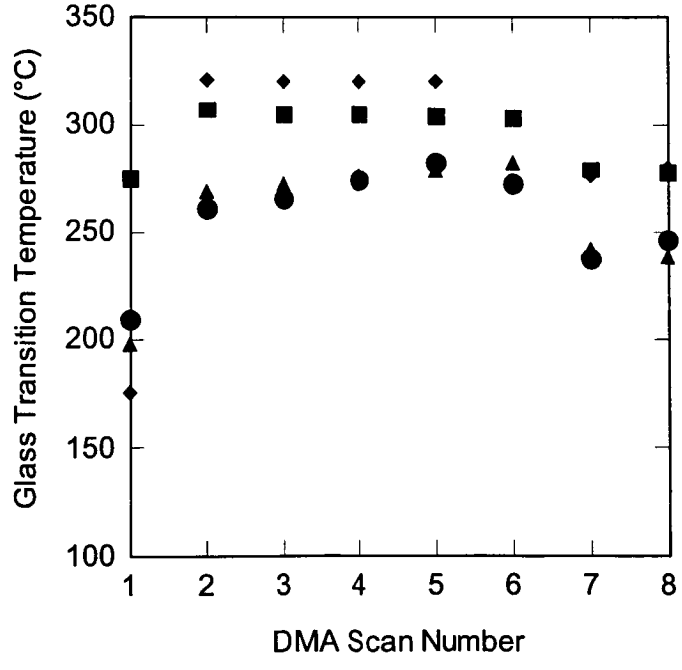

Figure 4.10 Glass transition temperature changes of Sn^{4+} catalyzed LECY during thermal cycling and water exposure. (■) 0 ppm, (♦) 150 ppm, (▲) 300 ppm. (●) 600 ppm.

However, these trends areis not as significant in the copper catalyzed LECY, even though higher concentration of copper will also lead to lower Tgs. Also, the cycles needed to reach maximum Tg are less for the tin catalyzed LECY except for high catalyst concentrations which may be inducing decomposition reactions. This observation is in agreement with the purported lower activation energy of the tin catalyst system.

Compared to the catalyzed systems, the non-catalyzed LECY, exhibited a lower Tg after full cure and a more pronounced decrease resulted from the thermal cycling. This suggests that a poor structure was formed without the presence of the catalyst and that such structures may be susceptible to decomposition.

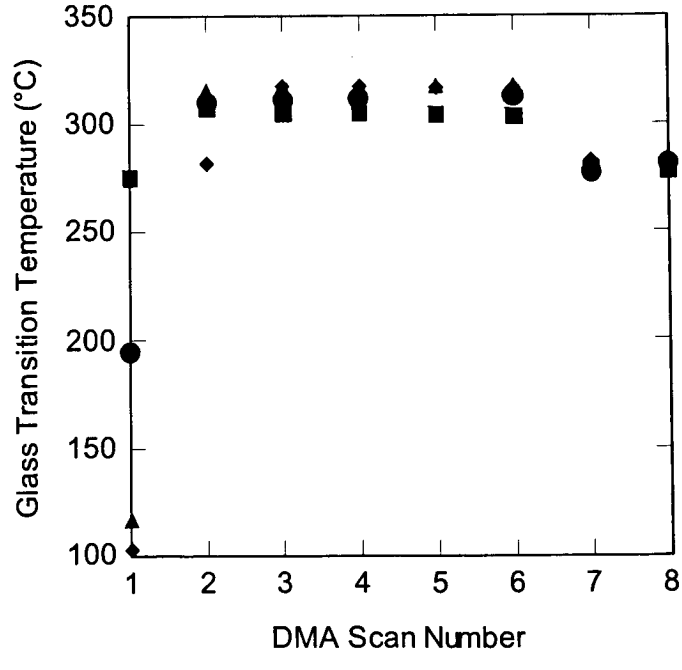

Figure 4.11 Glass transition temperature changes of Cu^{2+} catalyzed LECY during thermal cycling and water exposure. (■) 0 ppm, (♦) 150 ppm, (▲) 300 ppm, (●) 600 ppm.

Table 4.2 Glass transition temperature values after thermal cycling and water uptake with respect to catalyst amount, species.

Amount	1st run	2nd run	3rd run	4th run	5th run	6th run	water 7th run	water 8th run	down
0 ppm	275°C	307°C	305°C	305°C	304°C	303°C	279°C	278°C	25°C
150ppm Cu	102°C	282°C	317°C	317°C	316°C	316°C	282°C	283°C	33°C
150ppm Tin	176°C	320°C	320°C	320°C	320°C	319°C	276°C	280°C	39°C
300ppm Cu	116°C	316°C	317°C	317°C	317°C	317°C	281°C	283°C	34°C
300ppm Tin	198°C	269°C	272°C	276°C	279°C	283°C	242°C	238°C	45°C
600ppm Cu	195°C	310°C	311°C	312°C	312°C	312°C	277°C	281°C	31°C
600ppm Tin	210°C	261°C	266°C	274°C	282°C	272°C	238°C	246°C	26°C

Based on the above discussion, it is concluded that for the cure of LECY, there exists a competition between polymerization and decomposition resulting in an optimum high temperature time of cure.

The deterioration of structure resulting from hydrolysis is another factor that leads to the decrease in Tg which is also shown clearly in Figure 4.10 and 4.11, based on data given in Table 4.2. After exposure to water, in all cases there is a dramatic decrease Tg which is not recovered upon reheating. This suggests that the changes are permanent chemical changes and not physical plasticization effects. With the increase of the amount of catalyst, the tendency is more pronounced for tin catalyzed LECY, whereas the drop in Tg after water uptake is uniform for LECY catalyzed with copper at different concentrations. Combined with the cure process, there is a clear trend showing that the final Tg will decrease with the increase of catalyst, particularly for tin catalyzed LECY. The non-catalyzed system exhibited less decrease in Tg due to water exposure; nevertheless, the final Tgs of the copper catalyzed system are still higher than non-catalyzed system.

The mechanisms regarding loss of Tg due to the thermal cycling to 330°C and water uptake were investigated by FT-NIR in combination with TGA. The results are shown in Figure 4.12 for a series of NIR spectra taken at various stages of cure and exposure to water and temperature of LECY catalyzed using 300 ppm tin. These stages include: (a) cure at 105°C for 5 hours followed by cure at 130°C for 2 hours, (b) six DMA scans to 330°C at 10°C/min, (c) water uptake at 70°C in water for 5.5 hours, (d) drying at 105°C for one hour and (e) after 1 DMA scan following drying. Thermal cycling leads to a small OH peak (7000 cm^{-1}) but no water peak is observed. Water

uptake leads to a significant amount of water absorbed by the resin, as reflected in the water peak at 5250 cm^{-1}, along with a slight increase of the hydroxyl peak. After one hour drying at 105°C, there was still a significant amount of water in the resin suggesting that more time was needed to dry the sample at this temperature. Following a thermal scan to 330°C, the water peak disappeared and the hydroxyl peak increased. Hence water hydrolyzed the LECY. The disappearance of the water could also be partially attributed to evaporation. This observation proved that water absorbed in resin can result in the hydrolysis of the polycyanurate chain.

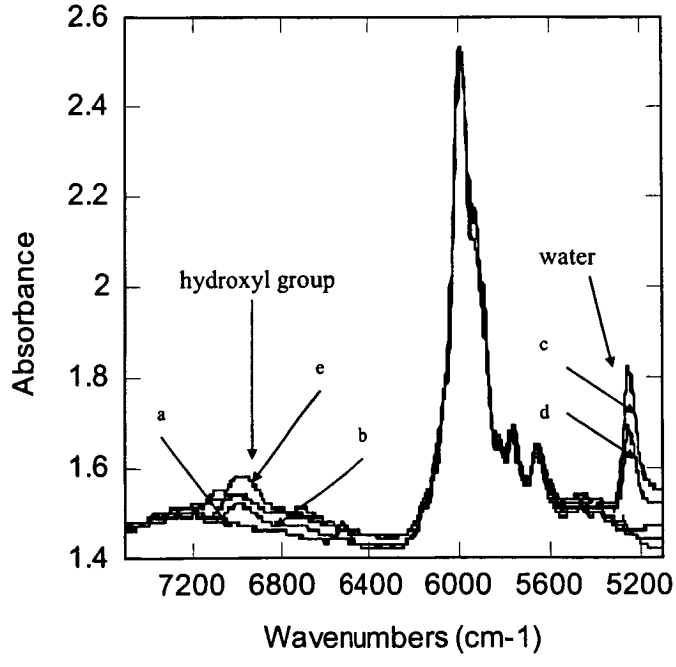

Figure 4.12 Different stage of 300 ppm tin catalyzing LECY cure monitored by FT-NIR. (a) cure @ 105°C (5hrs) + 130°C (2hrs), (b) 6 DMA runs up to 330°C, (c) water uptake @ 70°C (5.5hrs), (d) water uptake @ 70°C (5.5hrs) and drying @ 105°C (1hr), (e) DMA run after drying @ 105°C (1hr).

This conclusion is collaborated in Ramirez [11] who states that thermoxidative degradation proceeds via rapid hydrolysis of the ether oxygen bond between the phenyl and triazine rings in the presence of moisture at temperatures of 350-420°C, and by the work of Korshak [8, 12, 13]. However, our study shows that this kind hydrolysis can occur even around 330°C.

4.2.4 Comparison of water uptake behavior of LECY and BACY

In the preceding section, the hydrolytic decomposition of the cyanate ester — LECY was observed. It was found that this material absorbs water and that upon moderate heating the water can participate in hydrolysis of the cyanate ester. It is therefore important to understand how much water cyanate esters absorb and if the cyanate ester type influences the decomposition behavior.

The water absorption behavior of LECY and BACY (chemical structure see Figure 3.3) cured using no catalyst, 150, 300, and 600 ppm Cu^{2+} catalyst was investigated by measuring the % weight increase of samples of constant dimensions (33 mm × 11mm × 3.2 mm) conditioned in boiling water. The chemical difference between LECY and BACY is an additional methyl group on the backbone of the monomer. BACY is used in many commercial formulations. Figure 4.13 and 4.14 show the water uptake behavior for LECY and BACY systems respectively. Figure 4.15 combines the data for LECY and BACY systems. The water absorption behavior of both systems is very similar. Weight gain approaches equilibrium after 80 hours of exposure to boiling water and an equilibrium water uptake ranging from 2.5~2.7 wt.% was observed for all systems. The uncatalyzed systems absorb slightly more water.

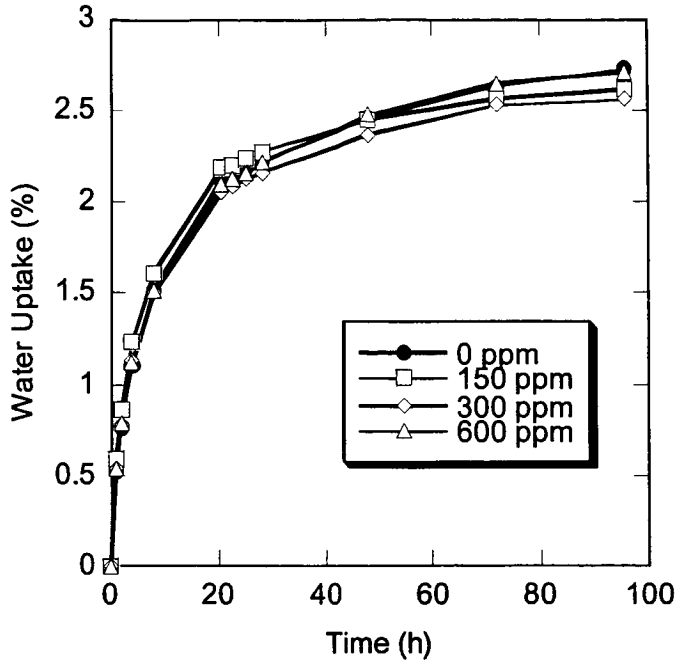

Figure 4.13 Water uptake profile of LECY with different amount of Cu^{2+}.

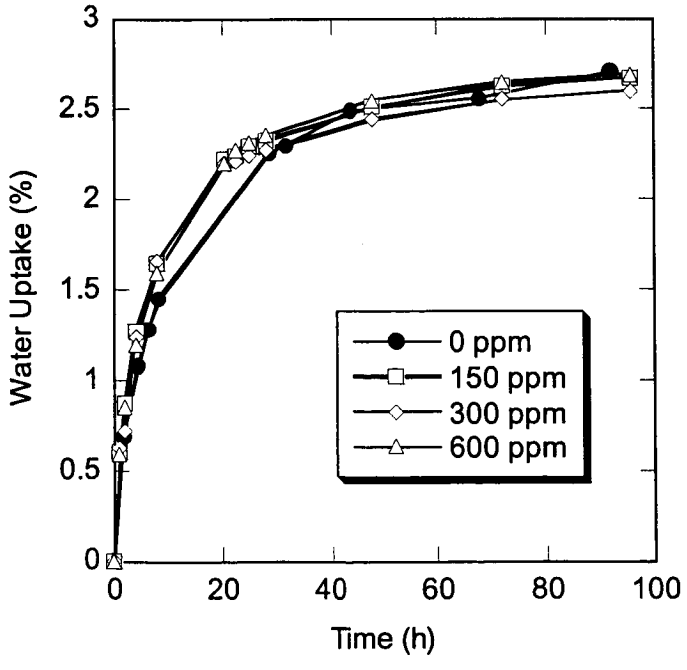

Figure 4.14 Water uptake profiles of BACY with different amount of Cu^{2+}.

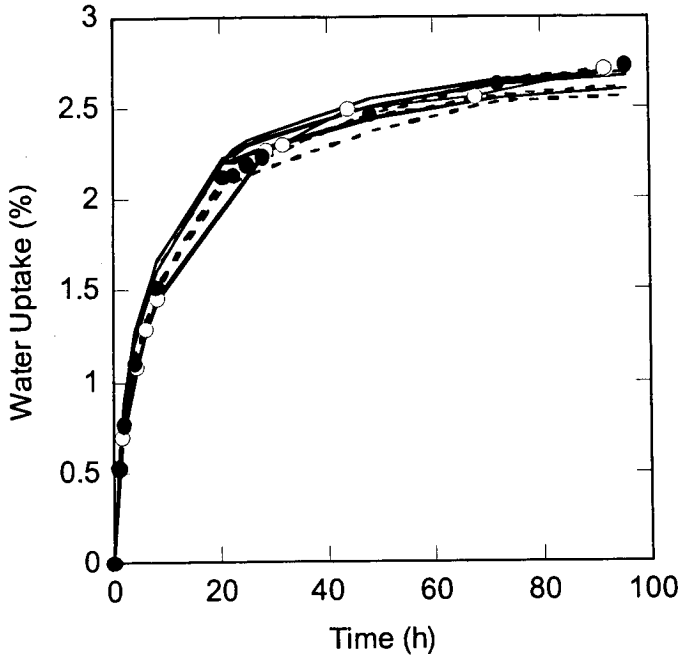

Figure 4.15 Water uptake profiles of LECY and BACY with different amount of Cu^{2+}.

The following analysis provides a rough estimate of the water diffusion coefficient (D) in the cyanate ester resins. The most common approach to modeling water diffusion is to consider Fick's law applied to simple-free-phase diffusion [14]. After a series of deductions, the initial absorption for an infinitely large plate is given by Springer as:

$$\frac{M_t}{M_\infty} = \frac{4}{h}\left(\frac{Dt}{\pi}\right)^{0.5} \qquad 4.2$$

where M_t is the mass of water absorbed at time t, M_∞ is the mass of water absorbed at saturation, and h is the thickness of specimen [15].

In this work, Equation 4.2 was employed to estimate the initial diffusion coefficient ignoring edge effects. The values of M_t/M_∞ as a function of $t^{0.5}/h$ are plotted in Figure 4.16.

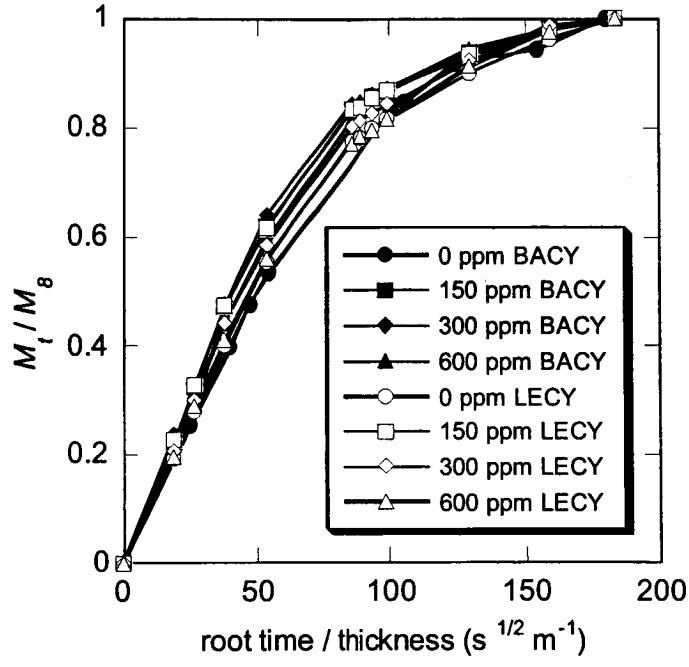

Figure 4.16 Water uptake profiles of LECY and BACY plotted as M_t/M_∞ versus [(square root of time/thickness)] at different concentrations of Cu^{2+}.

It can be observed from Figure 4.16 that at the initial stage, M_t/M_∞ has a linear relationship with $t^{0.5}/h$. Based on the slopes of the lines, D_{ini} can be obtained. The calculated D_{ini} values are summarized in Table 4.3.

Table 4.3 D_{ini} of LECY and BADCY in water uptake for different Cu^{2+} concentrations.

Cyanate ester	Cu^{2+} concentration (ppm)	D_{ini} (mm^2/s)
LECY	0	2.06×10^{-5}
LECY	150	2.87×10^{-5}
LECY	300	2.43×10^{-5}
LECY	600	2.19×10^{-5}
BADCY	0	2.07×10^{-5}
BADCY	150	2.85×10^{-5}
BADCY	300	3.18×10^{-5}
BADCY	600	2.67×10^{-5}

It can be concluded that at the initial stage of water uptake of LECY and BADCY, specimens without catalyst possess the lowest diffusion coefficient.

The decrease in Tg resulted from hydrolysis was compared for these two types of cyanate esters with results showing in Figure 4.17. It was found LECY possessed higher Tg after water uptake even though its Tg is lower than BADCY after fully cure, which shows BADCY suffered from water exposure more severely than LECY.

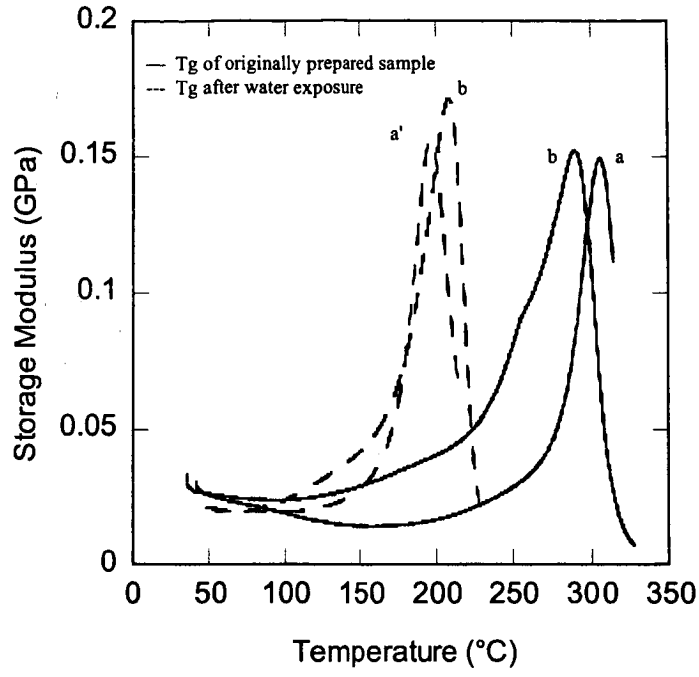

Figure 4.17 Tg change after water uptake for LECY and BADCY without catalyst. (a, a') BADCY with 0 ppm Cu^{2+}, (b, b') LECY with 0 ppm Cu^{2+}.

4.2.5 Determination of processing conditions — LECY cure kinetics

The reaction kinetics of both the uncatalyzed and the metal-catalyzed cure of cyanate esters can be adequately described by the semi-empirical model suggested by Simon [16].

$$d\alpha/dt = k_1(1-\alpha)^2 + k_2\alpha(1-\alpha)^2 \qquad 4.3$$

In the equation, α is the fractional conversion of cyanate group and k_1, k_2 are apparent rate constants. However, it was also pointed out by Dona [17] that in some cases, for both catalyzed and uncatalyzed systems an n^{th} order reaction satisfactorily explains the cure profile. This behavior was observed in many studies [18-21]. In addition, in view

of the high propensity of cyanate esters for catalysis by externally added catalyst, autocatalysis can be neglected in catalyzed systems and the reaction can be considered to follow the classical n^{th} order model given by Equation 4.4 [17]:

$$d\alpha/dt = k(1-\alpha)^n \qquad 4.4$$

Two classical methods for analyzing DSC kinetics data — the Kissenger and Coats-Redfern methods — were derived from the above equation [17, 22]. Both methods were preliminarily adopted in our study to investigate the kinetics of LECY by non-isothermal DSC. DSC results are summarized in Appendix II. Using Kissinger's method it was found that the cure process is a pseudo first order reaction, which is the same as Chen's conclusion for epoxies [23]. However, by the Coats-Redfern (C-R) method, the reaction order was determined to be 1.5. Nair *et al.* found the same number in their study on bisphenol A dicyanate's cure [17]. It was pointed out that Kissinger's method was based upon somewhat erroneous assumptions and theoretical development [24], which might account for the above discrepancy. Another interesting observation found in our study is that the activation energy of reaction, E, decreases linearly with increasing catalyst concentration, as displayed in Figure 4.18. For simplicity, it was assumed that the non-catalyst LECY cure would also follow the classical n^{th} order model, and the measured activation energy of pure LECY is about 133 KJ/mol, which is in the same range with Nair's result, but is much higher than the results determined by Leroy et al. (71 kJ/mol) [25] and Rodriguez-Arnold et al. 49 KJ/mol [26], which were derived by taking the reaction order as two and one respectively. Their results were similar to our

value derived by Kissinger method, which is 66 KJ/mol. Thus, this discrepancy is preliminarily believed to be a result of the different reaction order in kinetics expression equation adopted by different authors. In fact, there seemingly has no agreement on the reaction order. Therefore, further work on the accuracy of the derived kinetic parameters has both theoretical and technological significance.

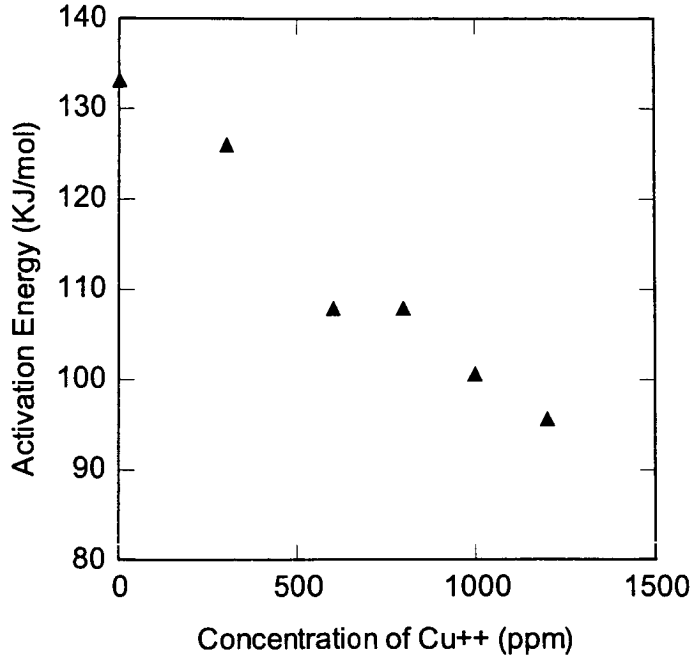

Figure 4.18 Plot of activation energy versus concentration of catalyst.

The amount of catalyst to be used for the synthesis of IPNs was determined based on the above information considering the processing time as well as the conversion of various functional groups in the system. The proper amount of catalyst should ensure the complete conversion of LECY at low temperature and in a short time. Since high temperature and long reaction time would unavoidably increase the conversion of C=C of

BMI and AMP. Acquiring a practical processing window is another factor in determining the parameters for LECY cure. Copper naphthenate was selected as the final choice based on the balance of its influence on the catalysis of polymerization and tempered hydrolysis of LECY polycyanurates. The measures of 0.25% and 0.5% of copper naphthenate based on the whole system weight corresponding to 150 ppm and 300 ppm respectively were adopted.

An FTIR technique was employed to monitor the chemical conversion of various functionalities during the processing of IPN systems catalyzed with 150 ppm and 300 ppm copper naphthenate with the results shown in Figure 4.19 and Figure 4.20 respectively.

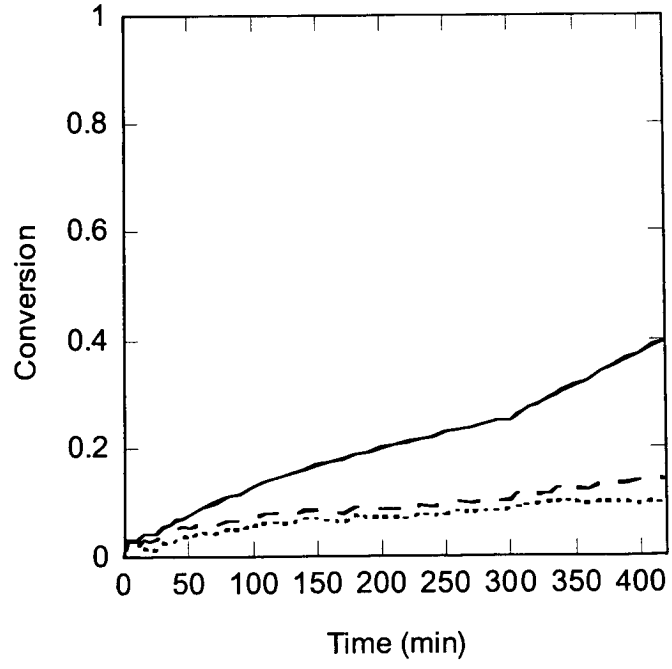

Figure 4.19 Mixture of 70% BMI and AMP (molar ratio 1:2) and 30% LECY with 150 ppm Cu^{2+}. (—) –OCN change, (---) C=C of BMI, (·····) C=C of AMP.

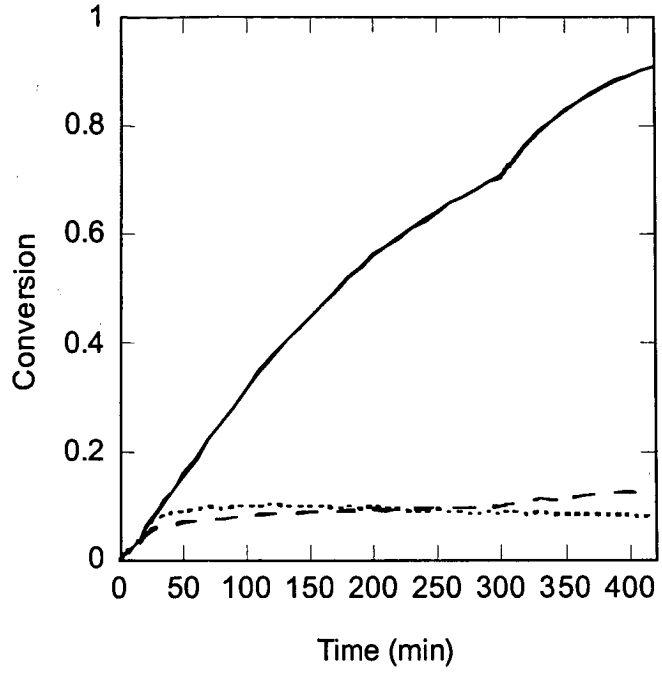

Figure 4.20 Mixture of 70% BMI and AMP (molar ratio 1:2) and 30% LECY with 300 ppm Cu^{2+}. (—) –OCN change, (---) C=C of BMI, (·····) C=C of AMP.

To circumvent the occurrence of excess exothermal heat resulting from the difficulty of heat dissipation associated with the gel formation, two consecutive cure processes with different temperatures, 110°C and 130°C were adopted. The higher temperature of 130°C was used to accelerate LECY cure but still avoid the reaction between BMI and AMP.

It can be concluded that compared to the concentration of Cu^{2+} at 150ppm, a concentration of 300 ppm could provide satisfactory results when combined with processing conditions so after two consecutive cures of 110°C and 130°C, the conversion of LECY can reach 91%, whereas the conversions of C=C of BMI and AMP are just 13% and 8% respectively.

4.3 Summary and Conclusions

As illustrated in Chapter 3, sequential IPNs based on LECY and BMI were successfully synthesized via EB irradiation. However, as a crucial component of the system, the catalyst for the LECY cure would significantly affect the final properties of the IPNs in connection with its marked influence on the processing of system as well as the hydrolysis of the polycyanurate network. Besides its amount and type, it was also observed that the sequence in which the catalyst was added significantly affects the processing behavior. An improper mixing method resulted in a fast gel whereby the processing window was greatly shortened and poor network structure was obtained. The utilization of DMA and FTIR techniques illustrated that thermal cycling to high temperature (330°C) with exposure to water results in hydrolysis of the polycyanurate network. This hydrolysis is accelerated in the presence of catalysts, and more prominent with some metals such as tin. The hydrolysis results in a sharp decrease of Tg and the formation of gaseous products. In our study, copper naphthenate was found to show a pronounced catalyzing effect in the LECY cure while maintaining the stability of both BMI and AMP at moderate temperatures. Moreover, this catalyst minimized hydrolysis of the polycyanurate and was selected for the cure of LECY in the synthesis of sequential IPNs with AMP-BMI. Mixing LECY and the catalyst first to form a complex in the presence of AMP, followed by the addition of BMI, was shown to be a good processing method. Consequently, the catalyst concentration of 300 ppm based on the whole system provides the appropriate balance between processibility and performance.

Additionally, it was found BACY does not demonstrate any advantage over LECY in lessening the hydrolysis resulting from water and thermal exposure. More

cyanate esters need to be investigated to determine if cyanate ester monomer structure can influence this aspect of polycyanurate long term stability .

List of References

1. Hamerton I. and S. Takeda. *A study of the polymerization of novel cyanate ester/acrylate blends.* Polymer 2000;41:1647-56.

2. Yong D. and G.C. Martin. *Diffusion phenomena during cyanate resin cure.* Polymer 1996;37(16):3593-601.

3. Fang T., D.A. Shimp. *Polycyanate esters: science and applications.* Progress in Polymer Science 1995;20(1):61-118.

4. Shimp D.A., J.R. Christenson and S.J. Ising. *Cyanate esters-an emerging family of versatile composite resins.* 34th International SAMPE Symposium, May 8-11, 1989.

5. Osei-Owusu, A., G.C. Martin. *Analysis of the curing behavior of cyanate ester resin systems.* Polymer Engineering and Science 1991;31(22):1604-9.

6. Shimp D.A. and S.J. Ising. *New cyanate ester resin with low temperature (125-200 ℃) cure capability.* 35th International SAMPE Symposium, April 2-5, 1990.

7. Gaku M. *Properties and applications of bisphenol A type cyanate resin.* Polymeric Materials Science and Engineering 1994;71:621-2.

8. Korshak V.V., P.N. Gribkova, A.V. Dmitrenko, A.G. Puchin, V.A. Pnakratov, and S. V. Vinogradova, Thermal and oxidative thermal degradation of polycyanates. Vysokomolekulyarnye Soedineniya 1974;seriya A:16(1):15-21.

9. Kasehagen L.J., I. Haury, C.W. Macosko, and D.A. Shimp. *Hydrolysis and blistering of cyanate ester networks.* Journal of Applied Polymer Science 1997;64(1):107-13.

10. Li W.F., W.L. Xin, G.H. Liang, X.Y. Ma, G.M. Zhu. *Cure reaction of cyanate ester resins and the catalyst.* Hangkong Cailiao Xuebao 2003;23(2):56-62.

11. Ramirez M.L., R. Walters, R.E. Lyon, E.P. Savitski. *Thermal Decomposition of cyanate ester resins.* Polymer Degradation and Stability 2002;78(1):73-82.

12. Korshak V.V., V.A. Pandratov, A.G. Puchin, S.A. Pavlova, I.V. Zhuiavleva, V.G. Danilov, and S.V. Vinogradova. *Effect of the structure of polycyanates produced by the polycyclotrimerization of aryl dicyanates on their thermal stability.* Polymer Science USSR 1975;17(3):554-9.

13. Korshak V.V., S.A. Pavlova, P.N. Gribkova, M.V. Tsirghiladze, V.A. Pandratov, S.V. Vinogradova, P.D. Tsiskarishvili, G.S. Papava. *Study of the decomposition of polycyanates with different structures.* Izvestiya Akademii Nauk Gruzinskoi SSR, Seriya Khimicheskaya 1977;3(1):7-15.

14. Dewimille B. and A.R. Bunsell. *The modeling of hydrothermal aging in glass fibre reinforced epoxy composites.* Journal of Physics D: Applied Physics 1982;(15):2079-91.

15. Shen C. H. and G.S. Springer. Effects of moisture and temperature on the tensile strength of composite materials. Journal of Composite Materials 1977;11:2-16.

16. Simon S.L. and J. K. Gillham. *Cure kinetics of a thermosetting liquid dicyanate ester monomer/high-Tg polycyanurate materials.* Journal of Applied Polymer Science 1993;(47):461.

17. Mathew D., C.P.R. Nair, K. Krishnan, K. N. Ninan. *Catalysis of the cure reaction of bisphenil A dicyanate. A DSC study.* Journal of Polymer Science Part A: Polymer Chemistry 1999;(37):1103-14.

18. Lu M.C. and J.L. Hong. *Cure kinetics and gravimetric analysis of a flexible aromatic dicyanate, cyanated phenylene sebacate oligomers.* Polymer 1994; 35(13):2822-27.

19. Osei-Owusu A., G.C. Martin. Analysis of the curing behaviour of cyanate ester resin systems. Polymer Engineering and Science 1991;31(22):1604-9.

20. Osei-Owusu A., G.C. Martin, J.T. Grotto. Characterization of bisphenol A-based cyanate ester resin systems. Polymeric Materials Science and Engineering 1991;65:304-5.

21. Osei-Owusu A., G.C. Martin, J.T. Grotto. Catalysis and kinetics of cyclotrimerization of cyanate ester resin systems. Polymer Engineering and Science 1992;32(8):535-41.

22. Kissinger H.E.. *Reaction kinetics in differential thermal analysis.* Analytical Chemistry 1957;29(11):1702.

23. Chen P., D.X. Zhang, L.J. Han. *Study of curing and cured compound of rare-earth organometallic compound /anhydride/epoxy resin system.* Acta materials Composite Sinica 1997;14(4):33.

24. Reed R.L., L. Weber, B.S. Gottfried. *Differential thermal analysis and reaction kinetics.* Industrial and Engineering Chemistry Research Fundamentals 1965;4(1):38-46.

25. Dupuy J., E. Leroy, A. Maazouz, J.P. Pascault, M. Raynaud, E. Bournez. *Validation in process-like conditions of the kinetic and thermophysical modeling of a dicyanate ester/glass fibers composite.* Thermochimica Acta 2002;(388):313-25.

26. Rodriquez-Arnold J., F.E. Arnold, R.E. Lyon. *Cure kinetics and thermal degradation of cyanate ester resins.* Recent Advances in Flame Retardancy of Polymeric Materials 1995;(6):80-97.

CHAPTER 5: N-ACRYLOYLMORPHOLINE—A UNIQUE REACTIVE DILUENT FOR BMI COPOLYMERIZATION

5.1 Introduction

EB irradiation can induce the addition polymerization of BMI, and thus aid in the low temperature processing of BMI. At low temperature the crystalline nature of BMI produces low conversion. One issue associated with the use of EB is the selection of an appropriate reactive diluent. Reactive diluents serve two purposes: (1) to improve the processibility of resin at low temperature, and (2) to improve the low temperature conversion of BMI without the use of solvent. The presence of solvent is detrimental to the final properties of the material. As pointed out in section 3.3, the reactive diluent must maintain the chemical stability of BMI at cure temperature during the formation of the first network. In this chapter, reactivity of BMI with a number of reactive diluents under thermal and EB conditions is evaluated. An understanding of the chemical factors that influence the reaction behavior of these co-monomers is developed, and this understanding is used to suggest appropriate reactive diluents for the sequential IPNs of cyanate ester and BMI being developed.

5.2 Experimental

5.2.1 Materials

The chemicals used in this study are as follows: 2-ethylhexyl vinyl ether (EHVE), cyclohexyl vinyl ether (CHVE), allyl phenyl ether (APE), styrene (St), divinylbenzene (DVB), 3-nitrostyrene (NSt), N-acryloylmorpholine (AMP), N-phenylmaleimide (PMI),

and bismaleimide (BMI). All of these were obtained from Aldrich Chemicals and used without further purification. The chemical structures of these materials are given in Figure 5.1.

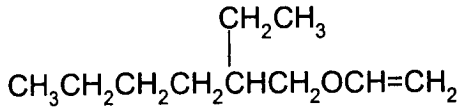

2-ethylhexyl vinyl ether (EHVE)

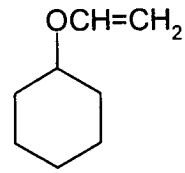

cyclohexyl vinyl ether (CHVE)

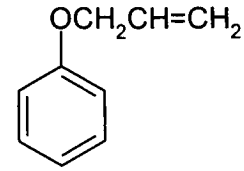

allyl phenyl ether (APE)

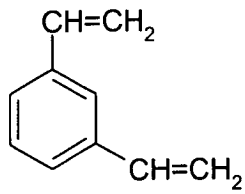

divinylbenzene (DVB)

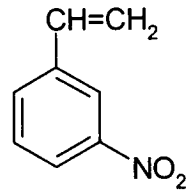

3-nitrostyrene (NSt)

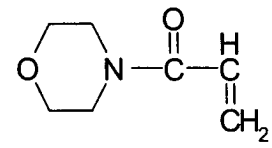

4-acryloylmorpholine (AMP)

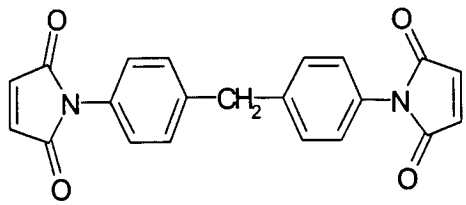

1,1'-(methylenedi-4,1phenylene)-bismaleimide (BMI)

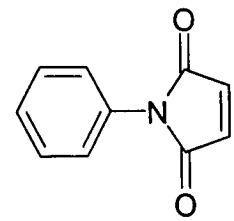

N-phenylmaleimide (PMI)

Figure 5.1 Chemical structures of materials used in current study.

5.2.2 Instruments and methods

A Thermo Nicolet Nexus 670 FTIR spectrometer was used. Mid IR experiments were conducted in transmission mode at 4 cm^{-1} resolution with 32 scans per spectrum. Near IR spectroscopy was also used to investigate the copolymerization parameters of free radical copolymerization with a resolution of 16 cm^{-1}.

Near infrared (NIR) spectroscopy technique was employed to monitor the variation of AMP double bond concentration under EB irradiation. The NIR measurements were performed using a Control Development, Inc. (CDI) infrared spectrometer. The spectrometer possesses a spectral range from 1160 nm to 2250 nm by using T.E. cooled, high performance linear InGaAs array detector. The infrared light was produced by a white light source that was connected to a sample holder by silica fiber optics obtained from RoMack, Inc. The sizes of the fiber core/clad/jacketing in μm were 400/440/465. This is a low O/H silica multicode step index fiber with protective furcation tubing and SMA 905 connectors. The silica fiber connecting the sample holder to the detector was obtained from Thorlabs, Inc. (catalog number FG-200-LCR) and consisted of the same fibers used in the RoMack, Inc. fiber optic cable. A specially designed sample holder was used to align the input and output light with the EB irradiation source so that precise location of the sample in the light path to obtain the optimum signal was possible. Heating elements were used for temperature control.

Differential Scanning Calorimetry (DSC) was performed at a heating rate of 10°C/min using a Perkin Elmer DSC 7 to obtain information regarding the cure behavior of these systems. The typical sample size was 8 mg, and the samples were placed in sealed aluminum pans under a nitrogen purge.

Perkin Elmer — High-Performance Liquid Chromatography (HPLC) with refractive index and UV detectors was used to detect the occurrence of the higher molecular weight materials resulting from EB irradiation.

Viscosity of resin systems as a function of temperature was evaluated using a Brookfield digital viscometer.

5.2.3 Electron beam curing parameters

EB irradiation experiments of vinylethers and AMP as reactive diluents were conducted on a 10 MeV electron beam induction accelerator. The principal parameters for EB cure of vinylethers with PMI were as follows: total dose of 200 kGy was applied to the sample in several passes with a dose for each pass as follows, 10, 20, 20, 50, 50, 50 kGy respectively. The operating parameters for the UDRI 3.5 MeV accelerator that was used to conduct the EB irradiation of AMP or the mixture of AMP and PMI were as follows: 25 pps, 150 mA/pulse, 12" air gap, with scan width 90%, corresponding to dose rate 3.5 kGy/min. The irradiation was performed continuously and the total dose was determined using film dosimetry in accordance with ASTM standards.

5.3 Results and Discussion

5.3.1 Influence of aggregation state on the conversion of phenylmaleimide under EB irradiation

As is well known, the aggregation state of a monomer — which is in direct relation to molecule activity — will markedly affect monomer conversion in thermal polymerization. EB irradiation induced polymerization generally follows the same limitations. To illustrate this idea, when free radical polymerization of phenylmaleimide

induced by EB irradiation was carried out at different temperatures, room temperature and 100° C respectively, the irradiation is conducted in the solid and the melt state. This is due to PMI's 91°C melting point obtained by the DSC thermoscan as seen in Figure 5.2. Furthermore, as shown by the exothermal peak in Figure 5.2, thermal initiation can induce the homopolymerization of PMI at temperatures near 250°C.

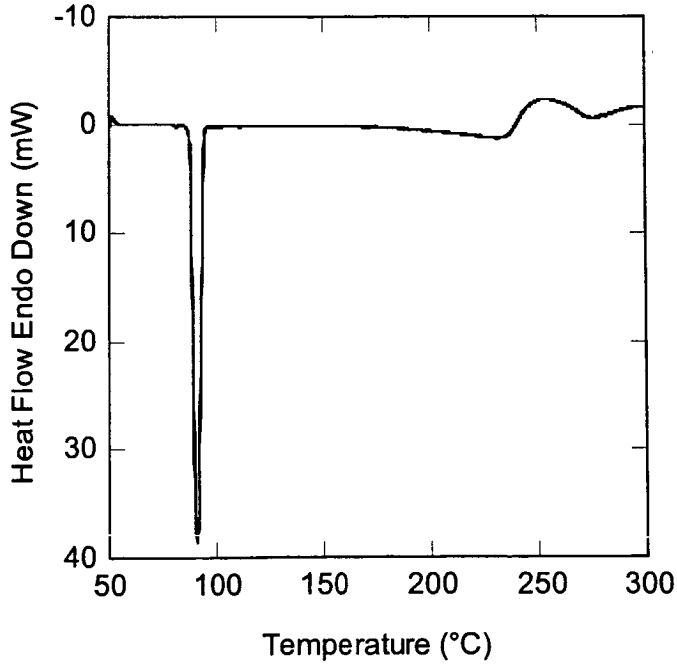

Figure 5.2 DSC thermogram of N-phenylmaleimide with a ramping rate of 10°C/min.

In Figure 5.3, HPLC analysis of the PMI following EB irradiation at room temperature shows no indication of the formation of high molecular weight molecules. Moreover, when this EB irradiated PMI sample was postcured at 105°C for 4 hours, the same result was obtained. Thus EB irradiation of PMI in the solid state does not induce polymerization.

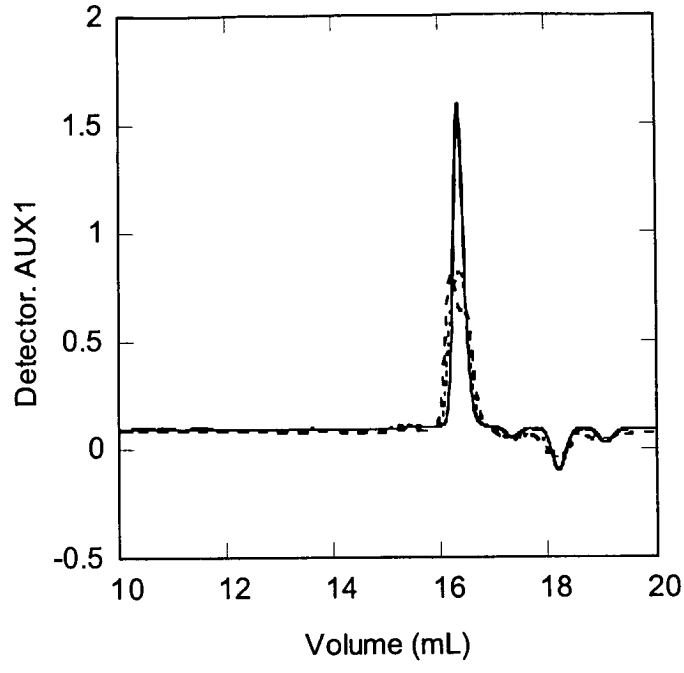

Figure 5.3 HPLC trace of PMI under EB irradiation at room temperature. (—) PMI before EB irradiation, (----) PMI after EB irradiation, (·····) PMI after EB and post heating to 105°C.

On the contrary, when the EB irradiation of PMI is conducted at 100°C, pronounced conversion of PMI C=C occurs as shown by the FTIR spectrum in Figure 5.4, wherein 833 cm^{-1} is attributed to the PMI C=C. By using the C=O peak (1710 cm^{-1}) as a reference, the conversion of PMI C=C in this case was found to be 46%. The reason for conversion observed in this case is attributed to the liquid state of PMI at 100°C. Thus the state of aggregation is of critical importance to the use of EB to induce free radical polymerization of maleimide functional monomers.

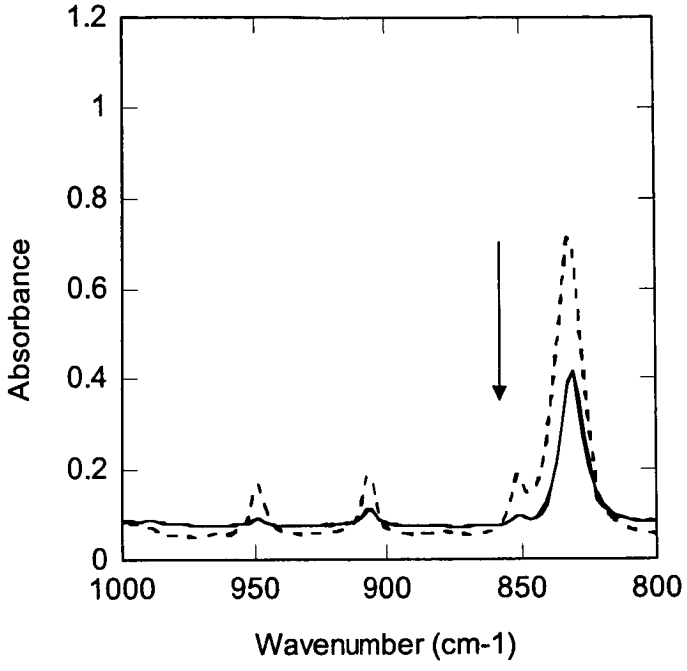

Figure 5.4 FTIR spectrum of PMI under different stages. (----) PMI before EB irradiation, (—) PMI with EB irradiating at 100°C.

5.3.2 Influence of reactive diluents on phenylmaleimide conversion via EB irradiation

The state of aggregation can also be changed by the introduction of a reactive diluent; accordingly, the conversion of PMI should also be altered. Allylphenylether (APE) was used to investigate the influence of the reactive diluent on the conversion of PMI C=C under EB irradiation. Figure 5.5 shows elution traces for the products of BMI and APE monomers of various concentrations subjected to EB irradiation. It is apparent that following EB irradiation, high molecular weight polymer is formed. The highest amount of high molecular weight material was formed for a 1:1 molar ratio of PMI to APE.

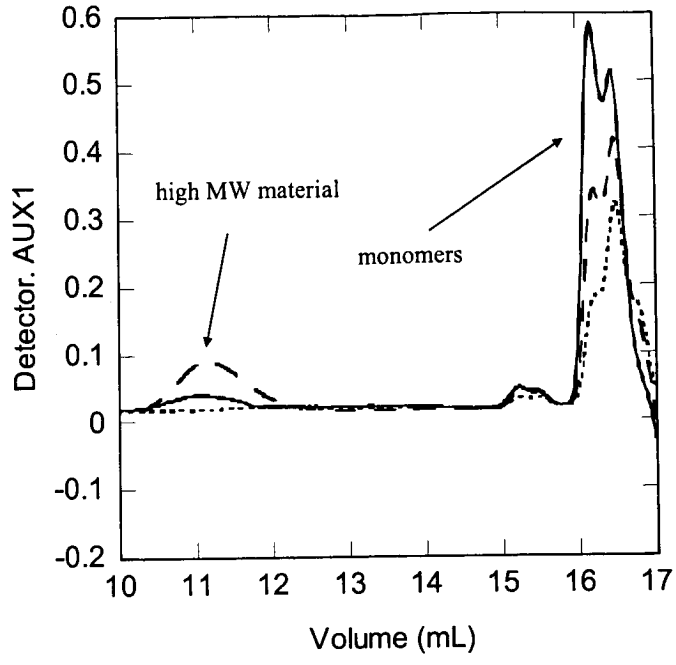

Figure 5.5 HPLC trace of PMI and APE with different molar ratio under EB irradiation. (—) 3:1 molar ratio of PMI to APE, (----) 1:1 molar ratio of PMI to APE, (·····) 1:3 molar ratio of PMI to APE.

FTIR was also used to substantiate this phenomenon. As can be seen from Figure 5.6, for an APE to PMI molar ratio of 1:1, a large change of PMI C=C peak height after EB irradiation is observed with little change in conversion after postcure.

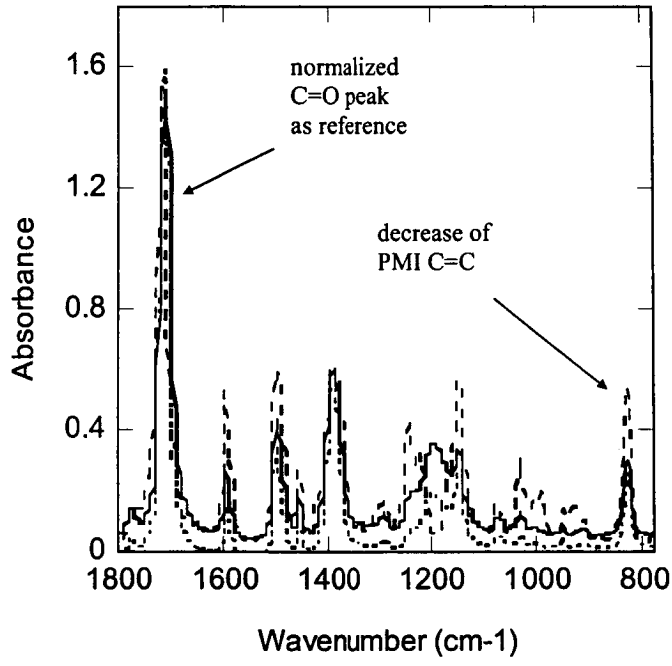

Figure 5.6 FTIR spectra of PMI and APE (molar ratio 1:1) at different stages. (----) before EB, (—) after EB, (·····) after EB and post cure.

On the other hand, Figure 5.7 shows that with a molar ratio of 3:1, the variation of PMI C=C resulting from EB irradiation is not pronounced. However, the subsequent postcure can lead to a significant conversion.

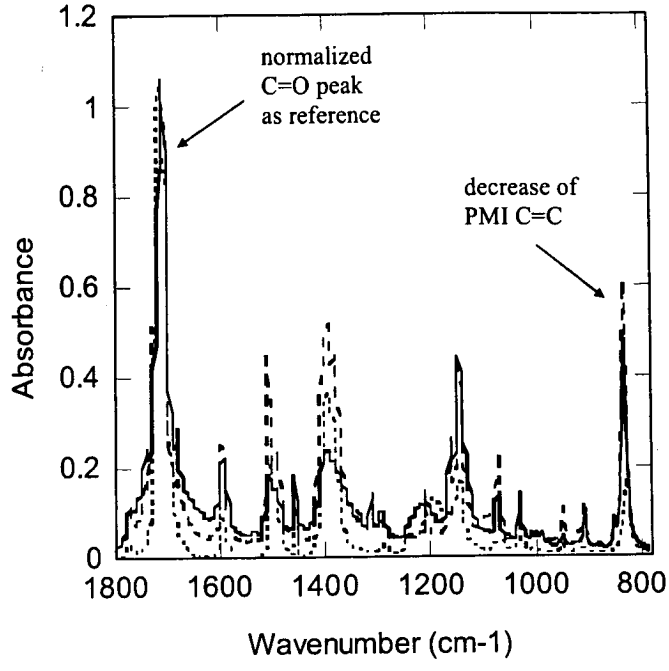

Figure 5.7 FTIR spectra of PMI and APE (molar ratio 3:1) at different stages. (----) before EB, (—) after EB, (·····) after EB and post cure.

A summary of these conversion results is given in Figure 5.8 where PMI C=C conversion is plotted as a function of APE molar fraction. The graph shows that after EB irradiation, the system with a 3:1 PMI to APE molar ratio has a PMI C=C conversion of 27%, while the system with molar ratio of 1:1 attains a 74% PMI C=C conversion. With a molar ratio of PMI to APE of 1:3, PMI C=C shows no obvious conversion. After postcure, which was carried out under the same conditions described for the reaction of pure PMI, the conversions of PMI C=C with molar ratios of 3:1 and 1:3 were greatly improved. Thus a feed composition that yields maximum PMI conversion exists for the APE/PMI system.

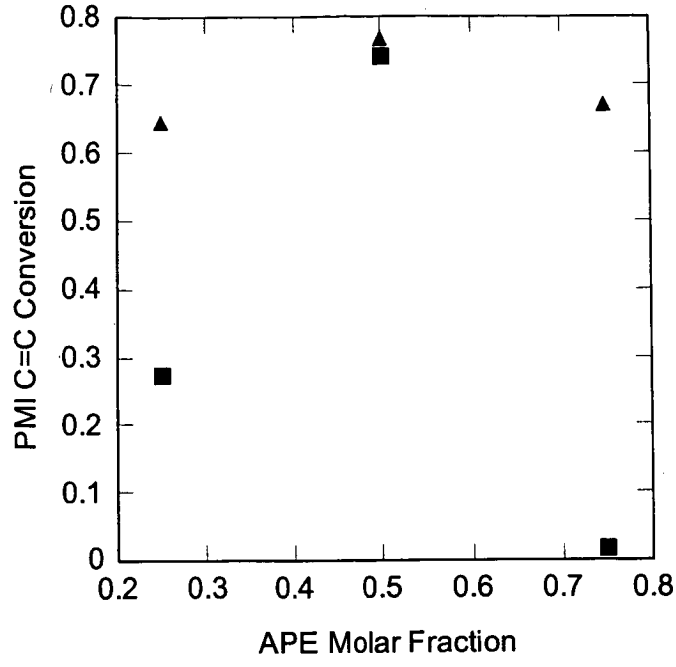

Figure 5.8 Conversion of PMI C=C under EB irradiation and postcure as a function of APE molar fraction. (■) EB, (▲) EB + postcure.

The behavior of PMI with APE under EB irradiation can be elucidated by understanding charge-transfer reaction mechanisms. Free radical reactions are often made more likely when there is a large disparity of charge between two molecules, i.e., an electron rich molecule will donate an electron to an electron deficient molecule. Such mechanisms are termed donor/acceptor or charge transfer reactions. The charge-transfer interaction lowers the energy for the formation of reactive centers and so the polymerization maybe carried out under more moderate conditions [1]. In this case, the C=C of PMI can be regarded as an electron acceptor due to its electron deficient property resulting from the presence of two carboxyl groups which are characterized by electron drawing ability. On the other hand, the C=C of APE can be considered as an electron donor. Thus, a complex based on these two different monomers will form and the

copolymerization will proceed. Two marked characteristics associated with this kind of free radical copolymerization are: (1) the tendency toward alternation increases as the difference in polarity between the two monomers increases, and (2) a most dramatic and useful aspect of alternating copolymerization is the copolymerization of monomers that show little or no tendency to homopolymerize [2]. In this study, the non-homopolymerization of APE under EB irradiation and thermal methods was substantiated by the HPLC technique, as shown by Figure 5.9 where no high molecular weight material is detected after EB exposure.

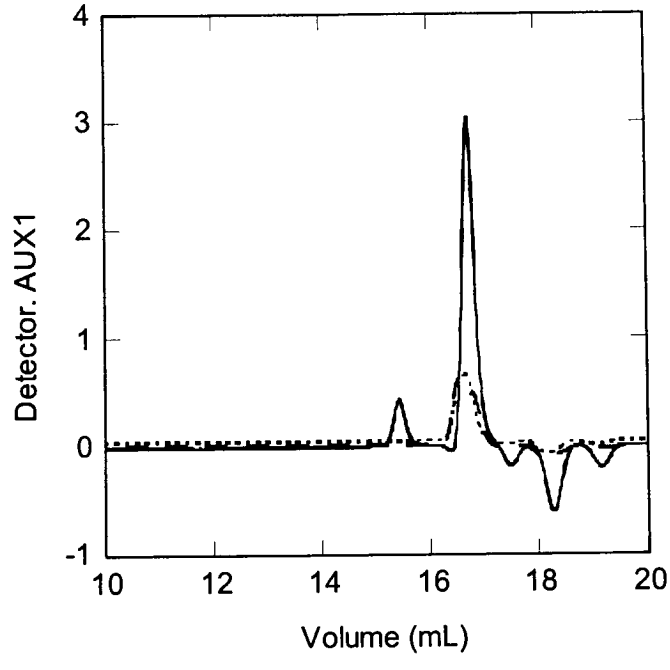

Figure 5.9 HPLC spectrum of APE under different stages. (—) APE before EB irradiation, (----) APE after EB irradiation, (·····) APE after EB and post heating.

Meanwhile, two mechanisms have been proposed to explain the strong alternating tendency between electron-donor and electron-acceptor monomers [2]. One, suggested by Cowie — which is also prevalently verified — pointed out that alternating copolymerization results from homopolymerization of a 1:1 complex, formed between donor and acceptor monomers. Therefore, in this case, the highest output of polymer corresponding to the 1:1 feed composition can thus be attributed to the maximum concentration of such a complex.

Other types of vinylethers such as 2-ethyl-1-hexyl vinyl ether (EHVE) and cyclohexyl vinyl ether (CHVE) were selected and used in the same experiment as APE and the results summarized in Figure 5.10. The same general tendency was found in these systems with an exception for CHVE.

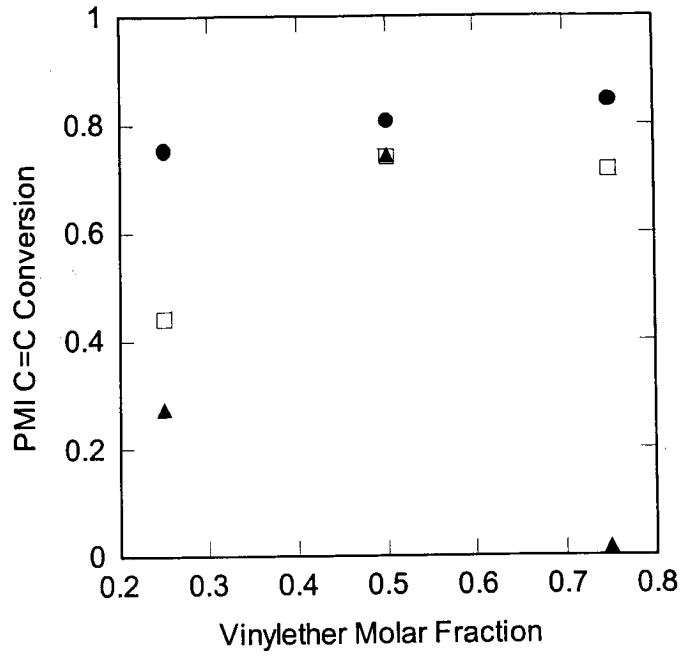

Figure 5.10 Conversion of PMI under EB with different kinds of vinyl ethers. (□) EHVE, (▲) APE, (●) CHVE. A characteristic maximum is not observed for CHVE.

For CHVE, with the increase of vinylether molar fraction, a maximum in conversion was not observed, and this may be attributed to the higher intrinsic reactivity of CHVE with PMI compared to the other vinylethers. In other words, the activation energy of complex formation may be significantly lower in this case, leading more easily to the reaction under a wide range of compositions. This is reflected in the DSC measurement conducted on mixtures of various vinyl ethers with PMI.

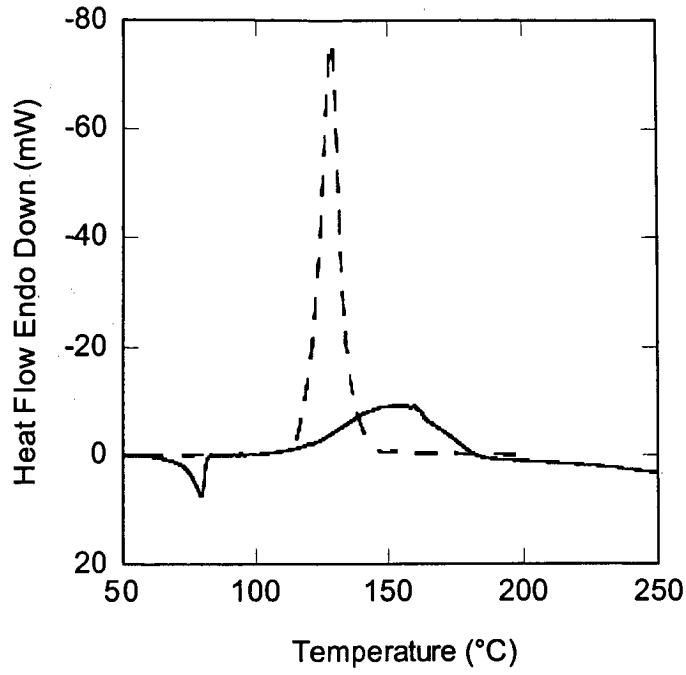

Figure 5.11 DSC thermogram of PMI with CHVE (----) and EHVE (—). Weight ratio of PMI to vinyl ether is of 1:2.

As can be seen in Figure 5.11, the reaction peak of PMI with CHVE is 128°C, whereas the reaction peak of PMI with EHVE occurs at 159°C. This means that the activation energy of complex formation for PMI with EHVE is higher than that of PMI with CHVE. Thus the reaction via the charge transfer mechanism for PMI and EHVE occurs at higher temperatures.

5.3.3 Influence of the side groups on the reactivity of reactive diluents

Two aspects are critical in selecting reactive diluents to be used for processing of BMI via EB irradiation: (1) making sure that the reactive diluent can react with BMI under EB irradiation, (2) ensuring that no reaction will occur near the processing temperature so as to provide a window for BMI processing of composites by methods

like Resin Transfer Molding (RTM) or Vacuum Assisted Resin Transfer Molding (VARTM). However, this presents a dilemma in choosing reactive diluents, particularly for vinylethers. Due to its high melting point and specific structure, BMI can only be dissolved in a high polarity solvent such as DMF, NMP, while common solvents can only dissolve BMI at elevated temperatures, generally above 100°C. From the perspective of reactivity however, at high temperatures, polymerizations between common reactive diluents and BMI may also occur. This incompatibility prohibited the use of many commonly used reactive diluents; such as styrene and some vinylethers, from consideration in this study.

Experiments were conducted with styrene and substituted styrenes with the idea of incorporating electron withdrawing moieties on the ring capable of altering the reactivity of the vinyl groups with the maleimide functional monomers. For mixtures of styrene, divinylbenzene, and nitrostyrene with PMI, DSC scans were used to evaluate relative reactivities of the diluents. The reactivity of reactive diluents towards maleimide double bonds can be reduced by introducing electron withdrawing group to their chemical structure. Figure 5.12 shows the DSC results. The relative reactivity was determined based on the reaction peak positions. The reaction peak of styrene with PMI is at 120°C, whereas the reaction peak of DVB with PMI shifted to 140°C. Furthermore, the peak of 3-nitrostyrene with PMI moved to a very high temperature of 190°C. Since the electron withdrawing ability of the nitro group is more pronounced than that of the benzene group, it is reasonable to conclude that the DSC peak position shifts are a result of the difference of electron withdrawing ability of the diluent vinyl group relative to that of BMI.

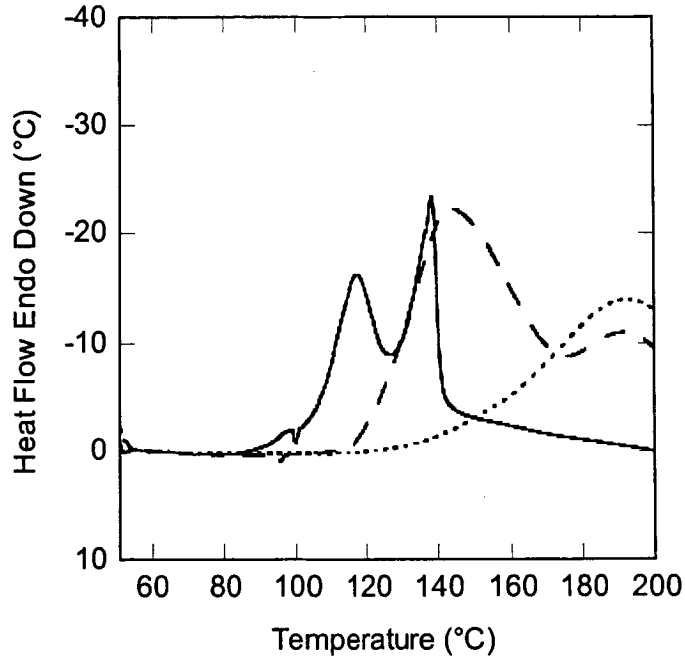

Figure 5.12 DSC therogram of PMI with St (—), DVB (---), and NSt (·····). Weight ratios of PMI to various diluents are of 1:2.

5.3.4 A new reactive diluent: N-acryloylmorpholine

Though 3-nitrostyrene could be a promising candidate for processing of BMI, its low reaction onset temperature ~ 130°C still limits the processing window of BMI blends. Thus another attempt is needed to find a more proper reactive diluent to limit the reactivity of BMI at high temperatures. At the same time, the selected diluent should possess some degree of electron-donating ability relative to BMI so that the formation of donor-acceptor complex during EB irradiation will allow for charge-transfer copolymerization. From this perspective, N-acryloylmorpholine (AMP) was found to process good features as a reactive diluent for BMI. N-vinylpyrrolidone (NVP) is a polar reactive diluent capable of dissolving BMI. However, it is well know that NVP is

characterized by much stronger electron donating ability than vinyl ethers. This makes the charge transfer reaction proceed more easily with NVP than vinylethers. This is believed to be because the nitrogen atom, which connects to the double bond, improves the electron donating ability of C=C greatly. Although the solubility of BMI in NVP is better than it is in vinyl ethers, the higher reactivity negates this benefit. On the other hand, when examining the AMP chemical structure, it was found that electron withdrawing group C=O lies in between the C=C and nitrogen atom and may partly counteract the electron donating effect delivered by nitrogen atom. Therefore, it was predicted that AMP may possess an optimum level of reactivity that allows for reaction with BMI under EB irradiation while maintaining the stability of BMI at high temperatures.

Solubility, of course, is another important factor in the selection of a reactive diluent. AMP might also be a good candidate in this regard. High polarity solvents like dimethylformamide (DMF) and N-methylpyrrolidone (NMP) that are capable of dissolving BMI, have the —N—C=O moiety in common which is also similar to the structure of BMI. So it can be reasonably concluded that the similarity in structure is the main factor that determines the solubility of BMI in these solvents. And this similarity can be found in the AMP structure as well.

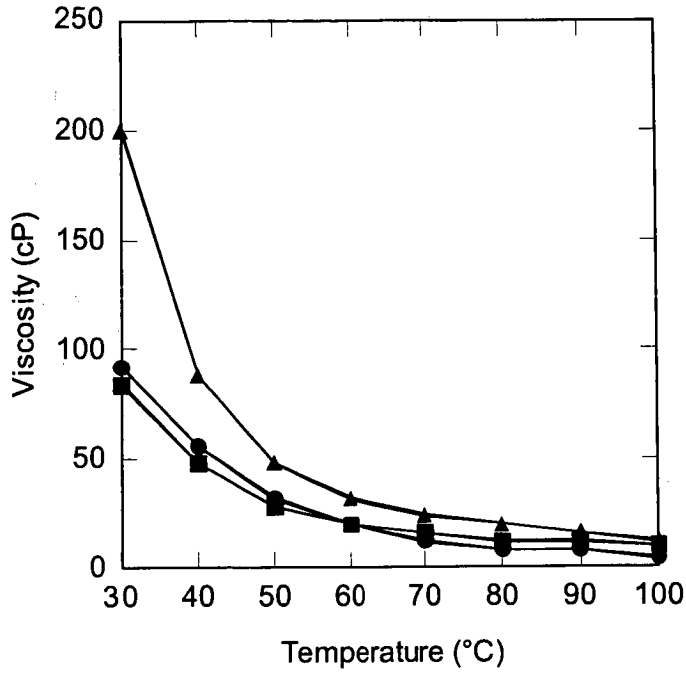

Figure 5.13 Viscosity change of three systems with the increase of temperature. (-▲-) molar ratio of BMI to AMP 1:2, (-●-) molar ratio of BMI to AMP 1:3, (-■-) molar ratio of BMI to AMP 1:4.

Figure 5.13 contains viscosity versus temperature plots for a number of BMI-AMP blends in the temperature range from 30 to 100°C. These plots clearly show the good solubility behavior of AMP and also the low viscosity that is attained at relatively low temperature thus imparting good processibility to the resin system for VARTM and RTM applications. The DSC thermoscans of BMI, AMP and a 1:4 molar ratio of BMI to AMP are shown in Figure 5.14. These results indicate that the mixture of BMI and AMP will remain stable at temperatures as high as 140°C displaying no reaction to that point. Compared to the low temperature homopolymerization of AMP and BMI, the mixture of BMI and AMP shows a strong tendency for copolymerization with the reaction peak shifting to the much higher temperature ~ 280°C. However, the FTIR data given in

Figure 5.15 of a 1:4 molar ratio of BMI with AMP indicate that AMP can copolymerize with BMI under EB irradiation even at room temperature since both AMP and BMI C=C peaks show significant decreases after irradiation.

In light of these observations, it is concluded that not only can AMP dissolve the BMI at low temperature, but it also limits BMI chemical reactivity. More importantly, AMP can copolymerize with BMI at low temperature by EB irradiation. Therefore, one fundamental shortcoming associated with BMI processing, which is a narrow processing window [3], can be satisfactorily resolved by using AMP as a reactive diluent for polymerization by EB irradiation.

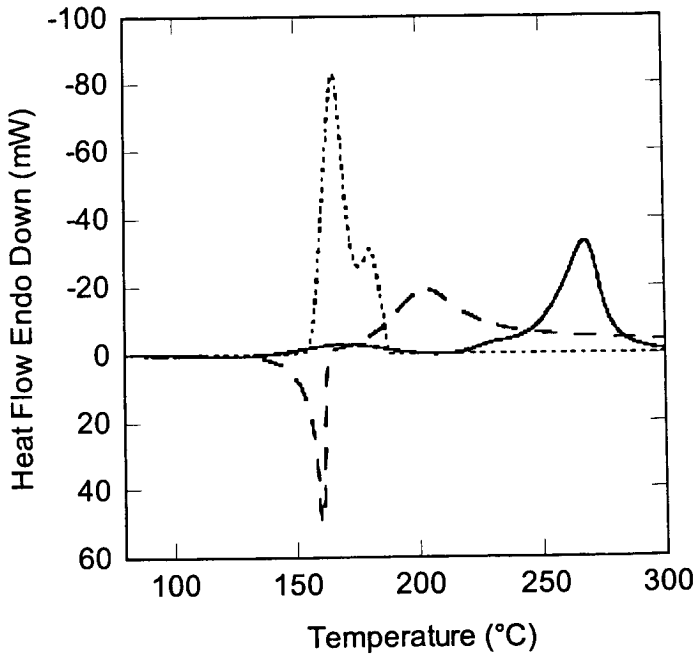

Figure 5.14 Overlay DSC plots of BMI, AMP, and mixture of BMI and AMP (molar ratio 1:4). (—) BMI+AMP (molar ratio 1:4), (----) BMI, (·····) AMP.

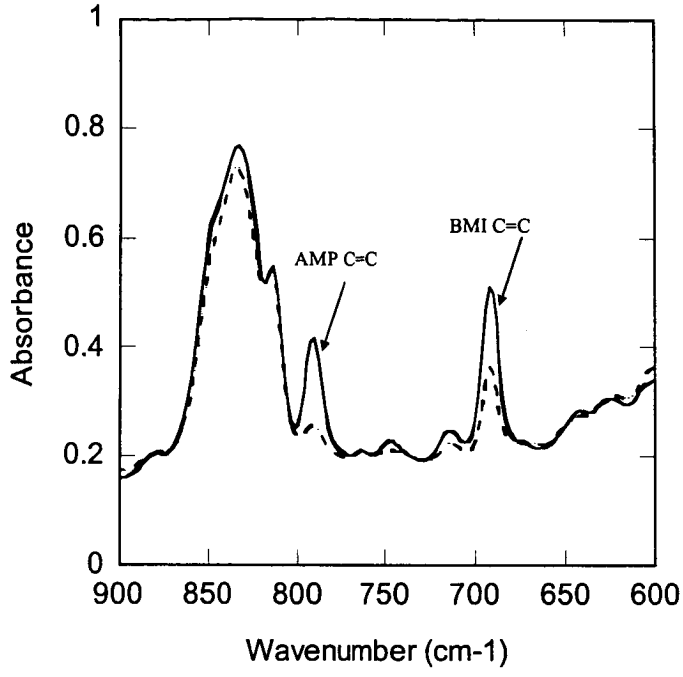

Figure 5.15 FTIR spectra of BMI and AMP mixture (molar ratio 1:4). (—) before EB irradiation, (----) after EB irradiation at room temperature.

The exact mechanism behind EB induced copolymerization of BMI and AMP is still unclear to us, following is an attempt at a simple explanation. BMI is an electron deficient monomer, and itself can polymerize by thermally initiated free radical homopolymerization with a reaction peak at 200°C [4] as shown in Figure 5.14. Compared to BMI, AMP can be regarded as an electron donating monomer due to the weaker electron drawing effect on the double bond by a single carboxyl group. Thus a donor-acceptor complex reaction center can also be formed between AMP and BMI; however, this interaction is not as strong as those formed with common reactive diluents that possess stronger electron donating capability. This viewpoint is supported by Hopewell's conclusion that a donor-acceptor complex can be formed even in BMI

homopolymerization by thermal initiation [5]. The tendency to form a donor-acceptor complex seems also be embodied in our DSC study. The DSC thermoscans of Figure 5.14 show that the starting reaction temperature of the BMI and AMP mixture is slightly lower than that of either component. This small scale reaction might be attributed to the formation of a small amount of the donor-acceptor complex. The small amount formed would be a result of the high activation energy associated with the small difference in polarity of the double bonds of these two monomers. Thus in the thermal copolymerization of BMI and AMP, a charge-transfer mechanism is not believed to predominate. Therefore, as shown in Figure 5.14, the exothermal peak of the thermally initiated BMI and AMP system is 267°C, which is much higher than the reaction peak of either component.

In thermally induced copolymerization, charge-transfer interactions take place in the ground state and it is expected that EB irradiation would result in similar interactions taking place in excited states [1]. This would suggest that EB induced charge-transfer polymerizations need weaker charge-transfer interactions and could therefore encompass a much wider range of donor-acceptor combinations. Therefore, PMI and AMP combinations might be expected to polymerize more readily under EB radiation. This viewpoint is supported by the phenomenon observed in our kinetics study that under EB irradiation, copolymerization can proceed at room temperature and that the PMI C=C conversion can reach 80% under these conditions. This is similar to results obtained by initiator induced thermal copolymerization at 110° C.

It is obvious that alternating copolymer would be achieved by the charge-transfer mechanism, which also means intrinsic reactivity ratios for two monomers should be 0.

In our study of the copolymerization parameters of PMI and AMP systems under EB irradiation at room temperature, discussed in Chapter 6, the monomer reactivity ratios of these two constituents were 0 and 0.5 respectively, which provides another piece of evidence for the suggested charge-transfer mechanism.

The influence of AMP concentration on the conversion of BMI C=C was investigated by using PMI as a mono-functional model compound since it possesses a lower melting point and does not result in cross-linked polymers. The results, depicted in Figure 5.16, show that the conversion of PMI C=C increases with increasing AMP concentration. This contrasts sharply with results obtained for the vinylether type reactive diluents. Thus, adding more AMP to the system can increase the conversion of BMI. Additionally, increasing AMP content can reduce processing problems by decreasing the viscosity of the system. However, adding more AMP might also bring about the following undesired effects: (1) the residual amount of AMP will increase, (2) the final Tg of system will decrease, and (3) the polymer chain structure will be altered. Therefore, finding the optimum amount of AMP in order to obtain the best overall properties is the aim of the study of kinetics of copolymerization of AMP and BMI under EB irradiation reported in next chapter.

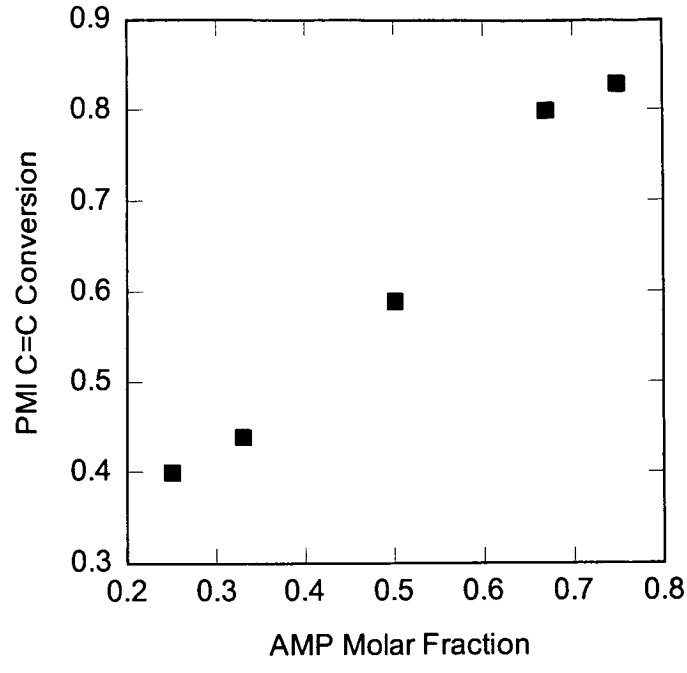

Figure 5.16 Conversion of PMI C=C under EB irradiation at room temperature as a function of AMP concentration.

Unlike vinylethers, the carboxyl group that connects to the C=C in AMP makes the homopolymerization of AMP possible, whether induced by heat or EB irradiation. This is shown by the NIR spectra in Figure 5.17, which were obtained by *in-situ* monitoring of the conversion of AMP C=C under EB irradiation at room temperature.

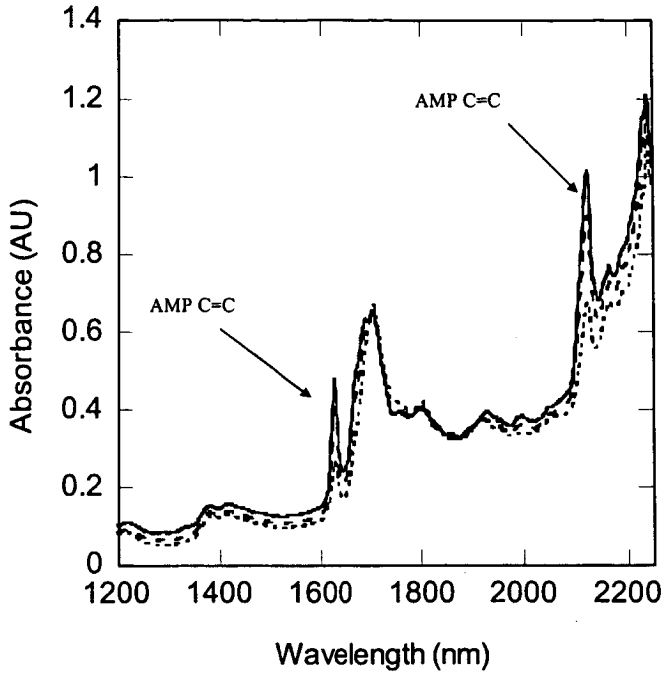

Figure 5.17 *In-situ* NIR monitoring of AMP C=C variation under EB irradiation with dose rate at 3.5 KGy/min and temperature of 22°C, (—) before EB irradiation, (----) after 5 sec of EB irradiation, (·····) after 10 sec of EB irradiation.

The conversion of AMP C=C with time is plotted in Figure 5.18. As can be seen, the conversion of AMP C=C after 5 sec can reach 20%, and after 10 sec of 55%. Finally, the conversion reaches values greater that 90%. The homopolymerization of AMP can also follow the charge-transfer mechanism. Thus, a larger amount of AMP would result in the increase of PMI conversion under EB irradiation, which is different than the behavior embodied by the vinylether-type reactive diluents. This may be reasonably attributed to higher concentrations of donor-acceptor complex being formed in the system through which higher throughput of copolymer can be obtained. More interestingly from a practical viewpoint, the homopolymerization of AMP under EB irradiation has the

advantage of eliminating unreacted monomers from blends of BMI and AMP regardless of initial composition.

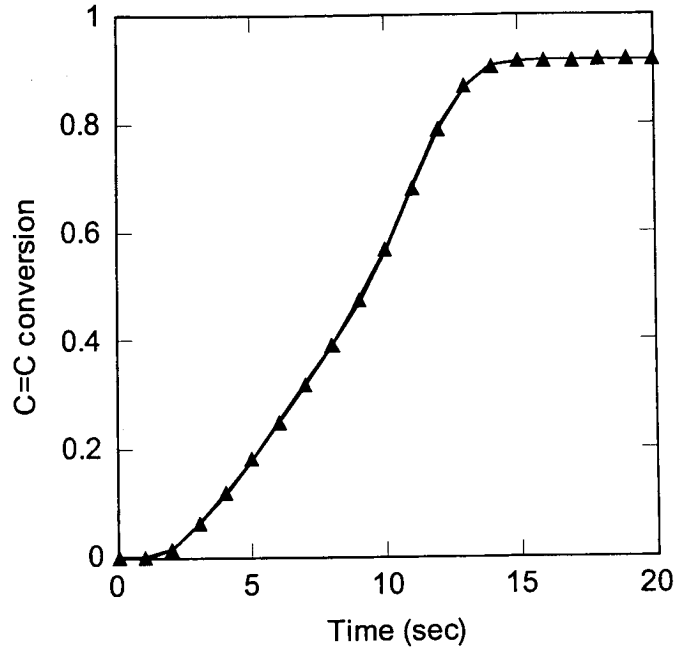

Figure 5.18 Conversion of AMP C=C with time under EB irradiation with dose rate as 3.5 KGy/min and temperature as 22°C.

5.4 Summary and Conclusions

In the foregoing chapter we have discussed the selection of a reactive diluent that enables the development of high Tg thermosetting polymers based on interpenetrating polymer networks of cyanate esters with BMI that can be processed at relatively low temperature by EB induced free radical polymerization. A reactive diluent is necessary because it eliminates the use of solvents which must be removed after reaction. However, two important criteria must be met for the reactive diluent to be effective: (1) the BMI should dissolve readily in the diluent and (2) the diluent should react with BMI, but not at

the processing temperature of the IPNs first network. Common reactive diluents for BMI are not well suited for the application. Many like vinylethers show poor solubility at low temperature and when heated react readily with BMI restricting the processing window and yet are not prone to homopolymerization. Others like NVP dissolve BMI very well but are also extremely reactive at low temperature because of strong donor-acceptor interactions that facilitate the charge transfer mechanism of reaction.

The keys to finding an appropriate reactive diluent are to enhance the solubility of BMI which requires strongly polar characteristics with donor acceptor interactions and to control the difference of electrophilicity between the BMI and reactive diluent double bond so as to balance stability with EB reactivity. N-acryloylmorpholine was found to be a diluent that uniquely satisfies these requirements. Following are some of this diluent's characteristics: (1) AMP can dissolve BMI at 110°C with a 1:2 molar ratio of BMI to AMP; it maintains BMI stability for long period time at temperatures as high as 140°C which brings about a broad processing window for BMI/AMP blends, (2) AMP can copolymerize with BMI under EB irradiation through charge-transfer mechanism at low temperature whereby the conversion of BMI can greatly be improved, (3) an alternating copolymer chain is more likely to be formed as a consequence of the charge-transfer mechanism — this is explained in detail in Chapter 6, and (4) AMP can also homopolymerize thus limiting unreacted diluent after polymerization for a broad range of BMI to AMP composition ratios. This copolymerization can be achieved irrespective of the initial monomer ratio, which makes the formulation and processing of system more flexible.

In conclusion, from both practical and theoretical perspectives, AMP has been found to be a novel reactive diluent when considered for low temperature processing of BMI via EB irradiation to manufacture high temperature composite materials. Some drawbacks associated with this material include potential toxicity and thermal stability that could be improved (Chapter 7).

Nevertheless, our discovery and investigation of this material has provided the fundamental knowledge needed for designing improved diluents for BMI copolymerization under EB irradiation.

List of References

1. Li T., W.X. Cao and X.D.Feng. *Photoinduced charge-transfer polymerizations of vinyl monomers.* JMS-REV. Macromolecular Chemistry and Physics 1989:C29(2&3);153-99.

2. Odian G.. *Principle of polymerization. 3rd edition*, John Wiley & Sons, INC. New York, 1991.

3. Liu Y.L., Y.J. Chen. *Novel thermosetting resins based on 4-(N-maleimideophenyl)glycidylether: II. Bismaleimides and polybismaleimides.* Polymer 2004;45:1797-1804.

4. Hopewell J.L., D.J.T. Hill and P.J. Pomery. *Electron spin resonance study of the homopolymerization of aromatic bismaleimides.* Polymer 1998;39(23):5601-07.

5. Hopewell J.L., G.A. George and D.J.T. Hill. *Quantitative analysis of bismaleimide-diamine thermosets using near infrared spectroscopy.* Polymer 2000;41(23):8221-29.

CHAPTER 6: KINETICS OF EB INDUCED BMI-AMP FREE RADICAL COPOLYMERIZATION

In the preceding chapter, the rationale for the selection of AMP as the appropriate and uniquely suited reactive diluent for EB copolymerization of BMI was presented. It is important now to understand the type of polymer structure that is formed between BMI and AMP. For example, do AMP and BMI form block copolymer or alternating copolymer or simply react separately? For the IPN being contemplated, the structure of a second network formed after free radical copolymerization under EB radiation is dictated by many factors, such as the initial monomer concentration ratio, monomer reactivity ratio and diffusion limitation. These factors determine the sequence distribution of monomers in polymer chains, crosslinking density and other related factors. EB processing parameters such as dose rate, total dose, which are believed to affect the network structure via initiation and termination, constitute another important aspect of this study. Accordingly, the kinetics of EB induced free radical copolymerization was investigated with the particular emphasis on copolymerization behavior.

6.1 Introduction and Background

6.1.1 Kinetics of EB induced free radical polymerization

The radiation polymerization of bulk methyl methacrylate was studied at low and medium dose rates by a number of investigators as early as 1974. A comprehensive account of this work has been presented by Chapiro [1]. The kinetics and other features of the polymerization were found to be very similar to those observed with corresponding

chemically initiated systems; a pronounced gel effect is observed and a square-root dependence of the rate on dose rate was found up to about 0.02 Gy/sec followed by a decreased dependence of reaction rate on irradiation dose.

At low dose rate, the kinetics scheme is the same as the conventional reaction mechanism of free-radical polymerization, which is modeled as follows:

Initiation

$$M \xrightarrow{k_1} 2\,R^{\bullet} \qquad 6.1$$

$$R^{\bullet} + M \xrightarrow{k_2} RM^{\bullet} \qquad 6.2$$

Propagation

$$RM_n^{\bullet} + M \xrightarrow{k_3} RM_{n+1}^{\bullet} \qquad 6.3$$

Termination

$$RM_n^{\bullet} + RM_m^{\bullet} \xrightarrow{k_4} RM_{n+m}R \qquad 6.4$$

At higher dose rates, it is considered that additional termination may occur owing to the strong and fast radiolysis of the system. These reactions may be represented in the following way:

$$RM_n^{\bullet} + R^{\bullet} \xrightarrow{k_5} RM_nR \qquad 6.5$$

$$R^{\bullet} + R^{\bullet} \xrightarrow{k_6} RR \qquad 6.6$$

According to the usual termination, i.e., the termination step reaction (6.4), the rate of polymerization R_p and degree of polymerization $\overline{DP}_n$ are found to be:

$$R_p = k_3 \frac{(k_1 I)^{1/2} (M)^{3/2}}{k_4^{1/2}} \qquad 6.7$$

$$\overline{DP}_n = \frac{2k_3[M]^{3/2}}{[k_4 k_1 I]^{1/2}} \qquad 6.8$$

Equations 6.7 and 6.8 show that the rate of propagation R_p is proportional to, and the degree of polymerization $\overline{DP}_n$ is inversely proportional to, the square root of the dose rate.

At high dose rates, when Equation 6.5 is considered, R_p and $\overline{DP}_n$ can be derived as:

$$R_p = \frac{k_3 k_2 [M]^2}{k_5} \qquad 6.9$$

$$\overline{DP}_n = \frac{2k_2 k_3 [M]}{k_1 k_5 I} \qquad 6.10$$

Unlike the former case, here the rate is independent of dose rate while the degree of polymerization is inversely proportional to the dose rate. In the same way, as termination step 6.6 comes into play, the rate and molecular weight begin to drop further until only dimmers and simple radiolysis products result.

An interesting phenomenon is that at high dose rate the activation energy increases. Also it has been shown that for a wide range of dose rates the EB free radical polymerization seems to follow the same kinetic behavior.

Polymerization reactions of methyl methacrylate (MMA) and methyl, ethyl, and *n*-butyl acrylates were carried out by γ-ray and electron beam irradiation using a wide range of dose rates, $0.1\text{-}10^4$ Gy/sec by Kanae *et al.* [2] in 1988. However, only EB curing is concerned here. In the aforementioned article the relationships among polymerization rate, molecular weight distribution (MWD) and dose rate were investigated. What is worth paying attention to is that high energy EB irradiation can also induce degradation of the polymer formed, which competes with polymerization and cross-linking reaction. Because of these results, the authors concluded that in MMA two different mechanisms of polymerization are taking place concurrently at high dose rates; the main reaction is certainly attributable to conventional radical polymerization, but the cause of the other is not clear. Meanwhile, the relation of polymerization rate to dose rate was found to agree with the equation obtained by Allen *et al.* for a very wide dose rate range.

6.1.2 Kinetics and mechanism of copolymerization

Copolymerization is the phenomenon in which more than one type of monomer unit enters the same polymer chain [3]. The kinetics of copolymerization are different from that of homopolymerization in that they involve two or more species of monomers and can provide the information on the relative reactivities of a variety of radicals towards a single monomer or on the relative reactivities of a series of monomers towards a reference radical.

Copolymer composition leads to the final structure of a polymer chain, and hence the network structure. However, it cannot be determined simply from knowledge of the homopolymerization rates of the two monomers [4]. In the following section, the factors

that influence the copolymer composition will be discussed based on the copolymerization mechanism. The formation of a binary copolymer is used as an example in which the reactivity of the growing chain is determined solely by the nature of the terminal unit. The two monomers are designated M_1 and M_2, and two growing chains are $M_1\bullet$ and $M_2\bullet$. The four possible propagation reactions are:

$$M_1\bullet + M_1 \xrightarrow{k_{11}} M_1\bullet \qquad 6.11$$

$$M_1\bullet + M_2 \xrightarrow{k_{12}} M_2\bullet \qquad 6.12$$

$$M_2\bullet + M_1 \xrightarrow{k_{21}} M_1\bullet \qquad 6.13$$

$$M_2\bullet + M_2 \xrightarrow{k_{22}} M_2\bullet \qquad 6.14$$

where k_{11} is the rate constant for a propagating chain end in M_1 adding to monomer M_1, k_{12} that for a propagating chain ending in M_1 adding to monomer M_2, and so on. For the formation of high molecular weight polymer, monomer disappears principally by the propagation reactions so that,

$$-\frac{d[M_1]}{dt} = k_{11}[M_1\bullet][M_1] + k_{21}[M_2\bullet][M_1] \qquad 6.15$$

$$-\frac{d[M_2]}{dt} = k_{12}[M_1\bullet][M_2] + k_{22}[M_2\bullet][M_2] \qquad 6.16$$

Dividing Equation 6.15 by Equation 6.16 yields the ratio of the rates at which the two monomers enter the copolymer, that is, the copolymer composition, viz;

$$\frac{d[M_1]}{d[M_2]} = \frac{k_{11}[M_1\bullet][M_1] + k_{21}[M_2\bullet][M_1]}{k_{12}[M_1\bullet][M_2] + k_{22}[M_2\bullet][M_2]} \qquad 6.17$$

The assumption of a stationary state concentration of both types of radicals automatically implies that the concentration of one cannot grow at the expense of the other. In other words, the rates of reactions 6.12 and 6.13 are equal.

$$k_{21}[M_2\bullet][M_1] = k_{12}[M_1\bullet][M_2] \qquad 6.18$$

Equation 6.18 can be arranged and substituted in Equation 6.17 to yield

$$\frac{d[M_1]}{d[M_2]} = \frac{[M_1]}{[M_2]} \times \frac{r_1[M_1] + [M_2]}{r_2[M_2] + [M_1]} \qquad 6.19$$

where $r_1 = k_{11}/k_{12}$ and $r_2 = k_{22}/k_{21}$ are know as the "reactivity ratios" of monomers M_1 and M_2 respectively. Therefore, it can be deduced based on Equation 6.19 that the copolymer composition is dependant upon the monomer reactivity ratios and initial monomer concentration ratios.

Copolymerization parameters are the key factors in regulating the final structure of a polymer chain, and hence the network structure. However, as far as we know, no one has investigated the copolymerization behavior of AMP and BMI until now, and especially not under EB irradiation.

Near FT-IR techniques haves been widely used to investigate the cure process of resins, such as epoxy and BMI, due to advantages of simplicity, broader bands, low cost, and remote monitoring capability compared to the mid-IR [5-8].

In this study, in order to elucidate the copolymerization behavior of AMP with BMI in the absence of a cross-linking reaction, the model compound *N*-phenylmaleimide (PMI) was used as a surrogate for BMI. These two monomers were mixed at different molar ratios and were irradiated by EB radiation for a number of dose rates. In addition, the influence of temperature was also investigated. Polymerizations were conducted at 22°C, 50°C, and 80°C. For comparison, thermal copolymerization induced by an initiator was also studied. The difference between EB and thermally induced polymerization was explored.

In addition to avoiding cross-linking reaction, PMI was used instead of BMI because PMI has a lower melting point, making dissolution in AMP more tractable and allowing the molar ratios of these components to be widely varied. It was assumed that the intrinsic reactivity of the PMI double bond is very close to that of BMI double bonds and that diffusion effects on the PMI kinetics are reduced because of the absence of crosslinking reactions. (see chemical structures in Figure 6.1)

Near IR spectroscopy was employed to measure the variation of PMI and AMP double bond concentration with time. The copolymerization parameters of the maleimide double bond and N-acryloylmorpholine double bond using the Mayo-Lewis method [9].

6.2 Experimental

6.2.1 Raw materials and sample preparation

N-phenylmaleimide (PMI) and N-acryloylmorpholine (AMP) shown in Figure 6.1 were obtained from Aldrich Chemicals and were used without further purification. These two compounds were mixed homogeneously to obtain a clear yellow solution, and a small amount of this solution was injected into a glass tube (ID = 1.7 mm, OD = 3.04 mm) with one end sealed using a Bunsen burner. The solution was placed at the sealed end. The height of the solution column in the tube was about 0.5 cm. After sealing the other end, the samples were placed in the freezer before EB irradiation. The compositions investigated were 1:1, 1:2, 1:3 (molar ratio of PMI to AMP). Prior to irradiation, the samples were heated at 80°C to ensure that any recrystallized PMI was fully dissolved in AMP. The samples were then placed in the sample holder at the designed temperature to be irradiated. A thermal initiator, 2,5-bis(tert-butylperoxy)-2,5-dimethylhexane (Luperox 101) was purchased from Aldrich Chemicals and directly used in the thermal copolymerization study at a concentration of 0.1 mol% (based on the moles of double bond). The initiator has a relatively high thermal decomposition temperature so that at 108°C, $t_{1/2}$ = 10 hours.

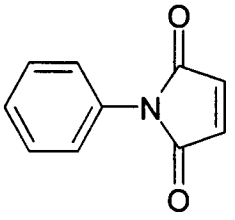

N-phenylmaleimide (PMI)

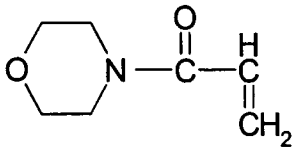

N-acryloylmorpholine (AMP)

Figure 6.1 Chemical structures of monomers used in current study.

6.2.2 Fiber optic Near-IR spectroscopy

Near infrared (NIR) spectroscopy was employed to monitor the variation of double bond concentration under EB irradiation remotely in order to investigate the copolymerization behavior of PMI with AMP. The experimental apparatus consisted of a NIR spectrometer, a temperature controller, and a specially designed sample holder. The schematic diagram of the sample holder is shown in Figure 6.2 and a schematic of entire set-up is shown in Figure 6.3.

Near infrared (NIR) spectroscopy was employed to monitor the variation of AMP double bond concentration under EB irradiation. The NIR measurements were performed using a Control Development, Inc. (CDI) infrared spectrometer. The spectrometer possesses a spectral range from 1160 nm to 2250 nm by using T.E. cooled, high performance Linear InGaAs arrays detector. The infrared light was produced by a white light source (Optical Solutions Inc. model no. LS-E-NIR) that was connected to a sample holder via low hydroxyl silica fiber optics obtained from RoMack, Inc. The sizes of the fiber core/clad/jacketing in μm were 400/440/465. This is a low OH silica multicode step index fiber with protective furcation tubing and SMA 905 connectors. The silica fiber connecting the sample holder to the detector, was obtained from Thorlabs, Inc. (catalog number FG-200-LCR) and consisted of the same fibers used in the RoMack, Inc. fiber optic cable. A specially designed sample holder was used to align the input and output light with the EB irradiation source so that precise location of the sample in the light path to obtain the optimum signal was possible. Heating elements were used for temperature control. For monitoring the exotherm during EB irradiation, an apparatus designed by researchers in UDRI was used to measure internal sample temperature during irradiation.

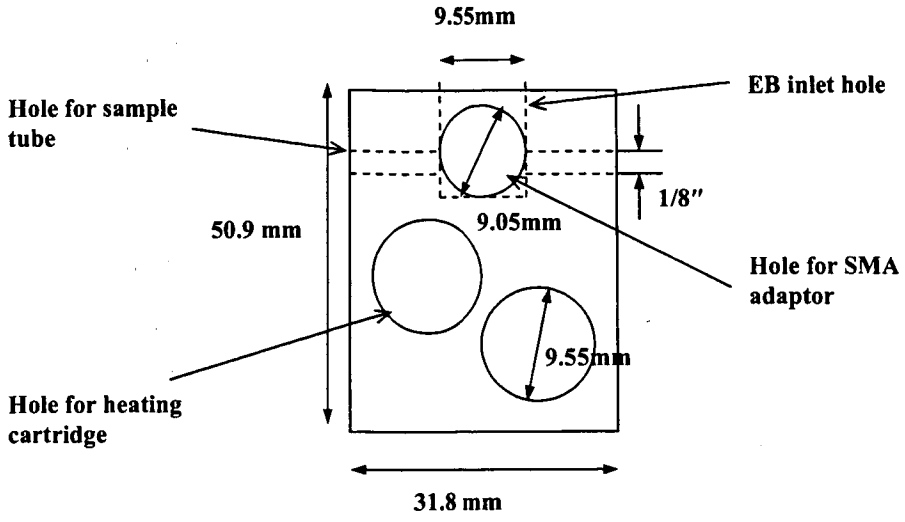

Front view of the sample cell

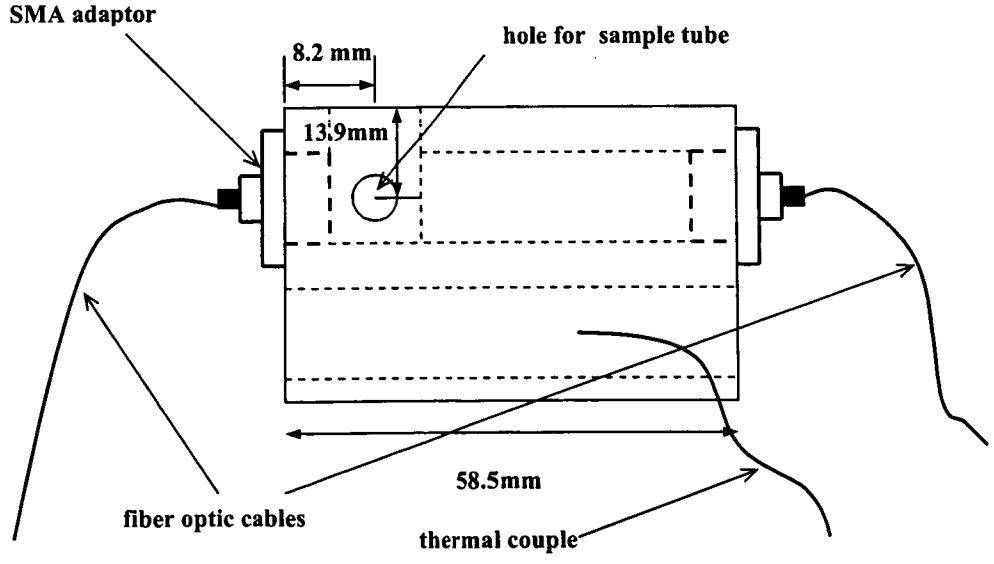

Side view of the sample cell

Figure 6.2 Schematic of sample cell configuration.

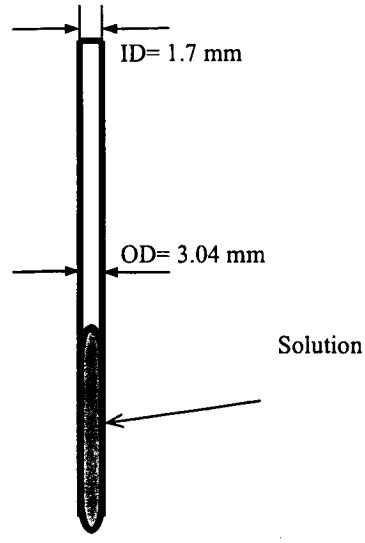

Sample tube

Figure 6.2 ***(continued)***

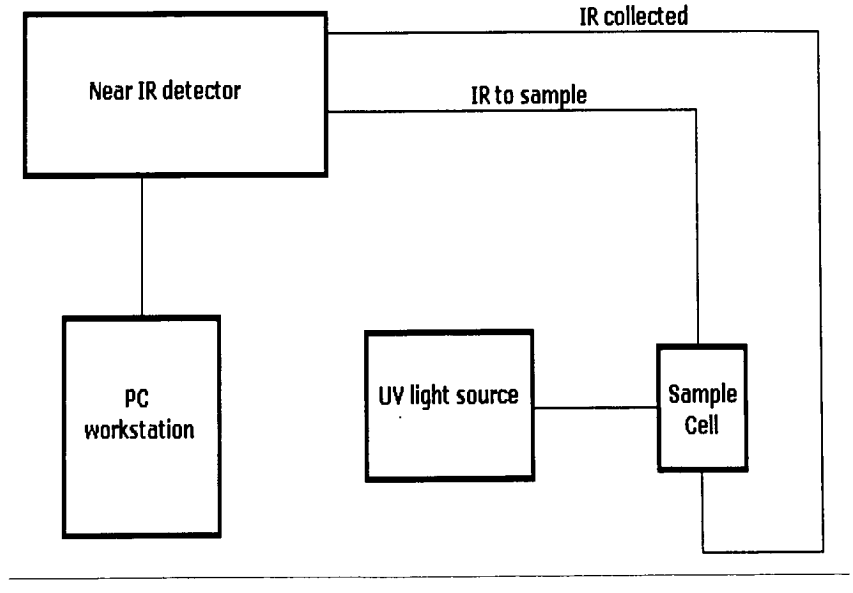

Figure 6.3 Schematic diagram of the entire set-up for remotely monitoring EB cure.

6.2.3 Electron beam curing parameters

EB irradiation experiments were conducted at University of Dayton Research Institute (UDRI), Dayton, OH, on an electron beam induction accelerator. The operating parameters for the cure experiment were as follows: 25pps, 150 mA/pulse, 12" air gap, with scan widths of 90%, 60%, and 40% corresponding to dose rates of 3.5 kGy/min, 4.5 kGy/min, and 7.0 kGy/min respectively. Dose and dose rates were quantified using film dosimetry. The experiments were carried out at nominal sample holder temperatures of 22°C, 50°C, and 80°C respectively. As will be discussed later, a slight exotherm was observed in the tubes as a result of EB heating and reaction exotherm.

6.2.4 FT-NIR monitoring of thermal copolymerization

A Thermo Nicolet Nexus 670 FTIR spectrometer in NIR mode with a resolution of 16 cm^{-1} was employed to monitor the variation of PMI and AMP C=C concentration during the thermally induced copolymerization of PMI and AMP in order to assess the difference between the two initiating methods. The sample preparation for thermally initiated polymerization was similar to that used in EB induced copolymerization monitoring with the exception that 2,5-bis(tert-butylperoxy)-2,5-dimethylhexane (Luperox 101) was added in the amount of 0.1 mole% on a monomer basis. Reaction were carried out in a similar sample holder in sealed glass tubes at a temperature of 110°C.

6.3 Results and Discussion

6.3.1 Near-IR monitoring of the EB and initiator induced copolymerization

Figure 6.4 shows a series of typical IR absorption spectra for sample with 1:3 molar ratio of PMI to AMP exposed to a dose rate of 3.5 KGy/min at 22°C. In these spectra, the peak at 1624 nm is attributed to the AMP double bond, whereas the 2052 nm peak is assigned to the PMI double bond. As seen from the spectra at different times, the height of both the peaks decreases as the sample is being irradiated. Consequently, C=C conversion of two monomers against time derived from the peak height variations are plotted in Figure 6.5.

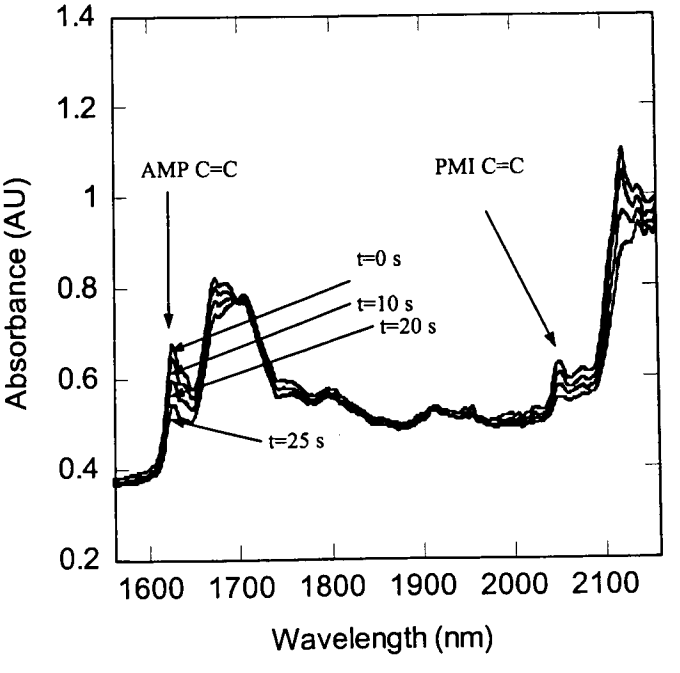

Figure 6.4 *In-situ* NIR spectra of the PMI/AMP system (dose rate = 3.5 kGy/min, T = 22°C, molar ratio PMI to AMP = 1:3).

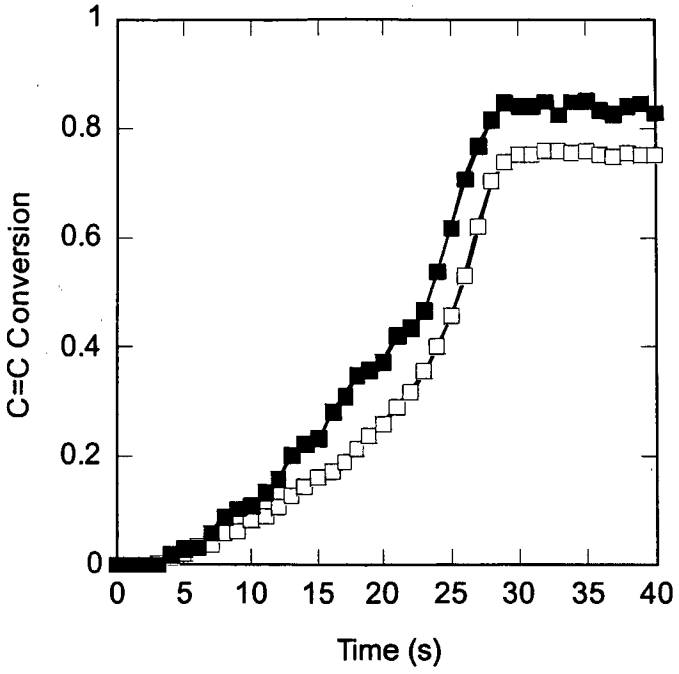

Figure 6.5 Plots of C=C conversion versus time under EB irradiation (dose rate = 3.5 kGy/min, T = 22°C, molar ratio PMI to AMP = 1:3): (-■-) PMI C=C, (-□-) AMP C=C.

An inhibition period is apparent which is probably due to the inhibitor added to commercial AMP to improve its stability. In this experiment, the inhibitor was not removed in order to maintain conditions as close as possible to those of practical EB processing and to maintain stability of the monomers during mixing. After the inhibition period, the reaction is representative of typical free radical copolymerization behavior. A marked acceleration in polymerization rate is observed at C=C conversion of about 20%. The overall behavior of this reaction is very similar to the behavior of methyl methacrylate (MMA) homopolymerization that was observed by Schulz and Harborth [10]. The autoacceleration can lead to a significant rise in temperature if dissipation of the heat of polymerization is inadequate. To some extent, this was observed in

experiments designed to monitor temperature and will be discussed later. The phenomenon of autoacceleration results from the decrease in rate of termination [10-12] associated with diffusion limitations of the active polymer chain end, resulting from the increase in molecular weight of the polymer being formed. This phenomenon is known as the "Trommsdorf effect". Additionally, full conversion is not observed at long times. Instead there is a sharp cut-off in the rate of reaction presumably as a result of more significant discussion limitations associated with vitrification. Post-curing at higher temperature resulted in nearly complete conversion of PMI and AMP double bonds.

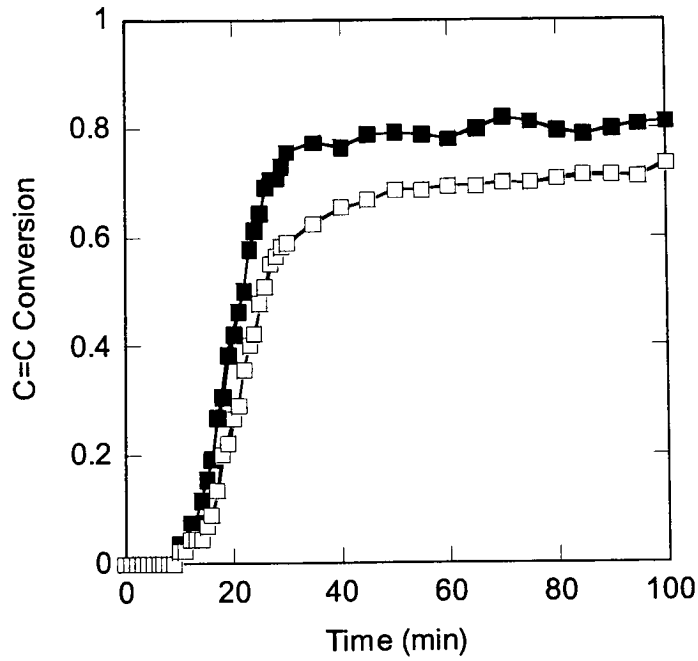

Figure 6.6 Plots of C=C conversion versus time for thermal induced copolymerization of PMI and AMP (molar ratio 3:1, T=110°C, 0.1 mol% Luperox 101): (-■-) PMI C=C conversion, (-□-) AMP C=C conversion.

As a comparison, the plots of conversion versus time for PMI and AMP with the same molar ratio polymerized by thermal initiation at 110°C are given in Figure 6.6. As with EB induced copolymerization, there also exists an induction period, which lasts significantly longer. It can be reasonably concluded therefore that the rate of free radicals generation is higher for EB irradiation than for thermal initiation for the polymerization conditions considered. After an induction period, the conversion of PMI and AMP was observed to increase sharply. The differences of behavior associated with the two polymerization methods may be attributed to the following factors, namely temperature as well as the number of free radicals produced per unit time by the different methods. The much higher temperature adopted in thermal copolymerization would be expected to diminish the influence of diffusion limitation at vitrification and increase the propagation rate. The greater number of free radicals produced per unit time by EB irradiation should lead to the high overall reaction rate at a relatively lower temperature because of a high concentration of propagating centers. For thermally induced polymerization, the number of active centers is low but the rate of propagation is much higher because of the higher temperature. Unexpectedly, the influence of diffusion limitation due to vitrification on final conversion is more evident in thermally induced copolymerization, even at much higher reaction temperature. From Figure 6.5 and Figure 6.6, the limits of conversion for EB induced copolymerization are higher than in thermally induced copolymerization. This may be attributed to the high free radical generation rate that could influence the characteristic diffusion distance necessary for reaction as well as the polymer structure as a function of conversion.

6.3.2 Influence of AMP concentration on the final conversion of double bond

Figure 6.7 and Figure 6.8 give the plots of the final conversion of PMI and AMP double bonds with the respect to the molar fraction of AMP for EB polymerizations conducted at 22°C for three dose rates. Conversion data regarding initiator induced thermal copolymerization of PMI and AMP are also given for a comparison. It is illustrated by Figure 6.7 that there exists a generally linear relationship between the PMI C=C conversion and the molar fraction of AMP used. With 75% mole fraction of AMP, which corresponds to the molar ratio of 1:3 PMI to AMP, the final conversion of PMI can reach values in excess of 80%, whereas with 25% mole fraction of AMP, the conversion of PMI C=C is only about 40%. Generally the influence of higher dose rate is to increase final conversion — this could be due to radical concentration effects as well as slightly higher temperature for higher dose rates. This will be discussed in more detail in the next section.

Compared with the thermal copolymerization behavior, it was observed that the conversion of PMI C=C by EB irradiation is much lower when the AMP molar ratio is low. This difference diminishes with increasing AMP. At a high molar fraction of AMP (75%), the conversion of PMI C=C obtained by EB radiation exceeds that obtained by the thermal method. This observation suggests that the reactive diluent will play a critical role in processing of BMI by EB irradiation to help the reaction proceed to completion.

In contrast, the final conversion of AMP C=C decreases with increasing molar fraction of AMP for both EB and thermally induced copolymerization. This behavior is shown in Figure 6.8. This effect is not as pronounced for EB induced polymerization.

Thus the benefit brought by AMP in PMI C=C conversion is counteracted by the low conversion of AMP.

It is important to remember here that the systems are not fully reacted. The polymerization ceases because of vitrification. The compositions that are locked in place are indicatives of the polymer structure that is formed.

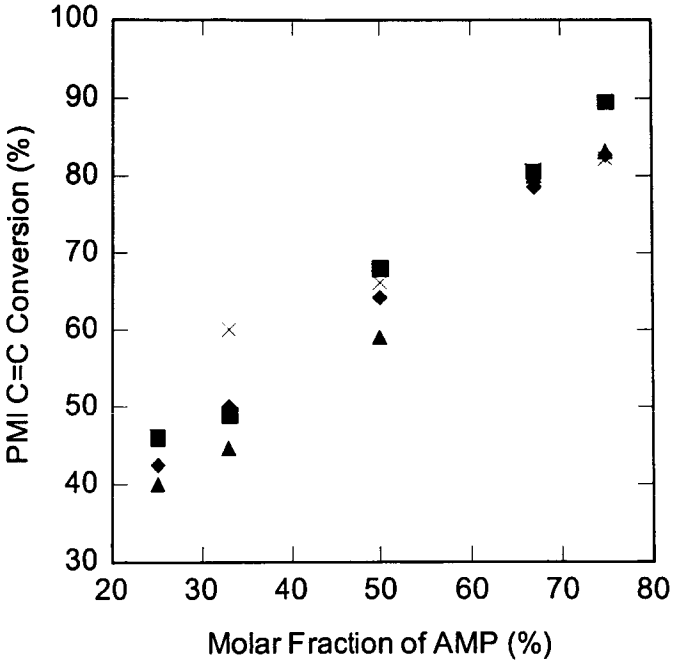

Figure 6.7 PMI C=C conversion with the increase of AMP amount (EB irradiation at 22°C): (▲) 3.5 kGy/min, (●) 4.4 kGy/min, (■) 7 kGy/min, (×) Thermal copolymerization (T = 110°C).

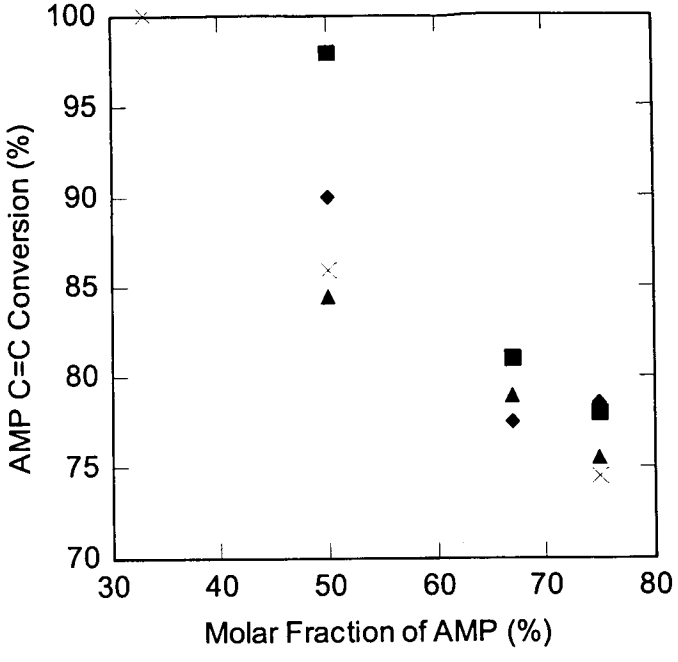

Figure 6.8 AMP C=C conversion with the change of AMP amount (EB irradiation at 22°C): (▲) 3.5 kGy/min, (●) 4.4 kGy/min, (■) 7 kGy/min, (×) Thermal copolymerization (T = 110°C).

For the purpose of further discussion, the residual amount of the PMI and AMP C=C after copolymerization based on the total numbers of moles in the system were calculated and plotted as Figure 6.9 and Figure 6.10 respectively. It can be seen from the figures, that for the compositions investigated, the residual amount of PMI C=C decreases with the increase of the AMP until it falls below 5%, while the residual amount of AMP C=C exhibits an increase until it reaches a value of about 15%. A similar result was obtained for thermally induced copolymerization. Furthermore, it was found that for low initial AMP molar fractions the residual molar ratio of PMI to AMP is much higher than the initial molar ratio and gets close to or even lower than the initial molar ratio with increasing AMP molar fraction. This indicates that with the increase of the AMP molar fraction, relatively more PMI C=C becomes part of

polymer chain. Under this circumstance, the lowest residual amount of PMI C=C and AMP C=C can not be obtained concurrently. Interestingly, with an AMP molar ratio as high as 75%, both PMI C=C and AMP C=C in EB induced copolymerization show higher conversion and lower residual amounts than those obtained by the thermal method, which suggests that EB irradiation may be advantageous in processing these materials. The questions arises: when BMI copolymerizes with AMP under EB irradiation, how can the best conversion for both monomers be obtained?

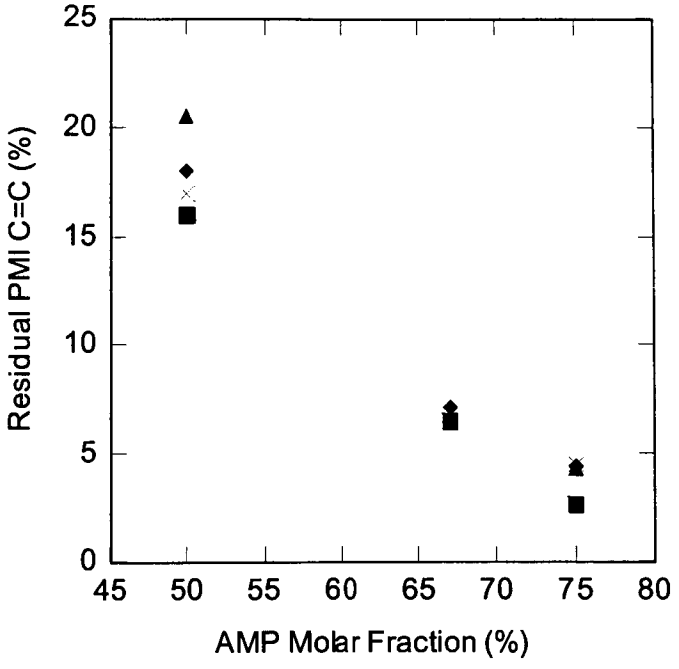

Figure 6.9 PMI C=C residual after EB and thermal (EB irradiation at 22°C): (▲) 3.5 kGy/min, (●) 4.4 kGy/min, (■) 7 kGy/min, (×) Thermal copolymerization (T = 110°C).

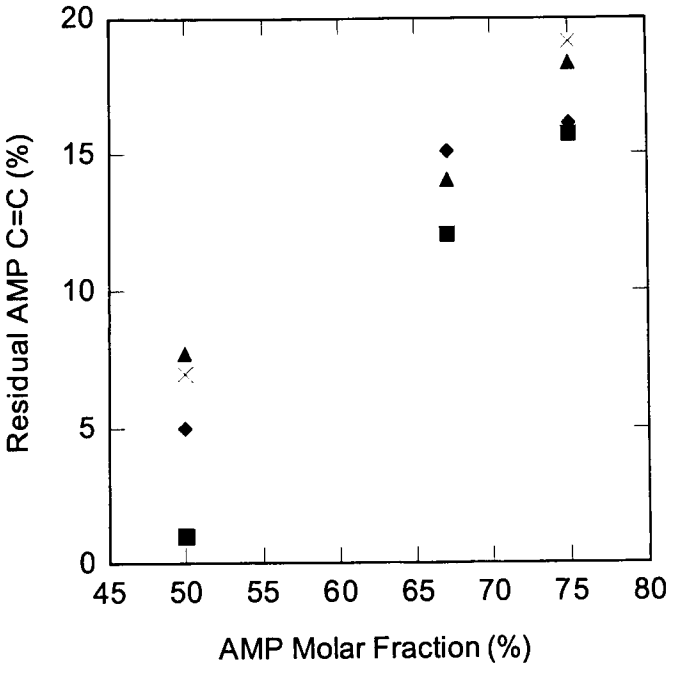

Figure 6.10 AMP C=C residual after EB and thermal (EB irradiation at 22°C): (▲) 3.5 kGy/min, (●) 4.4 kGy/min, (■) 7 kGy/min, (×) Thermal copolymerization (T = 110°C).

6.3.3 Influence of dose rate on the conversion of AMP and PMI

The influence of dose rate on the reaction rate and final conversion of AMP and PMI was investigated. The influence of dose rate on the reaction rate is presented in Figure 6.11, which shows representative conversion plots at 2 dose rates for the copolymerization of PMI and AMP (molar ratio 1:3) at 22°C. It was observed that the reaction rate increases with increasing dose rate during the initial stages of polymerization. Meanwhile, the polymerization at dose rate of 3.5 kGy/min possesses longer inhibition period of 3 second compared to that of 7 kGy/min, which is only 1 second.

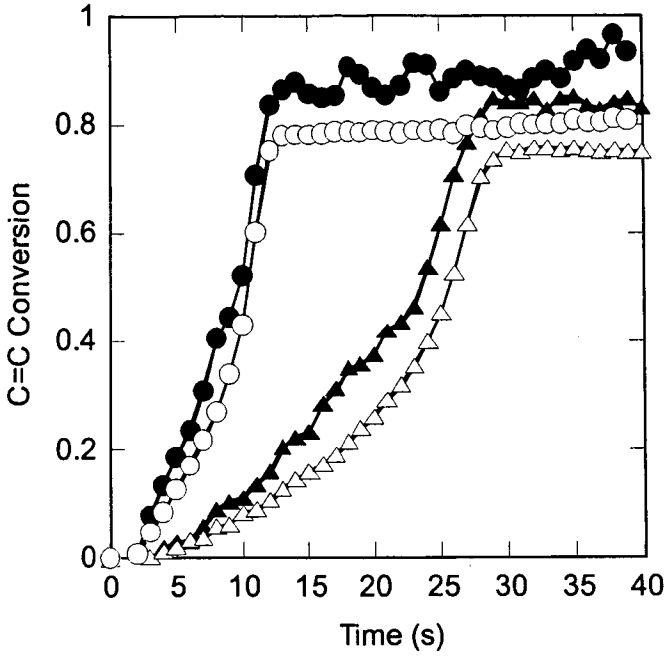

Figure 6.11 Plots of conversion vs. time for molar ratio of PMI to AMP as 1:3 with different dose rate at ambient temperature: (-■-) PMI (7 kGy/min), (-▲-) PMI (3.5 kGy/min), (-□-) AMP (7 kGy/min), (-Δ-) AMP (3.5 kGy/min).

To illustrate this observation more clearly, plots of the initial stages of the reaction (up to 20% conversion), neglecting the induction period, are shown in Figure 6.12 . The polymerization rate R_p of two kinds of C=C under different dose rates in the initial stage is obtained by taking the derivative of the curves in Figure 6.12. The values are summarized in Table 6.1

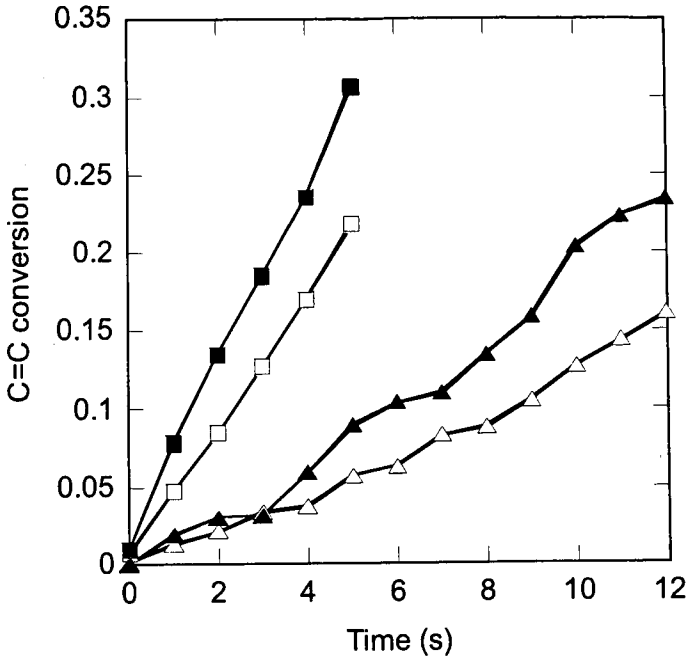

Figure 6.12 Initial stage plots of conversion vs. time for molar ratio of PMI to AMP as 1:3 with different dose rates at ambient temperature: (-■-) PMI (7 kGy/min), (-▲-) PMI (3.5 kGy/min), (-□-) AMP (7 kGy/min), (-Δ-) AMP (3.5 kGy/min).

Table 6.1 Polymerization rate R_p of different double bonds under different dose rates.

Dose rate (kGy/min)	Polymerization rate R_p (s^{-1})		
	PMI C=C	AMP C=C	Overall C=C
3.5	0.0202	0.0131	0.0333
7	0.0573	0.0419	0.0992

From the data in Table 6.1, it is seen that the rate of polymerization increases with increasing dose rate. It is believed that the higher polymerization rate as well as the shorter inhibition period associated with higher dose rate of 7 kGy/min is the result of the

more active centers produced per unit time. Also the "Trommsdorf effect" is more pronounced in polymerization at dose rate of 7 kGy/min, as shown in Figure 6.11.

With regard to final conversion, Figure 6.7 and Figure 6.8 show that dose rate has an influence on the conversion of C=C for both PMI and AMP. In summary, the final conversion of both AMP and PMI exhibits a tendency to increase with the increase of the dose rate. This influence decreases in significance at lower AMP molar fraction. This observation supports the assertion that a higher rate of free radical generation leads to higher conversion; however, the influence of the dose rate on final conversion is also affected by diffusion limitation associated with vitrification. First, higher AMP content lowers Tg of the copolymer so that higher conversion may be attained before Tg reaches T_{cure}, and secondly the exotherm may be influenced by the initial composition and dose rate.

6.3.4 Determination of the copolymerization parameters under different dose rate

A goal of this work is to understand how AMP co-reacts with PMI so that an understanding of how AMP would be incorporated into a BMI network can be reached. For the purpose of giving satisfactory explanations for the above experimental results, copolymerization parameters were determined in our study. The Mayo-Lewis (M-L) method [9] based on Equation 6.19 was used to obtain the copolymerization parameters from the NIR data of experiments conducted at 22°C and three different dose rates for a number of AMP to PMI molar ratios.

The reactivity ratios of AMP and PMI are designated as r_A and r_P respectively. From the integrated equation for the copolymer composition, r_P is expressed as follows:

$$r_P = \frac{\log\frac{M_P^0}{M_P} - \frac{1}{p}\log\frac{1-p(M_A/M_P)}{1-p(M_A^0/M_P^0)}}{\log\frac{M_A^0}{M_A} + \log\frac{1-p(M_A/M_P)}{1-p(M_A^0/M_P^0)}} \qquad 6.20$$

where $p = (1 - r_A)/(1 - r_P)$. M_A^0 and M_P^0 are initial concentrations of AMP and PMI respectively while M_A and M_P are concentrations at time t of these two monomers. On the basis of Equation 6.20, each set of M_A^0, M_P^0, M_A and M_P that were measured by the NIR technique yielded corresponding values of r_P in the corporation of the arbitrary (positive or negative) values of the parameter p. r_A was then calculated for each value of p. Consequently, values of r_P and r_A were plotted with r_P as abscissa and r_A as ordinate yielding a straight line plot of r_A versus r_P.

Plots corresponding to experiments using three molar ratios under EB irradiation are given in Figure 13, 14, and 15 for dose rates of 3.5 kGy/min, 4.4 kGy/min, and 7 kGy/min respectively. The experiments were conducted at 22°C. For each dose rate, monomer concentration for different time ranges, i.e. 10s, 20s, 30s, were measured by *in-situ* NIR monitoring. The corresponding conversions for each monomer are given in Table 6.2. The points of intersection for these lines provide the reactivity ratios of N-acryloylmorpholine and N-phenylmaleimide. In the absence of experimental error, all of the lines would intersect at the same point, which would represent the proper values of r_A and r_P. In this experiment, an average point of intersection is taken to represent the best experimental pair of r_A and r_P.

Table 6.2 Conversions of PMI and AMP at different time periods in EB induced copolymerization with different dose rates.

Dose rate (kGy/min)	Time (s)	Molar ratio AMP:PMI	PMI conversion (%)	AMP conversion (%)
3.5	10	3:1	11	8
		2:1	31	31
		1:1	5	5
	20	3:1	37	26
		2:1	77	79
		1:1	27	26
	30	3:1	84	75
		2:1	77	78
		1:1	45	42
4.4	10	3:1	8	4
		2:1	15	14
		1:1	3	3
	20	3:1	24	17
		2:1	41	38
		1:1	15	27
	30	3:1	45	36
		2:1	79	76
		1:1	36	54
7	10	3:1	52	43
		2:1	20	21
		1:1	17	32
	20	3:1	87	79
		2:1	70	71
		1:1	54	83
	30	3:1	87	79
		2:1	82	82
		1:1	69	97

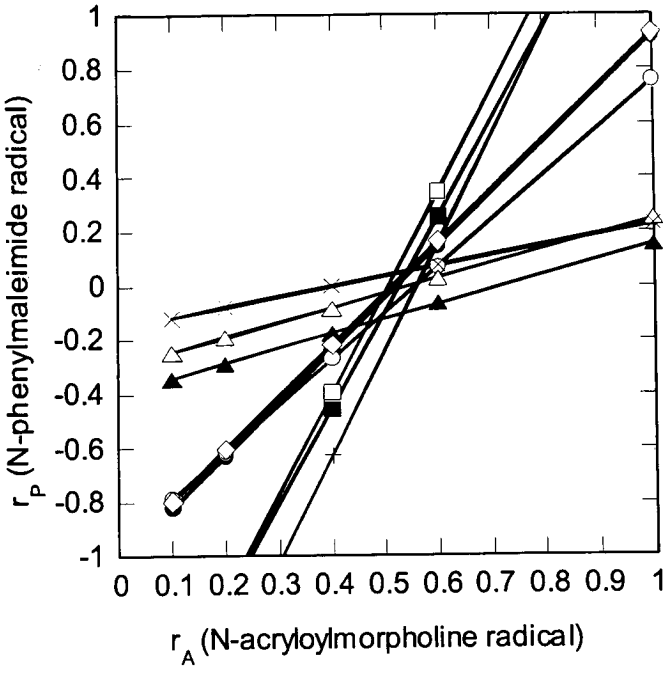

Figure 6.13 Copolymerization results with dose rate as 3.5 kGy/min (T = 22°C): (-■-) 3a1p (t = 10s), (-●-) 2a1p (t = 10s), (-▲-) 1a1p (t = 10s), (-□-) 3a1p (t = 20s), (-○-) 2a1p (t = 20s), (-Δ-) 1a1p (t = 20s), (-+-) 3a1p (t = 30s), (-◊-) 2a1p (t = 30s), (-×-) 1a1p (t = 30s).

In Figure 6.13, all the lines intersect at a point close to $r_P = 0$ and $r_A = 0.51$. And similarly, the values of 0 and 0.45 were assigned to r_A and r_P respectively from Figure 6.14.

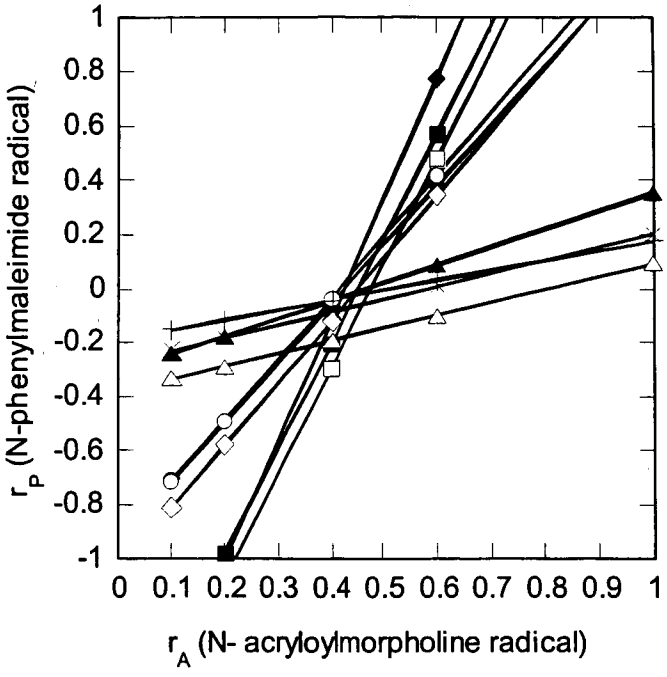

Figure 6.14 Copolymerization results with dose rate as 4.4 kGy/min (T = 22°C): (-■-) 3a1p (t = 10s), (-●-) 2a1p (t = 10s), (-▲-) 1a1p (t = 15s), (-□-) 3a1p (t = 20s), (-○-) 2a1p (t = 20s), (-Δ-) 1a1p (t = 20s), (-♦-) 3a1p (t = 30s), (-◊-) 2a1p (t = 30s), (-×-) 1a1p (t = 30s), (-+-) 1a1p (t = 35s).

As seen in Figure 6.15, the reproducibility of intersection is not as good at high dose rates, the value of r_A is in the range of 0.4~0.51 based on plots of r_P versus r_A at different time periods. The average value of r_p can be reasonably set as 0. Thus, it is reasonable to conclude that the reactivity ratio of PMI (r_P) is approximately 0 and the reactivity ratio of AMP (r_A) is in the range of 0.45-0.51. Moreover, it is concluded that the dose rate has no obvious effect on the copolymerization parameters of AMP and PMI at 22°C.

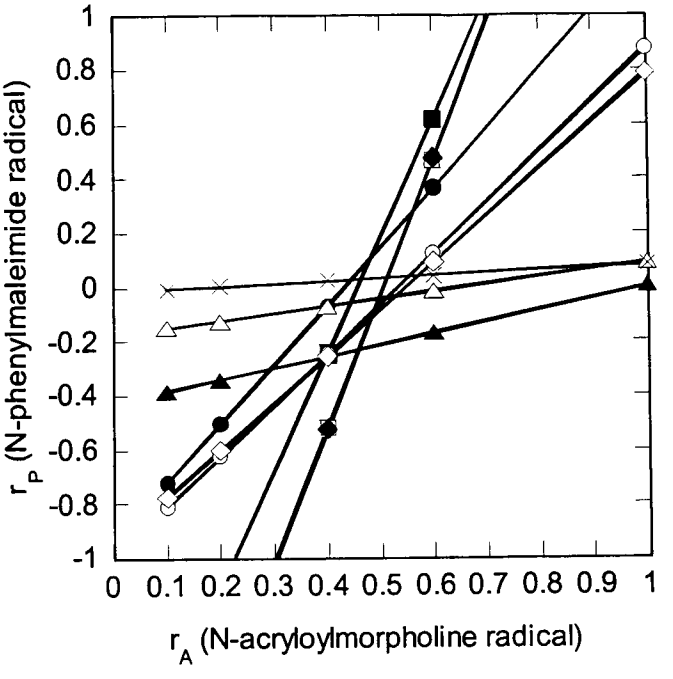

Figure 6.15 Copolymerization results with dose rate as 7 kGy/min (T = 22°C): (-■-) 3a1p (t = 10s), (-●-) 2a1p (t = 10s), (-▲-) 1a1p (t = 10s), (-□-) 3a1p (t = 20s), (-○-) 2a1p (t = 20s), (-Δ-) 1a1p (t = 20s), (-♦-) 3a1p (t = 30s), (-◊-) 2a1p (t = 30s), (-×-) 1a1p (t = 30s).

In the case of $r_P = 0$, the polymer chain end in PMI would not react with PMI monomer, instead it should react with AMP monomer. On the other hand, $r_A = 0.5$ means the polymer chain end in AMP would be more likely to react with PMI rather than with AMP. Therefore, it is believed that an alternating copolymer is generated for AMP copolymerizing with PMI under EB irradiation at 22°C.

6.3.5 Determination of initiator induced thermal copolymerization parameters

For comparison, the initiator induced thermal copolymerization parameters were also investigated using the Mayo-Lewis (M-L) method. The reaction time scales were

selected corresponding to conversion of AMP C=C of 10%, 30%, and 60%. As shown in Figure 6.16, data for a 3 to 1 molar ratio of AMP to PMI, obviously exhibits three separated groups of lines from left to right which correspond to three conversion ranges as 0~30% (stage I), 30%~60% (stage II), and above 60% (stage III) respectively.

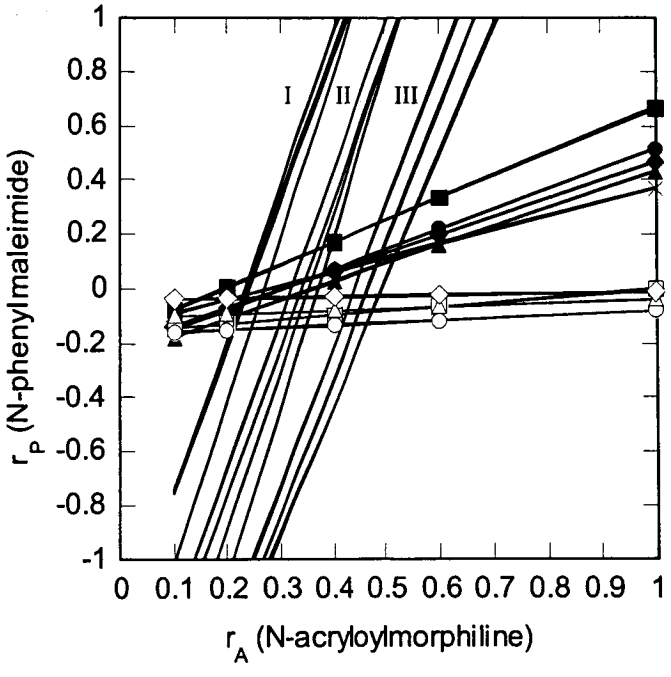

Figure 6.16 Copolymerization results for thermally polymerization at 110°C (Luperox 101 as initiator with concentration as 0.1 mol.%): (-■-)1a1p (t = 22min), (-●-) 1a1p (t = 25min), (-▲-) 1a1p (t = 30min), (-♦-) 1a1p (t = 35min), (-×-) 1a1p (t = 50min), (-□-) 1a2p (t = 16min), (-○-) 1a2p (t = 25min), (-Δ-) 1a2p (t = 30min), (-◊-) 1a2p (t = 35min). Three groups of lines correspond to three reaction stages I, II, and III in copolymerization of AMP and PMI at a molar ratio 3:1.

Therefore, the values of r_A based on the three intersecting points were 0.25, 0.3 and 0.4 respectively. The value of r_P showed just a slight variation around 0 for these three reaction stages. In Mayo's experiment [9], the phenomenon that a higher value of

the reactivity ratio would be obtained if longer reaction times and higher conversion of monomers were selected in measuring the monomer reactivity ratio, was observed. It was thought that the difference in monomer mobility which became more significant with the progress of copolymerization due to the diffusion limitation, is responsible for this. Thus for some monomer pairs, the whole copolymerization could be divided into several stages characterized by a different monomer reactivity ratio. The concept of intrinsic monomer reactivity ratio is used to describe the reaction behavior in the absence of diffusion limitations. Generally "intrinsic" parameters are obtained at low conversions. The increasing value of the AMP monomer reactivity ratio as copolymerization progresses, results from changes in monomer and polymer chain mobility. This may also be a reason for the fact that the monomer reactivity ratio of AMP in EB induced copolymerization at room temperature is of higher value.

To our knowledge, aside from this, no study on the determination of monomer reactivity ratio of PMI and AMP has been carried out. However, in Nair's work [13], it was reported that in the copolymerization of N-(4-hydroxyl phenyl) maleimide (HPM) with methyl methacrylate (MMA), the monomer reactivity ratio of HPM is 0 and that of MMA is in the range of 1-1.4, whereas for HPM with styrene, both values are close to 0. On the contrary, for the system of HPM with butyl acrylate (BuA), reactivity ratios of two monomers are in the range of 0.6-1.6 and 0.8-1 respectively depending on the solvent. The differences in results seem to arise from the electron donating ability of the coreactant with respect to HPM. BuA is electron-deficient just like HPM, while MMA is a moderately electron-rich monomer, and styrene is a well-known electron-rich monomer. Electron-rich and electron-deficient pairs can form an alternating copolymer by the

donor-acceptor mechanism, as is the case of HPM and styrene. On the other hand, it is pointed out [13] that in the case of HPM-BuA, both monomers are electron-deficient and hence their copolymerization is thermodynamically not favorable. It was discussed in Chapter 5 that the donating ability of AMP lies somewhat between that of styrene and MMA due to its special structure. We suspect that the interaction between the electron withdrawing nature of the carboxyl group and the electron donating of the nitrogen make AMP more like an electron donating monomer compared with MMA. This is reflected in a reactivity ratio as of 0.25 (thermal) compared to 0.6. Similarly, the electron donating ability of AMP is less than that of styrene due to the existence of the electron withdrawing carboxyl group connected directly with the C=C group. Thus a donor-acceptor complex is more easily formed in a PMI-St system. This is also supported by the DSC measurement studies (Figure 5.12 and Figure 5.14) which show the reaction peak temperature of the thermally induced copolymerization of PMI and St is lower than that of the AMP and PMI system.

In thermally induced copolymerization, charge-transfer interactions take place in the ground state and it is expected that EB irradiation would result in similar interactions taking place in excited states [14]. This would suggest that EB induced charge-transfer polymerizations need weaker charge-transfer interactions and could encompass a much wider range of donor-acceptor combinations. Therefore, PMI and AMP combinations would polymerize readily under EB radiation. This view is supported by the observations that under EB irradiation the copolymerization proceeds at room temperature and the PMI C=C conversion can reach 80%, a value similar to one obtained by initiator induced thermal copolymerization conducted at 110° C.

In fact, this characteristic is a prerequisite for AMP to be used as reactive diluent in the processing of BMI-CE IPNs in that it maintains AMP-BMI reaction stability up to 140°C, providing a wide processing window, yet it copolymerizes with BMI readily under EB radiation at low temperature by following a charge-transfer mechanism. This results in the incorporation of AMP into the copolymer.

6.3.6 Influence of temperature on the EB induced copolymerization behavior

The results of C=C conversion versus time for copolymerization of PMI and AMP with a 1:3 molar ratio are presented in Figure 6.17 for three reaction temperatures. Measurement of reaction exotherm for experiments were conducted at 50°C and 80°C by connecting a thermal couple to the sample tube. Figure 6.18 and 6.19 give the results of the measured exotherms at these two temperatures respectively. Note that the exotherm lasts much longer than the reaction. With the increase of temperature, the reaction rate shows an obvious increase as illustrated in Table 6.3, accompanied by a faster heat release that is supported by the exotherm observed in separate temperature monitoring experiments. The final conversion of PMI C=C is higher than that of AMP C=C at room temperature. However, this situation reverses at higher temperatures. Besides this, the final conversion of AMP C=C was improved with the increase of temperature. The abnormality in the AMP C=C conversion curve at 80°C shown in Figure 6.17 is a result of crack formation within the sample during the late stages of reaction, which resulted in an abnormal peak height of AMP C=C. Interestingly, the conversion of PMI C=C decreases with the increase of temperature from 22°C to 50°C and then increases again from 50°C to 80°C. This phenomenon is thought to be the outcome of various factors

such as reaction temperature, exotherm, mobility difference of two monomers and so forth. The further study need to be carried out to disclose it.

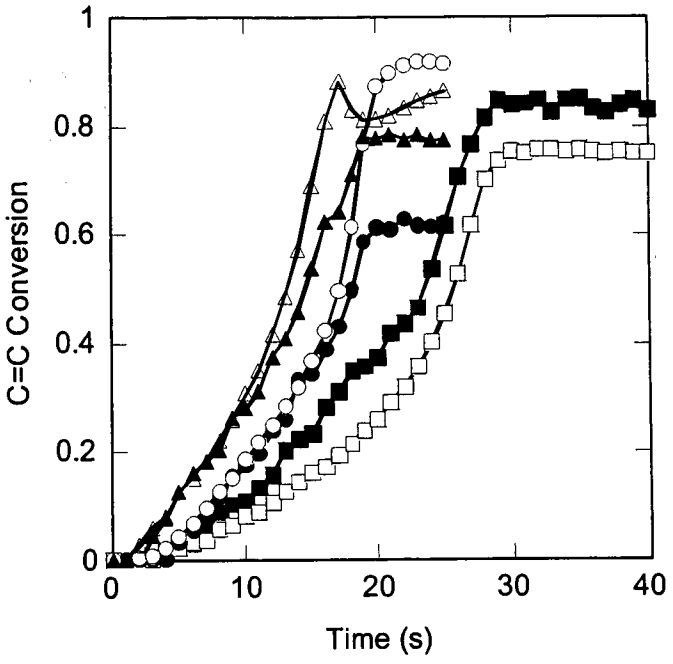

Figure 6.17 Plots of conversion vs. time for molar ratio of PMI to AMP as 1:3 with dose rate as 3.5 kGy/min under different temperatures: (-■-) PMI (22°C), (-●-) PMI (50°C), (-▲-) PMI (80°C), (-□-) AMP (22°C), (-○-) AMP (50°C), (-Δ-) AMP (80°C).

Table 6.3 Polymerization rate R_p of different double bonds with dose rate as 3.5 kGy/min under different temperatures.

Temperature (°C)	Polymerization rate R_p (s^{-1})		
	PMI C=C	AMP C=C	Overall C=C
22	0.0131	0.0087	0.0218
50	0.0185	0.0195	0.038
80	0.0313	0.0315	0.0628

It was found from exotherm experiments that the temperature remains fairly constant (within 1 or 2 degrees of the set temperature) during the first 10 sec of polymerization. During this time only modest conversion occur, for example at 80°C only 12% percent of C=C conversion is obtained. It can be reasonably deduced that at low conversion, the temperature within the sample tubes did not deviate greatly from the set temperature. This is especially true at 22°C and 50°C. Thus the following analysis of copolymerization parameters was done for a reaction time below 10 sec.

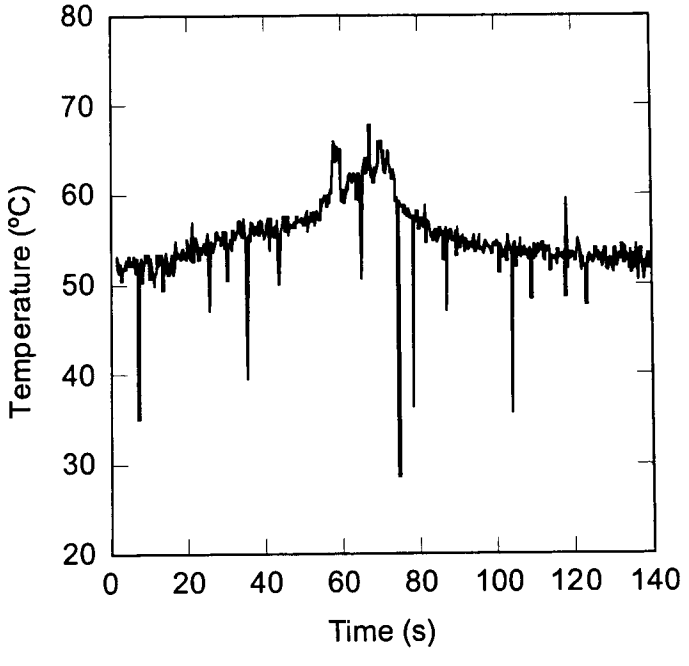

Figure 6.18 Temperature variation during the EB radiation at 50°C for 1:3 molar ratio of PMI to AMP (dose rate = 3.5 kGy/min).

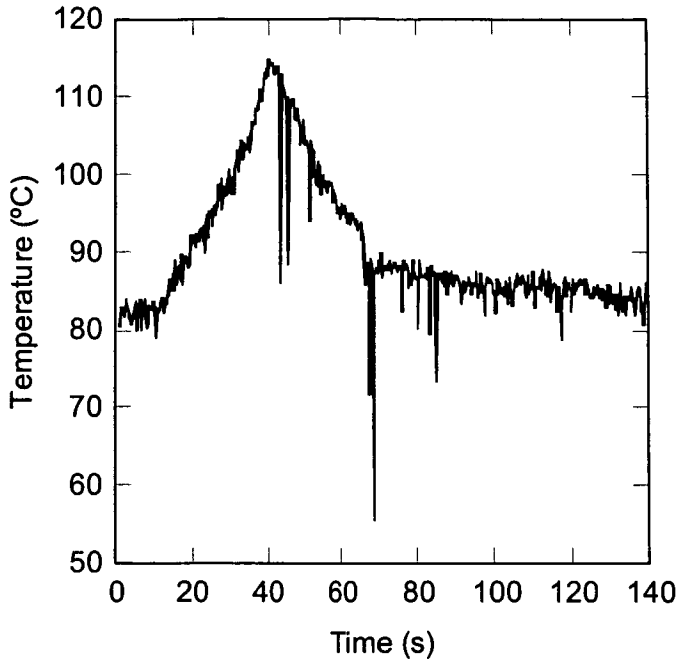

Figure 6.19 Temperature variation during the EB radiation at 80°C for 1:3 molar ratio of PMI to AMP (dose rate = 3.5 kGy/min).

To obtain a clear understanding of the temperature effect on copolymerization, the copolymerization parameters at different temperatures were evaluated and the results are presented in Figure 6.20 and Figure 6.21.

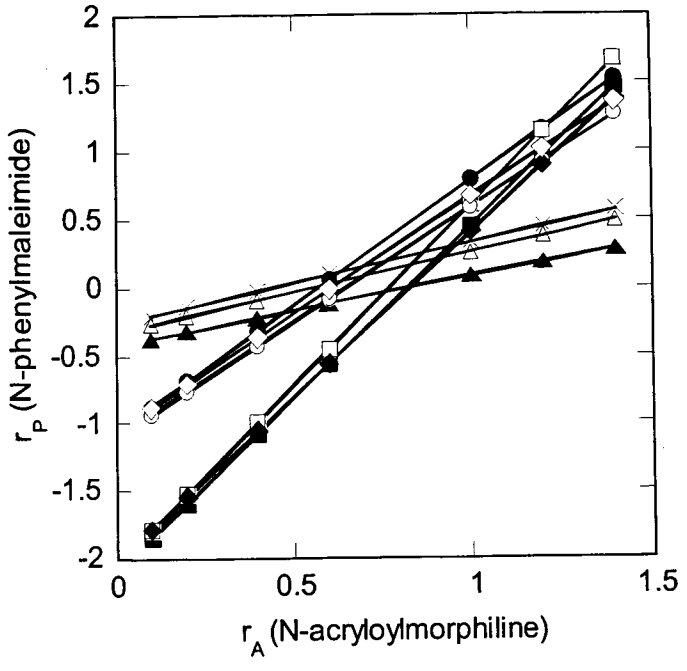

Figure 6.20 Copolymerization results with temperature as 50°C (dose rate = 3.5 kGy/min): (-■-) 3a1p (t = 5s), (-●-) 2a1p (t = 5s), (-▲-) 1a1p (t = 5s), (-□-) 3a1p (t = 7s), (-○-) 2a1p (t = 7s), (-Δ-) 1a1p (t = 7s), (-♦-) 3a1p (t = 10s), (-◊-) 2a1p (t = 10s), (-×-) 1a1p (t = 10s).

It can be concluded from the two figures that at temperature 50°C, the values of r_P and r_A are 0~0.4 and 0.6~0.8 respectively, while at temperature 80°C, the values are 0.6 and 1 respectively. Thus both the values of r_P and r_A increase but are less than 1 as the temperature increases. Flory [15] attributed this type of behavior to the difference in the activation energy which at least partially can account for the difference in relative rates of competing reactions with increasing temperature.

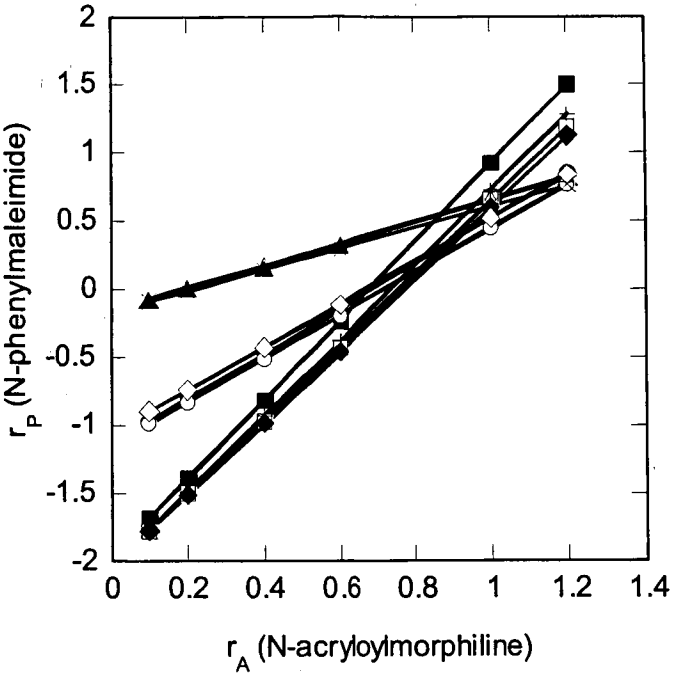

Figure 6.21 Copolymerization results with temperature as 80°C (dose rate = 3.5 kGy/min): (-■-) 3a1p (t = 5s), (-●-) 2a1p (t = 5s), (-▲-) 1a1p (t = 5s), (-□-) 3a1p (t = 8s), (-○-) 2a1p (t = 7s), (-Δ-) 1a1p (t = 8s), (-*-) 3a1p (t = 10s), (-◊-) 2a1p (t = 13s), (-×-) 1a1p (t = 10s), (-+-) 3a1p (t = 4s).

6.4 Summary

A Near-IR technique has been demonstrated to be an effective method for *in-situ* monitoring of free radical cure processes induced by EB radiation. The technique was employed in this study to investigate the copolymerization behavior of *N*-phenylmaleimide (PMI) and N-acryloylmorpholine (AMP) in order to obtain a clear understanding of the copolymerization mechanism of this system and to determine optimum processing parameters for EB cure. It was found that both the dose rate and the molar fraction of AMP will have an influence on the conversion of maleimide double bonds under EB irradiation for a given cure temperature. Furthermore, the complete

conversion of both maleimide C=C and AMP C=C can be accomplished by increasing the amount of AMP and increasing the reaction temperature in EB irradiation. As a critical parameters for understanding copolymerization behavior, monomer reactivity ratios of maleimide double bonds and AMP double bonds were obtained using the Mayo-Lewis (M-L) method. Typical values of 0 and 0.45~0.51 were obtained for PMA and AMP reactivity ratios respectively. Our analysis showed that the copolymerization behavior under EB irradiation was not appreciably affected by dose rate in the range investigated, but was significantly influenced by temperature in that an increase of reactivity ratio values for both components was observed at higher temperature. Based on these observations, it was deduced that a pseudo-alternating copolymer is likely formed under electron beam irradiation at low temperature, though a tendency to form block copolymer is likely to occur at high temperatures.

N-acryloylmorphiline is a promising candidate to improve the BMI processibility for cure by EB irradiation. PMI was used as a model compound in EB the cure kinetics study. AMP serves as an electron donor due to its electron rich character compared to PMI and thus can copolymerize with PMI easily and effectively under EB irradiation via a charge-transfer mechanism. The conversion of maleimide double bond under EB irradiation was greatly improved using AMP. At the same time, the existence of the carboxyl group in AMP, which is electron withdrawing, tempers its electron donating ability, and therefore maintains the thermal stability of the BMI and AMP upon heating. This balance is important because it provides a broad processing window for the system while maintaining high reactivity under EB.

List of References

1. Brown J.M., S. Srinivansan, A. Rau, T.C. Ward, J.E. McGrath, A.C. Loos, D. Hood, D.E. Kranbeuhl. *Production of controlled networks and morphologies in toughened thermosetting resins using real-time, in situ cure monitoring.* Polymer 1996;37(9):1691-6.

2. Mijovic J., W.V. Corso, L. Nicolais and D. Guglielmo. *In situ real-time study of crosslinking kinetics in thermal and microwave fields.* Polymers for Advanced Technologies 1998;9(4):231-43.

3. North A.M. *The kinetics of free radical polymerization. 1st edition,* Pergamon press, 1966.

4. Odian G.. *Principle of polymerization. 3rd edition*, John Wiley & Sons, INC. New York, 1991.

5. George G.A., P. Cle-Clarke, N.St. John, and G. Friend. *Real-time monitoring of the cure reaction of a TGDDM/DDS epoxy resin using fiber optic FT-IR.* Journal of Applied Polymer Science 1991;42(3):643-57.

6. Corso W.V. and J. Mijovic. *Comparison of microwave and thermal reaction kinetics via in-situ FTIR spectroscopy.* Ceramic Transactions (1997), 80 (Microwaves: Theory and Application in Materials Processing IV), 173-183.

7. Hopewell J.L., G.A.George, D.J.T. Hill. *Quantitative analysis of bismaleimide-diamine thermosets using near infrared spectroscopy.* Polymer 2000;41(23):8221-9.

8. Musto P., E. Martuscelli, G. Ragosta, L. Mascia, *Cure kinetics and ultimate properties of a tetrafunctional epoxy resin toughened by a perfluoro-ether oligomer.* Polymer 2001;42(12):5189-98.

9. Mayo F.R. and F.M. Lewis. *Copolymerization. I. A basis for comparing the behavior of monomers in copolymerization; The copolymerization of styrene and methyl methacrylate.* Journal of American Chemical Society 1944;(66):1594-601.

10. Schulz G.V. and G. Harborth. *Determination of molecular weight and of volume expansion of fibrous molecules by light scattering.* Makromolekulare Chemie 1947;(1):106-39.

11. Norrish R.G.W. and R.R. Smith. *Catalyzed polymerization of methyl methacrylate in the liquid phase.* Nature 1942;150:336-7.

12. Trommsdorff E., H. Köhle and P. Lagally. *Polymerization of methyl methacrylates.* Makromolekulare Chemie 1948;(1):169-98.

13. Nair C.P.R, D. Mathew and K.N. Ninan. *Free radical copolymerisation of N-(4-hydroxy phenyl) maleimide with vinyl monomers: solvent and penultimate-unit effects..* European Polymer Journal 1999;35(10):1829-40.

14. Li T., W.X. Cao, X.D. Feng. *Photoinduced charge-transfer polymerizations of vinyl monomers.* Journal of Macromolecular Science - Reviews in Macromolecular Chemistry and Physics 1989;C29(2&3):153-99.

15. Flory P.J. *Principles of Polymer Chemistry.* George Fisher Baker Non-Resident Lec, New York, 1953

CHAPTER 7: PROPERTIES OF THE SEQUENTIAL IPN AND CORRELATIONS WITH STRUCTURE

It is well known that the final properties of materials depend greatly on their chemical structure. Thus, the properties of the IPNs being developed are most easily and clearly understood when they are correlated with structure, in terms of the monomer, IPN composition, and crosslinking density. In this chapter the relationship between IPN structure and properties such as Tg, long term stability, thermal decomposition, and fracture toughness is investigated. Particular attention is placed on examining the question of potential property benefits associated with using IPNs and coupling the two networks of the IPN.

7.1 Effect of AMP Content on the Tg of the Formed Sequential IPNs

A number of sequential IPNs with varied AMP-BMI molar ratio were synthesized to acquire a preliminary understanding of how the amount of reactive affects the IPNs performance. Table 7.1 details the composition of the blends tested in this study. The second network formation for all these samples was completed by employing the thermal method rather than EB irradiation. The processing conditions and method for three IPNs were as follows. The blends of LECY and AMP were mixed with 300 ppm copper naphthenate (based on Cu^{2+}) at about 120°C until the color of the solution changed to deep green indicating that a complex between cyanate ester and Cu^{2+} was formed. Consequently, the appropriate amount of BMI and network coupler was added to the solutions to form homogeneous mixtures at 120°C. The mixtures were then cured at

110°C for 5 hours and 130°C for 2 hours to form the cyanurate network. The bismaleimide network formation was realized by a thermal scan to 310~330°C using a DMA instrument or by electron beam irradiation for which processing parameters are given in section 3.2.3.

Compositions in Table 7.1 contain molar ratios of BMI to AMP of 1:2, 1:3, and 1:4. They correspond to AMP molar fractions in the AMP-BMI components of the blends of 66.6%, 75% and 80% respectively. The molar fractions were selected based on the results of the investigation reported in Chapter 6 wherein the influence of monomer concentration, copolymerization parameters, as well as processing parameters such as temperature and dose rate on the performance of AMP and N-phenylmaleimide were reported.

Table 7.1 Compositions of samples in this study (all blends contained 1% copper naphthenate (6% Cu^{2+})).

Ref. of IPN	wt.% LECY	wt.% BMI	wt.% AMP
BA0-50	50	50	0
BA2-50	50	28	22
BA3-50	50	23	27
BA4-50	50	19	31

The Tg values of IPNs with varied amounts of AMP are summarized in Figure 7.1, with two lines (solid and dotted) representing the upper and lower limits for the Tg of the IPNs corresponding to Fox's rule (Equation 7.1) and the weighted average rule (Equation 7.2) respectively (Tg is in degrees K). Tgs of homopolymers derived from the monomers

of interest are given in Table 7.2. This table contains values of Tg measured in this study by DSC and DMA and values from literature.

$$\text{Lower bound: } 1/T_g = X_{Lecy}/T_{g\text{-}Lecy} + X_{BMI}/T_{g\text{-}BMI} + X_{AMP}/T_{g\text{-}AMP} \quad 7.1$$

$$\text{Upper bound: } T_g = X_{Lecy}T_{g\text{-}Lecy} + X_{BMI}T_{g\text{-}BMI} + X_{AMP}T_{g\text{-}AMP} \quad 7.2$$

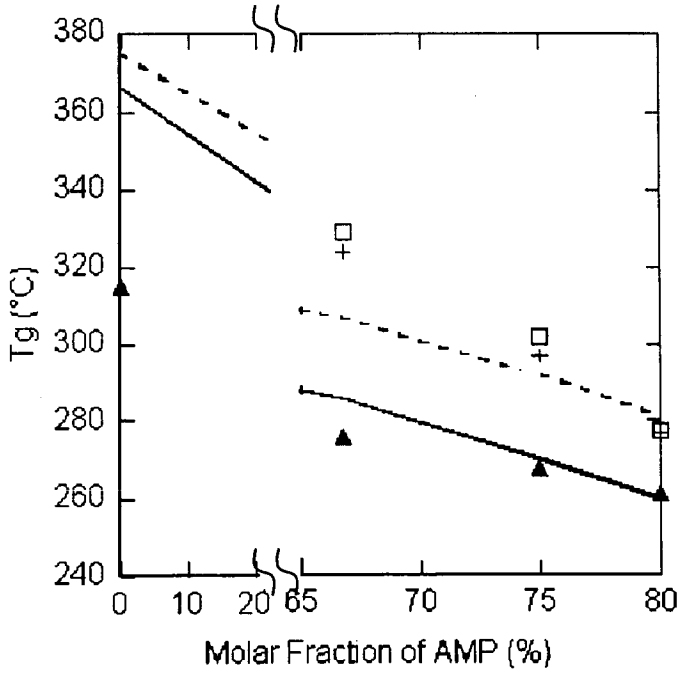

Figure 7.1 Tg results for the samples of 50 wt.% BMI and AMP 50 wt.% LECY with different amount of AMP: (—) lower bound (obtained by Fox's rule), (---) upper bound (obtained by weighted average rule), (-▲-) without adding of CPM, (-□-) after adding 10 wt.% to 20 wt.% of CPM, (-+-) predicted values of IPNs with different amount of CPM.

Table 7.2 Tgs of the various monomers employed in the current study.

Monomer name	measured by DMA	measured by DSC	reference value
AMP	142.5°C	120°C	147°C [1]
LECY	300°C	---	259°C [2]
BMI	450°C	430°C	380°C [3] ~ 430°C [4]
CPM	580°C *	560°C *	---

* values derived from experiment results by weighted average rule (see section 7.2)

As observed on the chart, without AMP, Tg of blends of 50 wt.% BMI and 50 wt.% LECY deviates greatly from the lower limit, whereas in the presence of AMP, the Tgs of the IPNs match up favorably with Fox's rule with a small deviation in the AMP molar fraction of 66.6% (corresponding to the AMP:BMI molar ratio of 1:2). In synthesizing IPNs composed of only BMI and LECY, a temperature of 140°C was employed to ensure the complete dissolution of BMI in LECY. However, concurrent reaction of BMI also takes place that leads to the occurrence of simultaneous IPNs, which may account for the marked deviation. The Tg of IPNs with an AMP/BMI molar ratio of 1:2 is higher than those with molar ratios of 1:3 and 1:4, but lower than that with 1:0. One explanation for this is that the addition of more AMP, whose polymer possesses the lowest Tg among the various components, lowers the ultimate Tg of the blends. Therefore, it can be reasonably concluded from these results that lessening the amount of AMP favors the ultimate Tg; on the other hand, the presence of a certain amount of AMP will also improve the processability of BMI and make the synthesis of sequential IPNs feasible. To further improve the Tg of the formed IPNs, the role of the network coupler in enhancing the ultimate Tg will be discussed in the following section.

7.2 Role of the Network Coupler in the Enhancement of Tg of Sequential IPNs

The influence of a network coupler was first investigated in terms of its quantity on the Tg of the neat resin. Table 7.3 gives the composition of the blends investigated. These samples were made by replacing the content of LECY in formulation given in Table 7.1 with increasing amount of CPM. The results are also given in Figure 7.1. Clearly, when adding CPM all three IPN systems result in a pronounced improvement of Tg that exceed or come close to the upper bound line computed earlier.

Table 7.3 Compositions of samples in this study (all blends contained 1% copper naphthenate (6% Cu^{2+})).

Ref. of IPN	wt.% CPM	wt.% LECY	wt.% BMI	wt.% AMP
BA2-30-20	20	30	28	22
BA3-35-15	15	35	23	27
BA4-40-10	10	40	19	31

Interlinking the networks appears to increase Tg substantially. Of course, another way to interpret these results is that CPM itself may have a Tg which is much higher than that of LECY when fully cured. There is no reference that provides the Tg of the CPM. One reason for this is that the Tg of CPM is extremely high so that prior to the detection of Tg by analytical methods, poly-CPM decomposes. For example, in our experiments, if a poly-CPM sample was postcured at 400°C, the Tg of CPM could reach 430°C, whereas simultaneously, the CPM underwent decomposition at this temperature due to the existence of the cyanurate ring. Accordingly, it seems impossible to obtain Tg of poly-CPM by using a pure poly-CPM sample. Therefore, the Tg of the CPM was derived from

the copolymers of the CPM and AMP of varied compositions whose Tgs were designed to be in the measurable range.

A series of CPM-AMP copolymer samples containing 1%, 5%, 10%, 15%, 20% of CPM (in weight fraction) were thus prepared according to the following procedure. CPM was mixed with corresponding amount of AMP at 120°C in the presence of 1.5% copper naphthenate (6% Cu^{2+}), the so obtained mixture was sealed tightly in a glass bottle which was then placed in oven at 130°C for 3 hours and held overnight at temperature of 210°C (approximately 12 hours) (except for 99% AMP 1%CPM which was kept at 170°C). Furthermore, DMA scans to 310°C were used for postcuring. One reason for selecting the above range of compositions is that when the amount of CPM exceeds 25%, phase separation was observed. Figure 7.2 and Figure 7.3 summarize the Tgs obtained by DMA and DSC analyses respectively. The DMA and DSC plots are given in Appendix III.

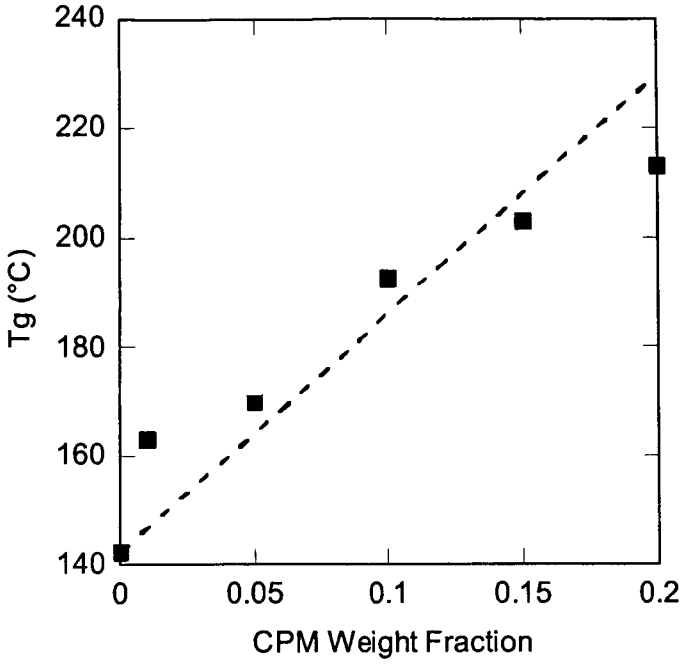

Figure 7.2 Tgs of copolymer of CPM and AMP with varied weight fraction of CPM (by DMA): (---) upper bound calculated by weighted average rule (obtained with presumed Tg of CPM as 580 °C).

To understand which mixing rule should be applied to predict CPM Tg from the data in Figures 7.2 and 7.3, as a reference, a series of BMI-AMP copolymer samples with similar composition were also synthesized by the following procedure. The copolymerization of BMI and AMP was carried out in the presence of Luperox 101 as thermal initiator (0.2% based on moles of C=C). The conditions for reaction were as follows: 110°C for 2 hours, and 170°C ~ 210°C for another 3 hours. Finally, thermal scan to 310°C was employed to fulfill a complete reaction.

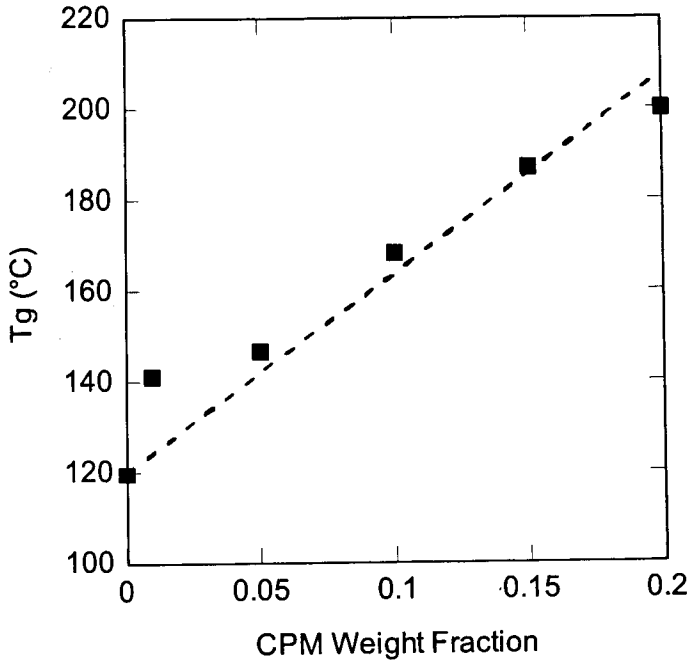

Figure 7.3 Tgs of copolymer of CPM and AMP with varied weight fraction of CPM (by DSC): (---) upper bound calculated by weighted average rule (obtained with presumed Tg of CPM as 560 °C).

The Tg results of the copolymer are shown in Figures 7.4 and 7.5, based on DMA and DSC analysis respectively. The DMA and DSC plots are also given in Appendix III. In general, there is a 20°C difference in Tg obtained by the two techniques. It was also found that for BMI weight fraction in excess of 50%, phase separation occurs. Using AMP Tg = 142°C (DMA) and BMI Tg = 450°C (DMA), the upper bond and lower bound mixing rules were used to predict Tg as a function of composition. Table 7.2 contains values of Tg for these systems obtained in our lab and from literature. For the purpose of analysis, herein the Tg values obtained with the same techniques used for testing the blends were adopted. It was found that the weighted average rule (upper bound) applies

to the BMI-AMP copolymer for the entire range of the BMI weight fractions investigated which is similar to those of the CPM-AMP systems investigated.

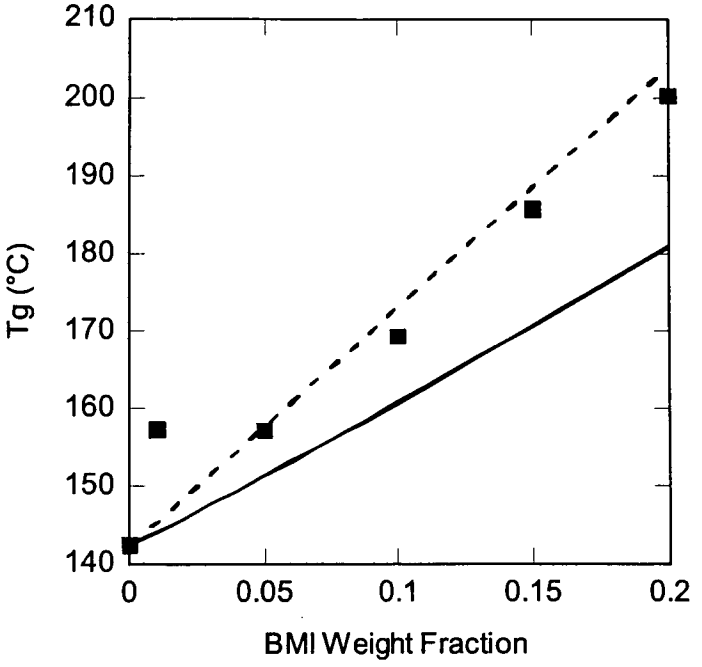

Figure 7.4 Tgs of copolymer of BMI and AMP with varied weight fraction of BMI (by DMA): (---) upper bound calculated by weighted average rule, (—) lower bound calculated by Fox's rule (both bounds were obtained with Tg of BMI as 450 °C).

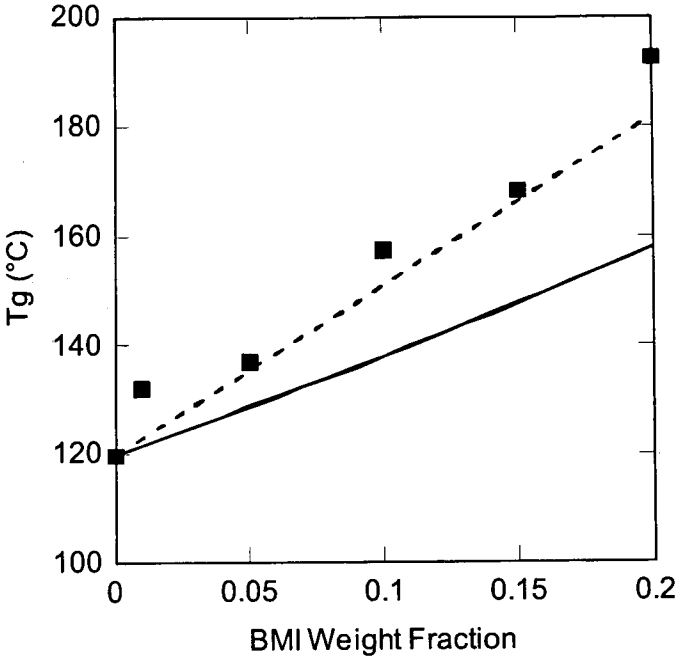

Figure 7.5 Tgs of copolymer of BMI and AMP with varied weight fraction of BMI (by DSC): (---) upper bound calculated by weighted average rule, (—) lower bound calculated by Fox's rule (both bounds were obtained with Tg of BMI as 430°C).

Assuming the same rule of mixtures applied for the CPM-AMP copolymer, Tgs of CPM are calculated to be 580° (for DMA data) and 560°C (for DSC data) respectively. Figures 7.2 and 7.3 contain the predicted Tgs based on this result. Interestingly, it was found that when a slightly higher value of Tg for AMP is used, the results match the weighted average rule more favorably in all cases. In fact, a lower Tg of the AMP was obtained and employed in our experiment compared to that found in the literature (147°C) [1].

By employing the value of 580°C as the Tg of CPM, deduced from DMA results, the theoretical Tgs of the IPNs were calculated by Fox's rule resulting in the points plotted in Figure 7.1. The good fit between the measured values and the theoretical values

imply that Fox's rule can be employed to predict the Tg of the interlinked IPNs as well. Therefore, the equation that can be used to predict the Tg of the sequential IPNs and therefore also for designing IPNs based on temperature requirements is as follows:

$$Tg = \frac{1}{\sum\left(w_i / Tg_i\right)} \qquad 7.3$$

where w_i is the weight fraction of each component and Tg_i is the Tg of each component.

The theoretical basis for predicting glass transition temperature from pure-component properties for compatible polymer blends was discussed in Couchman's work and is based on thermodynamic principles [5, 6]. In his work theoretical relations for the composition dependence of Tg was given on the basis of temperature-independent heat-capacity increments. The most general expression subsequently derived in terms of mass fraction is given as Equation 7.4.

$$\ln Tg = \frac{X_1 \Delta C_{p1} \ln Tg_1 + X_2 \Delta C_{p2} \ln Tg_2}{X_1 \Delta C_{p1} + X_2 \Delta C_{p2}} \qquad 7.4$$

If the ratio Tg_1/Tg_2 is not greatly different from unity, the logarithmic terms of Equation 7.4 may be approximated in the usual manner to give Equation 7.5.

$$Tg \sim \frac{X_1 \Delta C_{p1} Tg_1 + X_2 \Delta C_{p2} Tg_2}{X_1 \Delta C_{p1} + X_2 \Delta C_{p2}} \qquad 7.5$$

Accordingly, if the empirical rule $\Delta C_{pi}Tg_i \approx$ constant, substitution in Equation 7.4 gives the Fox equation. On the other hand, with two component system as an example, if $\Delta C_{p1}=\Delta C_{p2}$, simplification of Equation 7.5 yields the weighted average rule.

It can be deduced thereafter, for two components with similar ΔC_p, if the difference in Tg is not significant, such as vinylether and styrene, the Fox equation can be adopted to predict the Tgs of the copolymers based on the Tgs of the polymerized monomers; whereas, for components with large difference in their Tg such as BMI-AMP and CPM-AMP, the weighted average rule predicts the copolymer Tg more accurately. Meanwhile, the ultimate Tg of a multi-component system possessing less variation in component Tg might favor the use of Fox's rule rather than the weighted average rule.

7.3 Effect of CPM Amount on the Tg of Inter Linked Sequential IPNs

In order to assess the role of CPM in enhancing the Tg of interlinked sequential IPNs, as well as to verify the validity of the derived equation, a set of IPNs with different amounts of CPM were prepared via EB irradiation and thermal reaction methods as described by the procedures given in section 7.1. These IPNs maintained the molar ratio of BMI to AMP as 1:2 and weight fraction of LECY at 30%. Table 7.4 details the composition of the blends in this part of the investigation. The rationale for using 30% LECY in each composition is to maintain the necessary processibility and toughness. Moreover, it is known from preceding discussions that role of LECY in synthesizing IPNs relates to the formation of the first network. This network will limit the mobility of the semi-cured CPM and prevent its precipitation from solution which leads to macro

phase separation. The phase separation often found in CPM-AMP copolymerization did not occur even when the amount of CPM used in the IPNs was as high as 40%.

Table 7.4 Compositions of blends in this study (all blends contained 1% copper naphthenate (6% Cu^{2+})).

Blends designation	wt.% CPM	wt.% LECY	wt.% BMI	wt.% AMP
BC2-30-0	0	30	39	31
BC2-30-10	10	30	34	26
BC2-30-20	20	30	28	22
BC2-30-30	30	30	22	18
BC2-30-40	40	30	16	13

DMA plots of the interlinked sequential IPNs with different amounts of CPM are shown in Figures 7.6 and 7.7 with respect to storage modulus and loss modulus respectively.

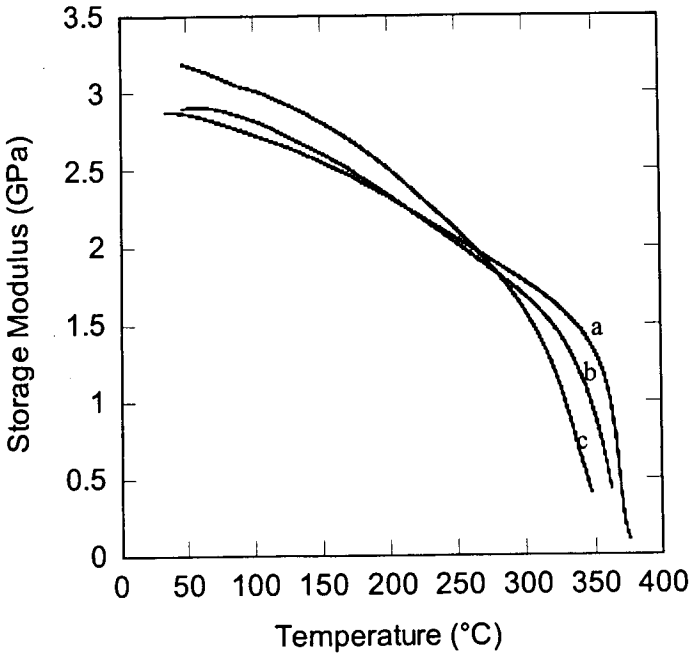

Figure 7.6 Dynamic mechanical spectra (storage modulus) of the interlinked IPNs: (a) BA2-30-40, (b) BA2-30-30, (c) BA2-30-20.

It is apparent that the higher loading of CPM increases the Tgs significantly which matches our predictions. Notably, BC2-40 gave the highest value of the Tg (Tg= 366°C). As a comparison, sequential IPNs formed via thermal cure were also prepared by DMA scanning to 330°C to ensure a complete cure.

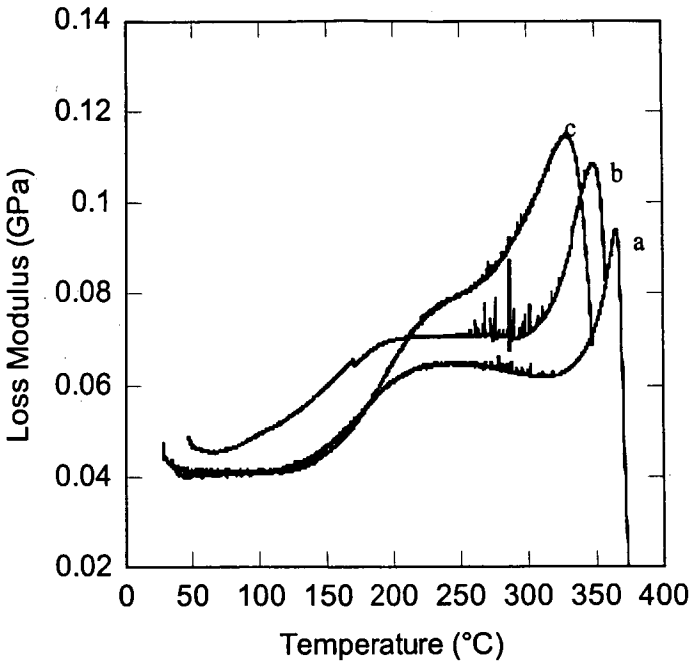

Figure 7.7 Dynamic mechanical spectra (Loss modulus) of the interlinked IPNs: (a) BA2-30-40, (b) BA2-30-30, (c) BA2-30-20.

The Tgs of both EB and thermal cured interlinked IPNs are summarized in Figure 7.8, together with the calculated upper and bottom bound by Fox's rule and the weighted average rule respectively. The Tgs obtained by EB irradiation are consistent with the ones obtained by the thermal cure. The measured values of Tg coincide with the ones predicted by Fox's rule and particularly well for high loading of CPM. This is consistent with previous observations. Furthermore, it can clearly be seen that with increasing CPM amount, the deviation between predicted values and actual values is diminished.

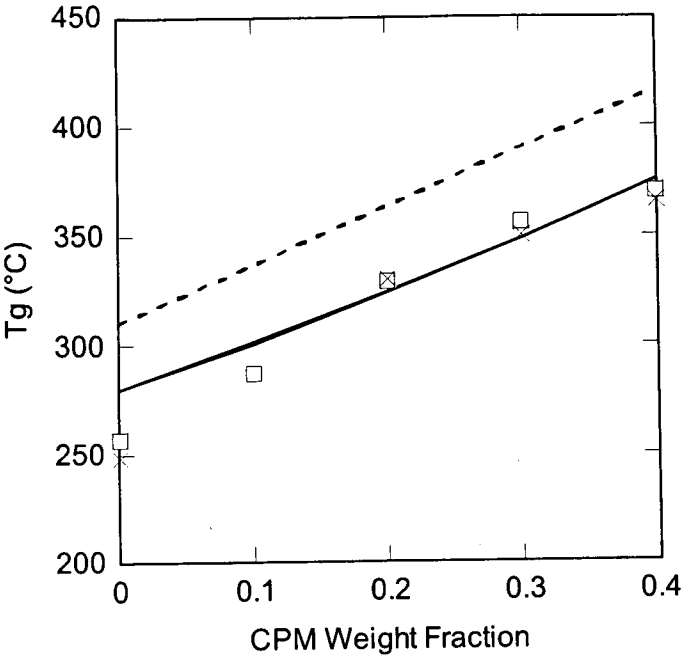

Figure 7.8 The change of Tg with the variation of CPM amount for IPN via different path: (-□-) Thermal cure, (-×-) EB irradiation, (---) upper bound obtained by weighted average rule, (—) lower bound obtained by Fox's rule.

The thermal cure behavior and postcure after EB irradiation can be differentiated by examining Figure 7.9, which displays two storage modulus plots for BC2-40 with different cure schedules. Shown on the chart, EB cured sample exhibits instant reaction with the progress of postcure that is reflected by the small peak in the glass transition region shoulder together with a broad decay zone for modulus. Whereas for the thermal cure sample, the sharp drop of the storage modulus indicates that once glass transition region of the first network is passed no reaction occurs for the next 100°C. The reaction in fact shows a lag period compared with the EB sample and begins to react at a temperature of 220°C. The different response of the EB cured sample to temperature of the environment implies that after EB irradiation, the unreacted free radicals produced in

EB irradiation are not terminated and are still sites of potential reactivity even though they will have lost mobility due to the vitrification. It is clear that postcure after EB irradiation is different from that of a thermally cured system since it requires less energy and possesses high cure efficiency.

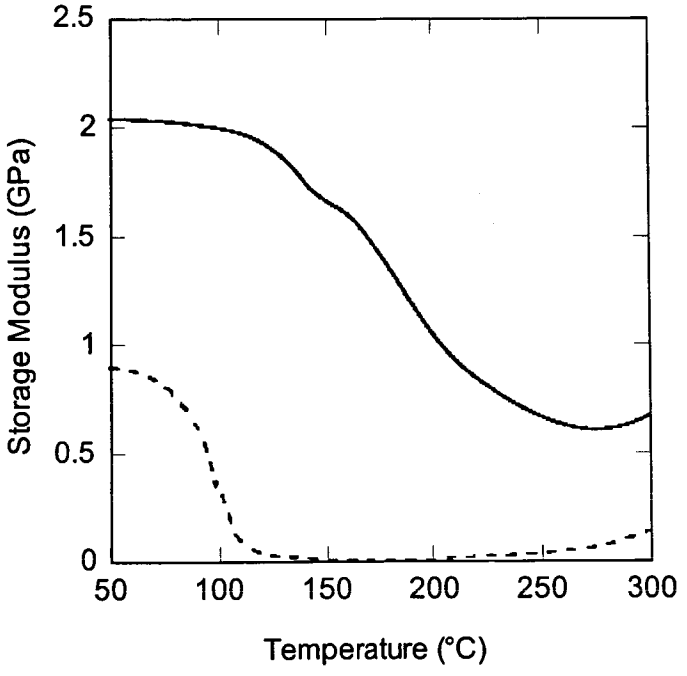

Figure 7.9 Dynamic mechanical analysis plots (Storage modulus) of the linked IPN: (—) EB BA2-30-40, (---) Thermal BA2-30-40.

7.4 Fracture Toughness of the Neat Resins

Fracture toughness of the neat resins and the interlaminar shear strength (ILSS) of the corresponding composite were evaluated using an Instron universal testing machine, model 8872. The procedure and the test results are summarized in Appendix IV.

For the fracture toughness measurement, two types of neat resin, with and without the presence of CPM, were tested. The formulations are as follows: Sample 1, IPNs—50% BMI and AMP (molar ratio 1:2), and 50% LECY; Sample 2, LIPNs—40% BMI and AMP (molar ratio 1:2), 30% LECY and 30% CPM. The corresponding Tgs are 280°C and 350°C respectively as reported previously. Based on the results given in Appendix IV, the fracture toughness values of sample 1 are consistent with insignificant variation. However, for sample 2, the values possess a larger variant. This difference is a result of sample preparation. For sample 2, there were some voids on the edge or in the center of the specimens. It is thought that the voids on the edge act as stress concentrators leading to the lower values whereas the voids in the center can dissipate more fracture energy by inducing more cracks that results in higher values. After averaging the reasonable values in the range of 80 J/m^2 to 187 J/m^2, the fracture toughness of sample 1 is 117 J/m^2 whereas the value of sample 2 is 122 J/m^2.

Table 7.5 summarizes the fracture toughness of various resins. The different values of fracture toughness of LECY were found in different references are thought to be the result of the different degrees of conversions also reflected in different values of Tg. Therefore, based on the Tg value of 300°C that was achieved in our work, fracture toughness of 160 J/m^2 is assigned to LECY. Meanwhile, it can be found from literature that the fracture toughness of bismaleimide resins is as low as 11 J/m^2 which corresponds to Tg as high as 430°C. Accordingly, for BMI applied in this study, it can be reasonably assumed that the fracture toughness is less than 11 J/m^2 in consideration of its higher Tg. This set of data clearly illustrated the necessity of modifying BMI for composite applications and amplify the potential role of LECY in modifying BMI.

Table 7.5 Fracture toughness of various resins.

Resin name	Fracture toughness (unit in J/m^2)	Tg (°C)
LECY (reference)	192 (1), 150~170 (2)	258 (1)
Bismaleimides	11 (2)	430 (2)
LECY (this study)	160*	300
BMI	<11*	450
IPNs	112	280
LIPNs	122	350

* Values are estimated based on the references

After investigating the sequential IPNs based on BMI and LECY however, as shown by the Table 7.5, although the fracture toughness is 112 J/m^2 which is significantly greater compared to pure BMI, the Tg decreases substantially at the same time. Additionally, the Tg of IPNs increases only 20°C compared to that of LECY whereas the toughness decreases is substantial. This observation shows that IPNs based on BMI and LECY alone are still not adequate to produce high temperature composite materials.

While on the other hand, after introducing CPM as an interlinker to the IPNs, both fracture toughness and Tg are improved. The LIPNs possess fracture toughness of 122 J/m^2, which is much higher than that of BMI. At the same time, the Tg of LIPNs is as high as 350°C and can provide excellent heat resistance when used as a composite matrix. In conclusion, the designed LIPNs based on BMI and LECY can indeed improve the fracture toughness of BMI while maintaining high Tg and processibility that meet with the requirements of high temperature composite manufacturing.

7.5 Thermal Stability of the Formed Sequential IPNs

7.5.1 Long term performance

The long time storage stability of the formed sequential IPNs was examined by conducting a series of comparison experiments in which postcured IPN samples and non-postcured samples with different composition were placed at ambient temperature for 7 months. Subsequently, the DMA analysis was conducted on each sample. Figure 7.10 gives representative results in connection with a formulation containing 20% CPM. It can be observed that after long time storage in ambient conditions, the postcured sample showed a remarkable decrease in T_g, whereas, for the non-postcured sample, when postcure was conducted 7 months later, the Tg did not reach the expected value and resulted in a material with performance even inferior to the aged postcured specimen.

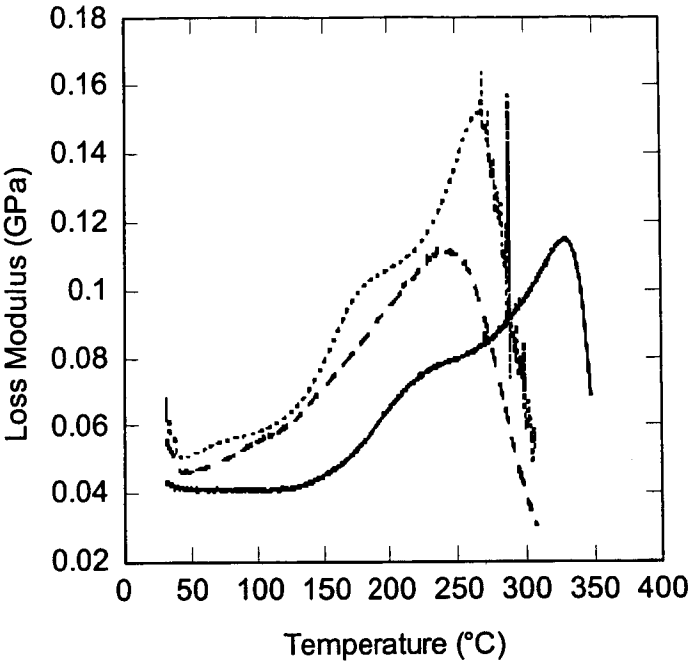

Figure 7.10 Tg change after 7 months for the sequential IPN comprised of 30 wt.% LECY and a 2:1 molar mixture of AMP and BMI together with 20 wt.% CPM with 1% Copper naphthenate as catalyst: (—) postcure immediately after EB irradiation (up to 330°C), (----) Postcure 7 months later after EB irradiation (up to 330°C), (·····) Postcured sample 7 months later (drying at 105°C @3hrs).

As revealed in Chapter 4, the hydrolysis of LECY accounts for this phenomenon. With regard to the other components in the system, namely BMI and AMP along with CPM, all of them are characterized by a strong water absorption capability. This is due to the existence of strong hydrophilic groups such as C=O, -O- in connection with their molecular structures which can bind water through hydrogen bonding and can take up water to a greater extent than LECY [7]. However, the water uptake associated with the BMI resin is a reversible process in that no appreciable difference in FT-IR spectra was observed after one absorption-desorption cycle. This indicates undetectable levels of chemical reaction during water absorption with the consequence that no permanent Tg

change resulting from water absorption is found for BMI [8], whereas LECY exposure to water will result in a pronounced decrease in Tg as a consequence of hydrolysis as shown in Figure 7.11 once the sample is heated.

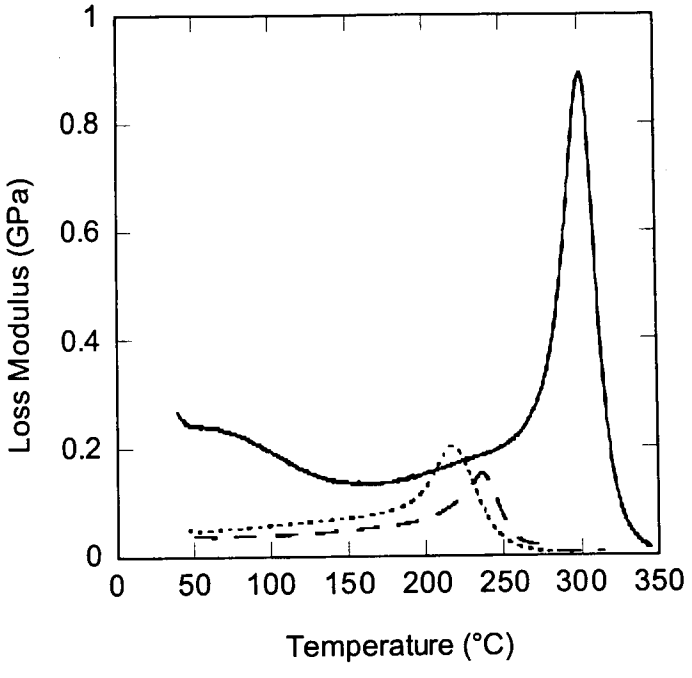

Figure 7.11 Long time storage of pure LECY cured with 600ppm Copper naphthenate: (—) after fully cure at 105°C for 12 hours, (----) 2 years later first scan, (·····) second scan.

As seen in Figure 7.11, water uptake induced hydrolysis can be accelerated when combined with high temperature as is evident by comparing the first scan with the second scan of the DMA conducted on the long time storage sample which shows a pronounced drop in Tg upon reheating. However, an improvement in resistance to boiling water can be achieved by increasing the conversion of cyanate groups via increasing the cure temperature [9]. Accordingly, to make LECY react as completely as possible by means of

applying optimum processing parameters to attain a good structure is critical to the water resistance of the final IPNs.

Another factor that generally affects the water uptake of the IPNs is the crosslink density of the network. A higher crosslink density will lead to a more open, less well packed structure which results in higher permeability [10]. This view is in accord with the observation that the water resistance of the sequential IPNs deteriorates with an increase in the amount of the network coupler, as represented by Figure 7.12.

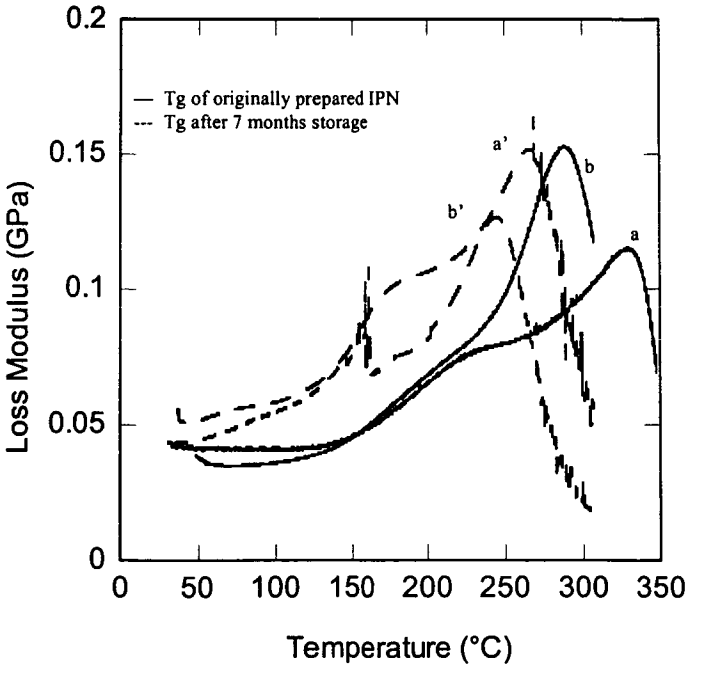

Figure 7.12 Influence of the network coupler amount on the water resistance of the formed sequential IPN: (a, a') 30 wt. % LECY and a 2:1 molar mixture of AMP and BMI together with 20 wt.% CPM with 1% Copper naphthenate as catalyst, (b, b') 40 wt.% LECY and a 2:1 molar mixture of AMP and BMI together with 10 wt.% CPM with 1% Copper naphthenate as catalyst.

7.5.2 Thermal degradation temperature (T_d)

The thermal stability is an important property of high temperature materials. In our investigation it was evaluated by thermogravimetric analysis (TGA) (conducted under a Nitrogen atmosphere); the result is shown in Figure 7.13 which focuses on the thermal decomposition behavior of various samples for a temperature range in which weight loss was less than 10%. It is observed that the IPN (50 wt.% LECY 50 wt.% BMI and AMP (molar ratio 1:2)) possesses the same thermal stability as LECY with temperatures up to 400°C; Up to this temperature there is two percentage loss of weight. However, when the temperature is above 400°C, accelerated decomposition occurs.

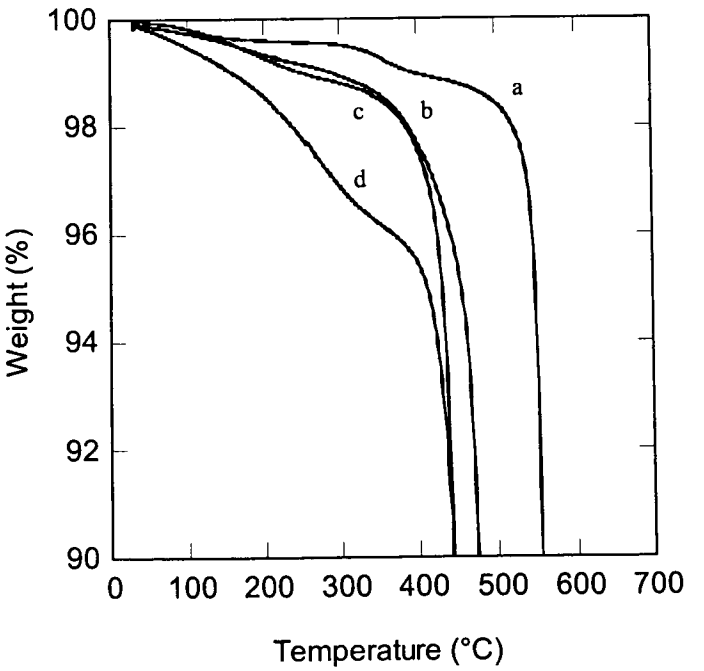

Figure7.13 TGA curves of different resins under nitrogen, (a) BMI, (b) LECY, (c) IPN, (d) AMP.

7.6 Summary

The concept of using bi-functional inter-network linking agents, or network couplers was introduced. Our preliminary investigation shows that the composition of systems, particularly the addition of CPM, can remarkably affect the formed sequential IPNs structure and hence, ultimately its Tg. The Tgs of copolymers comprised of two monomers having a distinct difference in Tg was found to be well described using a weighted average rule of mixtures whereas Tgs of the multi-component IPNs were found to follow Fox's mixing rule.

Accordingly, the Tg of the formed interlinked sequential IPNs can be enhanced greatly using interlinkers which themselves possess high Tg and this behavior can be predicted by applying Fox's equation. Thus low viscosity resin systems (< 500 cP at 30°C) with T_g as high as 370°C have been achieved.

Mechanical properties assessment was conducted using Instron and it was found that by employing the IPN technique, the fracture toughness of BMI can be improved significantly while maintaining high temperature resistance and improving processing characteristics.

The long time storage stability of the sequential IPNs was found to depend greatly on the humidity of the environment. The reason for this is the hydrolysis of LECY. Moreover, the presence of BMI, AMP and CPM in the IPNs formulation could accelerate the deterioration process because of the inherent hydrophilicity of these materials. Accordingly, keeping the sequential IPNs away from water is the key factor for successful long term storage of these materials.

On the other hand, the high temperature stability of the sequential IPNs lies in between LECY and BMI at temperatures of 400°C, which constitutes another pronounced feature of this sort of IPNs for the high temperature use.

List or References

1. Product instruction, PolySciences, Inc.

2. Shimp D.A. and W. M. Craig. Jr.. *New Liquid Dicyanate Monomer for Rapid Impregnation of Reinforcing Fibers.* 34th International SAMPE Symposium, May 8-11, 1989.

3. Hamerton I.. High-performance thermoset—thermoset polymer blends: a review of the chemistry of cyanate ester-bismaleimide blends. High Performance Polymers 1996;8:83-95.

4. Hamerton I., J. M. Barton, A. Chaplin, B. J. Howlin, S. J. Shaw.. *The development of novel functionalized aryl cyanate esters. Part. Mechanical properties of the polymers and composites.* Polymer 2001;42:2307-19.

5. Couchman P.R. and F.E. Karasz. *A classical thermodynamic discussion of the effect of composition on glass-transition temperature.* Macromolecules1978;11(1):117-9.

6. Couchman P.R.. *Compositional variation of glass-transition temperature. 2. Application of the thermodynamic theory to compatible polymer blends.* Macromolecules 1978;11(6):1156-61.

7. Chaplin A., I. Hamerton, H. Herman, A.K. Mudhar, and S.J. Shaw. *Studying water uptake effects in resins based on cyanate ester/bismaleimide blends.* Polymer 2000;41(11):3945-56.

8. Li R.B., F.Y. Albert, and C.Y.C. Lee. *Moisture absorption and hygrothermal aging in a bismaleimide resin.* Polymer 2001;42(17):7327-33.

9. Fang T. and D.A. Shimp. *Polycyanate esters: Science and Application.* Progress in Polymer Science 1995;20(1):61-118.

10. Lincoln J.E., R.J. Morgan and E. E. Shin. *Moisture absorption-network structure correlations in BMPM/DABPA bismaleimide composite matrices.* Journal of Advanced Materials 2000;32(4):24-34.

CHAPTER 8: PROCESSING AND PROPERTIES OF COMPOSITES

The long-term goal of the present study is to design a high performance composite material which can be potentially used in aerospace engineering and that is characterized by high temperature resistance, ease of processing, and excellent mechanical properties. The preceding chapters provide the foundation for a new class of materials that could be used to attain this goal. In those chapters detailed knowledge involving raw materials' selection, processing behavior, and structural characterization was presented. In this chapter, this understanding is used to make composite materials based on the BMI-LECY IPNs resins and to evaluate composite processing and mechanical behavior in order to illustrate the potential viability of these new material systems.

8.1 Composite Processing

8.1.1 Processability of IPNs neat resin

The resin comprised of 40 wt.% BMI and AMP (molar ratio 1:2), 30 wt.% LECY, and 30 wt.% CPM yields a Tg as high as 350°C. This formulation was used to produce resin for composite manufacturing. The viscosity versus temperature profile for this system is given in Figure 8.1. The dramatic decrease of viscosity, as a function of temperature is apparent. The viscosity drops from 130,000 cp at room temperature to 100 cp at 100°C, suggesting that the system is easily processed at a slightly elevated temperature by using a liquid molding technique.

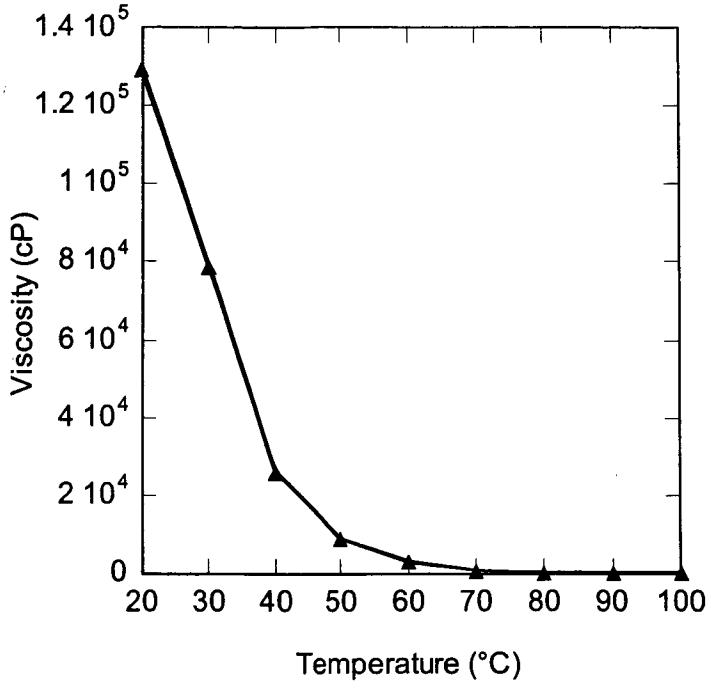

Figure 8.1 Change of IPNs neat resin viscosity with the increase of temperature.

8.1.2 Composite plaques prepared by liquid molding

Resin transfer molding (RTM) with the apparatus depicted schematically in Figure 8.2 was employed to conduct resin molding at low temperature.

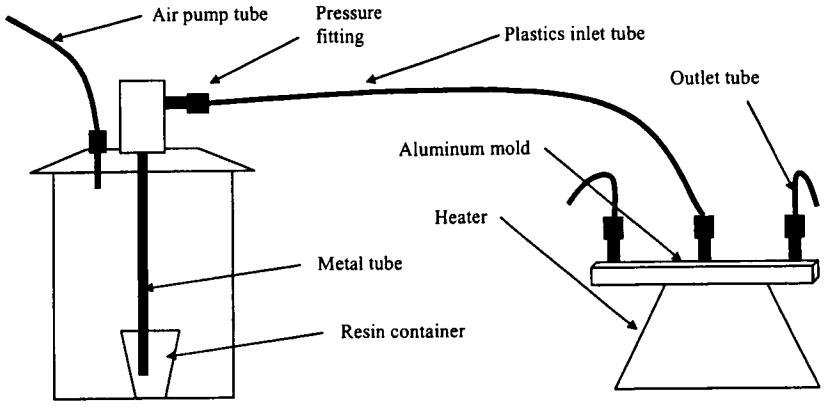

Figure 8.2 Schematic of the installation of the air pressure assisted RTM.

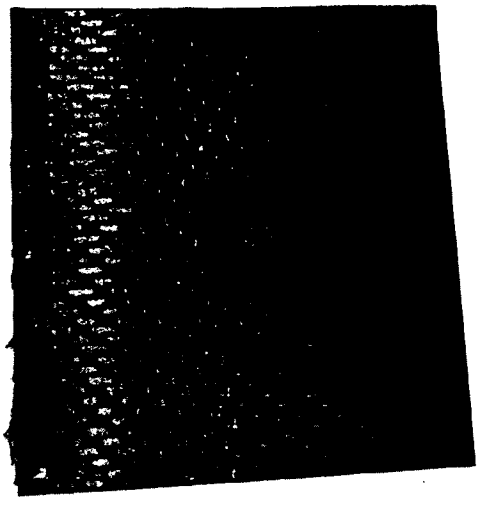

Figure 8.3 Representative picture of C-stage plaques.

The tightly sealed aluminum mold (see Appendix V) in which contained eight layers of THORNEL carbon fiber fabric with properties and characteristics given in Appendix V was placed on a heater to maintain the temperature at 100°C, in order to prevent the recrystallization of BMI from solution. The resin at 70°C was infused into the mold using 20 psi pressure until it appeared in the outlet tube, indicating the mold was filled with resin. Subsequently, the outlets and inlets of the mold were clamped tightly to prevent leaking. The mold was placed in an oven to cure at 105°C for 5 hours and 130°C for 2 hours consecutively. The resulting C-staged plaques with representative photo shown in Figure 8.3 were stored in a desiccator prior to EB processing.

8.1.3 Electron beam (EB) irradiation

EB irradiation experiments of the composite plaques were conducted at the University of Dayton Research Institute (UDRI), Dayton, OH, on an electron beam induction accelerator. Figure 8.4 illustrates the schematic of the E-beam equipment that was employed to conduct the EB cure. The EB processing cure parameters are summarized in Table 1. Prior to EB irradiation, the composite plaques were placed on an aluminum plate that was attached to a heater with the temperature set as 120°C; all of these parts were put on a track-mounted cart as shown in Figure 8.5. During irradiation, the cart traversed the electron beam at a specified speed several times. The irradiation dose was determined using standard dosimetry procedures and the cumulative irradiation dose was 208 kGy. All the processing parameters are summarized in Table 8.2. After EB irradiation, the temperature of the plaques was measured and found to be 150°C as a

result of the exothermal polymerization reaction and beam heating. The EB irradiated plaques were postcured at 310°C for 2 hours.

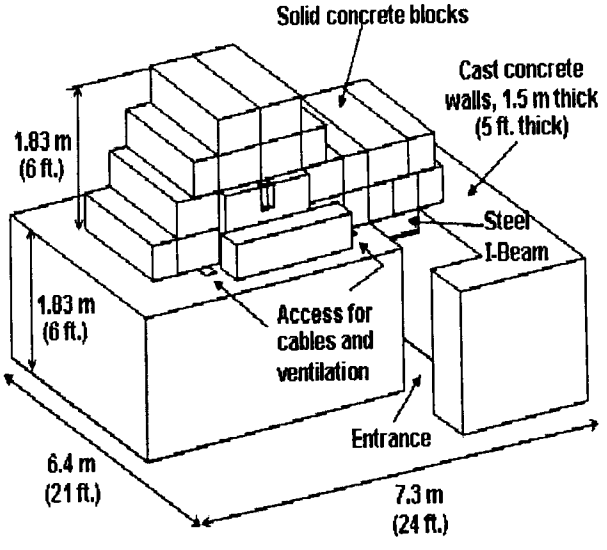
Solid concrete blocks
Cast concrete walls, 1.5 m thick (5 ft. thick)
1.83 m (6 ft.)
Steel I-Beam
1.83 m (6 ft.)
Access for cables and ventilation
Entrance
6.4 m (21 ft.)
7.3 m (24 ft.)

(A) Overall layout of UDRI E-beam facility

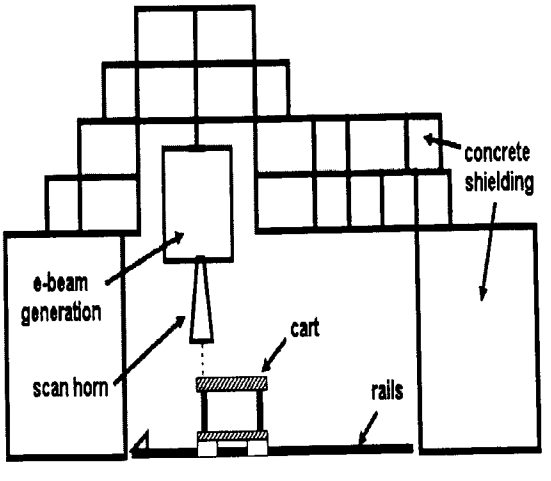

(B) Vault interior schematic

Figure 8.4 Schematic of the E-beam irradiation equipment.

Table 8.1 Processing parameters of the EB irradiation and postcure for composite plaques.

* Pulse rate = 150 pulses per second	* Scan Width = 60%
* Horn Air Gap = 12 inch	* Beam Current = 80~100 mA/Pulse
* Dose/Pass = ~16 kGy/pass	* Cart Speed = 5 inch/min
* Time for each pass = 120 sec	* Total Dose = 208 kGy
* Temperature = 120°C	* Postcure temperature = 310°C
* Postcure time = 2 hours	

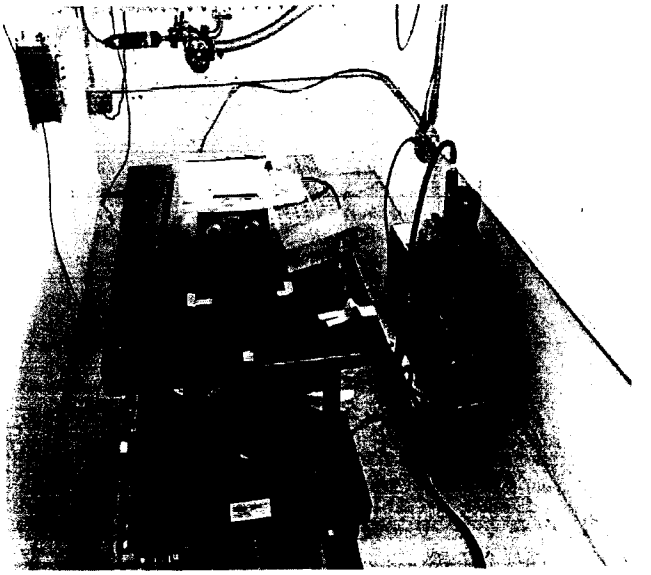

Figure 8.5 Photo of the cart and composite plaque installation.

8.2 Assessment of Composite Properties

8.2.1 High temperature behavior — Tg

Figure 8.6 gives the dynamic mechanical spectrum of the composite based on the above formulation. A Tg of 350°C was obtained. A sharp loss modulus peak indicates that minimal phase separation had occurred, which is the consequence of *in-situ* sequential synthesis of IPNs via EB irradiation.

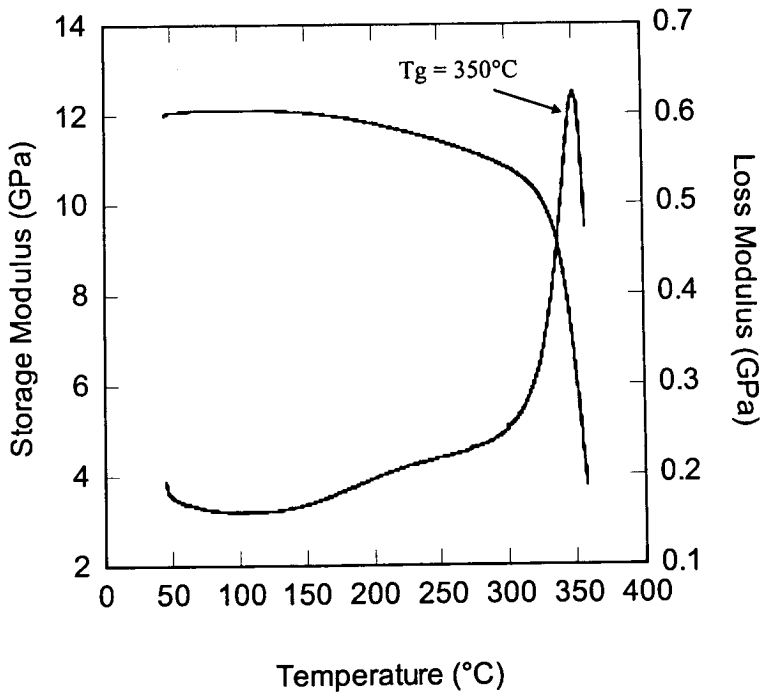

Figure 8.6 DMA spectrum for the composite based on LIPN resin comprising of 40 wt.% BMI and AMP (molar ratio 1:2) 30 wt.% LECY 30 wt.% CPM.

8.2.2 Interlaminar short beam shear (ILSS)

Interlaminar shear strength (ILSS) of the composite was determined by Short Beam Shear according to ASTM D2344-84 standard (See Appendix IV for details). Figure 8.7 shows a representative plot of flexure load against flexure extension obtained during ILSS testing.

Based on the maximum load as well as the specimen size, the ILSS was calculated. After averaging the values of twelve samples, the ILSS of this woven fabric composite is 7.2 Kpsi.

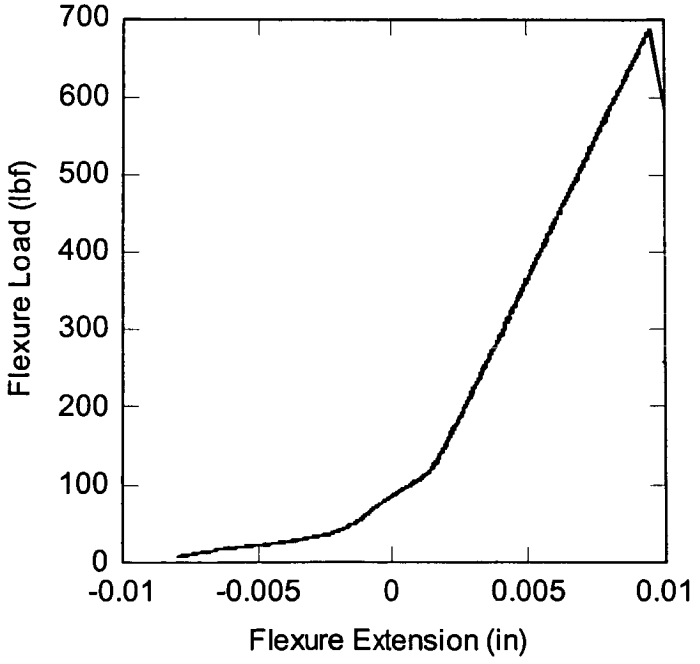

Figure 8.7 Representative ILSS test profile of the composite.

8.3 Summary

It has been demonstrated that the linked sequential IPN systems developed in this study can be used to fabricate composites using RTM at low temperature and pressure. Moreover it has been shown that such composites can be cured via EB irradiation resulting in materials with Tg = 350°C and adequate interlaminar shear strength following a short post-cure.

CHAPTER 9: CONCLUSIONS

In this chapter, accomplishments achieved in this investigation will be summarized together with important conclusions and observations. Additionally, based on our study, possible future work will be addressed.

9.1 Summary

As indicated in Chapter 1, one of the major issues regarding the use of high temperature polymers for composite applications is that the polymer's difficulty of processing often leads to a high cost. Another pronounced problem concerning the fabrication of high temperature polymer composite materials is that improvement in high temperature resistance can only be achieved by sacrificing toughness. Accordingly, engineering a high temperature polymer composite with good toughness and a low manufacturing cost constitutes the most important point of the investigation. This has involved the challenge of combining polymer science, experimental and analytical skills, and composite processing principles.

Bismaleimide resins are one type of addition polyimide that is becoming increasingly important in the manufacture of high temperature composite due to attributes that include high regularity and stiffness of the backbone, ability to crosslinking, and high crosslink density of the formed network among others, which all contribute to high temperature performance after cure. Thus, composite materials produced with bismaleimides can be used in highly demanding environments, particularly in the field of aerospace engineering.

However, two important aspects of bismaleimide resin systems limit their more widespread use. The first problem relates to the ease of processing of these systems. Bismaleimides generally possess a high melting point and high crystallinity which make them difficult to dissolve in common diluents and the resulting solution easily recrystallizes. As a result, it can not be effectively used in low cost processing such as low temperature RTM and VARTM. The second obstacle is that the high molecular rigidity and crosslink density result in very low fracture toughness of the fully cured resin.

In order to resolve the drawbacks associated with the current bismaleimide technology, the present study developed a high temperature system (Tg = 350°C) that can be used to fabricate composite materials with low temperature processing techniques such as RTM and VARTM. Our results demonstrate that synthesizing *in-situ* sequential IPNs of cyanate esters (CE) with BMI will result in a superior morphology characterized by (1) a minimum phase separation and hence small phase domain, (2) a clean interface, and (3) a high crosslinking density. All these improvements contribute to the ultimate high Tg, particularly when the interference between the two network reaction mechanisms is kept at a minimal level. After examining other techniques currently utilized to achieve BMI-CE sequential IPNs in terms of the synthetic routes, cure methods, as well as the ultimate results, it can be concluded that the sequential synthesis of IPNs based on these two components can only be truly carried out by the methodology designed in this study in which EB irradiation is employed to precisely control the sequence of network formation. Moreover, the EB irradiation induced *in-situ* formation of the second network in the vicinity of the first network, is conducive to good morphology and properties.

The methodology used, as discussed in Chapter 3, can be generalized by the following process: forming of the first cyanate ester based network is triggered by adding a catalyst at a temperature below 130°C in the presence of bismaleimide and a reactive diluent; the second network is obtained in the presence of the first by EB irradiation through the donor-acceptor free radical mechanism. The resulting sequential IPNs can provide both high temperature resistance and good toughness due to the synergic effect of the two networks. The EB irradiation offers the ease of processing with the help of a reactive diluent. Moreover, a network coupler can be introduced to the system to further improve the Tg of the IPNs by linking the two networks to form linked sequential IPNs or LIPNs with Tgs as high as 370°C.

The IPNs based on bismaleimide and cyanate ester possess the following features: (1) high Tg, (2) good toughness and (3) low temperature ease of processing. This suggests that more research activities on bismaleimide modification for high temperature material application could be fruitful. More importantly, the avenue pursued to realize EB irradiation assisted *in-situ* synthesis of sequential IPNs based on bismaleimide and cyanate ester lays the groundwork for the design of remarkable high performance polymer materials that can be processed at low temperature.

In studying the design of high temperature polymer resins, many observations and empirical relations were uncovered which deepen our understanding of sequential IPNs in terms of synthetic routes, morphology and ultimate properties. The results of this investigation enrich the guidelines for regulating the processing of such systems and determining the monomer parameters needed for the synthesis of IPNs. Furthermore this

work has the potential to accelerate the application of EB irradiation to the manufacturing of high temperature composite materials.

Specifically the challenges of this study include (1) selecting an appropriate reactive diluent based on the property and processing criteria suggested, (2) determining the optimum processing and material parameters to ensure the formation of sequential IPNs, and (3) investigating the structure-property-processing relationship in such systems to provide guidelines for improving and designing future IPN materials.

Selection of the reactive diluent plays a vital role in the implementation of this methodology in that the presence of a reactive diluent is necessary to resolve the processibility problem of bismaleimide as well as affect the chemical reactivity of bismaleimide. The latter is extremely important in controlling the sequence of network formation and diminishing the interference of the two reaction mechanisms. Current techniques using an allylphenol type monomer as the reactive diluent to improve the processibility are based on the Diels-Alder reaction between the two constituents. This is a thermally assisted process that demands an extremely high temperature environment for cure and is therefore a costly process. Moreover, the prevalent interference among different reaction mechanisms inherent in the system will undermine the network structures formed and inevitably suppress the ultimate Tg of such materials. A number of reactive diluents were investigated in this study as described in Chapter 5 and N-acryloylmorpholine was found to be a unique monomer able to enhance the processing ease of the bismaleimide resin based on the criteria of both good solubility and reactivity.

Our understanding of the process by which sequential IPNs can be produced is derived primarily from studies of the kinetics of two network formations as treated in

Chapters 4 and 6. For the first network formation, the cure kinetics of bisphenol E cyanate ester (LECY) was investigated. Based on this knowledge and on the influence of the catalyst on the hydrolysis of LECY, the catalyst type and corresponding amount was determined together with the processing parameters for first network formation including time, temperature as well as the sequence of adding the constituents. The kinetics and mechanisms underlying the EB induced free radical copolymerization were investigated with regard to the influence of dose rate and temperature on copolymerization behavior under EB irradiation. The significance of this part of study is that the processing parameters for the second network were determined based on knowledge of fundamental reaction behavior. More importantly, this preliminary understanding and basic observations regarding the kinetics of EB induced copolymerization elucidated in this study, have the potential to spur broader application of EB irradiation for the cure of composites in the future. The application of EB cure in composite manufacturing has been impeded by the lack of fundamental knowledge concerning the influence of processing parameters on cure behavior.

An understanding of the correlation of structure and properties for the CE-BMI/AMP sequential IPNs was developed and discussed in Chapter 7. Appropriate mixing rules were obtained for predicting the Tg of the sequential IPNs. As a means to improve the crosslink density a network coupler was introduced and the remarkable consequence of this was reflected by substantial increase of the ultimate Tg. Mixing rules were used to predict the behavior of linked systems as well. The relationships uncovered in this part of the work could be applied for the development of improved systems. In Chapter 8 the fabrication of carbon fiber composites using interlinked

sequential IPNs of LECY with BMI/AMP was described. The resin systems were found to be processed with ease using low temperature and pressure RTM followed by EB cure and the composite possessed favorable interlaminar shear strength and a Tg of 350°C.

9.2 Reactive Diluent Selection

In Chapter 5, the influence of the reactive diluent on the conversion of bismaleimide under EB irradiation was investigated together with the influence of side group on the reactivity of reactive diluents. It was suggested that bismaleimide could copolymerize with a reactive diluent under EB by following a charge-transfer mechanism whereby the conversion of bismaleimide can be improved. Common reactive diluents can only dissolve the BMI monomer at high temperatures thus sacrificing stability. However, the electron donating ability of reactive diluents can be tempered by introducing an electron-withdrawing group to the molecular structure.

N-acryloylmorpholine was accordingly selected as appropriate reactive diluent to resolve the processibility of BMI according to the following facts: (1) it can dissolve the bismaleimide at low temperatures (~100°C) due to the similarity in structure; (2) it can reduce the chemical reactivity of bismaleimide so that the bismaleimide will be stable during the formation of the first network formation — for practical purposes the stability of bismaleimide with AMP can be maintained at temperatures as high as 200°C; (3) it can also be regarded as an electron donor that can copolymerize even at room temperature with bismaleimide under EB irradiation through the charge-transfer mechanism. It was found that with appropriate initial composition, BMI and AMP form a pseudo-alternating copolymer that enhances material properties.

9.3 Processing and Materials Parameters

For the formation of the polycyanurate network (first network of the sequential IPN), copper naphthenate was found to be the appropriate catalyst in that it is not detrimental to the stability of the second network components, it is highly active for triazine ring formation and has a minimal propensity for catalyzing hydrolysis of LECY upon water uptake and heating. In the investigation of LECY cure kinetics, the activation energy for polymerization was found to decrease linearly with increasing concentration of catalyst. Based on this new information, the cure processing parameters, amount of catalyst, cure temperature, and time were selected for first network formation.

Moreover, the EB cure kinetics related to the second network formation were also investigated in terms of the influence of dose rate and temperature on cure behavior using phenylmaleimide as a non-crosslinking model compound for bismaleimide. The charge transfer mechanism was partially substantiated by measuring reactivity ratios using an *in-situ* fiber optic NIR spectroscopy technique. It was also found that dose rate does not significantly affect the copolymerization behaviors, whereas increasing temperature can increase monomer reactivity ratios for both monomers.

9.4 Structure-Property Correlation

The effects of the amounts of the reactive diluent and network coupler on the ultimate Tg were investigated. A network coupler can greatly improve the compatibility of IPNs by increasing the crosslinking density of the network and thus enhance the ultimate Tg by forming a linked sequential IPN.

The *in-situ* polymerization induced by E-beam radiation of BMI with AMP to form the second network can ensure the formation of the best IPN structures with both high crosslinking density and a good interface between phase domains.

It was found that the Tg of copolymers comprised of two monomers with distinct differences in Tg follow a weighted average mixing rule whereas the Tgs of the multi-component sequential IPNs follow the Fox equation.

Data obtained by thermogravimetric analysis (TGA) demonstrated that the thermal stability of the sequential IPNs exhibits behavior similar to that of LECY up to 400 °C in that there is only a one percentage loss of weight, which is quite similar to the BMI resin in this temperature range.

9.5 Future Work

Although it was shown by our work that AMP is an effective reactive diluent for modifying BMI, there are still however some disadvantages in its application: (1) it is regarded as a highly toxicity material, (2) its polymer possesses low thermal stability in a high temperature environment. This prompts us to seek other more optimum reactive diluents.

We propose nitrostyrene as a starting point for exploring new reactive diluents for BMI in light of its significantly better thermal stability when copolymerized with BMI compared to AMP and other diluents. However, to limit second network formation during the LECY cure, we must allow LECY to cure completely at low temperatures. This can be accomplished by: (1) increasing the concentration of catalyst to decrease the activation energy, (2) introducing the cyanate ester group to the backbone of the BMI

(There are two roles that the cyanate ester group can play. First, it can lower the melting point of BMI; second, the unreacted LECY groups can be directly connected to the IPN network.), and (3) introducing the proper amount of the hydroxyl group to the system so as to catalyze LECY cure and increase the final conversion of LECY at low temperatures. The decrease of cure temperature of cyanate ester was discovered in Hu's work [1]. Meanwhile the formation of hydrogen bonding due to the hydroxyl group can increase the C-stage compatibility of components. This is beneficial to the *in-situ* polymerization induced by E-Beam irradiation in that it has the potential for diminishing phase separation of final product. Moreover, it can be beneficial to allow interactions between polymer chains. This can diminish the influence of defects in the IPNs structure. As to network coupler design, we propose to synthesize multi-functional compounds to further improve crosslinking density.

The cyanate ester employed in the current study is LECY, which possesses a relatively low Tg. Accordingly, other cyanate ester monomers should be evaluated. Some commercial cyanate esters possess Tg as high as 360°C as well as a low melting point (liquid state at room temperature). Based on our current understanding of structure-property relationships the use of these new CE monomers could improve the ultimate Tg of the IPNs further. Meanwhile, another promising method for improving sequential IPN properties would be to directly introduce C=C group to currently available cyanate ester in order to avoid the utilization of our network coupler CPM, which is not currently commercialized.

9.6 Concluding Remarks

Few attempts have been made to process BMI resin at low temperature for high temperature applications (Tg > 300°C) using sequential IPN formation and EB radiation. This methodology has now been demonstrated to yield resins with the interesting characteristics of low cost, ease of processing at low temperature, and promising high temperature material properties (Tg up to 370°C). Although the material system based on BMI-LECY/AMP that was developed possesses some shortcomings, the fundamental understanding of cure behavior and structure-property relationships of these complex systems can serve to help design the next generation of such materials. Additionally, This work has provided some insight into copolymerization using EB radiation which in itself should further the application of EB in processing of polymer.

List of References

1. Hu X., J. Fan, C.Y. Yue. *Rheological study of crosslinking and gelation in bismaleimide/cyanate interpenetrating polymer network.* Journal of Applied Polymer Science 2001;80:2437-45.

2. Liu Y., B. Malcolm, and Y. Huglin. *Effective crosslinking densities and elastic moduli of some physically crosslinked hydrogels.* Polymer 1995;36(8):1715-8.

Appendix I: SYNTHESIS OF 4-CYANATOPHENYL MALEIMIDE (CPM)

The basic idea of synthesizing 4-cyanatophenyl maleimide, simplified as CPM in this study, can be illustrated by the following chemical equation:

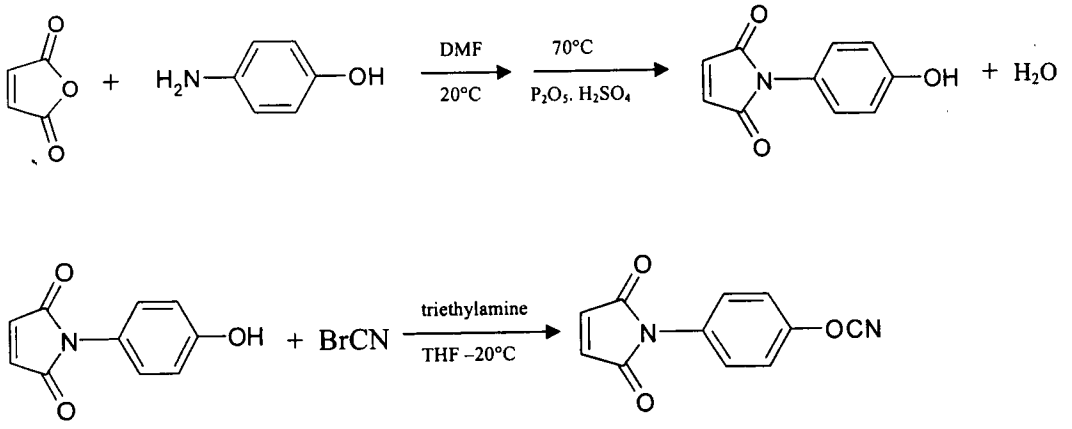

Seen clearly, the overall process includes two steps: synthesis of N-hydroxyphenyl maleimide (simplified as HPM in this study) and the succeeding synthesis of CPM. Whereas 4-aminophenol, maleic anhydride, and cyanogen bromide are starting materials, phosphorus pentoxide and triethylamine play the roles of catalysts in the reactions by absorbing the small molecules produced in two separate reactions which are water and hydrogen bromide respectively. In this way, both the speed and yield of the reaction can be improved significantly. Though sulfuric acid can also absorb water, what is more, it is also beneficial to the solvation of phosphorus pentoxide in the THF.

Otherwise it would be very difficult to carry out due to the high melting point of phosphorus, above 350°C.

The present procedure synthesizing the HPM and its succedent CPM, is the result of some rectifications being made to the reported literature [1,2], with regard to the solvent amount and reaction conditions, considering the actual situation. In the following section, the procedure adopted will be detailed as to the synthesis of HPM and CPM. Meanwhile, the analysis of the result obtained as well as the comparison of the results with reported results will be summarized.

1. Synthesis of N-hydroxyphenyl maleimide (HPM)

The chemicals reagents used in this step were as follows: 4-aminophenol, maleic anhydride, DMF, phosphorus pentoxide, sulfuric acid. All of them were purchased from Aldrich and directly used without further purification.

The apparatus for this experiment was: a 300ml conical flask, a 500ml round bottom flask, an oil bath, a vacuum pump, a Buchner filter, together with a hot plate with magnetic stirring.

The amount of chemicals used in the reactions was determined based on the reported formulation as well as by the devices in the lab with the aim of achieving the greatest production in one time, with formulation shown in Table A.I.1.

Table A.I.1 Formulation in the synthesis of HPM.

Chemical	4-aminophenol	maleic anhydride	DMF_1	P_2O_5	H_2SO_4	DMF_2
Amount	43.6g	43.2g	204ml	22.8g	10g	140ml

DMF_1 and DMF_2 stand for the DMF amounts used for the different purposes of dissolving starting materials and catalysts respectively. However, two times the amount of DMF as that used in the reference [1] was applied to ensure the complete solvation of 4-aminophenol. Thus the reaction time was increased correspondingly.

The procedure with regard to the synthesis of HPM is as follows. A conical flask charged with 43.2g maleic anhydride and 204ml DMF was put on a plate with magnetic stirring to prepare a solution with a white color. The solution was poured into another conical flask with 43.6g 4-amionphenol in it to form a clear yellow solution by stirring. Both of these steps were carried out at room temperature. Then the solution was transferred into a round bottom flask and heated to 70°C with the help of an oil bath, and a solution of 22.8g P_2O_5, 140ml DMF and 10g H_2SO_4 was added dropwise over a 30 minute period. The resulting solution was heated at 70°C for another 6 hours to ensure a sufficient reaction. Consequently, a clear dark brown solution was obtained. After cooling down, the resulting solution was then poured into ice water, accompanied by the yellow stuff that precipitated from the solution. After filtering, the rough HPM was obtained.

The product was then recrystallized in the presence of 2-propanol whose empirical amount was 3 ~ 4ml per gram of rough CPM. Then the mixture of 2-propanol

and the rough HPM was poured into a round bottomed flask with a reflux tube installed, stirred vigorously, and heated at 86°C, which is higher than the boiling point of 2-propanol in light of the temperature difference of the bath and the flask. Continuous heating lasted for about one hour until the rough HPM dissolved completely indicated by the formation of a clear dark brown solution. Then the HPM was recrystallized from the solution while cooling down to room temperature. After filtering and drying, the achieved HPM exhibited a needle shape with a golden yellowish color. The yield of the synthesis was around 60%, and the melting point of the obtained substance was 191°C, shown in Figure A.I.1. Thus, even though the yield is lower than reported (85%), a higher melting point, compared with the 182-184°C reported, can compensate for the loss.

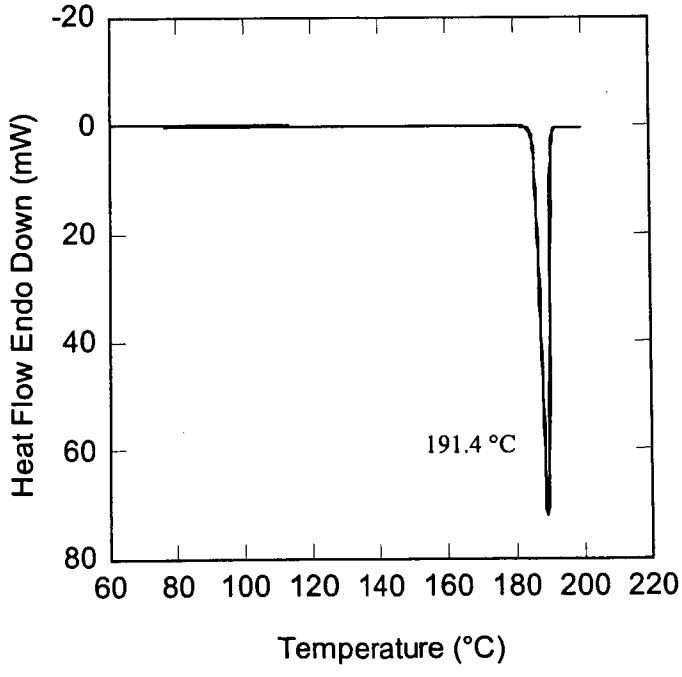

Figure A.I.1 DSC spectrum of the recrystallized HPM.

2. Synthesis of 4-cyanatophenyl maleimide (CPM)

The synthesis of CPM is based on the obtained HPM. The chemicals used, besides the obtained HPM, were cyanogen bromide, triethylamine, and THF as a solvent, all of which were purchased from Aldrich and directly used without further treatment.

The apparatus mainly includes a 1000 ml three-necked, round-bottomed flask equipped with a mechanical stirrer, as well as a constant temperature bath branded as Polystat, which was employed to satisfy the critical temperature requirement of –20°C for the reaction. The other devices were basically the same as those used in the first step.

The amount of chemicals used in this reaction was calculated based on the amount of the HPM according to Table A.I.2.

Table A.I.2 Formulation in the synthesis of CPM

Chemicals	HPM	cyanogen bromide	THF	triethylamine
Amount	4.85 g	4.08 g	30 ml	3.89 g

A little excess of cyanogen bromide was employed to make sure of the complete consumption of HPM. Meanwhile, a much larger amount of THF was adopted compared to the reference [2], to compensate for the loss resulting from evaporation during the reaction; another advantage of the excess amount of THF was in the rapid removal of the heat released in the reaction.

The detailed operation of this synthesis is as follows. A 1000 ml, three necked, round bottomed flask equipped with a mechanical stirrer was charged with a solution of

HPM, and a corresponding amount of BrCN and THF. This solution is stirred rapidly while cooling in a constant temperature bath to –20°C, and the triethylamine was added dropwise at such a rate that the temperature did not exceed –10°C. The obvious temperature increase together with the occurrence of a white solid stuff implied that the reaction was occurring. After reacting for two hours, the formed triethyl amine hydrobromide was filtered off, and the solution was precipitated into hexane. The filtered product was dried and recrystallized from isopropanol. However, the empirical amount of the isopropanol was about 18ml per gram of rough CPM. The overall time was about half an hour for all the rough CPM to completely dissolve in the isopropanol to form a clear light brown solution. Then the flask was removed from the oil bath and cooled down to room temperature. After filtering and drying, the obtained CPM exhibited a light greenish color, as shown in Figure A.I.2 (the little bit yellow color maybe resulting from chromatic aberration or the flashlight). Figure A.I.3 indicates that the synthesized CPM exhibits a melting point of 132.5°C. The overall yield was 64%. Both of the two indicatives were better than those of reference literature.

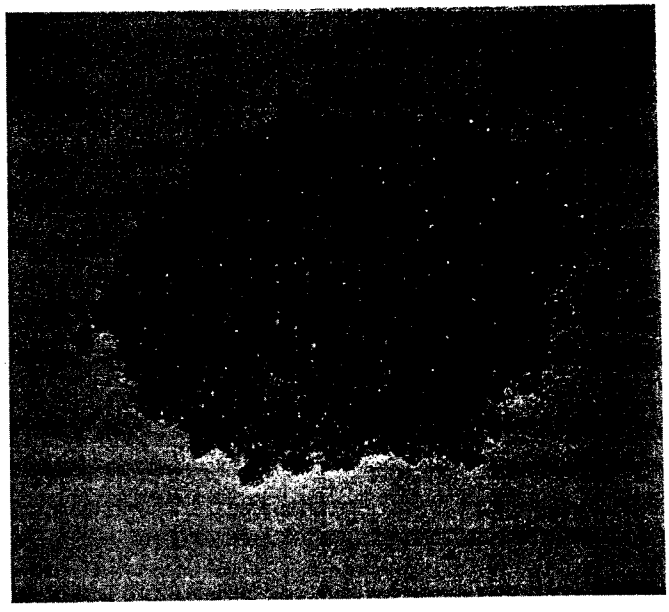

Figure A.I.2 Photo of the obtained CPM.

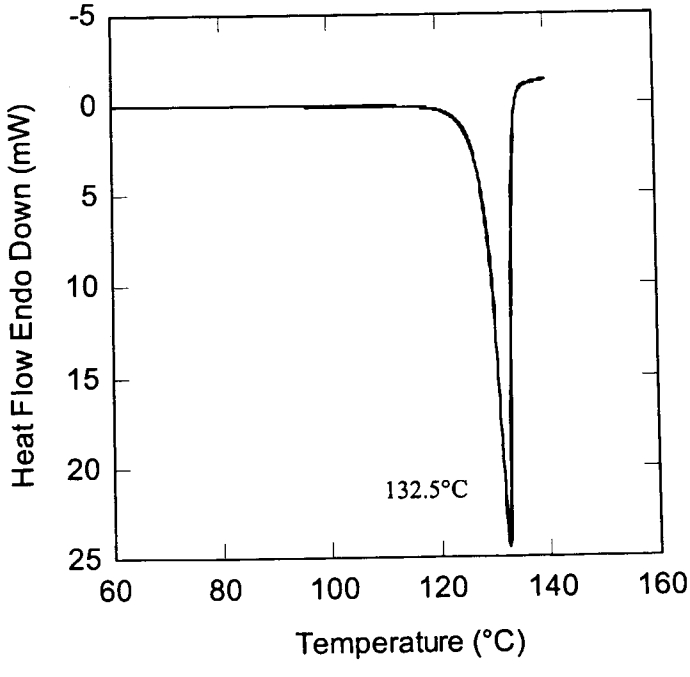

Figure A.I.3 DSC spectrum of the recrystallized CPM.

List of References

1. Park J.O. and S.H. Jang. *Synthesis and characterization of bismaleimides from epoxy resins.* Journal of Polymer Science Part A: Polymer Chemistry 1992;30(5):723-9.

2. Mathew D., C.P.R. Nair, K.N. Ninan. *Pendant cyanate functional vinyl polymers and imido-phenolic-triazines thereof: synthesis and thermal properties.* European Polymer Journal 2000;36(6):1195-208.

Appendix II: DSC PLOTS IN LECY CURE KINETICS STUDY

DSC plots in relation to the calculation of kinetics parameters of catalyzed LECY cure based on the Coats-Redfern (C-R) method are summarized by the following eight figures with regard to the different concentrations of Cu^{2+}.

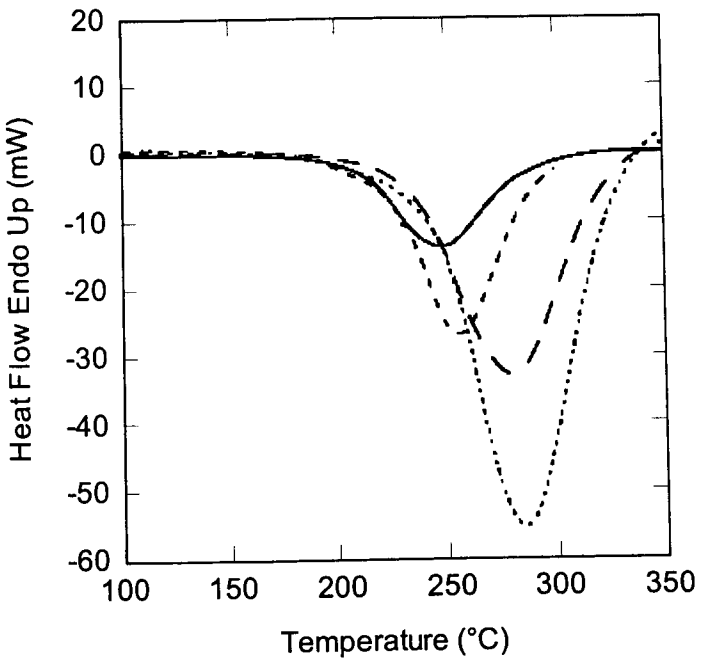

Figure A.II.1 DSC thermograms of pure LECY at different ramping rates. (—) 5°C/min, (– –) 10°C/min, (— —) 15°C/min, (·····) 20°C/min.

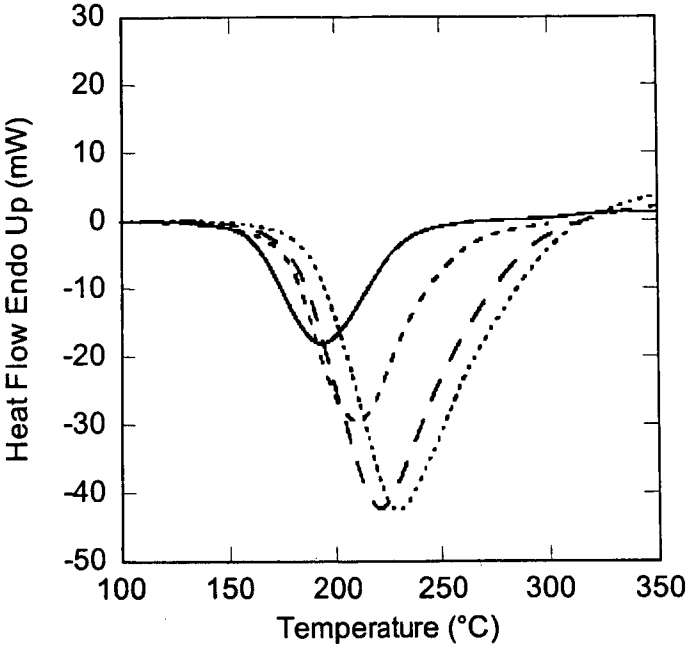

Figure A.II.2 DSC thermograms of LECY with 200ppm Cu^{2+} at different ramping rates. (—) 5°C/min, (– –) 10°C/min, (— —) 15°C/min, (·····) 20°C/min.

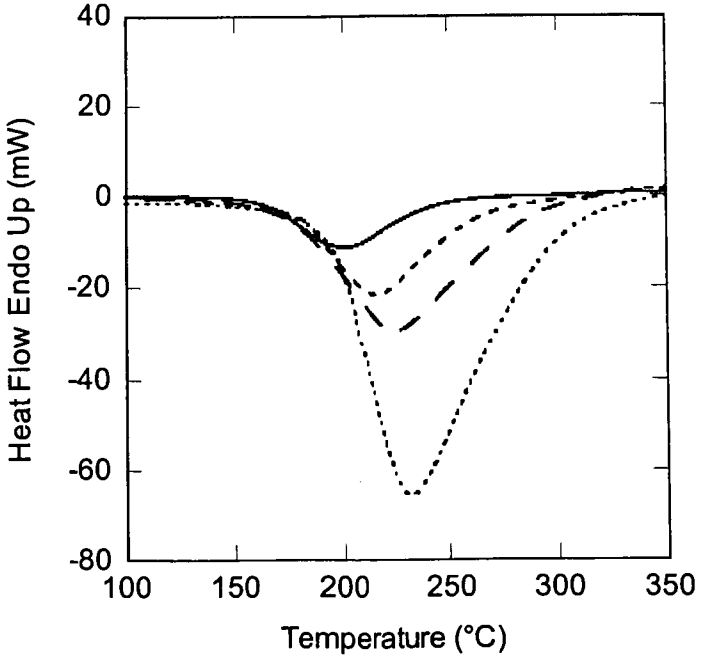

Figure A.II.3 DSC thermograms of LECY with 300ppm Cu^{2+} at different ramping rates. (—) 5°C/min, (– –) 10°C/min, (— —) 15°C/min, (·····) 20°C/min.

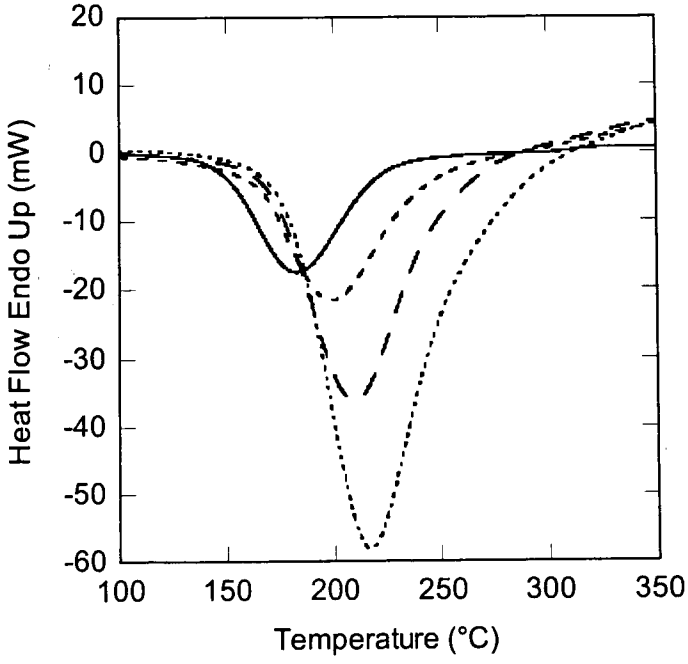

Figure A.II.4 DSC thermograms of LECY with 600ppm Cu^{2+} at different ramping rates. (—) 5°C/min, (– –) 10°C/min, (— —) 15°C/min, (·····) 20°C/min.

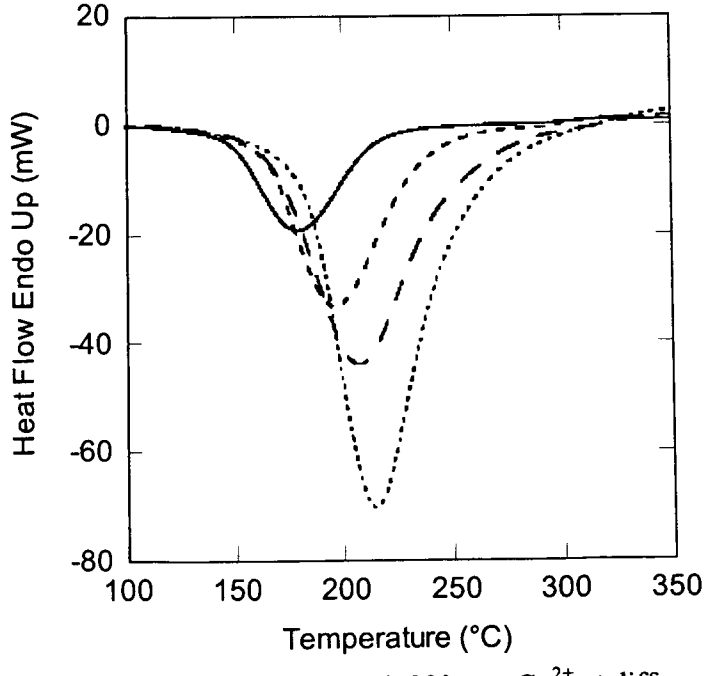

Figure A.II.5 DSC thermograms of LECY with 800ppm Cu^{2+} at different ramping rates. (—) 5°C/min, (– –) 10°C/min, (— —) 15°C/min, (·····) 20°C/min.

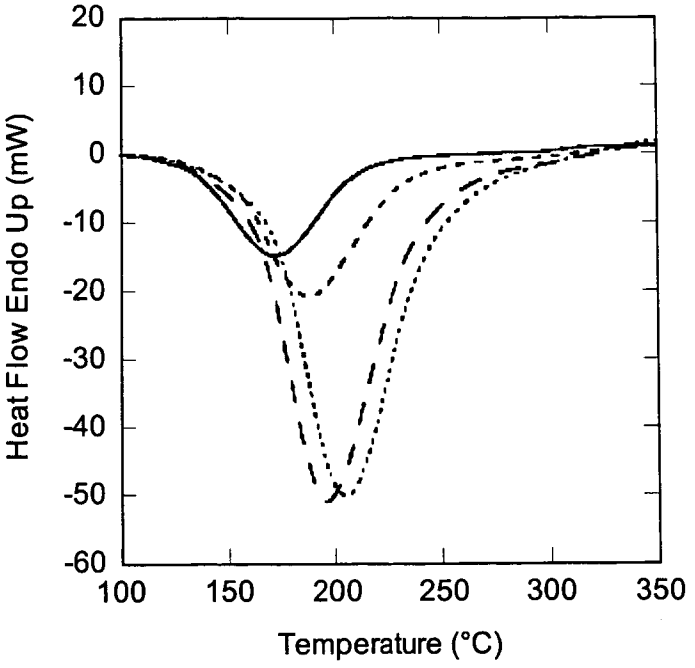

Figure A.II.6 DSC thermograms of LECY with 1000ppm Cu^{2+} at different ramping rates. (—) 5°C/min, (– –) 10°C/min, (— —) 15°C/min, (·····) 20°C/min.

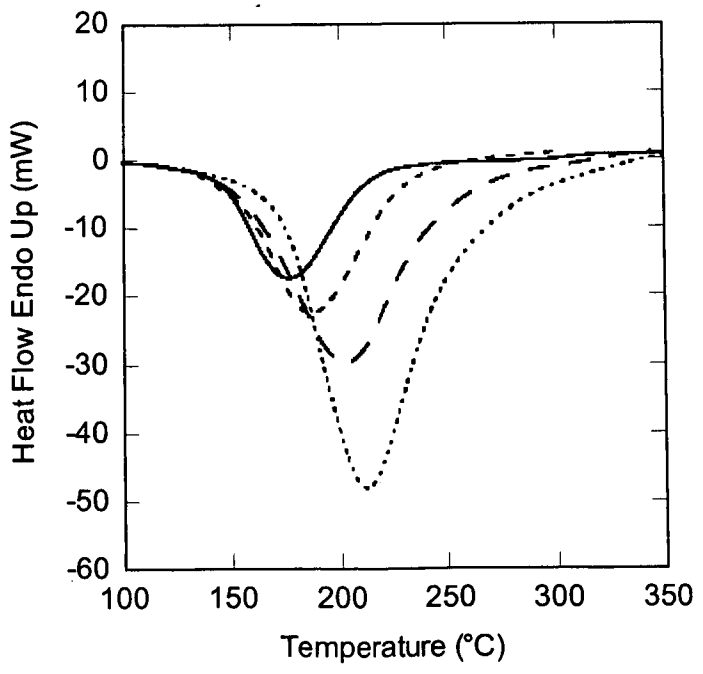

Figure A.II.7 DSC thermograms of LECY with 1200ppm Cu^{2+} at different ramping rates. (—) 5°C/min, (– –) 10°C/min, (— —) 15°C/min, (·····) 20°C/min.

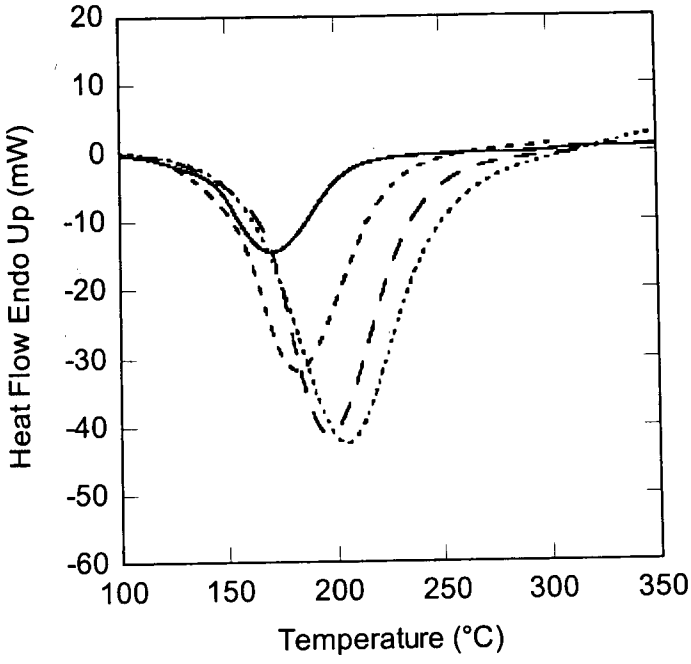

Figure A.II.8 DSC thermograms of LECY with 1400ppm Cu^{2+} at different ramping rates. (—) 5°C/min, (– –) 10°C/min, (— —) 15°C/min, (·····) 20°C/min.

Appendix III: DMA DSC RESULTS IN CPM Tg DETERMINATION

1. DSC Results

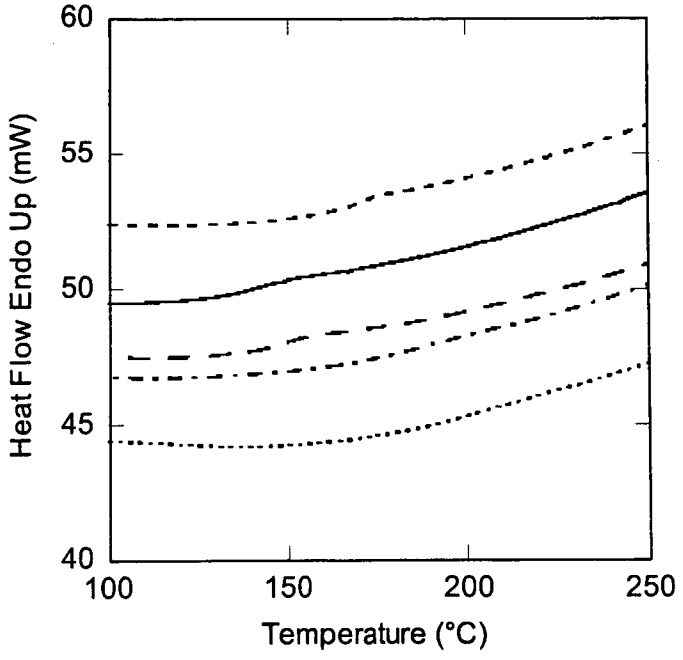

Figure A.III.1 DSC plots of CPM and AMP with different compositions. (—) 1 wt.% of CPM, (—) 5 wt.% of CPM, (---) 10 wt.% of CPM, (—·—) 15 wt.% of CPM, (····) 20 wt.% of CPM. Glass transition region will be clearer in small scale for high percentage of CPM. Tgs for these combinations with the increase of CPM amount are as follows: 141.3°C, 146.7°C, 168.4°C, 187.3°C, and 200.1°C.

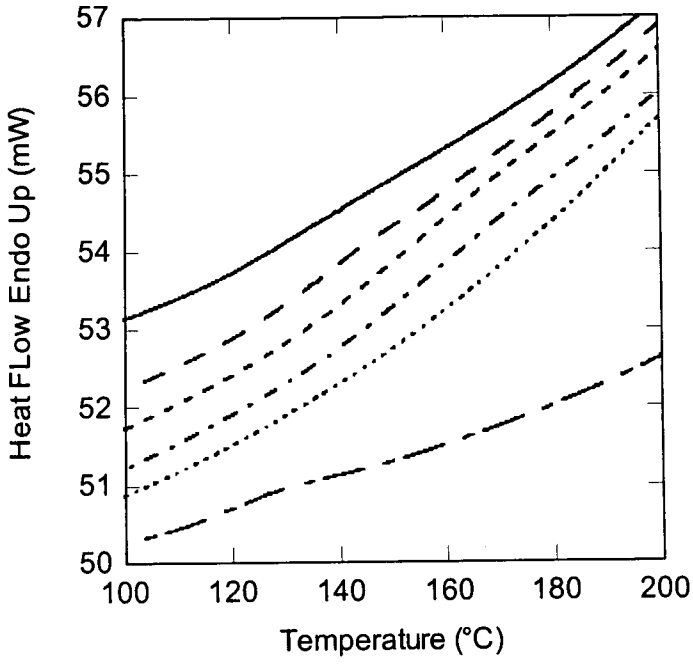

Figure A.III.2DSC plots of BMI and AMP with different compositions. (— –) 0 wt.% BMI (i.e. pure AMP), (—) 1 wt.% of BMI, (– –) 5 wt.% of BMI, (---) 10 wt.% of BMI, (–·–) 15 wt.% of BMI, (····) 20 wt.% of BMI. Glass transition region will be clearer in small scale for high percentage of BMI. Tgs for these combinations with the increase of BMI amount are as follows: 119.8°C, 132.1°C, 137°C, 157.3°C, 168.3°C, and 192.6°C.

2. DMA Results

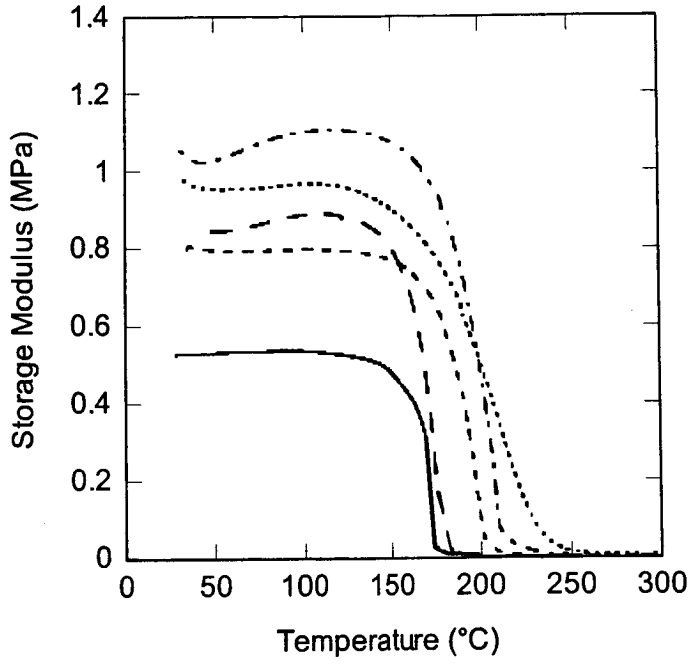

Figure A.III.3DMA plots concerning storage modulus of CPM and AMP with different compositions. (—) 1 wt.% of CPM, (—) 5 wt.% of CPM, (---) 10 wt.% of CPM, (-·-) 15 wt.% of CPM, (····) 20 wt.% of CPM. Tgs for these combinations with the increase of CPM amount are as follows: 163°C, 169.9°C, 192.6°C, 203°C, and 213.1°C.

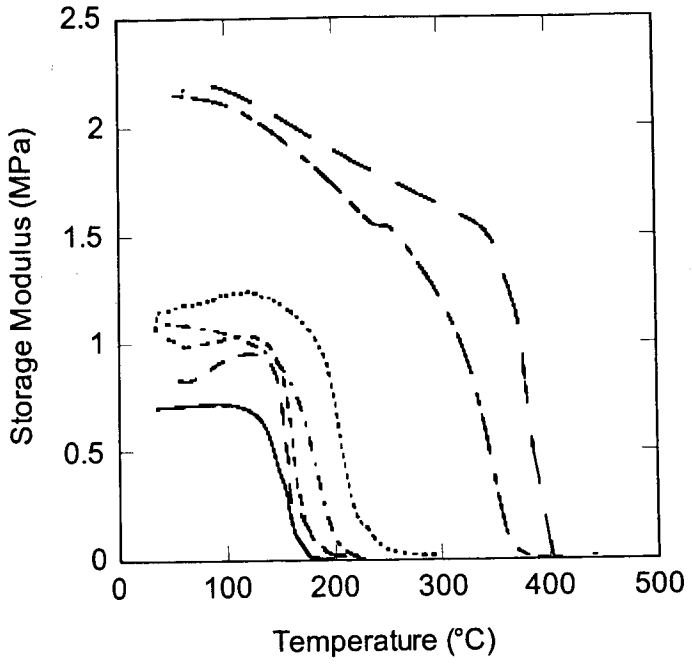

Figure A.III.4DMA plots concerning storage modulus of BMI and AMP with different compositions. (—) 1 wt.% of BMI, (—) 5 wt.% of BMI, (---) 10 wt.% of BMI, (–·–) 15 wt.% of BMI, (····) 20 wt.% of BMI, (— –) 50 wt.% of BMI, (——) 75 wt.% of BMI. Tgs for these combinations with the increase of BMI amount are as follows: 157.3°C, 157.2°C, 169.4°C, 185.7°C, 200.2°C, 337.2°C, and 384.9°C.

Appendix IV: MECHANICAL PROPERTIES ASSESSMENT OF IPNS NEAT RESIN AND COMPOSITE

1. Fracture toughness results

1.1 Test procedure

10 test specimens with thickness (~0.14 in), width (~0.5 in) and length (~2.5 in) were machined from flat, finished resin plaques. A notch with the length as half as the width of the specimen was cut in the middle position for each specimen except for one which would be used for a control test. After the control test, the specimen was placed on two supporters with un-notched side facing the loading nose. The support span was a little smaller than 2.5 in. The loading lose was then used to press the specimen until breakage. The force was then recorded. Calculations were performed to determine fracture toughness according to the following excel sheet, wherein notch length, thickness, depth, and breaking load were directly input based on the recording whereas the U and U_i were obtained by integrating the curve of loading against extension from sample and control test respectively. The following is a typical graph for a specimen. The area of the region circumvented by the curve of loading against extension, x axis, and dash line is the value of U. After the control test, plotting the U derived from each load against the load to gain a correlation between load and U, the U_i can then be obtained based on this correlation and the actual maximum load of each specimen.

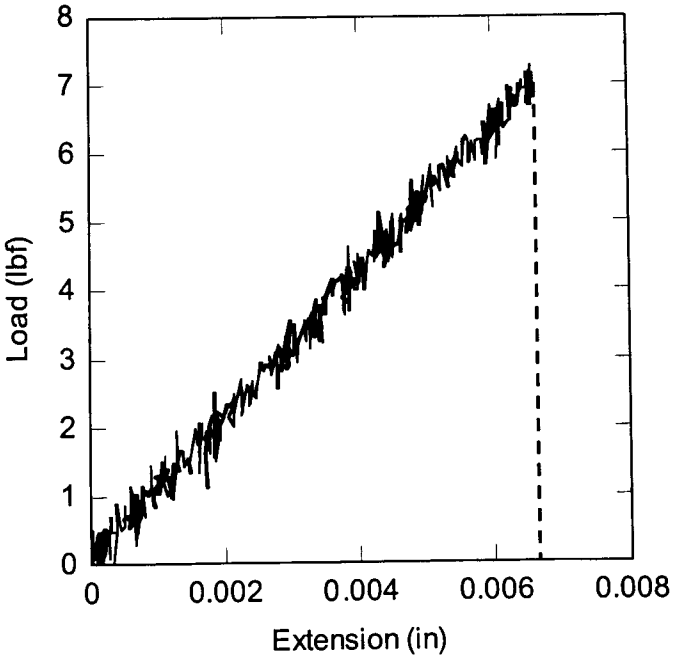

Figure A.IV.1 Representative plot of load against extension in fracture toughness measurement.

1.2 Result summary

Table A.IV.1 Neat resin comprising of 50% BMI and AMP (molar ratio 1:2) 50% LECY.

Sample	Notch Length, a in.	Thickness, B in.	Depth, W in.	B/W	Thickness, B Cm	a/W	f(x)	PQ lbf
1	0.239	0.1410	0.4750	0.2968	0.3581	0.503	10.758	5.830
2	0.236	0.1400	0.4690	0.2985	0.3556	0.503	10.759	7.600
3	0.275	0.1410	0.5090	0.2770	0.3581	0.540	12.156	10.032
4	0.222	0.1380	0.4550	0.3033	0.3505	0.488	10.253	6.288
5	0.252	0.1390	0.5140	0.2704	0.3531	0.490	10.329	7.501
6	0.260	0.1390	0.5200	0.2673	0.3531	0.500	10.650	6.714
7	0.255	0.1390	0.5070	0.2742	0.3531	0.503	10.751	6.575

Table A.IV.1 ***(continued)***

PQ	Depth, W	KQ	A	dA/dx	phi	U	Ui	U	GIc
kN	cm	MPa.m0.5				lbf. In.	lbf.In.	mJ	J/m2
0.0260	1.207	0.710	37.926	231.276	0.245	0.02227	0.01193	1.167	110.43
0.0338	1.191	0.938	37.936	231.334	0.245	0.03201	0.01807	1.574	151.90
0.0447	1.293	*1.333	47.620	294.332	0.225	0.06396	0.02833	4.023	*385.91
0.0280	1.156	0.762	34.562	210.398	0.253	0.02404	0.01341	1.200	117.13
0.0334	1.306	0.855	35.063	213.470	0.252	0.02916	0.01770	1.294	111.61
0.0299	1.321	0.785	37.203	226.744	0.246	0.02448	0.01486	1.086	94.59
0.0293	1.288	0.785	37.880	230.986	0.245	0.02109	0.01438	0.758	*68.13

Table A.IV.2 Neat resin comprising of 40% BMI and AMP (molar ratio 1:2) 30% LECY 30% CPM.

Test 1:

Sample	Notch Length, a	Thickness, B	Depth, W	B/W	Thickness, B	a/W	f(x)	PQ
	in.	in.	in.		Cm			lbf
1	0.262	0.1330	0.5230	0.2543	0.3378	0.501	10.682	6.701
2	0.266	0.1400	0.5240	0.2672	0.3556	0.508	10.913	16.630
3	0.261	0.1410	0.5230	0.2696	0.3581	0.499	10.618	15.302
4	0.253	0.1400	0.5200	0.2692	0.3556	0.487	10.209	6.177
5	0.255	0.1400	0.5220	0.2682	0.3556	0.489	10.272	7.021
6	0.260	0.1400	0.5240	0.2672	0.3556	0.496	10.522	12.946
7	0.265	0.1410	0.5240	0.2691	0.3581	0.506	10.846	3.672
8	0.259	0.1400	0.5240	0.2672	0.3556	0.494	10.459	6.794

Test 1 ***(continued)***

PQ	Depth, W	KQ	A	dA/dx	phi	U	Ui	U	GIc
kN	cm	MPa.m0.5				lbf. In.	lbf.In.	mJ	J/m2
0.0298	1.328	0.818	37.420	228.104	0.246	0.02341	0.01225	1.259	114.16
0.0740	1.331	1.970	38.976	237.897	0.242	0.11578	0.05635	6.710	585.35*
0.0681	1.328	1.752	36.987	225.394	0.247	0.10730	0.04902	6.579	560.33*
0.0275	1.321	0.687	34.275	208.635	0.254	0.01896	0.01061	0.943	79.15
0.0313	1.326	0.784	34.688	211.165	0.253	0.02739	0.01329	1.592	133.69
0.0576	1.331	1.478	36.348	221.415	0.248	0.08150	0.03711	5.011	426.33*
0.0163	1.331	0.429	38.525	235.045	0.243	0.00883	0.00370	0.579	49.91*
0.0302	1.331	1.000*	35.928	218.810	0.249	0.02376	0.01255	1.266	404.54*

Test 2:

Sample	Notch Length, a in.	Thickness, B in.	Depth, W in.	B/W	Thickness, B Cm	a/W	f(x)	PQ lbf
1	0.249	0.1250	0.4930	0.2535	0.3175	0.505	10.823	6.121
2	0.251	0.1240	0.4910	0.2525	0.3150	0.511	11.039	5.835
3	0.248	0.1230	0.4970	0.2475	0.3124	0.499	10.616	4.007
4	0.236	0.1240	0.4760	0.2605	0.3150	0.496	10.509	5.241
5	0.245	0.1250	0.4880	0.2561	0.3175	0.502	10.720	6.756
6	0.158	0.1390	0.3760	0.3697	0.3531	0.420	8.389	4.410

Test 2 *(continued)*

PQ	Depth, W	KQ	A	dA/dx	phi	U	Ui	U	GIc
kN	cm	MPa.m0.5				lbf. In.	lbf.In.	mJ	J/m2
0.0273	1.252	0.830	38.371	234.077	0.244	0.02281	0.01458	0.929	95.92
0.0260	1.247	0.815	39.835	243.348	0.240	0.02671	0.01349	1.493	158.13
0.0178	1.262	0.540	36.976	225.324	0.247	0.00865	0.00720	0.163	16.75*
0.0233	1.209	0.708	36.263	220.887	0.249	0.01845	0.01132	0.805	85.08
0.0301	1.240	0.912	37.671	229.672	0.245	0.03312	0.01711	1.807	187.32
0.0196	0.955	0.477	22.838	141.506	0.293	0.01288	0.00849	0.496	50.18*

2. Short bean shear test

The test procedure based on the ASTM D2344-84 is described as follows. The test specimens with thickness (~3.12mm) and width (~12.6mm) were machined from flat, finished composites. The thickness and width of the test specimen were measured before conditioning. The specimen was placed on a horizontal shear test fixture so that the fibers are parallel to the loading nose. The support span was 12.34 mm. The loading lose was then used to flex the specimen at a speed of 1.3 mm/min until breakage. The force was then recorded. Calculations were performed to determine shear strength according to the following equation, and the results are given by Table A.IV.3.

$$\textit{Shear strength} = \frac{0.75 \times breakingload}{width \times thickness}$$

Table A.IV.3 Result summary.

Sample ID	width (mm)	thickness (mm)	Breaking Load (lbf)	Shear Strength (Kpsi)
1	12.34	3.12	625	7.609419804
2	12.34	3.12	525	6.391912636
3	12.34	3.11	600	7.328531896
4	12.34	3.12	625	7.609419804
5	12.34	3.11	550	6.717820905
6	12.34	3.13	525	6.371491189
7	12.34	3.09	590	7.253032997
8	12.34	3.14	567	6.859295802
9	12.34	3.13	687	8.337551328
10	12.34	3.13	588	7.136070132
11	12.34	3.12	630	7.670295163
12	12.34	3.11	543	6.632321366

Appendix V: FIBER CHARACTERISTICS AND MOLD DESIGN

1. Fiber characteristics (with reference to THORNEL Product Information)

THORNEL Carbon Fiber T-650/35 3K was used in the composite processing, which is a continuous length, high strength, high modulus fiber made from a polyacrylonitrile precursor. The fiber surface is treated to increase the interlaminar shear strength in a resin matrix composite. Its typical properties and characteristics are summarized in Table A.V.1 and A.V.2.

Table A.V.1 Properties and characteristics of THORNEL Carbon Fiber T-650/35 3K.

Property	U.S. Customary Units	S.I. Units
Tensile Strength	660 $lb/in^2 \times 10^3$	4.55 GPa
Tensile Modulus	35 $lb/in^2 \times 10^3$	241 GPa
Density	0.064 $lb/in^2 \times 10^3$	1.77 Mg/m^3
Filament Diameter	6.8 μ	6.8 μ
Elongation at Break	1.75%	1.75%
Elastic Recovery	100%	100%
Carbon Assay	94%	94%
Surface Area	0.5 m^2/g	0.5 m^2/g
Longitudinal Thermal Conductivity	8 BTU-ft/hr(ft^2)(°F)	14 W/mK
Electrical Resistivity	14.9 Ohm-cm $\times 10^{-4}$	14.9 μOhm-m
Longitudinal CTE at 70°F (21°C)	-0.3 PPM/°F	-0.5 PPM/K

Table A.V.2 Typical Strand Properties of THORNEL Carbon Fiber T-650/35 3K.

Property	U.S. Customary Units	S.I. Units
Yield	2534 yd/lb	5.1 m/g
Denier	1763 g/9000m	1763 g/9000m
Twist	0	0
Filaments/Strand	3000	3000
Fiber Area in Yarn Cross Section	$17.2\ in^2 \times 10^{-5}$	$0.111\ mm^2$

2. Mold design

The mold was designed for pressure assisted resin transfer mold processing. In addition, the leaking of AMP needed to be prevented due to its toxicity. Accordingly, three aluminum parts were attached to each other tightly with a sealant O-ring. This created a space for packing fiber and infusing resin while being airproofed, as is shown in the following scheme. Pressure fittings were also installed to ensure pressurization. Information of O-ring and pressure fittings is given in Table A.V.3. The mold design schemes are given in the following four figures.

Table A.V.3 Specification of parts

Part name	Specification
Sealant O-ring	silicon O-ring with OD as
Pressure fitting	for tube with OD as 0.192'' and stand 20Psi

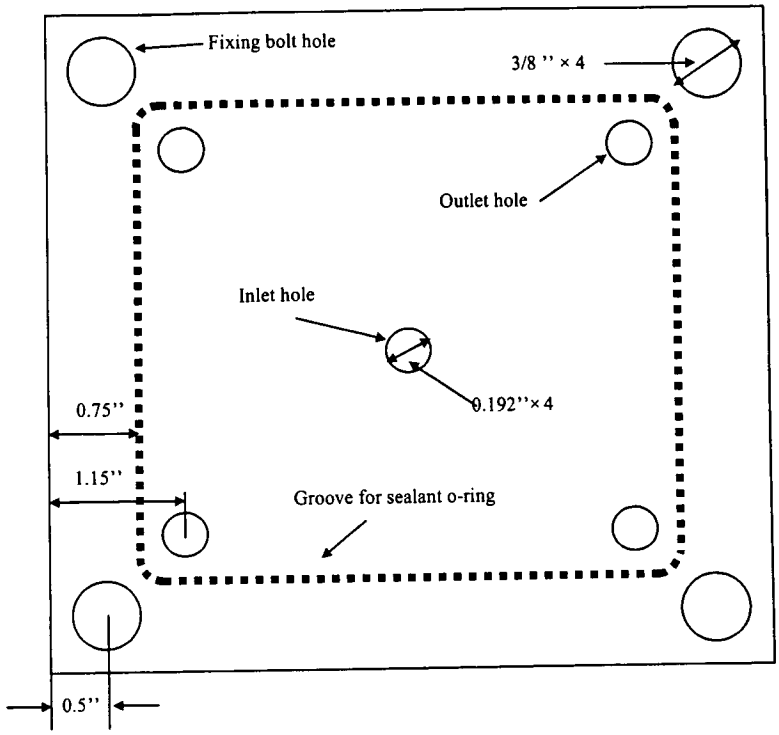

Upper layer (top view)

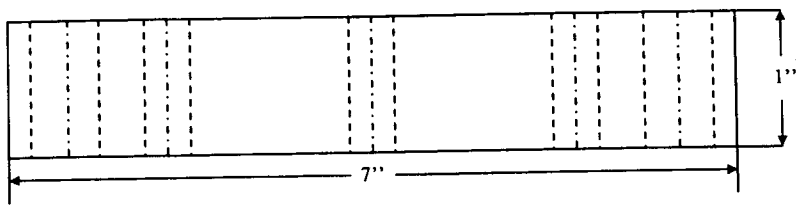

Upper layer (side view)

Figure A.V.1 Design scheme for the upper layer.

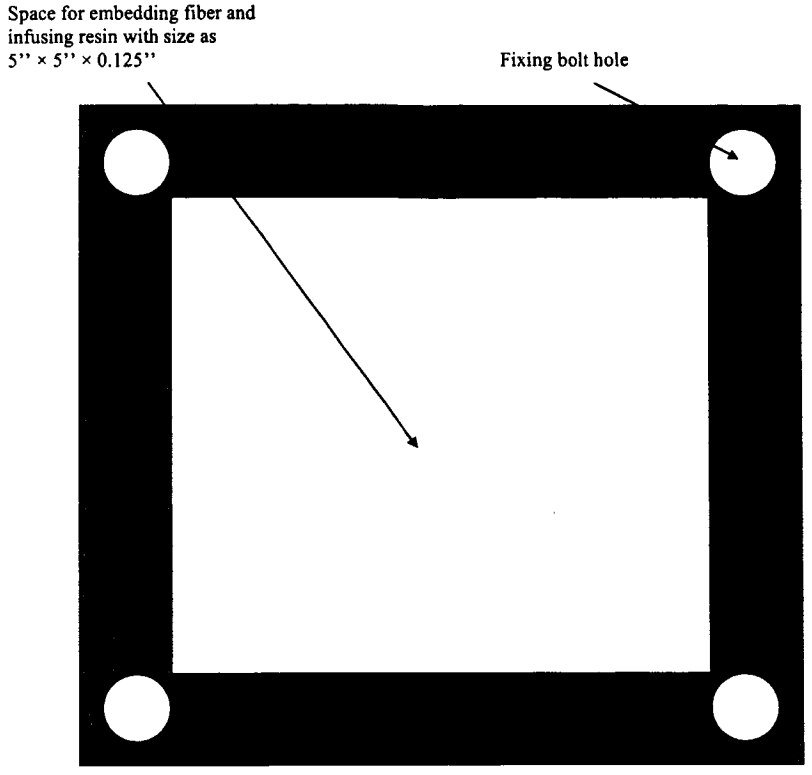

Middle layer (top view)

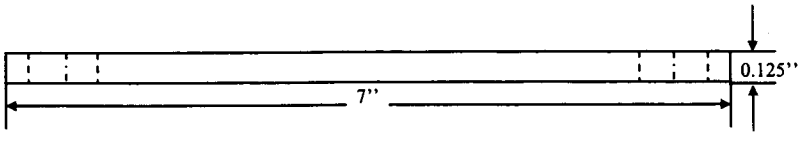

Middle layer (side view)

Figure A.V.2 Design scheme for the middle layer.

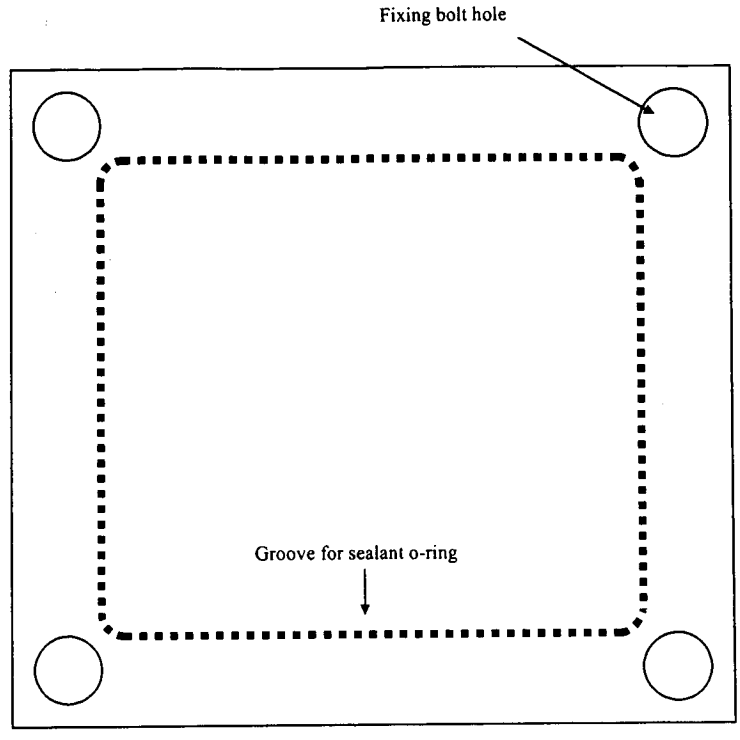

Bottom layer (top view)

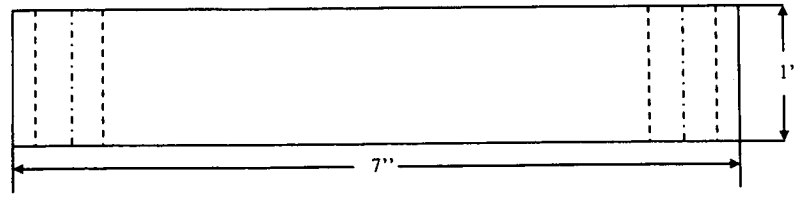

Bottom layer (side view)

Figure A.V.3 Design scheme for the bottom layer.

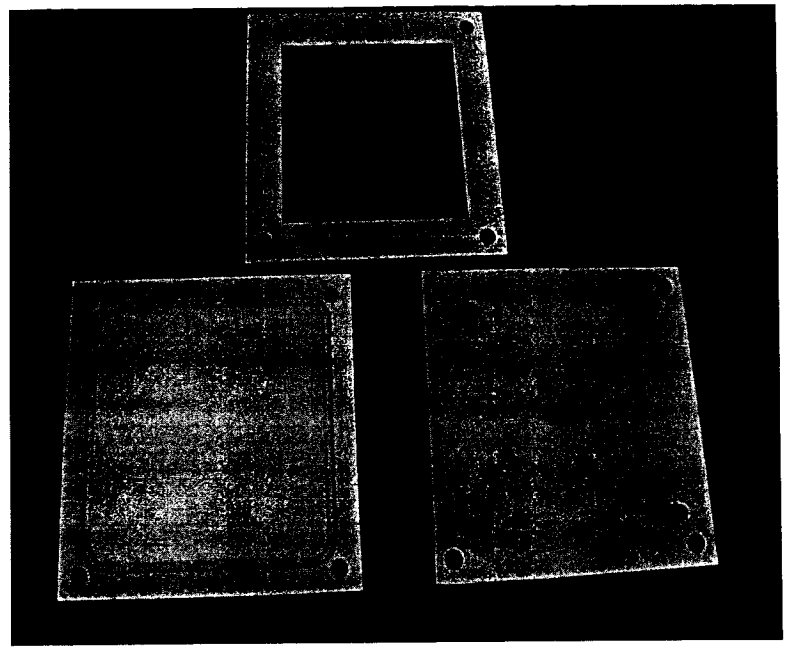

Figure A.V.4 Photo of the designed mold.

VITA

Name: Xing Geng **Date of Birth:** April 26, 1970 **Citizenship:** P. R. China

Education:

Ph. D. Chemical Engineering (Polymer Composite Materials), Drexel University, 2005
M. S. Minerals Processing Engineering (Water-borne Construction Composite Materials), University of Science and Technology Beijing, 1997
B. S. Polymer Chemical Engineering, Hebei University of Technology, 1991

Professional Experience:

Research Trainee (Polymer Materials and Technology)
Osaka Municipal Technical Research Institute, Osaka, Japan 1995.5-1995.9
Research Assistant Engineer
Hebei Research and Design Institute of Building Materials, Shijiazhuang, China 1991-1995

Selected Presentations:

Xing Geng and Giuseppe R. Palmese, *Development of Cyanate Ester - Bismaleimide E-Beam Cured Composite Systems*, Annual Meeting of the American Institute of Chemical Engineers, Indianapolis, IN, 3-8 November, 2002.

Xing Geng and G.R.Palmese, *Synthesis of Bismaleimide and Cyanate ester Based Sequential IPNs via EB Irradiation*, (Poster Honorable Mention), Drexel University Annual Research Day 2003, April 2003.

Xing Geng and G.R.Palmese, *Synthesis of Bismaleimide and Cyanate ester Based Sequential IPNs Via EB Irradiation*," Proceedings of the 48th International SAMPE Symposium/Exhibition, Long Beach, CA, May 2003.

Xing Geng, Giuseppe R. Palmese, *Bismaleimide and Cyanate Ester Sequential IPNs for High Temperature Composite Liquid Molding Applications,* ASC/ASTM-D30 Joint 19th Annual Technical Conference, Georgia Tech, Atlanta, GA, Oct. 17-20, 2004

Selected Publications:

Xing Geng and G.R. Palmese, *Synthesis of Cyanate Ester Modified Bismaleimide Resin Via Electron Beam Irradiation for High Temperature Applications*, submitted to Polymer

Xing Geng and G.R.Palmese, *Studies in Electron Beam Induced Free Radical Copolymerization of N-Acryloylmorpholine and N-Phenylmaleimide*, Journal of Polymer science: part B Polymer Physics (to be submitted)

Xing Geng and G.R.Palmese, *Study in the Reactive Diluents for the EB Irradiation Processing of Bismaleimide Resin: N-Acryloylmorpholine as a Novel Reactive Diluent for BMI Processing via EB Irradiation*, Journal of applied polymer science (to be submitted)

Xing Geng and G.R.Palmese, *Bisphenol E Based Cyanate Ester as a Co-reactive Diluent in the Bismaleimide Processing. Catalysis, Hydrolysis and Their Influences on the Final Properties*, , Journal of applied polymer science (to be submitted)

Xing Geng and G.R.Palmese, In-situ Synthesized Sequential Interpenetrating Polymer Networks from Bisphenol E Based Cyanate Ester and Bismaleimide via EB Irradiation. Synthesis, Characterization, and Properties , (to be submitted)